KU Leuven
Biomedical Sciences Group
Faculty of Medicine
Department of Cellular and Molecular Medicine

KU LEUVEN

DOCTORAL SCHOOL
BIOMEDICAL SCIENCES

SYNTHESIS AND APPLICATION OF PROBES FOR SERINE AND CYSTEINE HYDROLASES AND THE POLYAMINE TRANSPORT SYSTEM

Roeland Vanhoutte

KU Leuven
Groep Biomedische Wetenschappen
Faculteit Geneeskunde
Departement Cellulaire & Moleculaire
          Geneeskunde

KU LEUVEN

DOCTORAL SCHOOL
BIOMEDICAL SCIENCES

SYNTHESE EN TOEPASSING VAN PROBES VOOR SERINE EN CYSTEINE HYDROLASES EN HET POLYAMINE TRANSPORTSYSTEEM

Roeland Vanhoutte

Acknowledgements

Dear reader,

This is likely the first part of my thesis that you will read, for me however it is the last part that I write. After four great years, my research is done and my manuscript is written. I only have one last thing to do: give a big thank you to all of those who helped me throughout my PhD.

First and foremost my promotor, professor Steven Verhelst. Steven, thank you for your guidance in these past years. You have been a mentor who looks after his people rather than a supervisor. I know that this is not a given, especially in academia, and I am very grateful for it. Thank you for making a lab with such a nice working environment and for giving me freedom in my research. I could not have wished for a better promotor.

I want to thank my jury: professor Mario van der Stelt, professor Thomas Böttcher, professor Wim Dehaen and professor Eveline Lescrinier for reading my thesis and for their valuable feedback on my work. I want to thank dr Steven De Jonghe and professor Wim Dehaen once more for being part of my doctoral committee throughout the years. I have always enjoyed our yearly discussions on my work with you.

I am lucky that Steven hired such wonderful colleagues that have made me very happy to come to the lab every morning. Jian, Suravi, Merel, Marta, JP, Dimitris, Hester, Yvonne, Snezhana, Jonathan, Michaela and Shanping, it's been a real pleasure. All the discussions on science I have had with you were essential for my PhD, but so were the (pizza)lunches, labawats, skiing and China trips, Christmas parties, potlucks, barbecues, TAFKAPs, Friday afternoons (including Friday afternoon music) in the lab and random nights at the oude markt. As the only Belgian in the lab for most of my PhD, I have greatly enjoyed my inverse Erasmus with you guys. I'm very happy that I can call my colleagues my friends.

Also thank you to the non-Leuvenlab members of the Verhelstlab: Tim, Minh, Suyuan, Daniel, and Joachim. We saw each other less often, but it was always nice hearing from you guys on Thursdays and on the labawats.

Thank you to my masterstudents Fien and Elien for their hard work and enthousiasm.

Some other people from the department also deserve a thank you. Thanks to the neighbours of the Gelenslab for all the fun in our shared labspace and on our joint lab activities. Also thanks to my collaborators at LCTS group for their help with the characterization of the polyamineprobes, and to

Table of Contents

Table of Contents

List of Abbreviations

17-ODYA	17-octadecynoic acid
aa	amino acid
ABHD	Alpha/beta-hydrolase domain containing enzyme
ABP	Activity-based probe
ABPP	Activity-based protein profiling
ACN	Acetonitrile
Ad_N	Nucleophilic addition
Ahx	6-aminohexanoic acid
Ala	L-alanine
Alloc	Allyloxycarbonyl
AOMK	Acyloxymethylketone
APEH	Acylaminoacyl-peptide hydrolase
APT-1	Acyl-protein thioesterase 1
APT-1/2	Acyl-protein thioesterases 1 and 2
APT-2	Acyl-protein thioesterase 2
Arg	L-arginine
Asn	L-asparagine
Asp	L-aspartic acid
ATPase	Adenosine triphosphatase
AzaGln	Aza-glutamine
Azt	Azetidine
BCA	Bicinchoninic acid
BK channel	Big potassium channel
Boc	*tert*-Butyloxycarbonyl
Boc-ON	2-(*tert*-butoxycarbonyloxyimino)-2-phenylacetonitrile
BODIPY	5,5-Difluoro-5H-4λ^5-dipyrrolo[1,2-*c*:2',1'-*f*][1,3,2]diazaborinin-4-ylium-5-uide
BSA	Bovine serum albumin
CC_{50}	Half maximal cytotoxic concentration
Covid-19	Coronavirus disease-19
CPP	Cell-penetrating peptide
Cryo-EM	Cryogenic electron microscopy
CuAAC	Copper(I)-catalyzed azide-alkyne cycloaddition
Cys	L-cysteine
DAGL	Diacylglycerol lipase
DAPI	4',6-diamidino-2-fenylindole
DCM	Dichloromethane
DIC	*N,N'*-diisopropylcarbodiimide
DIEA	*N,N*-diisopropylethylamine
DIFMU	6,8-difluoro-7-hydroxy-4-methylcoumarin
DMEM	Dulbecco's modified Eagle medium
DMF	*N,N*-dimethylformamide
DMSO	Dimethylsulfoxide
DNA	Deoxyribonucleic acid
DPP	Depalmitoylation probe
DTT	Dithiotreitol

List of Abbreviations

EC$_{50}$	Half-maximal effective concentration
EDTA	Ethylenediaminetetraacetic acid
eGFP	Enhanced green fluorescent protein
ESI-MS	Electrospray ionization mass spectrometry
EtOH	Ethanol
FAAH	Fatty acid amide hydrolase
FASN	Fatty acid synthase
FBS	Fetal bovine serum
Fmoc	Fluorenylmethyloxycarbonyl
FP	Fluorophosphonate
FP-Rh	Fluorophosphonate-Rhodamine
GAP-43	Growth-associated protein 43
Gln	L-glutamine
Gln(Me)$_2$	*N,N*-dimethyl-L-glutamine
GTPase	Guanidine triphosphatase
HBTU	*N,N,N',N'*-Tetramethyl-O-(1H-benzotriazol-1-yl) uronium
HDFP	Hexadecyl fluorophosphonate
HEPES	4-(2-hydroxyethyl)-1-piperazineethanesulfonic acid
HPLC	High pressure liquid chromatography
His	L-histidine
HOBt	1-Hydroxybenzotriazole
HRMS	High resolution mass spectrometry
IC$_{50}$	Half maximal inhibitory concentration
IC$_{50}^{App}$	Apparent half maximal inhibitory concentration
Inp	Isonipecotic acid
IPTG	Isopropyl β-D-1-thiogalactopyranoside
kDa	Kilodalton
K$_i$	Inhibition constant
KIAA1363	Neutral cholesterol ester hydrolase 1
k$_{inact}$	Rate of enzyme deactivation
k$_{obs}$	Observed rate of inactivation
LC-MS	Liquid chromatography-mass spectrometry
Leu	L-leucine
LIPG	Endothelial lipase
Lys	L-lysine
Lys(N$_3$)	ε-azido-L-lysine
MAGL	Monoacylglycerol lipase
MALDI-TOF	Matrix-assisted laser diffractionionization-time of flight
MANT	*N*-methylanthranyloyl
MeOH	Methanol
MERS-CoV	Middle-eastern respiratory syndrome coronavirus
M^{pro}	Main protease
mRNA	Messenger RNA
MS	Mass spectrometry
NBD	Nitrobenzofurazan
NIR	Near infrared
NMR	Nuclear magnetic resonance
NHS	*N*-hydroxysuccinimidyl
nsp	Non-structural protein
NTPase	Nucleoside triphosphatase

OD$_{600}$	Optical density at wavelength 600 nm
PalmB	Palmostatin B
PalmM	Palmostatin M
PBS	Phosphate-buffered saline
Phe	L-phenylalanine
PMSF	Phenylmethyl sulfonylfluoride
PNPLA	Patatin-like phospholipase domain containing protein
pp1A	polyprotein 1a
pp1ab	polyprotein 1ab
PTM	Post-translational modification
PTS	Polyamine transport system
Put	Putrescine
PyBrOP	Bromotripyrrolidinophosphonium
Pyr	Pyrrolidine
Ras	Rat sarcoma virus protein
RDP	Ratiomeric depalmitoylation probe
RNA	Ribonucleic acid
RT	Room temperature
SARS-CoV	Severe acute respiratory syndrome coronavirus
SARS-CoV-2	Severe acute respiratory syndrome-coronavirus-2
Scrib	Scribbled planar cell polarity protein
SDS	Sodium Dodecyl sulfate
SDS-PAGE	Sodium dodecyl sulfate polyacrylamide gel electrophoresis
Ser	L-serine
SH	Serine hydrolase
S_N2	Bi-molecular nucleophilic substitution
S_NAr	Nucleophilic aromatic substitution
$S_N2(P)$	Nucleophilic substitution at phosphorus center
Spd	Spermidine
Spm	Spermine
SPPS	Solid-phase peptide synthesis
TAT	Transactivating transcriptional activator
TAMRA	Carboxytetramethylrhodamine
TEA	Triethylamine
TFA	Trifluoroacetic acid
THF	Tetrahydrofuran
THPTA	Tris-hydroxypropyltriazolylmethylamine
TIS	Triisopropyl silane
TLC	Thin-layer chromatography
Tle	L-*tert*-leucine
TMR	Tetramethylrhodamine
Tris	Tromethamine
UV	Ultraviolet
VS	Vinyl sulfone
WH	Warhead
zDHHC	Zinc finger DHHC domain containing enzyme

Summary

Activity-based probes (ABPs) are small molecular tools that allow the detection and monitoring of enzyme activity by covalently binding onto the active site of the enzyme. They consist of a warhead that binds the enzyme, a recognition element that alters the selectivity of the probe and a detection tag that allows the visualization, quantification or purification of probe-labeled enzymes. ABPs are applied to elucidate enzyme function, enzyme localization and the involvement of enzymes in health and disease. They can furthermore be used as screening tools for drug candidates.

To monitor the activity a single enzyme, the selectivity of an ABP has to be steered towards this target. This often requires a difficult and time-consuming synthetic process, and as a result, selective ABPs have only been developed for relatively few enzymes expressed in human cells. One enzyme family of which only a few members have selective ABPs are the serine hydrolases. To speed up the process of ABP development for serine hydrolases, solid-phase synthesis procedures that allow a fast synthesis of six classes of serine-reactive probes were developed in **Chapter III**. The application of these procedures is shown by the combinatorial on-resin synthesis of a library of ABPs. These probes bear a recognition element made up of an aromatic moiety and a piperidine/piperazine ring, and a serine reactive warhead. Two probes with a triazole urea warhead were found to be reactive and selective for acyl-protein thioesterases 1 and 2 (APT-1/2) in a screening on serine hydrolases present in mouse brain.

Chapter IV describes the use of the solid-phase synthesis procedures established in Chapter III to synthesize a library of triazole urea ABPs, based on the APT-1/2 reactive ABPs found in the previous chapter. In this library, changes were made in the recognition elements of the probes to drive their reactivity towards one of the APT-isoforms and creating isoform-selective ABPs. Although this yielded no selective probes, several probes with a higher reactivity for both APT-isoforms than the original probes were discovered.

In **Chapter V**, the development of ABPs for the SARS-CoV-2 main protease (M^{pro}) is described. M^{pro} is a cysteine protease that is the key player in the proteolytic maturation of the non-structural proteins of the SARS-CoV-2 virus by cleavage of its polyproteins. It has gained a lot of attention as a potential target for antiviral drugs to combat the Covid-19 pandemic. In this chapter, azapeptidic ABPs for M^{pro} are synthesized that can be fully made on resin. The recognition element of these probes consists of the preferred P_1, P_2 and P_3 substrates of M^{pro}, of which the P_1 residue is an aza-amino acid. The ABPs are capped with a cysteine-reactive warhead on the P_1 aza-residue. A probe with a chloroacetamide warhead was found to be very potent in labelling M^{pro} and to have a very low detection limit. This

probe could furthermore inhibit cell death in SARS-CoV-2 infected cells and can potentially be used for labeling M^{pro} in live cells.

The mammalian polyamine transport system was a mystery at the start of this research project, as no proteins had been identified as polyamine transporters. **Chapter VI** describes the synthesis of azide-functionalized polyamines, which were converted to fluorescent probes through "click" chemistry with an alkyne-BODIPY fluorophore. Through a SAR study with polyamine probes with different lengths, different positionings of the fluorophore and a different amount of positive charges, it was found that probes in which the fluorophore is attached to an outer amine of the polyamine get taken best into cells. These polyamine probes have since been used by other research groups in the identification of polyamine transporters.

In summary, this thesis describes the synthesis and validation of probes that target APT-1/2, SARS-CoV-2 M^{pro} and the polyamine transport system. These probes can be synthesized efficiently via solid-phase synthesis or click chemistry. The developed solid-phase synthesis procedures are applicable for the synthesis of probes for other targets as well.

Samenvatting

Activity-based probes (ABPs) zijn moleculaire gereedschappen die covalent binden aan de actieve site van enzymen. Met behulp van deze gereedschappen kan enzymatische activiteit worden gedetecteerd en gemonitord. ABPs bestaan uit drie delen: een "warhead", die bindt met het enzym; een herkenningselement, waarmee de selectiviteit van een probe kan worden beïnvloed; en een detectielabel, waarmee probe-gelabelde enzymen kunnen worden gevisualiseerd, gekwantificeerd of opgezuiverd. ABPs worden toegepast om de functie of lokalisatie van enzymen te bepalen. Ze kunnen verder ook gebruikt worden om de rol van enzymen in ziektebeelden te bepalen of bij de screening van potentiële geneesmiddelkandidaten.

Om de activiteit van een enkel enzym te monitoren moet de selectiviteit van een ABP gestuurd woden naar dit ene doelwit. Hiervoor is een synthetisch proces nodig dat in de meeste gevallen erg tijdrovend is. D aarom zijn er slechts relatief weinig selectieve ABPs ontwikkeld voor enzymen die tot expressie worden gebracht in menselijke cellen. Een enzymenfamilie waarvan slechts enkele enzymen selectieve ABPs hebben zijn de serine hydrolasen. Om het proces van ABP-ontwikkeling voor serine hydrolasen te versnellen, werden vaste-fasesynthese procedures ontwikkeld in **Hoofdstuk III**, waarmee zes types van serine-reactieve probes kunnen worden gemaakt. Met behulp van deze procedures werd een combinatorische bibliotheek gemaakt van ABPs die een herkenningselement bevatten met een aromatische groep en een piperidine/piperazinering, en een serine-reactieve warhead. Van twee probes van deze bibliotheek met een triazoolurea warhead werd gevonden dat ze reactief en selectief zijn voor acyl-proteine thioesterases 1 en 2 (APT-1/2) in een screening op de serine hydrolasen die aanwezig zijn in een muizenbrein.

In **Hoofdstuk IV** worden de procedures die ontwikkeld werden in Hoofdstuk III gebruikt om een bibliotheek van ABPs te maken met een triazoolurea warhead, gebaseerd op de APT-1/2-reactieve probes die ontwikkeld werden in het vorige hoofdstuk. In deze nieuwe bibliotheek werden er veranderingen aangebracht in de herkenningselementen van de probes om hun reactiviteit en selectiviteit voor de APT-isovormen te proberen sturen. Deze bibliotheek leverde geen isovorm-selectieve probes op, maar er werden wel verschillende probes gevonden met een hogere activiteit voor de beide APT-isovormen dan de originele probes.

Hoofdstuk V beschrijft de ontwikkeling van ABPs voor het SARS-CoV-2 main protease (M^{pro}). M^{pro} is een cysteine protease dat een sleutelrol speelt in de proteolytische maturatie van de niet-structurele eiwitten van het SARS-CoV-2 virus door het klieven van de polyproteinen die tot expressie worden gebracht door het virus. M^{pro} is daarom een belangrijk potentieel doelwit voor de ontwikkeling van

antivirale geneesmiddelen voor de behandeling van Covid-19. In dit hoofdstuk worden azapeptidische ABPs ontwikkeld die reageren met het SARS-CoV-2 M^{pro}. Het herkenningselement van dez probes bestaat uit de P_1-, P_2- en P_3-voorkeurssubstraten van M^{pro}, waarvan het P_1-substraat een aza-aminozuur is. De ABPs zijn gecapped op het P_1 aza-aminozuur met een cysteine-reactieve groep. Van een ABP met een chloroacetamide warhead werd gevonden dat deze erg potent reageert met M^{pro} en een lage detectielimiet heeft voor probe-labeling. Deze ABP kon ook celdood verhinderen in cellen die besmet zijn met SARS-CoV-2 en kan potentieel gebruikt worden voor het labelen van M^{pro} in levende cellen.

Hoofdstuk VI behandelt de ontwikkeling van fluorescente polyamine probes. Aan het begin van dit onderzoeksproject was het polyamine transport in zoogdieren een mysterie, daar er nog geen eiwitten waren geïdentificeerd als zijnde polyamine transporters. In dit hoofdstuk werden polyamines ontwikkeld die gefunctionaliseerd werden met azides, waarmee via "click" chemie met alkyn-gefunctionaliseerde BODIPY fluoroforen fluorescente polyamineprobes werden gemaakt. Deze polyamineprobes hebben verschillende lengtes, een verschillende positionering van het fluorofoor ten opzichte van het polyamine en een verschillend aantal positieve ladingen. Er werd gevonden dat polyamine probes waarbij de fluorofoor verbonden is aan een van de buitenste amines van het polyamine beter opgenomen wordt dan probes waarbij de fluorofoor aan een van de middelste amines zit. Deze lineaire probes zijn sindsdien gebruikt door andere onderzoeksgroepen om moleculaire spelers in polyamine transport te identificeren.

Samengevat beschrijft deze thesis de synthese en toepassing van probes die als doelwit APT-1/2, SARS-CoV-2 M^{pro} of het polyamine transport systeem hebben. Deze probes werden op efficiënte manieren gesynthetiseerd door vaste-fasesynthese of click chemie. De ontwikkelde vaste-fasesyntheseprocedures kunnen ook gebruikt worden voor de ontwikkeling van probes die andere serine of cysteïne hydrolasen als doelwit hebben.

Chapter I: Introduction

1.1. Activity-based protein profiling

Around the year 2000, activity-based protein profiling (ABPP) was reported for the first time by the groups of Cravatt[1] and Bogyo[2]. This technique was developed to overcome a lacking in molecular biology: the quantification of the active fraction of a proteome. In ABPP, small molecules called activity-based probes (ABPs) are employed, which bind covalently with the nucleophile in the active site of enzymes and allow the active enzyme to be visualized, quantified or purified. Through their mechanism of action, ABPs take into account the tight activity regulation of many enzymes by various post-translational mechanisms, which is not possible with mRNA quantification or protein quantification.

1.1.1. Activity-based probes

ABPs consist of three parts: a warhead that binds covalently onto the active site nucleophile, a spacer with or without a recognition element that influences the selectivity of the probe for a specific (group of) enzyme(s) and a detection tag, which enables probe-labeled enzymes to be detected (Figure **1.1**).
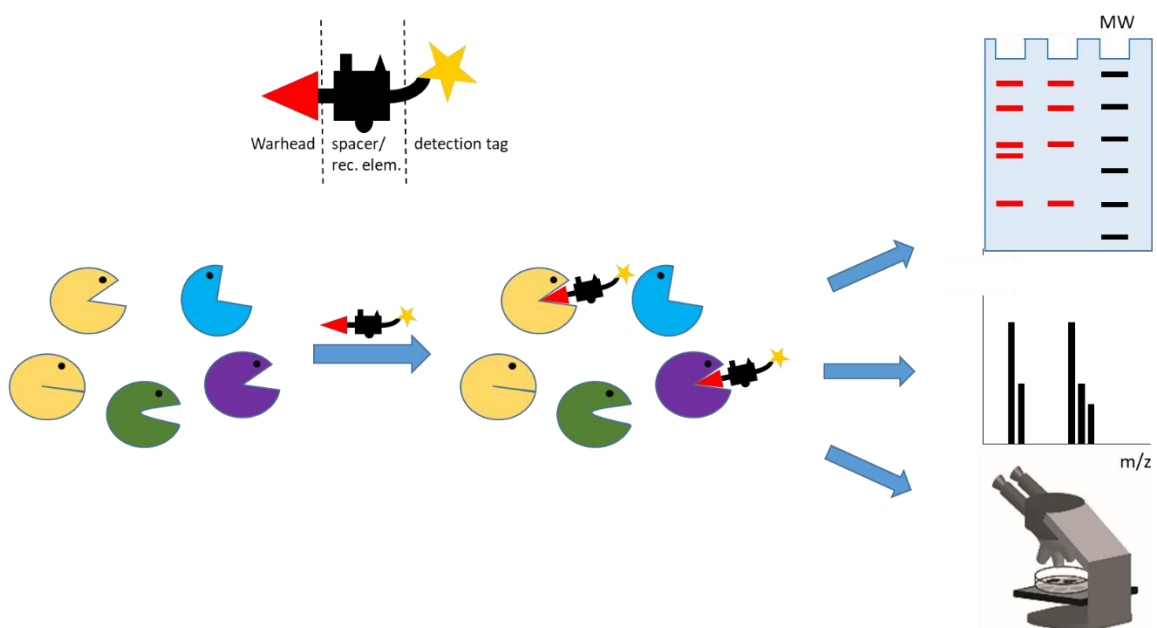
Figure 1.1. General structure of ABPs (top) and workflow of direct ABP labelling, with gel-based MS-based and microscopy read-out (bottom).

1.1.1.1. Detection tags

Detection tags of ABPs are chosen dependent on the read-out. For visualization experiments, this can be a fluorophore, such as rhodamine or a radioactive tag, such as [125]I (Figure **1.2A**). For affinity purification of probe-labeled enzymes, biotin tags are commonly used. One limitation of these aforementioned tags is their relatively large size, which may present a steric clash or prevent cell permeability. To overcome this problem, bio-orthogonal detection tags have been introduced into ABPP by Ovaa and Overkleeft[3], and Speers and Cravatt[4]. These bio-orthogonal tags are "click" handles such as azides or alkynes. The benefit of click tags is that they are small and therefore make minimal alterations to the physicochemical properties of activity-based probes.[5] Additionally, they allow a wide variety of readouts through bio-orthogonal chemistry to a reporter tag of choice after probe-labelling. Click reactions used in ABPP include Copper(I)-catalyzed azide-alkyne cycloaddition and Staudinger ligation (Figure **1.2B**).[6]
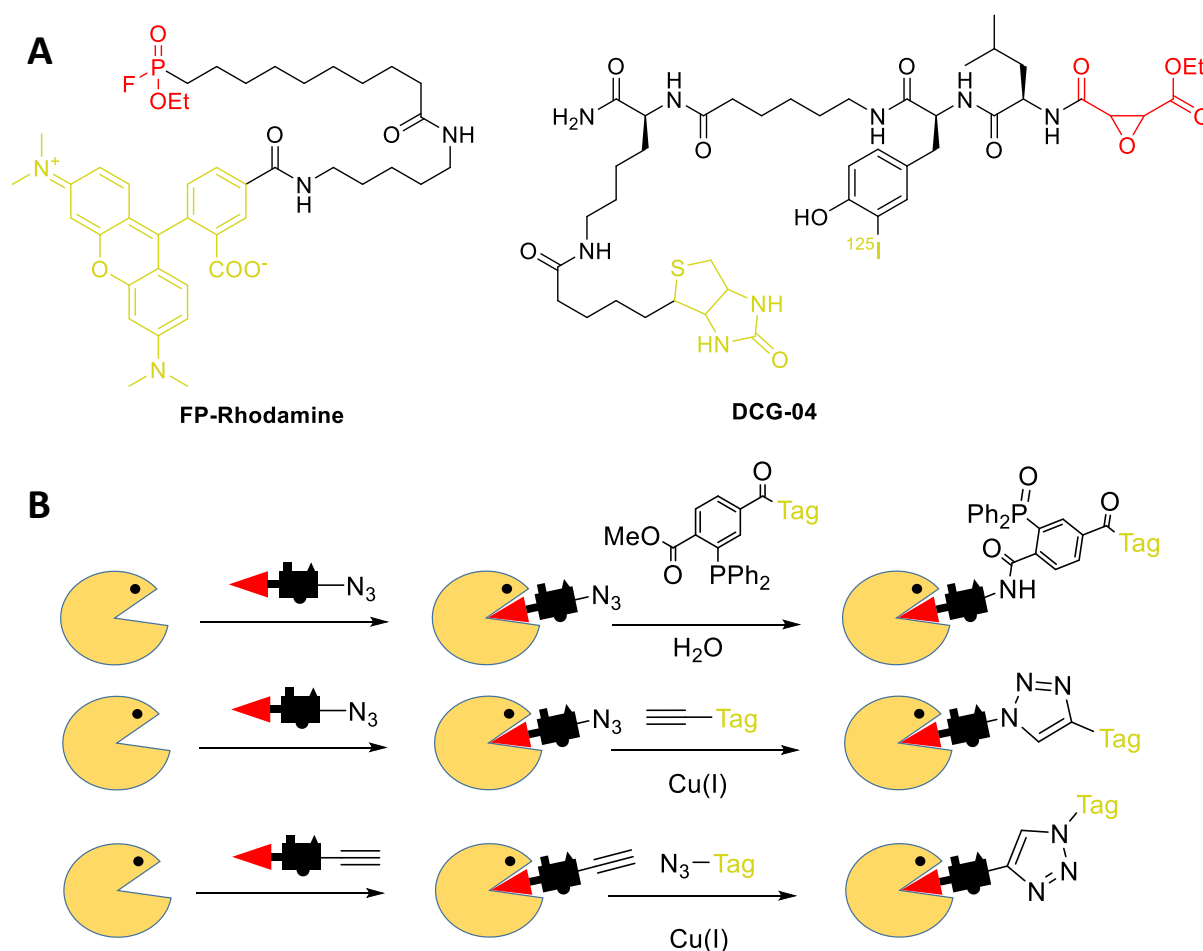
Figure 1.2. A. Molecular structures of FP-Rhodamine and DCG-04. Warheads are depicted in red, spacers in black and detection tags in yellow. **B.** Labeling of an enzyme with a probe bearing an alkyne or azide detection tag, followed by bio-orthogonal ligation of probe-labeled enzyme complexes to detection tags via Staudinger ligation (top) and CuAAC (bottom).

1.1.1.2. Recognition elements/spacer

Spacers serve two purposes: creating distance between warhead and detection tag to prevent strong influence of the tag on the probe binding and, if desired, increasing the specificity of an ABP for a specific (group of) enzyme(s) with an incorporated recognition element. An example of an ABP that has a spacer without a recognition element is FP-Rhodamine (Figure **1.2A**). This probe is a general serine reactive ABP, labelling >80% of mammalian serine hydrolases.[7] As a result, this probe is commonly used to assess general serine hydrolase activity in proteomes and in competitive ABPP with serine hydrolase inhibitors and probes (see paragraph 1.1.3.1.). However, probes as FP-Rhodamine are not suited for imaging experiments in which the localization of a particular serine hydrolase needs to be assessed, because of their general serine reactivity.

Probes that contain a recognition element in their spacer to increase their selectivity, such as DCG-04 (Figure **1.2A**), preferentially label one enzyme or a group of related enzymes. For DCG-04, these are clan CA proteases.[2,5,8,9] Probes that contain a recognition element and are selective for specific enzymes are very valuable study tools for determining the activity and localization of specific enzymes, and can be applied in visualization experiments on whole cells, besides gel-based experiments.

1.1.1.3. Warheads

Warheads form a covalent bond between the probe and the active site nucleophile. They also influence the selectivity of probes, as hard electrophilic warheads preferentially label hard active site nucleophiles such as serine residues and soft electrophilic warheads label soft active site nucleophiles such as cysteine residues.[10,11] Reactivities of different warheads for a nucleophile differ, which also influences probe selectivity. In the next two sections, serine and cysteine reactive warheads will be discussed.

1.1.1.3.1 Serine reactive warheads

Two popular types of serine-reactive warheads are electrophiles that undergo an $S_N2(P)$ reaction and those that undergo an addition-elimination reaction (Figure **1.3**). The leaving group on the warhead heavily impacts the reactivity of phosphonate probes. FP-Rhodamine for example, is a very reactive probe because of the inductive effect the fluoride has on the phosphorous atom[12], which makes up for the poor leaving group qualities of the fluoride. Although diphenyl phosphoramidates possess a better leaving group, they make less reactive probes, because the phosphorous is less induced by the leaving groups.[13] Diphenyl phosphonates have a phosphorous with an electrophilicity higher than

diphenyl phosphoramidates and lower than fluorophosphonates and, as a result, have a reactivity in between these two classes of probes.[14]

Besides the electrophilicity of the atom in the warhead that is attacked by the nucleophilic side chain of the enzyme, the leaving group of the warhead (if present) also has an effect on the reactivity. This is also illustrated by a study of Wang et al., who made a series of phophonate probes bearing a phenol leaving group substituted with an electron-withdrawing group. Several of these probes labeled targets which were not labeled by FP-Rhodamine.[15] Furthermore, diphenyl phosphonates have a very strong labeling preference for serine proteases over other classes of serine hydrolases because the leaving group fits very well into the S_1 pocket of serine proteases.[16]

Reactivity of carbamate probes is also influenced by the leaving group on the warhead. Common O-substituents of carbamate-reactive ABPs are phenyl, *p*-nitrophenyl, hexafluoroisopropyl and N-hydroxyhydantoin. Chang et al. managed to increase the selectivity of a carbamylated ABP for MAGL and ABHD6 over FAAH by substituting the *p*-nitro phenyl moiety for a hexafluoroisopropyl moiety.[17]
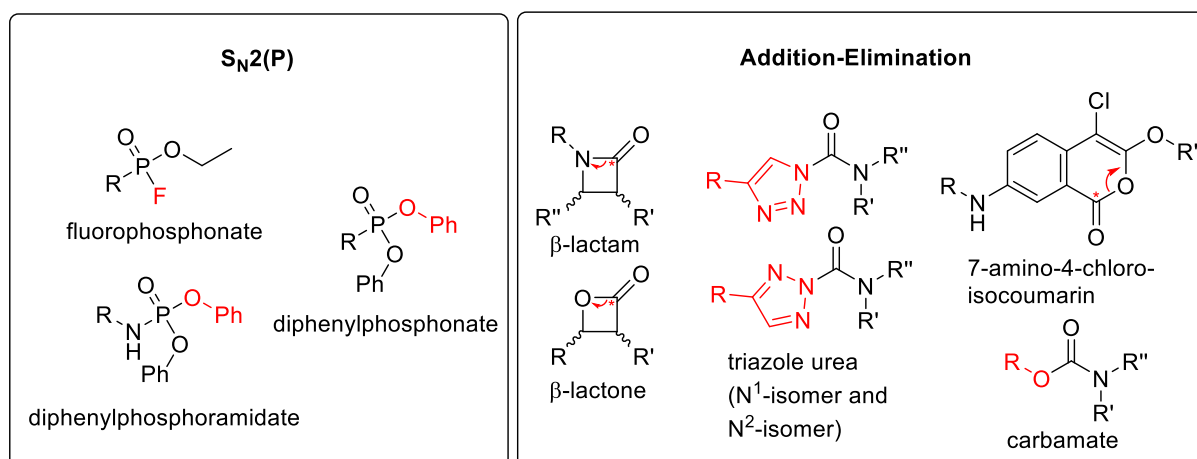
Figure 1.3. Selective list of serine-reactive warheads. Leaving groups are indicated in red. For intramolecular leaving groups, the site of attack is indicated with a red asterisk and the ring opening mechanism with a red arrow.

1.1.1.3.2 Cysteine reactive warheads

Similar to serine reactive warheads, cysteine reactive warheads differ in reactivity depending on electrophilicity and mechanism.[11,18] Mechanisms for Cys-reactive warheads include Michael addition, S_NAr, Ad_N and S_N2 (Figure **1.4**). The reactivity of Michael acceptors is largely dependent on the strength of the electron-withdrawing group, which determines how easily the intermediate structure is formed. Vinyl sulfonamides are therefore more reactive Michael acceptors than acrylamides (Figure **1.4**).[11] The reactivity of vinyl sulfonamides is so strong however that it is difficult to create selective probes with this warhead. Weaker Michael acceptors such as acrylates are on the other hand more subjective

to the effects of recognition elements altering the probes selectivity and also find frequent usage in ABPP.[19,20]
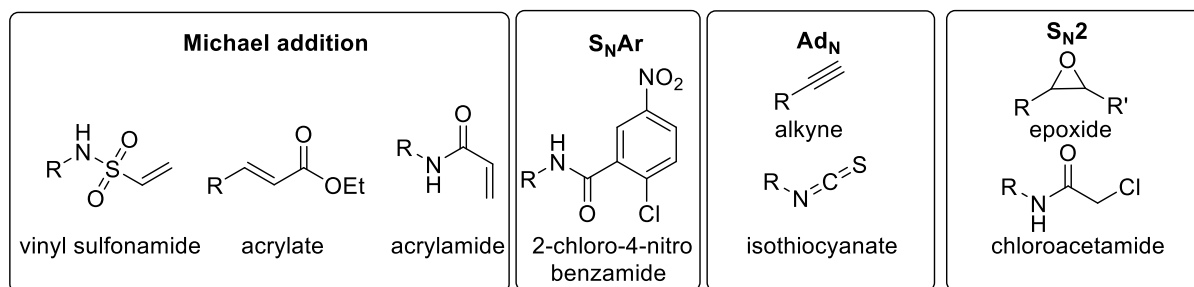
Figure 1.4. Selective list of cysteine-reactive warheads.

1.1.2. Solid-phase synthesis in ABP development

A major bottleneck for the development of ABPs is their synthesis, which is often a long process. Because irreversible inhibitors were unpopular for a long time for pharmaceutical purposes, there is a lacking of information on such inhibitors for most pharmacologically relevant targets, which can serve as easy starting points for the synthesis of ABPs. Furthermore, the solution-phase chemistry techniques used to synthesize ABPs are time consuming and take a long time to optimize. Therefore, scientists searched for methods to increase the speed at which probes can be synthesized and the amount of probes that can be synthesized simultaneously.[21]

One such method is solid-phase synthesis, in which a molecule is immobilized on a resin. Through solid-phase synthesis, ABPs can be built without long and tedious workups between reactions. The time and space efficiency of solid-phase synthesis makes it a very efficient method for simultaneous synthesis of large amounts of compounds.

Solid-phase synthesis has since its inception mainly been used for peptide synthesis[22], therefore solid-phase peptide synthesis procedures are well established. As a result, the technique is mainly applied in ABPP for the construction of protease probes that have recognition elements based on the consensus sequence of their substrate.[10] This has led to probes for cathepsins and the Sars-CoV-2 main protease.[2,23]

A drawback of solid-phase synthesis is that not all warheads can be introduced on resin. Reactions that work in solution phase synthesis, including some creating a reactive electrophilic center cannot always be reproduced on resin. The C->N directed nature of solid-phase synthesis makes it also difficult to introduce warheads which cannot be attached to nitrogen such as diphenylphosphonates. These drawbacks have been overcome however for the on resin synthesis of acyloxymethyl ketones.[23,24]

1.1.3. ABP labeling techniques

There is a multitude of applications in which ABPs can be used.[6,25] The labeling mechanisms used in these applications are twofold. Depending on whether an inhibitor is applied in the labeling or not, we can differentiate between competitive ABPP and direct ABP labeling.

1.1.3.1. Competitive ABPP

Competitive labeling is an approach in which cells, proteomes or purified enzymes are first incubated with an inhibitor, followed by labeling with an ABP (Figure **1.5**).[26,27] It can be applied to screen inhibitors against a single target using an enzyme-selective probe or against a range of enzymes by using a broad spectrum probe. The potency of the inhibitor for its targets is then assessed by the loss of ABP labeling of each target in a titration series of the inhibitor.[28,29] This approach has several advantages over classic substrate assays. For one, it allows inhibitor screening against enzymes that have no known substrates and enzymes of which the function is unknown. It also does not require any protein expression or purification, but allows target engagement on a multitude of enzymes in physiologically relevant settings.[29] When using a broad-spectrum probe, the technique allows the assessment of inhibitor selectivity for one enzyme over other enzymes labeled by that probe. This is frequently applied for the selectivity assessment of serine hydrolase inhibitors in complex proteomes via competitive ABPP with FP-Rhodamine.
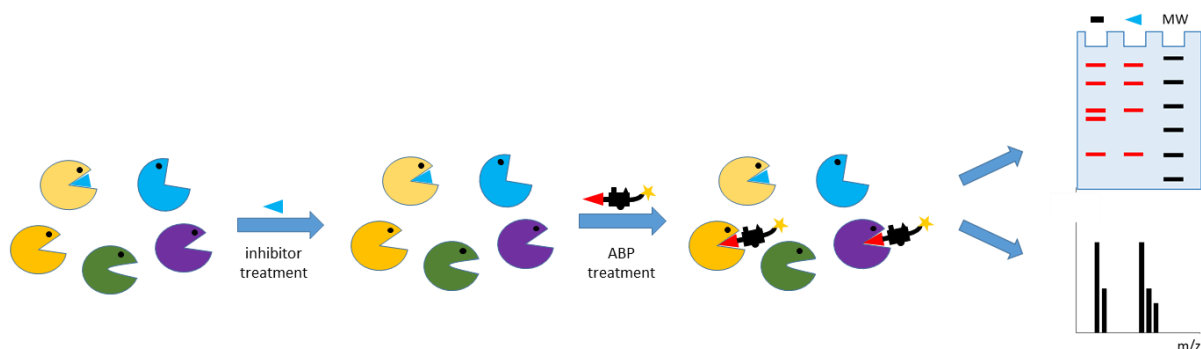
Figure 1.5. Schematic overview of competitive ABPP, with gel-based and MS-based readouts.

1.1.3.2. Direct ABP labeling

In direct probe labelling, a proteome is incubated with an activity-based probe, after which the targets are visualized or identified through the detection tag on the probe (**Figure 1.1**). This allows the visualization of all targets within a proteome that are labeled by the probe, whereas in competitive ABPP, only the targets of the inhibitor that are also targeted by the ABP that it competes with can be detected. Applications of direct probe labeling include: (1) Gel-based read-out of the targets hit in a proteome. This fast method allows the detection of all targets hit that are sufficiently expressed in the proteome. (2) The visualization of probe targets in live cells. Direct ABP labeling is a very valuable

method in combination with fluorescence microscopy, as it provides information on the localization and the activity of the probe targets within cells. (3) The identification of probe targets using mass spectrometry, which unambiguously identifies the whole set of targets labeled by the probe. By labeling probe-enzyme complexes with biotin, these enzymes can be isolated via streptavidin pull-down and identified by analysis of their peptides with LC-MS/MS after proteomic work-up.

1.2. Acyl-protein thioesterases

Acyl protein thioesterases are metabolic serine hydrolases, which are actors in the dynamic process of *S*-palmitoylation.[30] They are a group of poorly understood enzymes, the study of which is necessary to obtain a better view on the post-translational modification of *S*-palmitoylation. I will give an introduction about serine hydrolases, after which I will further discuss acyl-protein thioesterases.

1.2.1. Serine hydrolases

The enzyme superfamily of serine hydrolases is one of the largest and most diverse in nature. Around 1% of the human genome encodes serine hydrolases, with an estimated 240 unique enzymes expressed in humans. In humans, serine hydrolases are involved in practically all physiological and pathophysiological processes, including digestion, blood clotting, nervous system signaling, and inflammation.[31] They are furthermore involved in crucial processes in viruses and bacteria, including virulence, pathogen life cycle and drug resistance.[32,33] Serine hydrolases are divided into two classes: serine proteases and metabolic serine hydrolases.

Serine proteases are a group of enzymes that cleave amide bonds of proteins.[34] Their activity is tightly controlled, and dysregulation of their activity is associated with diseases such as cancer, diabetes and neurodegeneration.[35] To control their activity, most serine proteases are expressed as inactive zymogens, which get activated by proteolytic cleavage.[36] After cleavage, their activity is regulated by endogenous inhibitors such as serpins or through compartmentalization in specific organelles such as neutrophil granules.[37]

Metabolic serine hydrolases cleave a wider array of substrates than serine proteases. These substrates comprise peptides, small molecules and post-translational modifications on proteins. Depending on the substrate they cleave, metabolic serine hydrolases are subdivided into neutral lipases, phospholipases, amidases, Acyl-CoA hydrolases, cholinesterases, peptidases, protein hydrolases (enzymes that hydrolyse other bonds than the backbone amides) and glycan hydrolases.[38] Due to their wide substrate variety, metabolic serine hydrolases are included in most pathophysiological processes

in human. Dysregulation of their activity is associated with a very wide array of diseases, including neurological diseases and cancer.[39–41]

1.2.1.1. Catalytic mechanism of serine hydrolases

All serine hydrolases cleave their substrates (esters, thioesters or amides) via a nucleophilic serine residue in its active site (Fig. **1.6**). A basic residue, which is part of a catalytic dyad or triad in the active site of the enzyme activates this serine residue. The most frequently occurring activation mechanism for serine hydrolases in humans is the Ser-His-Asp triad. More than 60% of metabolic serine hydrolases contain this catalytic Ser-His-Asp triad, other known catalytic centers are a Ser-Ser-Lys triad or a Ser-Asp dyad.[31]
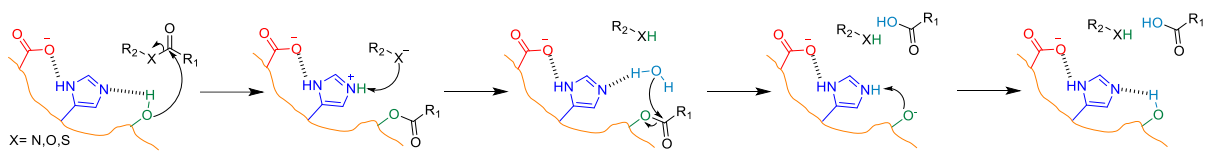
Figure 1.6. Mechanism of action of a serine hydrolase with a Ser-His-Asp triad.

1.2.2. *S*-palmitoylation

One process that involves metabolic serine hydrolases is protein *S*-(de)palmitoylation. *S*-palmitoylation is a post-translational modification (PTM) that describes the formation of a thioester-bond between Cys-residues and a fatty acid. Although named after the C16 fatty acid palmitic acid, the term *S*-palmitoylation covers the formation of thioesters with fatty acids that are 14-20 carbons long and is also referred to as *S*-acylation.[42,43]

Besides *S*-palmitoylation, other PTMs exist in humans that also involve the addition of fatty acids to proteins (Figure **1.7**).[44] These include *N*-myristoylation, in which a 14-carbon myristoyl group is transferred to an N-terminal glycine residue, and *N*-palmitoylation of lysine residues or N-termini. Two other post-translational lipidations exist that involve prenylation of C-terminal Cys residues: *S*-farnesylation and *S*-geranylgeranylation. The big difference between *S*-palmitoylation and these other post-translational lipidations is *S*-palmitoylation's reversibility. The palmitoyl-thioester bonds are quite labile and are readily cleaved by protein depalmitoylases, whereas the amide and thioether bonds of the other PTMs are permanent modifications.[43]

S-palmitoylation

N-palmitoylation

N-myristoylation

S-farnesylation

S-geranylgeranylation
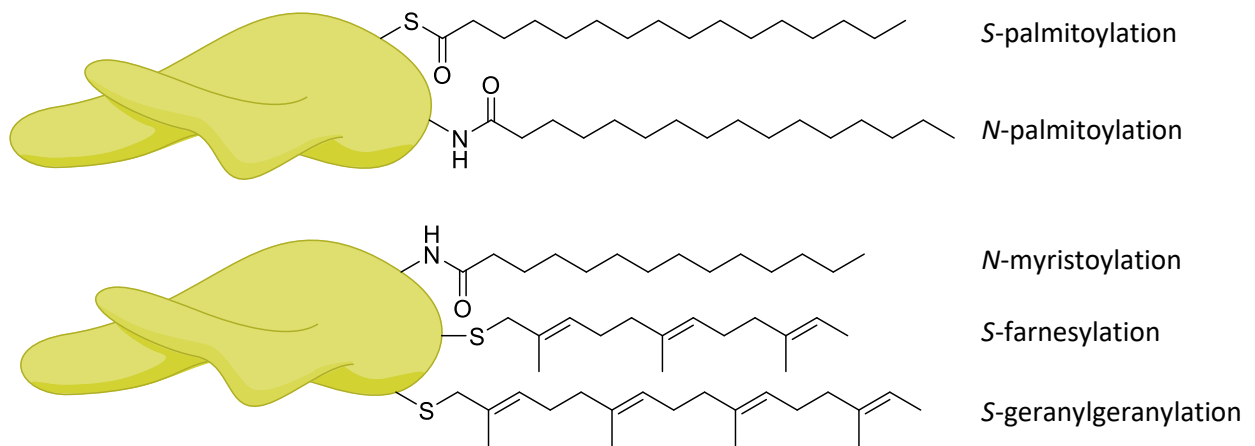
Figure 1.7. Lipid post-translational modifications. Figure adapted from Main et al.[43]

Protein S-palmitoylation facilitates the membrane attachment, localization and trafficking of proteins by equipping them with fatty acid "anchors" that allow them to bind with internal membranes, vesicles and the plasma membrane.[30,45] Depalmitoylation on the other hand causes proteins to detach from these membranes. This way, the dynamic S-palmitoylation/depalmitoylation cycle acts as a molecular switch, which regulates the spatial distribution of proteins. S-palmitoylation has also been reported to increase the half-life of several proteins by protecting them from ubiquitination[46,47] and can alter the conformation of proteins[48].

S-palmitoylation is associated with several biological processes, which include receptor-signaling, endocytosis, synaptic plasticity, cell growth and cardiac contractility.[49–52] Targets of protein palmitoylation include G-proteins, protein kinases, ion channels, transporters, pumps and receptors. Furthermore, this PTM is a crucial modification in the life cycle of parasites and viruses.[43,53]

1.2.3. Enzymes involved in protein S-palmitoylation and depalmitoylation

Protein S-palmitoylation is catalyzed by ZDHHC enzymes, whereas depalmitoylation is catalyzed by protein depalmitoylases. The protein depalmitoylases that have been identified so far are acyl protein thioesterases-1 and -2 (APT-1/2), ABHD10 and the ABHD17 enzyme family.[30,53,54] Palmitoyl protein thioesterase is another protein depalmitoylase[55], but this enzyme is only localized in lysosomes and late endosomes[56]. It likely only removes the thioester acyl chains during terminal protein degradation and is not involved in plasma membrane depalmitoylation.[30]

1.2.3.1. zDHHC enzyme family

zDHHC enzymes are a family of 23 transmembrane proteins that catalyze the formation of *S*-acyl thioesters on Cys residues in humans (Figure **1.8**). They are named after their distinct Asp-His-His-Cys motif and presumed Zn^{2+} binding domain.[57,58] Their mechanism of action works as follows: they first auto-acylate the Cys residue in their zDHHC domain with an acyl group that comes from a long chain fatty-acylCoA, which they subsequently transfer to their substrate.[59]
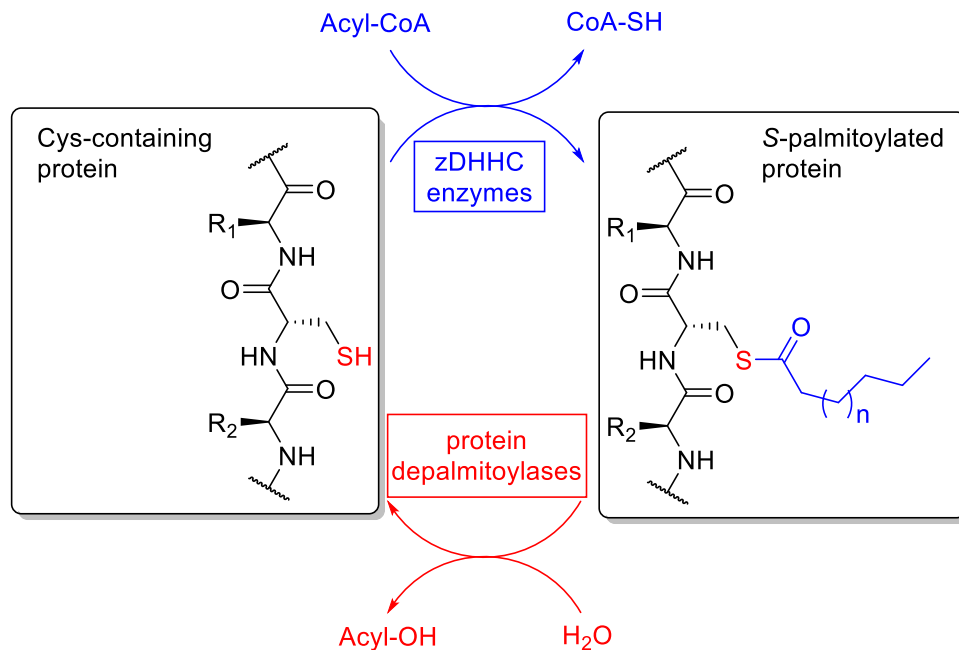
Figure 1.8. Scheme of the protein *S*-palmitoylation reaction. An acyl moiety from an acyl-CoA is covalently bound to a thiol group of a cysteine residue through a thioester bond in a reaction catalyzed by zDHHC enzymes. The hydrolysis of the *S*-acyl thioester is catalyzed by protein depalmitoylases. The typically attached acyl chain is C16:0 (palmitic acid), but can vary in length and degree of saturation. Figure adapted from Zaballa et al.[60]

1.2.3.2. APT-1/2

Whereas zDHHC enzymes install *S*-acyl thioesters, acyl protein thioesterases remove them (Figure **1.8**). The first enzyme that was discovered as a protein depalmitoylase was acyl protein thioesterase 1 (APT-1) in 1998 by Duncan and Gilman.[61] This protein was previously called lysophospholipase 1 (LYPLA-1) for its mild lysophospholipase activity until it was discovered to depalmitoylate Ras and Gα subunits of G proteins. Shortly after APT-1, APT-2 was discovered[62], a protein depalmitoylase that is highly homologous to APT-1 (68% similarity).[30] This enzyme was also first annotated to be a lysophospholipase, before it was discovered to have strong depalmitoylation activity. It also hydrolyzes prostaglandin-esters, in contrast to APT-1.[63]
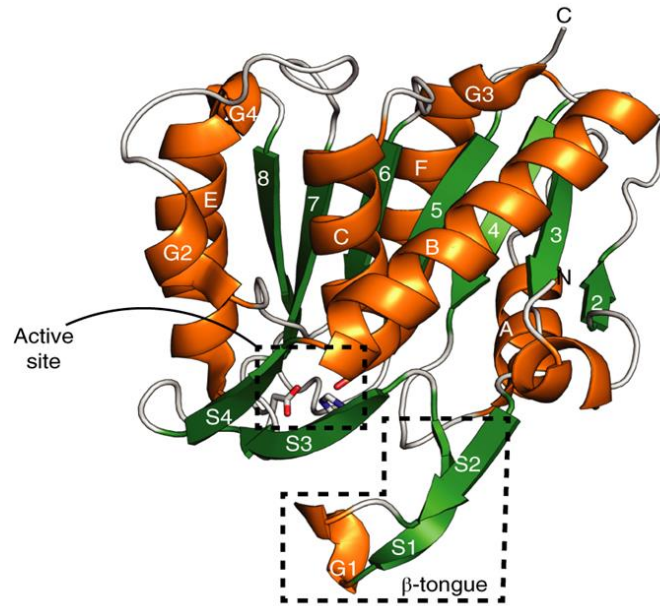
Figure 1.9. Ribbon structure of APT-1, with α-helices depicted in orange and β-strands in green. The active site and β-tongue are contoured in black. Figure republished with permission from Abrami et al.[64]

Both APTs are serine hydrolases with a classical Ser-His-Asp catalytical triad that belong to the enzyme family of the α/β hydrolases. These enzymes have a structure with a central 8-stranded β-sheet, surrounded by α-helices.[65] APT-1/2 have an atypical structure for α/β hydrolases, as they lack the first β-strand of the sheet and the fourth α-helix is much shorter than usual (Figure **1.9**). APT-1/2 are expressed as cytosolic enzymes, but can attach to membranes.[66]

The modus operandi of APT-1/2 was poorly understood for a long time, due to a lack of knowledge on how they associate to membranes and how they bind their substrates. A recent study by Abrami et al. however has shed some light on how these enzymes might interact with their substrates.[64] Through a combination of cellular, biochemical and molecular dynamics studies they revealed that APT-2 associates with membranes via palmitoylation, electrostatic interactions through a positively charged region on the protein, and a "β-tongue" that can dip into membranes (Figure **1.9**). This allows the enzyme to approach its membrane-bound target. They furthermore revealed that soluble APT-2 is more prone to ubiquitination, whereas in their membrane-bound state, the ubiquitination site of the protein is protected. This revealed the first evidence on the regulation of APT-2 activity in the cell. Similarly, the localization of APT-1 is also known to be regulated by dynamic palmitoylation, which allows its attachment to and detachment from membranes.[66]

Little is known about substrate specificity of APT-1/2. Only a few proteins have been identified that are selectively depalmitoylated by one of the APTs. These are zDHHC6[67], GAP-43[68] and Scrib[69] (by

APT-2) and BK channels[70] (by APT-1). To reveal more details about the substrate specificity of APT-1 and -2, Bogyo and coworkers used quenched fluorescent peptides in a positional scanning library, revealing that both APT-1 and APT-2 prefer Lys and Arg residues distal to the palmitoylation site of their substrate.[71] It still remains a mystery, however, what the differences in substrate selectivity are for these two enzymes. To help answer this question, an extensive toolkit has already been developed to study APT-1/2 and depalmitoylation in general (section 1.2.4.).

1.2.4. Molecular tools for the study of protein (de)palmitoylation

1.2.4.1. Detectable palmitic acid analogues
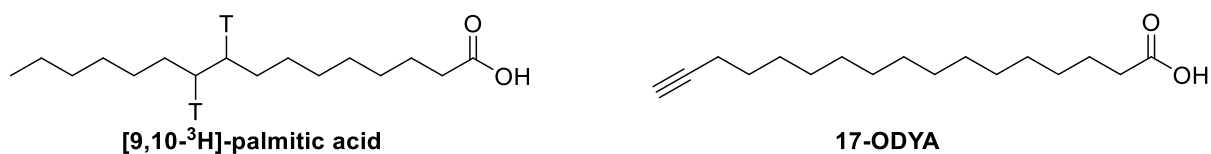
Figure 1.10. Structures of [9,10-^{3}H]-palmitic acid and 17-octadecynoic acid (17-ODYA): detectable palmitic acid probes that are used for metabolic labelling of *S*-palmitoylation

The first tool that was used for the metabolic labelling of palmitoylation sites was [9,10-^{3}H]-palmitic acid (Figure **1.10**). This tritiated palmitic acid analogue was already used as a research tool for fatty acid research before the observation of protein palmitoylation in 1979.[72,73] It is incorporated on Cys residues in proteins and is detected by immunoprecipitation of proteins followed by autoradiography. This method had some drawbacks however, such as long exposure times, low sensitivity and radioactive health hazards.[74] Despite these drawbacks, it remained the main tool for metabolic labelling of palmitoylation until the mid 2000's. To overcome the issues of [9,10-^{3}H]-palmitic acid, fatty acids with small, bio-orthogonal handles were developed. The currently most widely used one is 17-octadecynoic acid (17-ODYA) (Figure **1.10**).[75] 17-ODYA is incorporated on proteins as a palmitate mimic. It allows gel-based detection of palmitoylated proteins through CuAAC with azide-funcionalised dyes and can also be used for proteomics based identification of palmitoylated proteins after CuAAC with azide-functionalised biotin and affinity purification, which is a major advantage over the radioactive palmitate analogue. These proteomic studies have caused a major increase in the identification of proteins that undergo *S*-palmitoylation.[74]

Other proteomics-based methods for the identification of palmitoylated proteins are acyl-biotin exchange and acyl-resin assisted capture. In these methods, palmitic acid thioesters on Cys residues are replaced by biotin-containing, Cys-reactive scaffolds followed by affinity purification and proteomic work-up. Detailed information about these methods can be found in the review by Main et al.[43]

1.2.4.2. Substrates for acyl-protein thioesterases
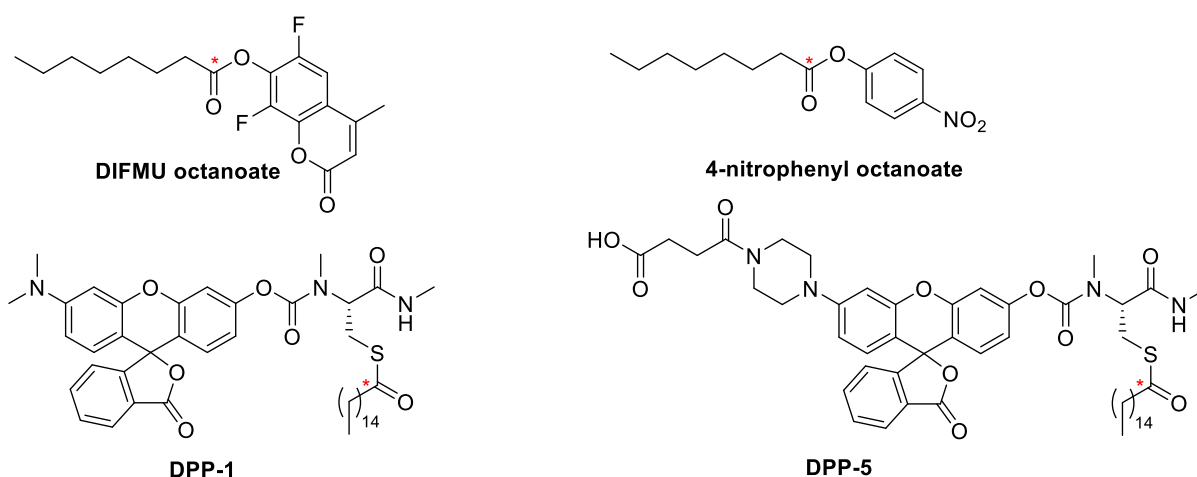
Figure 1.11. Substrates for acyl protein thioesterases. Cleaving sites are marked with a red asterisk.

Metabolic labels such as 17-ODYA cannot be used to measure activity of depalmitoylation inhibitors on purified enzymes. To this end, substrates such as DIFMU octanoate and 4-nitrophenyl octanoate (Figure **1.11**) can be used, which give respectively a fluorescent and chromogenic product upon cleavage of the ester by an APT.

When applied in live cells, 17-ODYA can be used to assess the global balance between protein *S*-palmitoylation and depalmitoylation, but not to assess the regulation of the different enzymatic players that influence the palmitoylation cycle.[42,76] To this end, turn-on probes were developed by the Dickinson group to monitor depalmitoylation activity. Two types have been developed. A first type are depalmitoylation probes (DPPs), such as DPP-5 (Figure **1.11**), which bear a modifiable rhodol-based parent fluorophore that becomes fluorescent upon reaction with a depalmitoylase (Figure **1.12**).[77] The signal produced by this probe is dependent on the cellular uptake of the probe however. To cancel out this factor, ratiomeric depalmitoylation probes (RDPs) were developed, such as RDP-1 (Figure **1.11**). This probe bears an aminocoumarin fluorophore that turns from green fluorescent to blue fluorescent upon reaction with a depalmitoylase (Figure **1.12**), allowing a more quantitative assessment of depalmitoylase activity.[78]
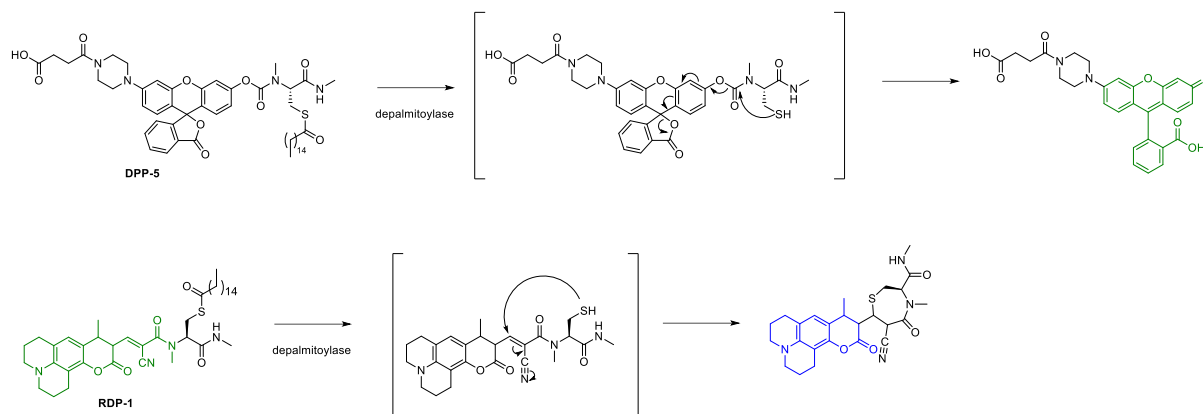
Figure 1.12. Mechanism of action of DPP-5 and RDP-1, probes that allow the measurement of depalmitoylase activity in live cells. After cleavage of the acyl thioester on the probe, an internal reaction creates or alters a fluorescent moiety on the probe.

1.2.4.3. APT-inhibitors

Inhibitors are useful tools to disturb the action of an enzyme in cells and study the resulting effect. Dekker et al. developed the β-lactone-based covalent inhibitors Palmostatin B (PalmB) and Palmostatin M (PalmM) as inhibitors for APT-1[79] (Figure **1.13**). These inhibitors turned out to target APT-2 as well. Although they are very potent APT-inhibitors (IC$_{50}$ PalmB < 5nM for both APTs), they also inhibit serine hydrolases ABHD6, ABHD16A, ABHD17A/B/C, PNPLA6 and FASN at concentrations needed for APT-inhibition.[30] Hexadecylfluorophosphonate (HDFP) (Figure **1.13**) is a general serine hydrolase reactive inhibitor, comparable to FP-Rhodamine (Figure **1.2**), which is commonly used in depalmitoylation studies. Similar to PalmB and PalmM, it also inhibits a wide array of serine hydrolases other than APT-1/2.[30,80] A more selective covalent probe for APT-1/2 is isocoumarin JCP174 (Figure **1.13**), of which the APT-1/2 activity was assessed by Child et al.[81] Similarly, triazole urea-based inhibitor ML211 (Figure **1.13**) also inhibits both APT-1 and APT-2. Such inhibitors are good starting points for the development of selective ABPs.

Selective inhibitors for APT-1 (ML348) and APT-2 (ML349) (Figure **1.13**), were discovered in a high throughput screening by Adibekian et al. These substituted piperazines are the first, and currently only, developed compounds that show good selectivity for one of the APT-isoforms. These compounds do not covalently inhibit the depalmitoylases however, which makes them unsuitable as ABPs.
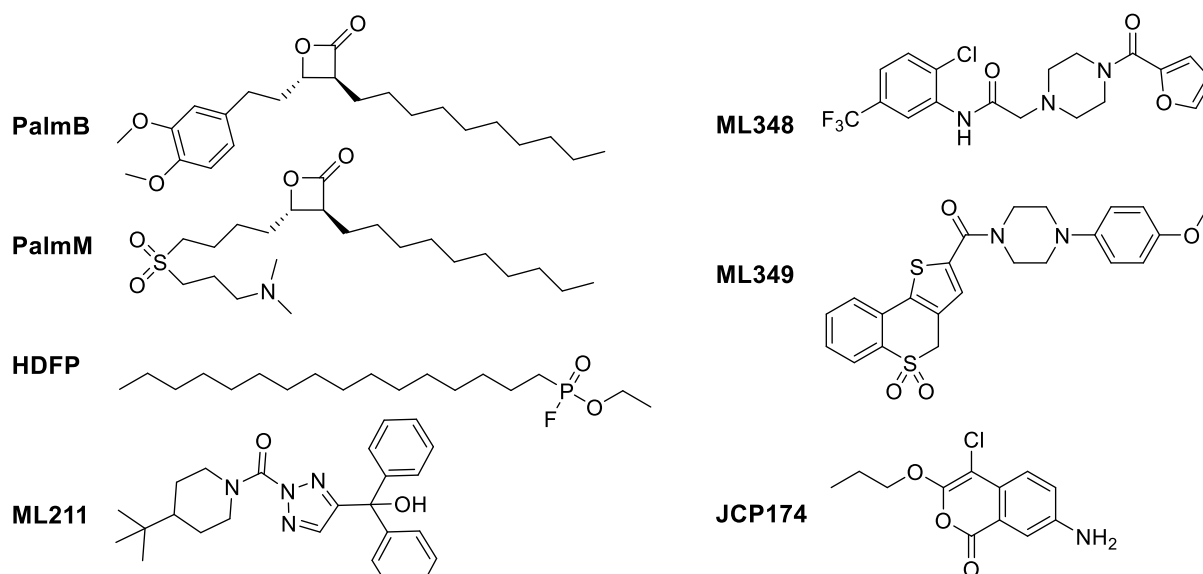
Figure 1.13. Structures of APT-inhibitors.

1.2.4.4. APT-reactive ABPs

So far, only dual-labelling activity-based probes have been discovered for APT-1/2. This includes JCP174-BT (Figure **14**), discovered by Garland et al. This is a BODIPY-TMR-tagged ABP derived from APT-1/2 inhibitor JCP174. Another dual-labeling probe is RV-152 (Figure **14**), discovered by Vanhoutte et al. and discussed more elaborately further on in this thesis. This probe is suitable for detection via CuAAC to its azide handle. ABPs that are selective for one APT-isoform would be indispensable tools for gaining insight in the differences in localization, activity and substrate specificity of APT-1 and APT-2, but are not yet discovered.
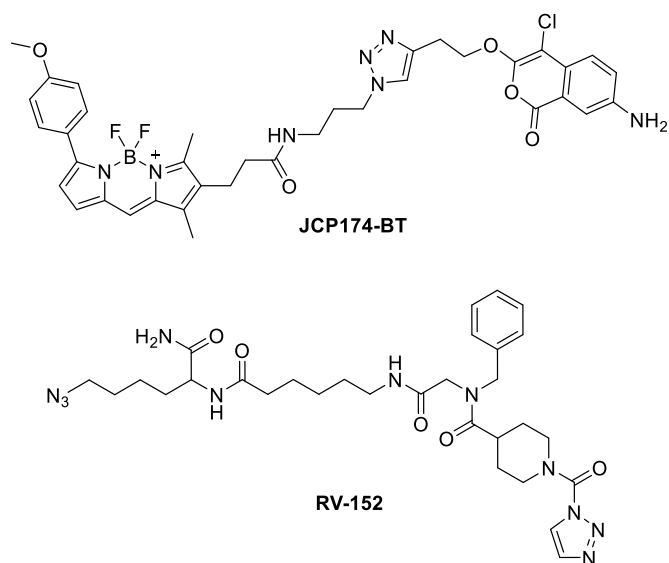
Figure 1.14. Structures of dual-labelling ABPs for APT-1/2.

1.3. SARS-CoV-2 main protease

The main protease of SARS-CoV-2 is a cysteine protease that is key in the proteolytic maturation of the non-structural proteins (nsps) translated by the RNA of the SARS-CoV-2 virus.[82–84] Preventing the cleavage of these nsps is a potential strategy for the treatment of Covid-19. I will give an introduction about cysteine proteases and the SARS-CoV-2 virus, after which I will further discuss the SARS-CoV-2 M[pro] and the probes and inhibitors developed against this target.

1.3.1. Cysteine proteases

Cysteine proteases are a group of enzymes, present in all forms of life, which cleave amide bonds using a nucleophilic Cys residue.[85] This Cys residue is part of a catalytic dyad or triad, the most common of which are Cys-His-Asn/Asp triads and Cys-His dyads.[36,86] Cysteine proteases are involved in a wide array of processes, including protein turnover, bone remodeling, antigen processing and presentation, and wound healing.[87] They are commonly expressed as inactive zymogens to prevent unwanted proteolytic activity and become active upon cleavage of their prodomain by either themselves or another protease.[36]

1.3.1.1. SARS-CoV-2

Coronaviruses are enveloped, positive-sense single stranded RNA viruses.[88,89] They are divided into four different genera: alpha-, beta-, gamma-, and deltacoronaviruses. Whereas gamma- and deltacoronaviruses mainly infect avian species, alpha- and betacoronaviruses also infect mammals.[90] Seven alpha- and betacoronaviruses are known to infect humans. Four of these make up 10-30% of common cold cases and generally do not cause severe symptoms in infected patients. Three betacoronaviruses however, can lead to life-threatening respiratory pathologies and have led to pandemics with a large human toll: the SARS virus in 2002, the MERS virus in 2011 and the SARS-CoV-2 virus since 2019.[89] The casualties claimed by SARS-CoV-2 have far surpassed those claimed by SARS and MERS, mainly due to the higher transmissibility of the virus.[91] The development of vaccines against the SARS-CoV-2 virus has caused a drop in infections and mortalities in vaccinated areas, but mutated strains of the virus are emerging against which the vaccines are less effective.[92] Potentially, new strains may emerge against which the vaccines can no longer effectively protect the human population. Therefore, there is a need for small-molecule therapeutics to treat SARS-CoV-2 infections that evade the immune response.

1.3.1.2. M^pro

A potential target for such therapeutics is the main protease (M^pro) of the SARS-CoV-2 virus.[82] M^pros of coronaviruses are cysteine proteases that are involved in most of the maturation cleavages of non-structural proteins (nsps) from the polyproteins expressed by the virus.[93] The SARS-CoV-2 M^pro is a homodimer that consists of two protomers, with a Cys-His catalytic dyad in its active site.[94,95] It is responsible for the proteolytic maturation of 12 of the 16 nsps from the two polyproteins expressed by the SARS-CoV-2 virus, pp1a and pp1ab (Figure **1.15A**). The nsps cleaved by M^pro include RNA-dependent RNA-polymerase nsp12 and NTPase/helicase nsp13, which are both essential for viral replication. Therefore, blocking the M^pro is an interesting strategy for development of an antiviral.
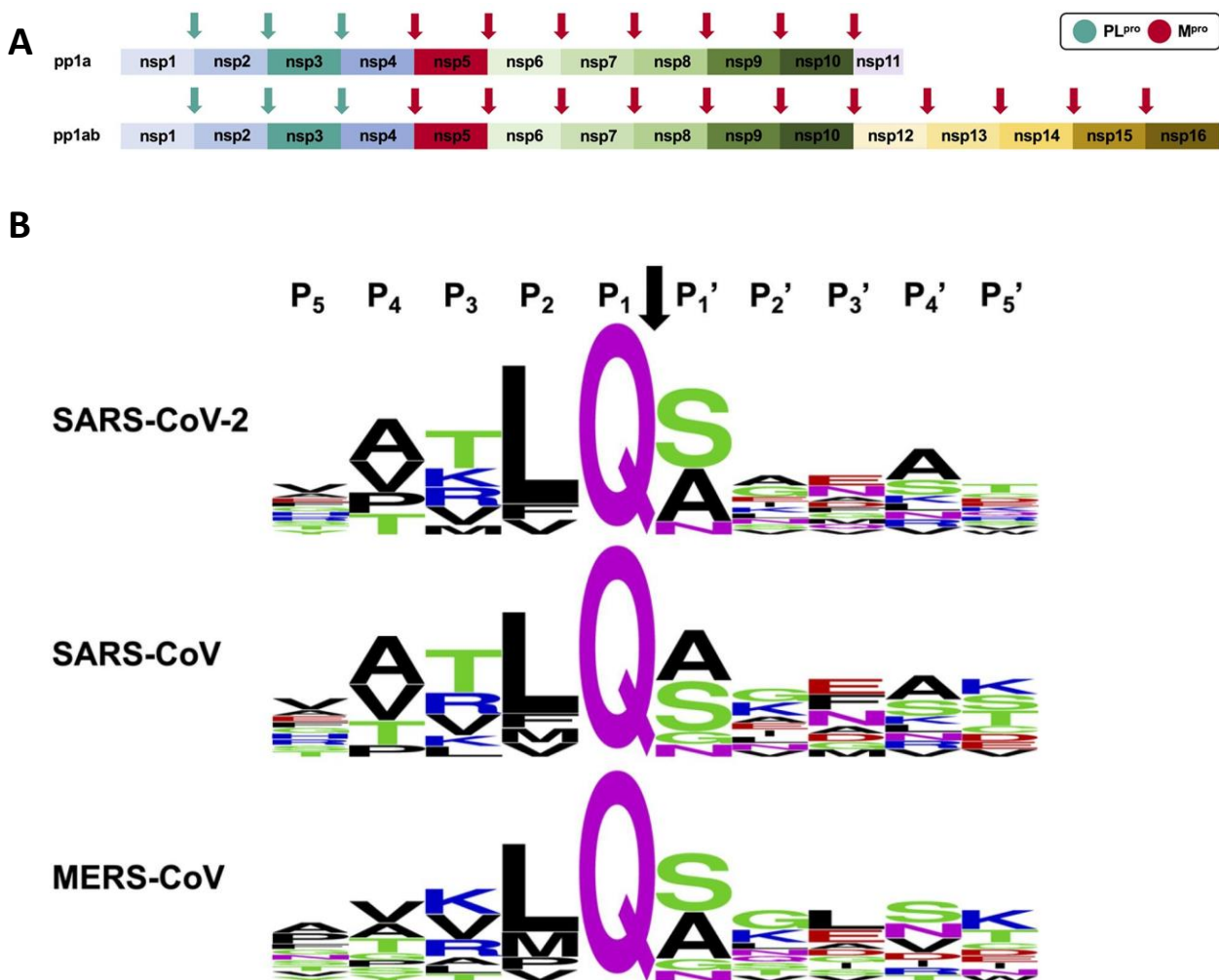
Figure 1.15. A. M^pro and PL^pro cleave the two polyproteins pp1a and pp1ab, expressed by the SARS-CoV-2 virus into its 16 non-structural proteins (nsp's). **B.** Substrate specificity of the SARS-CoV-2 M^pro compared to those of the SARS M^pro and MERS M^pro. Figure republished with permission from Ullrich et al.[82]

Analysis of the polyprotein cleavage sites of Sars-Cov-2 M^{pro} shows a result that is very alike to those of the SARS-CoV M^{pro} and MERS-CoV M^{pro} (Figure **1.15B**). They cleave only after P$_1$ Gln residues, tolerate hydrophobic residues in P$_2$ (mainly Leu) and prefer small residues such as Ser and Ala in P$_1$'.[96,97] No human enzymes are known to cleave after a P$_1$ Gln residue, which makes the development of peptidic inhibitors based on the substrate recognition sequence a potential strategy that could result in inhibitors with little off-targets.[82]

1.3.2. M^{pro} inhibitors and ABPs

The first inhibitors that were discovered against the SARS-CoV-2 M^{pro} were reported by the Hilgenfeld group in April 2020.[83] They found that 11r (Figure **1.16A**), a substrate-based inhibitor with a P$_1$ Gln residue masked in a γ-lactam and an α-ketoamide warhead was very effective in inhibiting the SARS-CoV-2 M^{pro} (IC$_{50}$ = 0.18 ± 0.02 µM). This compound was previously developed as a broad-spectrum inhibitor for coronavirus M^{pro}s and enterovirus 3C proteases. They synthesized structure 13a (Figure **1.16A**), analogous to 11r, which was slightly less active (IC$_{50}$ = 0.67 ± 0.18 µM), but had a better plasma stability and less plasma protein binding in mice than the original compound.

The Drag group used a positional scanning library of peptide-like structures with a P$_1$ glutamine and different natural and non-natural amino acids in the P$_2$-, P$_3$- and P$_4$-position to determine the preferred P$_2$-, P$_3$- and P$_4$-substrates are of the SARS-CoV-2 M^{pro}. [98] They found that the preferred residues were an L-Leucine in P$_2$, an L-tert-Leucine or D-Tyrosine in P$_3$ and L-aminobutyric acid in P$_4$-position. The same substrates were found to be optimal for SARS-CoV M^{pro}. Based on this information they created inhibitors (Ac-QS1-VS) as well as biotinylated ABPs and fluorescent ABPs (Bodipy-QS5-VS) bearing this substrate sequence and a vinyl sulfonamide warhead (Figure **1.16A**). This was the first study in which a probe (Bodipy-QS5-VS) was used to detect SARS-CoV-2 M^{pro} in samples of Covid-19 patients.

The groups of Gütschow and Müller created a library of azapeptide nitriles and halopyridinyl 1H-indolecarboxylates, of which compounds G8 (k$_{inact}$/K$_i$ = 37500 M^{-1}s^{-1},K$_i$ = 24.0 nM) and G17 (k$_{inact}$/K$_i$ = 29100 M^{-1}s^{-1},K$_i$ = 10.0 nM) were the most reactive against SARS-CoV-2 M^{pro}[99] (Figure **1.16A**). The azapeptide nitriles were also found to inhibit cathepsin L.

The Verhelst group created a library of clickable peptidic acyloxymethylketone (AOMK) ABPs that can be made on-resin.[23] Although a P$_1$ Gln residue was not very compatible with the warhead due to reversible cyclization between the two moieties, a P$_1$ dimethylated Gln in probe Hex-Tle-Leu-Gln(Me)$_2$-AOMK (k$_{obs}$/I = 47.1 ± 7.4 M^{-1}s^{-1}) (Figure **1.16A**) also gave very good reactivity with the SARS-CoV-2 M^{pro}.

Several drugs were found to act as SARS-CoV-2 M^{pro} inhibitors and can potentially be repurposed as Covid-19 therapeutics. Carmofur (Figure **1.16A**), a chemotherapeuticum that is mainly used as a treatment for colorectal cancers, was found to covalently bind the active site residue of M^{pro}. It is a potent inhibitor of M^{pro} in vitro (IC_{50} = 1.82 µM) and can inhibit viral replication in infected VeroE6 cells (EC_{50} = 24.3 µM).[84] Also Ebselen, a glutathione peroxidase mimic, shows good M^{pro} inhibition in vitro (IC_{50} = 0.67 ± 0.09 µM).[100] Remdesivir, an antiviral drug that is commonly used for treatment of Ebola and Marburg-infections, can also bind M^{pro} and prevents viral replication in VeroE6 cells (EC_{50} = 0.77 µM) (Figure **16A**).[101,102] The Lemieux group found that GC-373, an inhibitor of Feline Coronavirus main protease (FCoV M^{pro}) also potently inhibits SARS-CoV-2 M^{pro} (IC_{50} = 0.4 ± 0.05 µM). It's prodrug, GC376, which converts readily to GC373 (Figure **1.16B**), gave an even better result (IC_{50} = 0.19 ± 0.04 µM).[103]

A

11r

13a

Ac-QS1-VS

Bodipy-QS5-VS

G17

G8

Hex-Abu-Tle-Leu-Gln-AOMK

Carmofur

Ebselen

Remdesivir

B

GC376

NaHSO$_4$
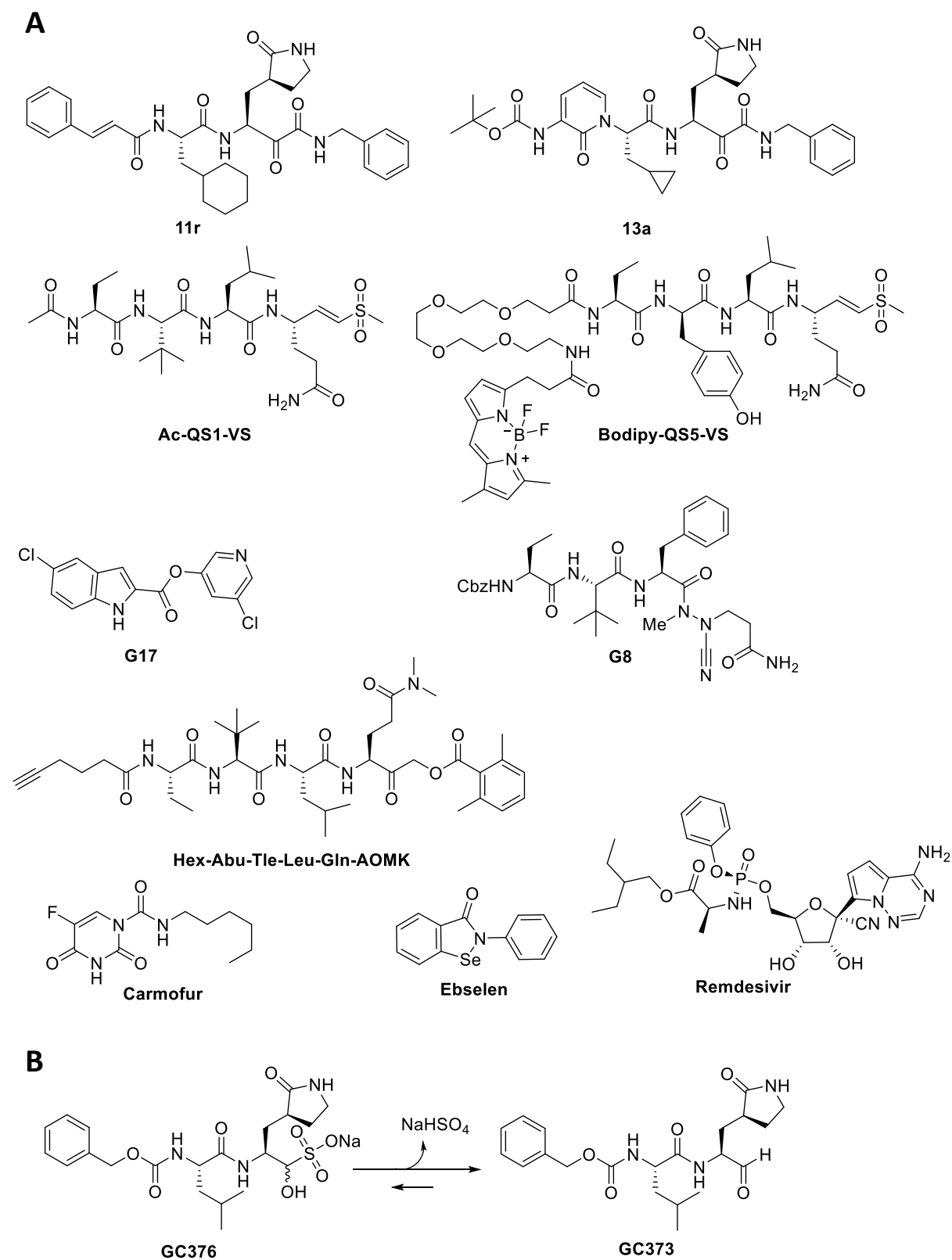
GC373

Figure 1.16. A. Structures of SARS-CoV-2 M^{pro} inhibitors and ABPs. **B.** Conversion of GC376, an M^{pro} inhibitor originally developed against FCoV M^{pro} to its active form GC373.

1.4. Polyamine transport system as a potential route for the internalization of probes

Probes are often hindered in reacting with their target because of poor cell-permeability. Especially for biotinylated probes, probes with high molecular masses and probes with charged functionalities this is a drawback when performing labeling experiments on live cells. To increase the cell-permeability of probes, several strategies have been applied already. I will first discuss these strategies and then go into further detail on an unexplored potential route for the internalization of probes: the polyamine transport system.

1.4.1. Methodologies for the internalization of probes

Already in the first papers about ABPP that were pubished, it was found probes were not always cell permeable. Bogyo et al. used a prodrug strategy of creating methyl esters from carboxylates to increase the cell permeability of a cathepsin B reactive ABP by masking its negative charge.[104]

Cell-penetrating peptides (CPP) have also been shown to be viable strategies for the internalization of ABPs. These peptides are short (typically <30 amino acids) cationic, amphipathic or hydrophobic peptides that permeate membranes through electrostatic and/or hydrophobic interactions with cell membranes.[105] Edgington et al. used this technology to enhance the cell permeability of a caspase-reactive ABP by attaching it to a cationic TAT peptide (RKKRRQRRR), for using it to monitor apoptosis.[106] In another study, Gui et al. attached a deubiquitylation probe to a TAT-peptide and to a cyclic polyarginine peptide (cR_{10}).[107] They found that the probe was better internalized when attached to the cR_{10} peptide.

Another method for increasing cell permeability of probes is by creating pores in the target cell. In 2014, Claessen et al. used Perfringolysin O, a pore-forming toxin, to increase the cell-permeability of a biotinylated deubiquitylation probe.[108] For the internalization of Ub-Dha, another deubiquitylation probe, Mulder et al. used electroporation to create a similar effect of creating pores in the cell membrane.[109] The latter is a more durable method, as the pores created by electroporation are small and transient and therefore have lower impact on the viability of the cells than those created by Perfringolysin O.

Biotinylated probes can also be taken up by cells via endocytosis by binding them to latex beads coated with streptavidin. This strategy was used by Lennon-Duménil et al. and Reich et al. to improve the uptake of DCG-04 in dendritic cells.[110,111]

1.4.2. Polyamine transport

A potential route for internalizing poor cell-permeable probes is by vectorising the probe to a polyamine for internalization through the polyamine transport system. In the below paragraph, I will explain the functions and metabolism of polyamines, after which I will go into further detail on polyamine transport.
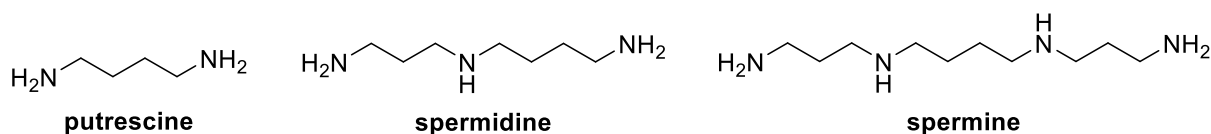
Figure 1.17. Structures of polyamines putrescine, spermidine and spermine

1.4.2.1. Structures and functions of polyamines

The most commonly occurring natural polyamines are putrescine, spermidine and spermine (Figure **1.17**). They are polycationic molecules at physiological pH. As a result, they interact with negatively charged molecules in the cell, such as DNA, RNA and negatively charged proteins. By binding to DNA and mRNA, polyamines stabilize these structures. The interaction between polyamines and DNA is essential in maintaining DNA structure and repairing DNA damage, as well as for transcription, histone acetylation and the formation of chromatin. Polyamine binding to mRNA is furthermore essential for translation; and interactions between proteins and polyamines are essential for proper functioning of several kinases and ion channels.[112]

Because of all their interactions with nuclear material, polyamines are indispensable for cell cycle progression and division. As a result, rapidly proliferating cells such as cancer cells have a high need for polyamines. Cells have two ways of maintaining their polyamine levels: via biosynthesis from ornithine within the cell, and via polyamine transport from outside of the cell (Figure **1.18**). Although mammalian polyamine biosynthesis and catabolism are two well described processes about which a lot of details are known, mammalian polyamine transport was a mystery at the beginning of my PhD research. The mechanism of polyamine uptake was unknown and no proteins had been discovered as being polyamine transporters. During my research project, the P5-type ATPases ATP13A2 and ATP13A3 were discovered as the first polyamine transporters.[113,114] For these studies, polyamine probes were used which are described in Chapter VI.[115]
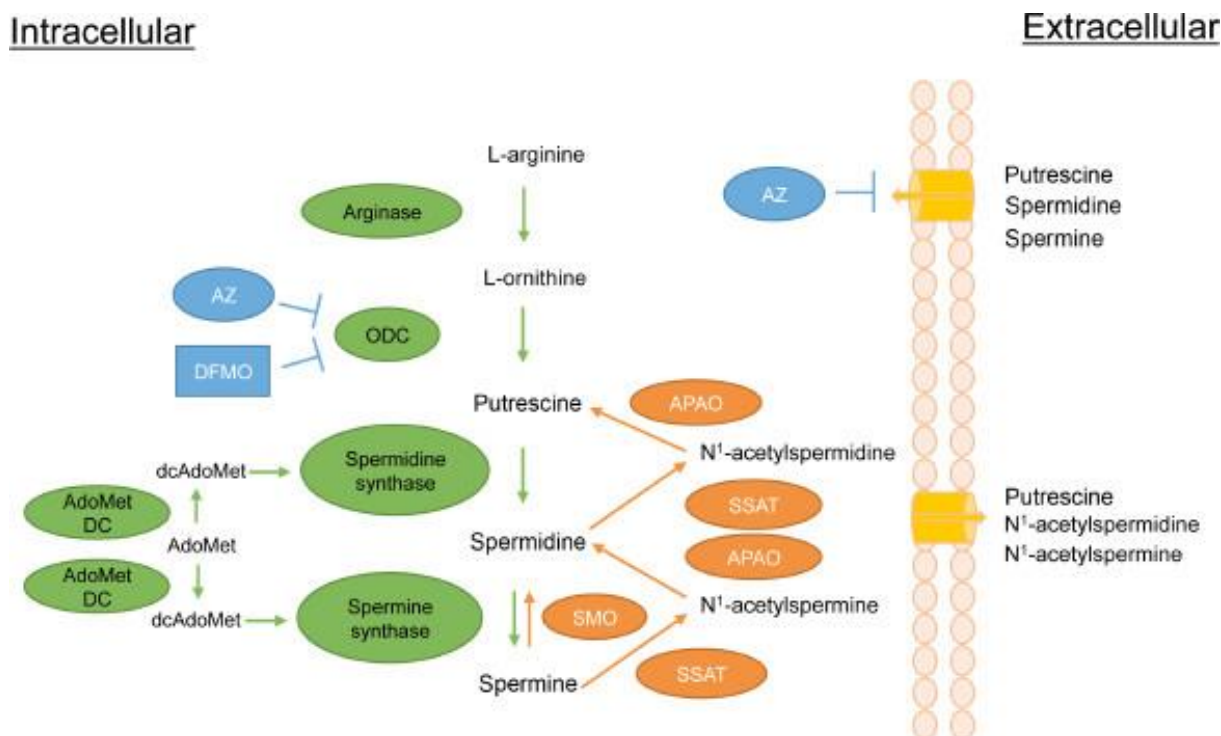
Figure 1.18. The polyamine pathway in mammalian cells. Metabolic enzymes are in green while enzymes of polyamine catabolism are in orange. Ornithine decarboxylase (ODC) inhibitors α-difluoromethylornithine (DFMO) and antizyme (AZ) are in blue. In addition to inhibiting ODC, AZ causes the ODC protein to be degraded and has the additional effect of inhibiting polyamine transport by an unknown mechanism. Other abbreviations are as follows: *S*-adenosylmethionine decarboxylase (AdoMetDC); *S*-adenosylmethionine (AdoMet); decarboxylated *S*-adenosylmethionine (dcAdoMet); Spermidine/spermine N^1-acetyltransferase (SSAT); N^1-acetylpolyamine oxidase (APAO); spermine oxidase (SMO). Figure and legenda republished with permission from Nowotarski et al.[116]

1.4.2.2. Polyamine transport system

The polyamine transport system shuttles naturally occurring polyamines spermine, spermidine and putrescine into the cell. The mechanism of this transport system is not proven yet. Theories suggest that polyamines are taken up through endocytosis and are then released into the cytosol by P-type ATPases, such as ATP13A2.[113,114] Cryo-EM studies on ATP13A2 suggest that after ADP-release and association to phosphatidylinositol-(3,5)-bisphosphate, ATP13A2 opens a long channel through which polyamines are imported.[117] This transport system is quite tolerant in its uptake, which is proven by the uptake of several fluorescent polyamines, such as spermidine-MANT and spermine-NBD (Figure **1.19**).[118,119] Whereas CPP are known to facilitate the uptake of large cargo's (see paragraph 1.4.1), it is unknown to which extent the channel of ATP13A2 allows the uptake of cargo attached to polyamines. A SAR study on where to attach fluorophores or other cargo on a polyamine to optimize its uptake was also not yet performed at the beginning of this thesis however. Such data would not only be useful for the rational design of polyamine probes, but could also give information on how to create other polyamine adducts for selective uptake through the polyamine transport system. The

latter can be used to create, for example, polyamine-chemotherapeuticum conjugates for the selective uptake of chemotherapeutics in cancer cells, as polyamine transport is significantly upregulated in cancer cells in comparison to non-cancer cells.[120]
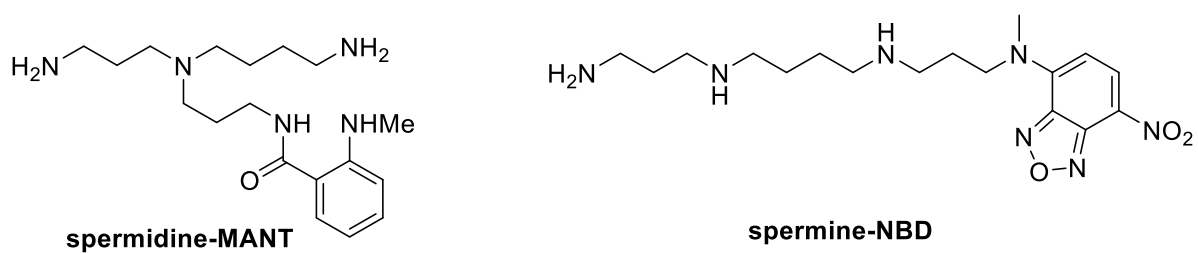
Figure 1.19. Structures of spermidine-MANT and spermine-NBD.

1.5. References

[1]   Y. Liu, M. P. Patricelli, B. F. Cravatt, *Proc. Natl. Acad. Sci. U. S. A.* **1999**, *96*, 14694–14699.

[2]   D. Greenbaum, K. F. M. Y, A. B. Y, M. Bogyo, *Chem. Biol.* **2000**, *7*, 569–581.

[3]   H. Ovaa, P. F. van Swieten, B. M. Kessler, M. A. Leeuwenburgh, E. Fiebiger, A. M. C. H. van den Nieuwendijk, P. J. Galardy, G. A. van der Marel, H. L. Ploegh, H. S. Overkleeft, *Angew. Chemie-International Ed.* **2003**, *42*, 3626–3629.

[4]   A. E. Speers, G. C. Adam, B. F. Cravatt, *J. Am. Chem. Soc.* **2003**, *125*, 4686–4687.

[5]   S. Chakrabarty, J. P. Kahler, M. A. T. van de Plassche, R. Vanhoutte, S. H. L. Verhelst, *Archivum Immunologiae et Therapiae Experimentalis*, **2019**, 253–281.

[6]   S. H. L. Verhelst, K. M. Bonger, L. I. Willems, *Molecules* **2020**, *25*.

[7]   D. A. Bachovchin, T. Ji, W. Li, G. M. Simon, J. L. Blankman, A. Adibekian, H. Hoover, S. Niessen, B. F. Cravatt, *Proc. Natl. Acad. Sci.* **2010**, *107*, 20941–20946.

[8]   Y. Yasuda, Z. Q. Li, D. Greenbaum, M. Bogyo, E. Weber, D. Bromme, *J. Biol. Chem.* **2004**, *279*, 36761–36770.

[9]   D. Greenbaum, A. Baruch, L. Hayrapetian, Z. Darula, A. Burlingame, K. F. Medzihradszky, M. Bogyo, *Mol. Cell. Proteomics* **2002**, *1*, 60–68.

[10]   L. E. Sanman, M. Bogyo, *Annu. Rev. Biochem.* **2014**, *83*, 249–273.

[11]   J. S. Martin, C. J. Mackenzie, D. Fletcher, I. H. Gilbert, *Bioorg. Med. Chem.* **2019**, *27*, 2066–2074.

[12]   M. A. Van Bochove, M. Swart, F. M. Bickelhaupt, *Chemphyschem* **2007**, 2452–2463.

[13]   U. R. Haedke, S. C. Frommel, F. Hansen, H. Hahne, B. Kuster, M. Bogyo, S. H. L. Verhelst, *ChemBioChem* **2014**, *15*, 1106–1110.

[14]   S. Serim, S. V Mayer, S. H. L. Verhelst, *Org Biomol Chem* **2013**, *11*, 5714–5721.

[15]   C. Wang, D. Abegg, B. G. Dwyer, A. Adibekian, *Chembiochem* **2019**, *20*, 2212–2216.

[16]   C. M. Brown, M. Ray, A. A. Eroy-Reveles, P. Egea, C. Tajon, C. S. Craik, *Chem. Biol.* **2011**, *18*, 48–57.

[17]   J. W. Chang, M. J. Niphakis, K. M. Lum, A. B. Cognetta, C. Wang, M. L. Matthews, S. Niessen, M. W. Buczynski, L. H. Parsons, B. F. Cravatt, *Chem. Biol.* **2012**, *19*, 579–588.

[18]   M. Hrast, A. Mitrovi, D. I. Roper, K. Horv, *Eur. J. Med. Chem.* **2018**, *160*, 94–107.

[19]   P. A. Jackson, J. C. Widen, D. A. Harki, K. M. Brummond, *J. Med. Chem.* **2017**, *60*, 839–885.

[20]   S. Klüter, J. R. Simard, H. B. Rode, C. Grütter, V. Pawar, H. C. A. Raaijmakers, T. A. Barf, M. Rabiller, W. A. L. Van Otterlo, D. Rauh, *Chembiochem* **2010**, *11*, 2557–2566.

[21]   A. J. Van Der Zouwen, M. D. Witte, *Front. Chem.* **2021**, *9*, 1–17.

[22]   R. B. Merrifield, *J. Am. Chem. Soc.* **1963**, *85*, 2149–2154.

[23]   M. A. T. Van De Plassche, M. Barniol-xicota, S. H. L. Verhelst, *ChemBioChem* **2020**, *21*, 3383–3388.

[24]   D. Kato, K. M. Boatright, A. B. Berger, T. Nazif, G. Blum, C. Ryan, K. A. H. Chehade, G. S. Salvesen, M. Bogyo, *Nat. Chem. Biol.* **2005**, *1*, 33–38.

[25]   J. Xu, X. Li, K. Ding, Z. Li, *Chem Asian J* **2020**, 34–41.

[26]   R. Serwa, E. W. Tate, *Chem. Biol.* **2011**, *18*, 407–409.

[27]   G. M. Simon, M. J. Niphakis, B. F. Cravatt, *Nat. Chem. Biol.* **2013**, *9*, 200–205.

[28]   E. Deu, M. Verdoes, M. Bogyo, *Nat. Struct. Mol. Biol.* **2013**, *19*, 9–16.

[29]   M. F. and M. Bogyo, *Curr. Pharm. Des.* **2007**, *13*, 253–261.

[30]   S. J. Won, M. Cheung See Kit, B. R. Martin, *Crit. Rev. Biochem. Mol. Biol.* **2018**, *53*, 83–98.

[31]   D. A. Bachovchin, B. F. Cravatt, *Nat Rev Drug Discov* **2012**, *11*, 52–68.

[32]   M. J. White, J. P. Savaryn, D. J. Bretl, H. He, R. M. Penoske, S. Scott, T. C. Zahrt, *PLoS One* **2011**, *6*, 18175.

[33]   H. S. and R. Hilgenfeld, *Curr. Top. Med. Chem.* **2010**, *10*, 323–345.

[34]   L. Hedstrom, *Chem. Rev.* **2002**, *102*, 4501–4524.

[35]   S. Patel, *Allergol. Immunopathol. (Madr).* **2017**, *45*, 579–591.

[36] A. R. Khan, M. N. James, *Protein Sci.* **1998**, *7*, 815–836.
[37] J. P. Kahler, R. Vanhoutte, S. H. L. Verhelst, *Arch. Immunol. Ther. Exp. (Warsz).* **2020**, *68*, 1–12.
[38] J. Z. Long, B. F. Cravatt, *Chem. Rev.* **2011**, *111*, 6022–6063.
[39] V. Chiurchi, L. Scipioni, B. Arosio, D. Mari, S. Oddi, *Biomolecules* **2021**, *11*.
[40] J. R. Piro, D. I. Benjamin, J. M. Duerr, Y. Pi, C. Gonzales, K. M. Wood, J. W. Schwartz, D. K. Nomura, T. A. Samad, *Cell Rep.* **2013**, *1*, 617–623.
[41] P.-K. Lo, Y. Yao, J. S. Lee, Y. Zhang, W. Huang, M. A. Kane, Q. Zhou, *Elife* **2018**, *7*, e31334.
[42] S. Azizi, R. S. Kathayat, B. C. Dickinson, *Acc. Chem. Res.* **2019**, *52*, 3029–3038.
[43] A. Main, W. Fuller, *FEBS J.* **2021**, 15781.
[44] L. H. Chamberlain, M. J. Shipston, *Physiol. Rev.* **2015**, *95*, 341–376.
[45] J. L. Daniotti, M. P. Pedro, J. Valdez Taubas, *Traffic* **2017**, *18*, 699–710.
[46] C. Kong, J. J. Lange, D. Samovski, X. Su, J. Liu, S. Sundaresan, P. D. Stahl, *Biochem. Biophys. Res. Commun.* **2013**, *434*, 388–393.
[47] A. Rossin, J. Durivault, T. Chakhtoura-Feghali, N. Lounnas, L. Gagnoux-Palacios, A. O. Hueber, *Cell Death Differ.* **2015**, *22*, 643–653.
[48] M. Joseph, R. Nagaraj, *J. Biol. Chem.* **1995**, *270*, 16749–16755.
[49] J. E. Smotrys, M. E. Linder, *Annu. Rev. Biochem.* **2004**, *73*, 559–587.
[50] M. E. Linder, R. J. Deschenes, *Nat. Rev. Mol. Cell Biol.* **2007**, *8*, 74–84.
[51] A. E. El-husseini, D. S. Bredt, *Nat. Rev. Neurosci.* **2002**, *3*, DOI 10.1038/nrn940.
[52] D. A. Mitchell, A. Vasudevan, M. E. Linder, R. J. Deschenes, *J. Lipid Res.* **2006**, *47*, 1118–1127.
[53] J. J. Chen, Y. Fan, D. Boehning, *Front. Mol. Biosci.* **2021**, *8*, 1–23.
[54] Y. Cao, T. Qiu, R. S. Kathayat, S. Azizi, A. K. Thorne, D. Ahn, Y. Fukata, M. Fukata, P. A. Rice, B. C. Dickinson, *Nat Chem Biol* **2020**, *15*, 1232–1240.
[55] L. A. Camp, S. L. Hofmann, *J. Biol. Chem.* **1993**, *268*, 22566–22574.
[56] L. A. Verkruyse, S. L. Hofmann, *J. Biol. Chem.* **1996**, *271*, 15831–15836.
[57] C. D. Gottlieb, S. Zhang, M. E. Linder, *J. Biol. Chem.* **2015**, *290*, 29259–29269.
[58] M. Fukata, Y. Fukata, H. Adesnik, R. A. Nicoll, D. S. Bredt, *Neuron* **2004**, *44*, 987–996.
[59] D. A. Mitchell, A. Vasudevan, M. E. Linder, R. J. Deschenes, *J. Lipid Res.* **2006**, *47*, 1118–1127.
[60] M. E. Zaballa, F. G. van der Goot, *Crit. Rev. Biochem. Mol. Biol.* **2018**, *53*, 420–451.
[61] J. A. Duncan, A. G. Gilman, *J. Biol. Chem.* **1998**, *273*, 15830–15837.
[62] T. Toyoda, H. Sugimoto, S. Yamashita, *Biochim. Biophys. Acta - Mol. Cell Biol. Lipids* **1999**, *1437*, 182–193.
[63] J. D. Manna, J. A. Wepy, K.-L. Hsu, J. W. Chang, B. F. Cravatt, L. J. Marnett, *J. Biol. Chem.* **2014**, *289*, 33741–33753.
[64] L. Abrami, M. Audagnotto, S. Ho, M. J. Marcaida, F. S. Mesquita, M. U. Anwar, P. A. Sandoz, G. Fonti, F. Pojer, M. Dal Peraro, et al., *Nat. Chem. Biol.* **2021**, *17*, 438–447.
[65] M. M. Gromiha, G. Pujadas, C. Magyar, S. Selvaraj, I. Simon, *Proteins Struct. Funct. Genet.* **2004**, *55*, 316–329.
[66] N. Vartak, B. Papke, H. E. Grecco, L. Rossmannek, H. Waldmann, C. Hedberg, P. I. H. Bastiaens, *Biophys. J.* **2014**, *106*, 93–105.
[67] L. Abrami, T. Dallavilla, P. A. Sandoz, M. Demir, B. Kunz, G. Savoglidis, V. Hatzimanikatis, F. G. van Der Goot, *Elife* **2017**, *6*, 1–24.
[68] V. M. Tomatis, A. Trenchi, G. A. Gomez, J. L. Daniotti, *PLoS One* **2010**, *5*, DOI 10.1371/journal.pone.0015045.
[69] J. L. Hernandez, D. Davda, M. Cheung See Kit, J. D. Majmudar, S. J. Won, M. Gang, S. C. Pasupuleti, A. I. Choi, C. M. Bartkowiak, B. R. Martin, *Cell Chem. Biol.* **2017**, *24*, 87–97.
[70] L. Tian, H. McClafferty, H. G. Knaus, P. Ruth, M. J. Shipston, *J. Biol. Chem.* **2012**, *287*, 14718–14725.
[71] N. Amara, I. T. Foe, O. Onguka, M. Garland, M. Bogyo, *Cell Chem. Biol.* **2019**, *26*, 35–47.e7.
[72] M. F. Schmidt, M. J. Schlesinger, *Cell* **1979**, *17*, 813–819.
[73] R. F. Glascock, V. A. Welch, *J. Dairy Sci.* **1974**, *57*, 1364–1370.
[74] X. Gao, R. N. Hannoush, *Cell Chem. Biol.* **2018**, *25*, 236–246.

[75]   R. N. Hannoush, N. Arenas-Ramirez, *ACS Chem. Biol.* **2009**, *4*, 581–587.

[76]   O. Rocks, M. Gerauer, N. Vartak, S. Koch, Z. P. Huang, M. Pechlivanis, J. Kuhlmann, L. Brunsveld, A. Chandra, B. Ellinger, et al., *Cell* **2010**, *141*, 458–471.

[77]   R. S. Kathayat, P. D. Elvira, B. C. Dickinson, *Nat. Chem. Biol.* **2017**, *13*, 150–152.

[78]   M. W. Beck, R. S. Kathayat, C. M. Cham, E. B. Chang, B. C. Dickinson, *Chem. Sci.* **2017**, *8*, 7588–7592.

[79]   F. J. Dekker, O. Rocks, N. Vartak, S. Menninger, C. Hedberg, R. Balamurugan, S. Wetzel, S. Renner, M. Gerauer, B. Schölermann, et al., *Nat. Chem. Biol.* **2010**, *6*, 449–456.

[80]   S. J. Won, B. R. Martin, *ACS Chem. Biol.* **2019**, *13*, 1560–1568.

[81]   M. A. Child1, C. I. Hall, J. R. Beck, L. O. Ofori, V. E. Albrow, M. Garland, P. W. Bowyer, P. J. Bradley, J. C. Powers, E. Boothroyd, John C. Weerapana, et al., *Nat. Chem. Biol.* **2013**, *9*, 651–656.

[82]   S. Ullrich, C. Nitsche, *Bioorganic Med. Chem. Lett.* **2020**, *30*, 127377.

[83]   L. Zhang, D. Lin, X. Sun, U. Curth, C. Drosten, L. Sauerhering, S. Becker, K. Rox, R. Hilgenfeld, *Science.* **2020**, *368*, 409–412.

[84]   Z. Jin, Y. Zhao, Y. Sun, B. Zhang, H. Wang, Y. Wu, Y. Zhu, C. Zhu, T. Hu, X. Du, et al., *Nat. Struct. Mol. Biol.* **2020**, *27*, 529–532.

[85]   S. Verma, R. Dixit, K. C. Pandey, *Front. Pharmacol.* **2016**, *7*, 107.

[86]   L. Sanchez-Pulido, C. P. Ponting, *Bioinformatics* **2016**, *32*, 1441–1445.

[87]   O. Vasiljeva, T. Reinheckel, C. Peters, D. Turk, V. Turk, B. Turk, *Curr. Pharm. Des.* **2007**, *13*, 387–403.

[88]   P. V'kovski, A. Kratzel, S. Steiner, H. Stalder, V. Thiel, *Nat. Rev. Microbiol.* **2021**, *19*, 155–170.

[89]   E. Hartenian, D. Nandakumar, A. Lari, M. Ly, J. M. Tucker, B. A. Glaunsinger, *J. Biol. Chem.* **2020**, *295*, 12910–12934.

[90]   V. M. Corman, D. Muth, D. Niemeyer, C. Drosten, *Adv. Virus Res.* **2018**, *100*, 163–188.

[91]   E. Petersen, M. Koopmans, U. Go, D. H. Hamer, N. Petrosillo, F. Castelli, M. Storgaard, S. Al Khalili, L. Simonsen, *Lancet Infect. Dis.* **2020**, *20*, e238–e244.

[92]   J. L. Bernal, N. Andrews, C. Gower, E. Gallagher, R. Simmons, S. Thelwall, J. Stowe, E. Tessier, N. Groves, G. Dabrera, et al., *N Engl J Med* **2021**, *385*, 585–594.

[93]   K. Anand, G. J. Palm, J. R. Mesters, S. G. Siddell, J. Ziebuhr, R. Hilgenfeld, *EMBO J.* **2002**, *21*, 3213–3224.

[94]   W. Dai, B. Zhang, X. M. Jiang, H. Su, J. Li, Y. Zhao, X. Xie, Z. Jin, J. Peng, F. Liu, et al., *Science* **2020**, *368*, 1331–1335.

[95]   Z. Jin, X. Du, Y. Xu, Y. Deng, M. Liu, Y. Zhao, *Nature* **2020**, *582*, 289-293.

[96]   R. Hilgenfeld, *FEBS J.* **2014**, *281*, 4085–4096.

[97]   L. Zhang, D. Lin, Y. Kusov, Y. Nian, Q. Ma, J. Wang, A. Von Brunn, P. Leyssen, K. Lanko, J. Neyts, et al., *J. Med. Chem.* **2020**, *63*, 4562–4578.

[98]   W. Rut, K. Groborz, L. Zhang, X. Sun, M. Zmudzinski, B. Pawlik, X. Wang, D. Jochmans, J. Neyts, W. Młynarski, et al., *Nat. Chem. Biol.* **2021**, *17*, 222–228.

[99]   J. Breidenbach, C. Lemke, T. Pillaiyar, L. Schäkel, G. Al Hamwi, M. Diett, R. Gedschold, N. Geiger, V. Lopez, S. Mirza, et al., *Angew. Chemie - Int. Ed.* **2021**, *60*, 10423–10429.

[100]   K. Amporndanai, X. Meng, W. Shang, Z. Jin, M. Rogers, Y. Zhao, Z. Rao, Z. J. Liu, H. Yang, L. Zhang, et al., *Nat. Commun.* **2021**, *12*, 1–7.

[101]   H. L. Nguyen, N. Q. Thai, D. T. Truong, M. S. Li, *J. Phys. Chem. B* **2020**, *124*, 11337–11348.

[102]   M. Wang, R. Cao, L. Zhang, X. Yang, J. Liu, M. Xu, Z. Shi, Z. Hu, W. Zhong, G. Xiao, *Cell Res.* **2020**, *30*, 269–271.

[103]   W. Vuong, M. B. Khan, C. Fischer, E. Arutyunova, T. Lamer, J. Shields, H. A. Saffran, R. T. McKay, M. J. van Belkum, M. A. Joyce, et al., *Nat. Commun.* **2020**, *11*, 1–8.

[104]   M. Bogyo, S. Verhelst, V. Bellingard-Dubouchaud, S. Toba, D. Greenbaum, *Chem. Biol.* **2000**, *7*, 27–38.

[105]   J. Xie, Y. Bi, H. Zhang, S. Dong, L. Teng, R. J. Lee, Z. Yang, *Front. Pharmacol.* **2020**, *11*, 1–23.

[106]   L. E. Edgington, A. B. Berger, G. Blum, V. E. Albrow, M. G. Paulick, N. Lineberry, M. Bogyo, *Nat.*

Med. **2009**, *15*, 967–974.

[107] W. Gui, C. A. Ott, K. Yang, J. S. Chung, S. Shen, Z. Zhuang, *J. Am. Chem. Soc.* **2018**, *140*, 12424–12433.

[108] J. H. Claessen, M. D. Witte, N. C. Yoder, A. Y. Zhu, E. Spooner, H. L. Ploegh, *Chembiochem* **2013**, *14*, 343–352.

[109] M. P. C. Mulder, K. Witting, I. Berlin, J. N. Pruneda, K. P. Wu, J. G. Chang, R. Merkx, J. Bialas, M. Groettrup, A. C. O. Vertegaal, et al., *Nat. Chem. Biol.* **2016**, *12*, 523–530.

[110] A. M. Lennon-Duménil, A. H. Bakker, R. Maehr, E. Fiebiger, H. S. Overkleeft, M. Rosemblatt, H. L. Ploegh, C. Lagaudrière-Gesbert, *J. Exp. Med.* **2002**, *196*, 529–539.

[111] M. Reich, P. F. van Swieten, V. Sommandas, M. Kraus, R. Fischer, E. Weber, H. Kalbacher, H. S. Overkleeft, C. Driessen, *J. Leukoc. Biol.* **2007**, *81*, 990–1001.

[112] A. E. Pegg, *J. Biol. Chem.* **2016**, *291*, 14904–14912.

[113] S. van Veen, S. Martin, C. Van den Haute, V. Benoy, J. Lyons, R. Vanhoutte, J. P. Kahler, J. P. Decuypere, G. Gelders, E. Lambie, et al., *Nature* **2020**, *578*, 419–424.

[114] N. N. Hamouda, C. van den Haute, R. Vanhoutte, R. Sannerud, M. Azfar, R. Mayer, Á. C. Calabuig, J. V. Swinnen, P. Agostinis, V. Baekelandt, et al., *J. Biol. Chem.* **2021**, *296*, 100182.

[115] R. Vanhoutte, J. P. Kahler, S. Martin, S. van Veen, S. H. L. Verhelst, *ChemBioChem* **2018**, *19*, 907–911.

[116] S. L. Nowotarski, D. J. Feith, L. M. Shantz, *Cancer Growth Metastasis* **2015**, *2015*, 17–27.

[117] J. Tillinghast, D. Bowser, K. Pak, K. Lee, *BioArchiv* **2021**.

[118] P. M. Cullis, R. E. Green, L. Merson-Davies, N. Travis, *Chem. Biol.* **1999**, *6*, 717–729.

[119] J. P. Annereau, V. Brel, C. Dumontet, Y. Guminski, T. Imbert, M. Broussas, S. Vispé, S. Bréand, N. Guilbaud, J. M. Barret, et al., *Leuk. Res.* **2010**, *34*, 1383–1389.

[120] A. A. Abdulhussein, H. M. Wallace, *Amino Acids* **2014**, *46*, 655–660.

Chapter II: Aims of the study

This thesis describes the development of activity-based probes (ABPs) for serine hydrolases and the SARS-CoV-2 main protease using solid-phase synthesis, and the development of fluorescent chemical probes for the polyamine transport system.

Aim 1: Fast development of serine hydrolase ABPs

Serine hydrolases are a very large family of enzymes that are involved in a wide variety of biochemical processes. The exact function of most of its ~200 members remains elusive however. Activity-based protein profiling (ABPP), which uses small molecule ABPs, can be used to elucidate the function of enzymes. The synthesis of selective ABPs for a single enzyme or group of closely related enzymes is a difficult and time-consuming process however, and as a result, few selective serine-reactive ABPs have been reported. Therefore, a first aim is **to develop solid-phase synthesis procedures that allow a fast, on-resin synthesis of serine-reactive ABPs.** This work is presented in Chapter III.

Aim 1b: Optimization of APT-1/2 reactive ABPs to more potent and selective APT-probes

During research on aim 1, ABPs were discovered that bind acyl protein thioesterases-1/2 (APT-1/2), two closely related protein depalmitoylases. No selective ABPs have been discovered yet for the individual APT-isoforms. Using the solid-phase synthesis procedures established in Chapter III, it was attempted to modulate the ABPs synthesized in this chapter to **obtain probes with higher reactivity towards APT-1/2 or high selectivity for one of the APT-isoforms.** This work is presented in Chapter IV.

Aim 2: Development of ABPs for the SARS-CoV-2 main protease (M^{pro})

The M^{pro} of the SARS-CoV-2 virus has gained a lot of attention as a potential drug target in the search for antiviral therapies to treat Covid-19, because it is the main actor in the proteolytic maturation of the non-structural proteins of the virus. A second aim of this thesis is **to synthesize ABPs for the SARS-CoV-2 M^{pro} using solid-phase synthesis**, which can be used as study tools for this protease. This work is presented in Chapter V.

Aim 3: Development of fluorescent polyamine probes

The mammalian polyamine transport system remains a mystery. To elucidate the mechanism and molecular players of the polyamine transport system, probes are needed that are taken up by it. A last aim is to **develop azide functionalized polyamine derivatives** with different characteristics, which can be converted into probes through CuAAC "click chemistry" and used to determine which characteristics are important for uptake through the polyamine transport system. Eventually, these polyamine derivatives may also be used as vectors to shuttle cargo molecules into the cell through the polyamine transport system. This work is presented in Chapter VI.

Chapter III: Rapid solid-phase construction of serine hydrolase probes results in selective activity-based probes for acyl protein thioesterases-1/2

Abstract

Serine hydrolases are a large, diverse family of enzymes that play various biomedically important roles. Their study has been substantially advanced by activity-based protein profiling, which makes use of covalent chemical probes for labeling of the active site and detection by various methodologies. However, highly selective probes for individual serine hydrolases are scarce, because probe synthesis usually takes place by time-consuming solution phase chemistry. We here report a general solid phase synthesis towards serine hydrolase chemical probes, which will speed up probe library synthesis. It involves construction of a recognition element ending in a secondary amine followed by capping with different electrophiles. We illustrate the power of this approach by the discovery of selective chemical probes for the depalmitoylating enzymes APT-1/2. Overall, this study provides new methodologies to synthesize serine hydrolase probes, while providing new reagents to study protein depalmitoylation.
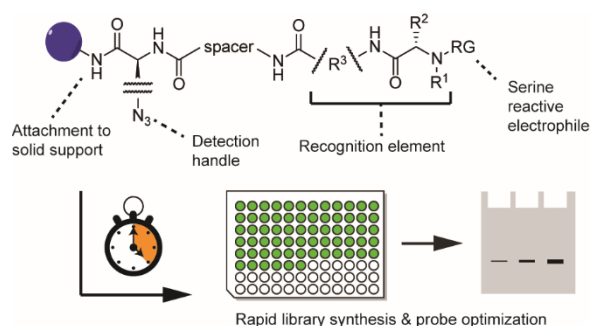
3.1. Introduction

Activity-based protein profiling (ABPP) emerged two decades ago to help discover the function of enzymes.[1] ABPP uses small molecules called activity-based probes (ABPs), which bind covalently to the active site of the enzymes of interest, allowing a multitude of read-out possibilities and application areas,[2] including profiling in different disease states, imaging, target identification as well as inhibitor screening by competitive ABPP (Figure **3.1A**). ABPs generally consist of three parts: a warhead, which binds covalently to a catalytic residue of the target enzyme, a recognition element, which influences the selectivity of a probe, and a reporter tag to visualize probe labeled proteins.

Fluorophosphonate (FP) probes (Figure **3.1B**) were developed as the first serine hydrolase reactive ABPs – either equipped with a biotin tag (FP-Biotin)[3] or a fluorophore (FP-rhodamine; FP-Rh).[4],[5] Serine hydrolases (SHs) are an enzyme superfamily comprising 1-2% of the human genome. Amongst them are several pharmaceutically interesting proteins,[6] such as monoacyl glycerol lipase (MAGL) and α,β-hydrolase domain containing protein 6 (ABDH6), which play a role in the generation of endocannabinoids in the nervous system,[7] acyl protein thioesterases-1/2 (APT-1/2; previously known as lysophospholipases-1/2; LYPLA-1/2), which are involved in depalmitoylation of Ras GTPase,[8] and protein phosphatase methyl esterase 1, which plays a role in neuroblastoma.[9] For most SH members, however, the exact function remains elusive. Conveniently, FP-Rh reacts with more than 80% of all metabolic SHs in mice.[10] Hence, FP-Rh has not only been useful for the study of well known SHs, but also for uncharacterized ones. However, there are also some limitations of this reagent: (1) The synthesis is not trivial and takes considerable effort. (2) It may not react with all SHs. (3) Because of its general nature, it is problematic to implement this probe in studies for visualization of a single SH of interest. Therefore, serine-reactive ABPs with other warheads and recognition elements have been developed over the past two decades. These have the potential to be used for in vivo imaging studies, as recently illustrated for MAGL.[11], [12] Nevertheless, it is extremely challenging and time-consuming to obtain highly selective ABPs, because the synthesis and optimization of these ABPs usually takes place by solution phase chemistry. Hence, selective SH ABPs have only been reported for a few SHs, including neutral cholesterol ester hydrolase 1 (KIAA1363),[13] diacylglycerol lipase (DAGL),[14], [15] and MAGL,[16] although probes for the last two showed some crossreactivity towards ABDH6. In order to produce and optimize ABPs in a fast and efficient manner, we set out to speed up the process of SH probe development by applying solid phase synthesis. Here, we present a mix-and-match strategy of recognition elements and serine reactive warheads for the design and full on-resin synthesis of a SH ABP library. Triazole urea probes in this library were potent and selective against APT-1/2, and represent new tools for the study of protein depalmitoylation.
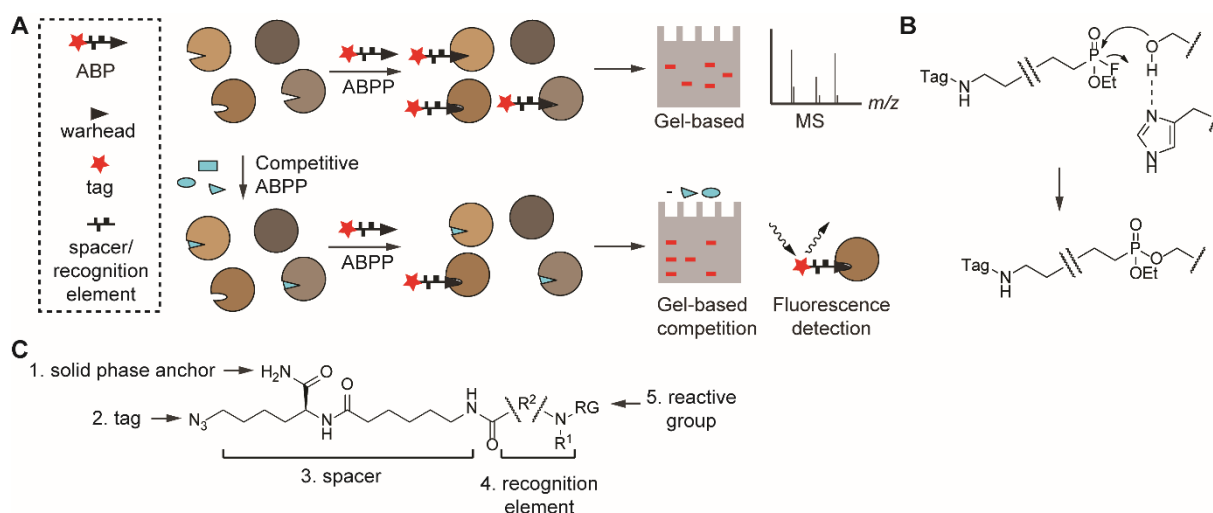
Figure 3.1. ABPP and ABPs. **A.** Left (boxed): ABPs generally consist of three elements: a reactive electrophile as warhead that engages in a mechanism-based reaction with the active site nucleophiles of the target, a tag that allows detection and a spacer and/or recognition element to prevent a steric clash of the tag in the active site and to influence the selectivity of the probe. Right: ABPP allows the tagging of active enzyme targets in a complex proteome, such as a cell lysate, whole cell or in vivo setting, followed by various types of read-out. Inhibitor evaluation in complex proteomes may be done by 'competitive ABPP', in which the proteome is first treated with a potential inhibitor before incubation with the ABP. Disappearance of gel bands in SDS-PAGE will then reveal inhibitor selectivity. **B.** Structure of fluorophosphonate-based probes and the mechanism of reaction with serine hydrolases: the active site serine side chain, activated by hydrogen bonding to a histidine residue, engages in a mechanism-based reaction and results in a stable, covalent phosphonate ester probe-protein complex. **C.** A modular design of SH ABPs for construction on solid support.

3.2. Results and discussion

Design & synthesis of probes. We aimed at making ABPs for SHs in a time-efficient manner by a full on resin synthesis. Therefore, our probes comprised the following modular design (Figure **3.1C**): (1) a C-terminal amide which forms the anchor to the common Rink amide resin, (2) an azide tag amenable to click chemistry-mediated detection of probe targets and incorporated in (3) an azidolysine-aminohexanoic acid spacer that connects to (4) a recognition element consisting of a natural amino acid, an unnatural amino acid or a peptoid (or a combination thereof), and (5) a serine reactive electrophile. In this design, the reactive group is introduced on resin as an N-terminal cap in the very last step prior to resin cleavage. As warheads, we selected five types of reactive electrophiles (Scheme **3.1A**) which have previously been shown to react with serine hydrolases and that can potentially be installed at an amine in a last step on solid support: a diphenylphosphoramidate,[17] an N-hydroxysuccinimidylcarbamate (NHS carbamate),[16] a (nitro-)phenylcarbamate, a 2-aminopyridineurea[18] and a 1,2,3-triazoleurea.[19] The introduction at this point of the synthesis would minimize the incompatibilty with any used reagents and conditions except for the coupling conditions

35

of the reactive group and the cleavage conditions from the resin. Whereas diphenylphosphoramidates have already been synthesized on resin,[17] this possibility has not yet been explored for the other reactive electrophiles. In a pilot experiment (Scheme **3.1A**), we explored coupling these reactive groups to recognition elements ending in a primary amine (a phenyl alanine), a secondary amine (a phenylalanine peptoid) or a secondary amine in a six-membered ring (an isonipecotic acid). We found that primary amines capped as hydroxysuccinimidylcarbamates converted into hydantoins (Figure **S3.1**) and could therefore not be formed, we could neither form triazole ureas onto primary or non-cyclic secondary amines. However, all reactive groups could be placed onto the piperidine ring of isonipecotic acid as detected by LC-MS of crude compound mixtures after resin cleavage (Figure **S3.2**). This inspired us to make a series of recognition elements, consisting of a piperidine or piperazine-moiety connected to an additional aromatic group, a combination which has previously shown to have affinity for various serine hydrolases.[19] [20] [21] [22]
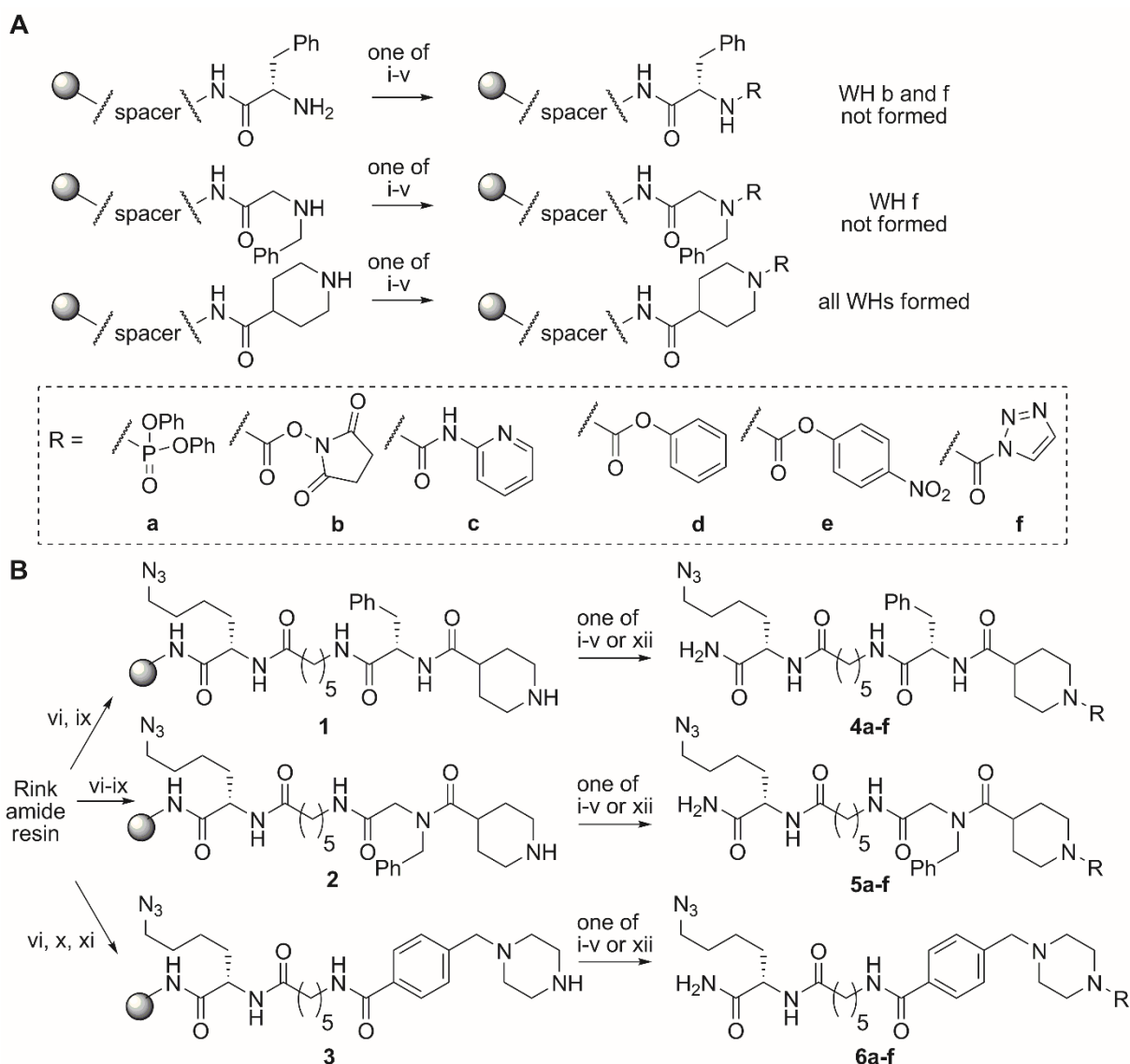
Scheme 3.1. Synthesis of mix-and-match SH ABP libraries. **A.** On resin coupling of warheads to different types of amines. *Reagents and conditions*: (i) Diphenylphosphoryl chloride, DIEA, DCM. (ii) Disuccinimidylcarbonate, DIEA, DCM. (iii) 2-aminopyridinyl phenyl carbamate, DIEA, DCM. (iv) phenyl chloroformate, DIEA, DCM. (v) 1. Triphosgene, DIEA, DCM, 30 minutes; 2. 1*H*-1,2,3-triazole, DIEA, DCM. **B.** Library synthesis towards compounds **4a-6f**. (vi) SPPS elongation by 1. DMF/piperidine 4/1, 15 min; 2. Fmoc-aa-OH, HBTU, DIEA, DMF. (vii) 1. DMF/piperidine 4/1, 5 min; 2. Bromoacetic acid, DIC, HOBt, DMF. (viii) Benzylamine, DIEA, DMF. (ix) Fmoc-Inp-OH, DIC, HOBt, DMF. (x) p-Bromomethylbenzoic acid, PyBrOP, DIEA, DMF. (xi) Piperazine, DMF. (xii) 4-nitrophenyl chloroformate, DIEA, DCM.

Library synthesis. The three recognition elements in the probe library (Scheme **3.1B**) comprised of isonipecotic acid coupled to phenylalanine (**1**), isonipecotic acid coupled to a phenylalanine peptoid (**2**), or *para*-piperazinylmethyl benzoic acid (**3**). These recognition elements were synthesized by modified SPPS and installed onto a Lys(N$_3$)-Ahx click-tag/linker moiety. Specifically, elongation with Phe took place under standard conditions, whereas the peptoid Phe was synthesized by coupling a bromoacetic acid followed by on resin nucleophilic substitution of the bromide by benzylamine. These

two recognition elements were completed by coupling of isonipecotic acid (Inp) under influence of DIC/HOBt. The third recognition element was formed by installation of a 4-bromomethylbenzoyl substituent followed by S_N2 substitution with piperazine. All three recognition elements were then capped with six warheads. Gratifyingly, these compounds were all compatible with Rink amide resin cleavage conditions, giving a 3x6 library of ABPs **4a-6f**.

Activity against SHs in competitive ABPP. Next, we set out to test whether these compounds display reactivity against SHs. Mouse brain lysate was chosen as a suitable proteome for screening, because it contains a wide variety of pharmacologically interesting SHs. Previous studies have identified between approximately 25 and 40 different SHs in this lysate and conveniently, the retention of several of these on SDS-PAGE is known.[23] [24] [25] Hence, the cytosolic and membrane fractions of mouse brain lysates were pretreated with compounds **4a-6f** and residually active SHs were labeled with FP-Rh (Figure **3.2A**). Interestingly, this competitive ABPP experiment revealed that five library members (the three triazole ureas **4f**, **5f** and **6f**, and two NHS-carbamates **5b** and **6b**) showed selective inhibition of two close-running gel bands that have previously been identified as APT-1/2 (Figure **3.2A**).[26] A titration of these compounds showed that the potency of the NHS carbamates **5b** and **6b** for these targets was moderate (see Figure **S3.3**), whereas the triazole ureas were much more potent (low to mid nanomolar range) (Figure **3.2B**, see also Figure **S3.4** for representative gels).

Probe **4f**, with a Phe-Inp recognition element had an apparent IC_{50} of 460 ± 50 nM for APT-1/2. For the other targets of FP-rhodamine, this probe had apparent IC_{50} values above 30 μM (Figure **S3.4**), resulting in a larger than 65 fold selectivity. Remarkably, the potency for APT-1/2 increased 37 fold by replacing the Phe in the recognition element by its peptoid analog in **5f** (IC_{50}^{App}= 11.8 ± 1.8 nM) (Figure **3.2B**), while having an excellent selectivity (over 2500 fold, as measured by apparent IC_{50} values against the other FP-Rh targets, which were above 30 μM, see Figure S4). Probe **6f**, with a linear benzyl-piperazinyl recognition element also showed high activity against APT-1/2 (IC_{50}^{App} = 27.9 ± 2.8 nM), although at micromolar concentrations this probe also inhibited ABHD6 (Figure S4) with an apparent IC_{50} of 7.4 ± 1.7 μM (approximately 250 fold selectivity).

We next compared probe **5f** with the chloro-isocoumarin-based probe JCP-174-alk[27] and the isoform selective APT-1 and APT-2 inhibitors ML-348 and ML349.[26] To this end, competitive ABPP was performed in the soluble fraction of mouse brain lysate. We found that the gel bands that are competed with probe **5f** also disappear upon treatment with JCP-174-alk (Figure **3.2C**, left panel). Moreover, inhibitors ML-348 and ML-349 only compete one of the two close-running gel bands inhibited by probe **5f**. Overall, this reveals that **5f** has similar inhibitory capacity and confirms APT-1/2 as target. We assessed the cell permeability of probes **5f** and **6f** using the human squamous carcinoma

cell line A431. In a competitive ABPP assay with FP-rhodamine both **5f** and **6f** fully inhibited all active APT-1/2 at 1 μM concentration (Figure **3.2D**), confirming their target engagement in live cells.
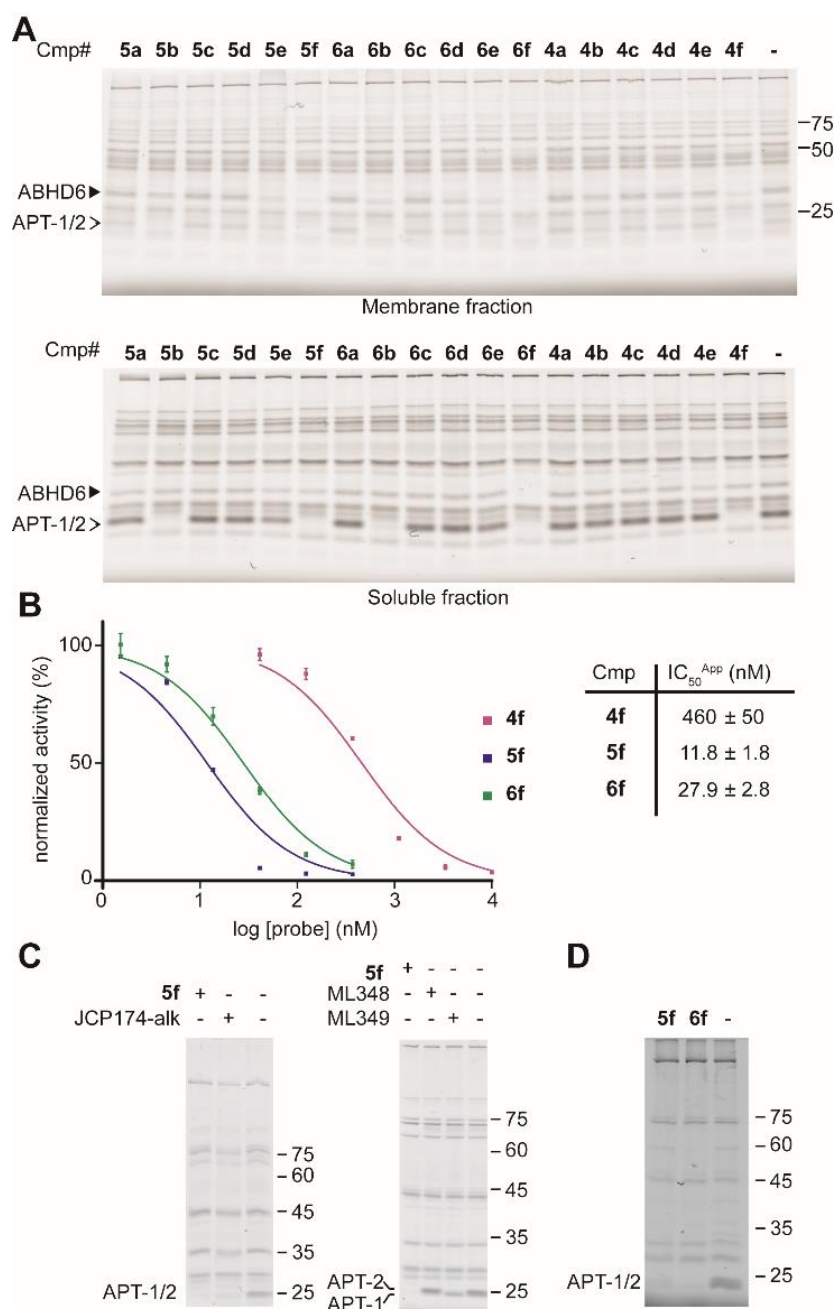
Figure 3.2. Screening of SH ABP library for inhibition by competitive ABPP. **A.** Fluorescent gels of competitive ABPP in the membrane fraction (upper) or soluble fraction (lower) of mouse brain lysates. Pretreatment of lysate with the indicated probe was followed by measurement of residual SH activity with FP-Rh. **B.** Apparent IC$_{50}$ curves were determined by competitive ABPP of serial dilutions, followed by quantification using gel band densitometry. **C.** Competitive ABPP in mouse brain lysate (soluble fraction) with known APT1/2 inhibitor JCP-174-alk (left panel) or APT1-selective inhibitor ML348 and APT2-selective inhibitor ML349 (right panel) in comparison with compound **5f**. Residual SH activity in treated tissue lysates was measured by incubation with FP-Rh. **D.** Inhibition of APT1/2 by compounds **5f** and **6f** in live A431 cells. After treatment, compounds were washed out, and residual SH activity in cell lysates was detected with FP-Rh.

Direct profiling of probe targets. To show the utility of the synthesized molecules as novel, highly selective ABPs against SHs, probes were applied in a labeling experiment using copper-catalyzed azide alkyne cycloaddition (CuAAC) with an alkyne-functionalized fluorophore. At 1 µM concentration, all three probes showed strong labeling of the APT-1/2 band, and this labeling was even retained at 100 nM concentration for probes **5f** and **6f** (Figure **3.3A-B**). Interestingly, a few other targets besides the APT-1/2 gel bands were revealed in this direct labeling experiment (indicated with a red asterisk, Figure 3A-B), which were not detected in the competitive ABPP experiment that made use of FP-Rh. This illustrates that not all probe targets overlap with general SH probe FP-rhodamine. Specifically, probe **6f** showed strong labeling of a soluble protein at 30 kDa (Figure **3.3A**) and membrane proteins at 35 and 55 kDa (Figure **3.3B**). Probes **4f** and **5f** both showed reactivity towards a different membrane protein at 33 kDa at 1 µM. However SDS-PAGE analysis of **5f** at 100 nM concentration did not show any other labeling than APT-1/2 (Figure **3.3B**, right panel).

Previously reported proteomics based assessments of the targets of FP-rhodamine in brain lysates show that it labels APT-1/2 as targets at 25 kD.[24] Given our competitive based ABPP results with FP-rhodamine, we suspected these as being the targets of our NHS-carbamate and triazole ureaprobes. To confirm that these close-running gel bands correspond to APT-1/2, we incubated mouse brain lysates with **5f** or **6f**, followed by click labelling of the probe-enzyme complexes with a trifunctional TAMRA-biotin-alkyne detection tag. This tag allowed affinity-based enrichment of the probe hits on streptavidin-coated beads, followed by both fluorescent visualization (Figure **3.3C**, upper panels, full gels in Figure **S3.5**) as well as Western blot analysis (Figure **3.3C**; lower panels). The detected bands with anti-APT-1 and anti-APT-2 antibodies in the samples treated with probe, but not in DMSO controls unequivocally reveal the identity of the probe target.

Model of probe binding. To gain insight into the binding mode of the two most active compounds **5f** and **6f** towards their targets, we performed covalent docking using the flexible sidechain methods of Autodock 4.2.[28] [29] In a crystal structure of APT-1 with a bound palmitate molecule (PDB code: 6QGS), both probes overlay well with this substrate (Figure **3.3D-E**) and occupy a long, hydrophobic channel, which is also the binding site of the recently reported, reversible APT-1 inhibitor ML348 (Figure **S3.6**).[30] The Inp residue of the most potent probe **5f** seems locked between hydrophobic residues F73, I75, W145 and L176, whereas its peptoid Phe moiety binds into a pocket created by the residues F73, I75, I76 and the alkyl chain of E84 (Figure **3.3D**). Although the slightly less active probe **6f** does not have the peptoid Phe, it may compensate for this by a stacking interaction of the benzoyl group in its backbone with W145, whereas its piperidine ring has similar hydrophobic interactions as the Inp in probe **5f** with L30, I75, W145 and L176 (Figure **3.3E**).
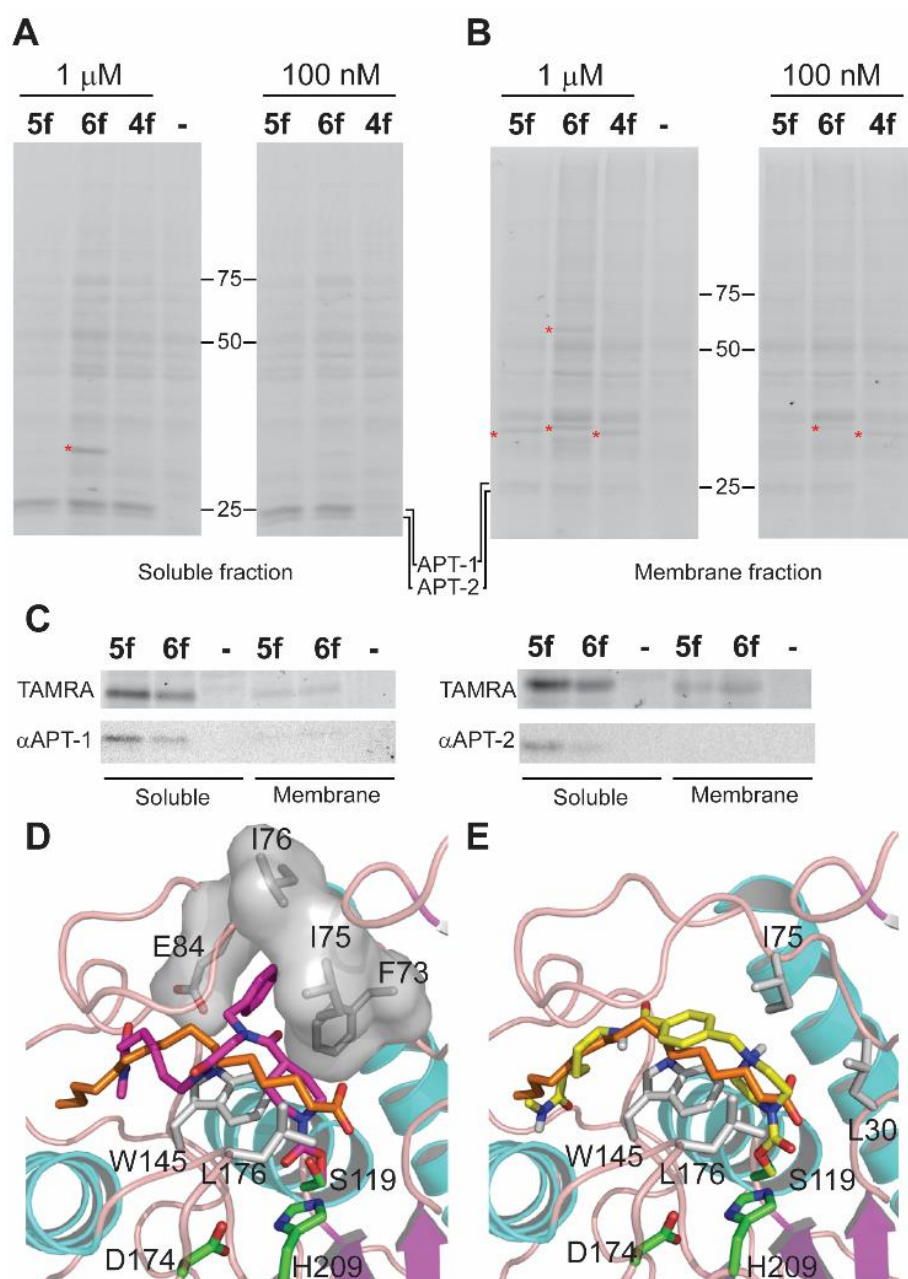
Figure 3.3. Covalent interaction with APT-1/2. **A.** Labeling of a soluble fraction of mouse brain lysate with probes **4f-6f**, followed by click chemistry with a TAMRA-alkyne derivative shows selective detection of the ATP-1/2 gel bands. DMSO control (-) shows click background. Other protein targets than APT-1/2 are indicated by a *. **B.** Same as A. but in the membrane fraction of mouse brain lysate. **C.** After click chemistry with a trifunctional biotin-TAMRA-alkyne tag and enrichment on streptavidin beads, fluorescent detection (upper panels) confirms target engagement of the probes, while detection by anti-APT-1 or anti-APT-2 antibodies (lower panels) confirms target identity. Note that the targets in the membrane fraction were very low abundant and led to very weak bands. Full fluorescent gels in Figure S5. **D.** Covalent docking of **5f** in a crystal structure of APT-1 (PDB code: 6QGS). Protein in cartoon format with α-helices in cyan, β-sheets in magenta and random coil in pink. A co-crystallized palmitate is shown in orange sticks, whereas **5f** is shown in magenta. Active site residues are depicted in green, whereas interacting residues are shown in white. Picture rendered with PyMol.[31] **E.** Covalent docking of **6f** (in yellow) overlayed with co-crystallized palmitate (in orange) in a crystal structure of APT-1.

41

3.3. Conclusion

In conclusion, we report synthetic procedures for a full on-resin synthesis of SH chemical probes compatible with six different types of serine-reactive electrophiles. Using this procedure, we constructed a library of ABPs by combining the electrophiles with three different recognition elements consisting of an aromatic unit and a piperidine or piperazine moiety. Evaluation of these compounds in a serine-hydrolase rich mouse brain lysate revealed activity of five of these compounds against protein depalmitoylases APT-1 and APT-2, with triazole urea **5f** showing nanomolar potency and excellent selectivity. The structure-activity relationship from this work may provide new information on pharmacophores for the design of drug-like APT-1/2 inhibitors and the in silico docking presented here provides a plausible model of the binding mode of these compounds. Compared with other recently reported inhibitors and probes for APT1/2,[26] [27] the compounds presented here can be readily synthesized on solid support and allow for easy future optimization by medicinal chemistry studies.

We expect that the novel selective ABPs **5f** and **6f** resulting from this work will find application in the study of APT1/2-mediated protein depalmitoylation. Furthermore, the synthetic procedures reported in this work may be automated in future work and facilitate more rapid development of SH inhibitors and ABPs by library synthesis on solid support. Since many SHs are still poorly characterized, we expect that this will open the door to functional studies of these.

3.4. Experimental section

General materials and methods
All starting materials for chemical reactions were purchased from commercial suppliers and used without purification. All solvents were of synthesis grade or higher. Progress of solution phase reactions was monitored by TLC on pre-coated 0.20 mm thick ALUGRAM® TLC sheets (silicagel-60 with UV indicator) using UV light and/or staining with cerium ammonium molybdate or ninhydrin followed by heating. Nuclear magnetic resonance spectra were recorded on a Bruker Ultrashield™ 300 or 600 MHz NMR Spectrometer. Chemical shifts are reported in ppm relative to the residual solvent peak. LC-MS spectra were recorded on a Prominence Ultra-fast Liquid Chromatography system (Shimadzu) using a Waters X-bridge 2.1 mm C18 column with a gradient of 5%-80% acetonitrile in water (with 0.1% formic acid) over 22 min. HPLC purification was performed on a Prominence Ultra-fast Liquid Chromatography system (Shimadzu) using a Waters X-bridge 150 mm C18 prep column with a gradient of acetonitrile in water (with 0.1% trifluoroacetic acid) over 32 min. Purity >95% of all final compounds was assessed by integration of LC chromatograms.

Solid phase chemistry procedures
Fmoc protected Rink amide resin (1.35 g, 0.74 mmol/g) was treated with 20% piperidine in DMF for 5 min to swell the resin and deprotect the Fmoc group. Next, the resin was washed three times with DMF. All following Fmoc deprotections were performed according to this procedure.

Backbone synthesis

Method 1. Fmoc-L-Lys(N$_3$)-OH was coupled to 1 mmol of deprotected rink amide resin by adding amino acid (1.5 eq.), HBTU (1.5 eq.) and DIPEA (3 eq.) in 4 mL of DMF to the resin and incubating for 4 hours at room temperature. After this and each following coupling, the resin was washed three times with DMF and three times with DCM. After deprotection, Fmoc-6-aminohexanoic acid was coupled by adding amino acid (2 eq.), HBTU (2 eq.) and DIPEA (4 eq.) in 4 mL DMF to the resin and incubating overnight at room temperature.

Recognition element synthesis

After synthesis of the peptide backbone, the resin was divided into portions of 100 µmol on which the different recognition elements were formed. Peptide bonds in recognition elements were formed with the corresponding (amino)acid (3 eq.), DIC (3 eq.) and HOBt (3 eq.) in 1.5 mL DMF overnight at room temperature unless stated otherwise.

Method 2.1. Phe-peptoid was formed by coupling Br-acetic acid to the peptide backbone under standard SPPS conditions and subsequent substitution with benzylamine (20 eq.) and DIPEA (10 eq.) in 1.5 mL DMF per 100 µmol overnight at room temperature. Next, Fmoc-Isonipecotic acid was coupled using standard SPPS conditions.

Method 2.2. 4-Bromomethyl phenylacetic acid (3 eq.) was coupled to the peptide backbone with PyBrOP (3 eq.) and DIPEA (6 eq.) in 1.5 mL DMF per 100 µmol overnight at room temperature. Subsequently, the bromide was substituted for piperazine (20 eq.) using DIPEA (10 eq.) in 1.5 mL DMF overnight at room temperature.

Method 2.3. Fmoc-L-Phe-OH was coupled to the peptide backbone using standard SPPS conditions, followed by coupling of Fmoc-Isonipecotic acid under standard SPPS conditions.

Warhead coupling

After synthesis of the recognition elements, the resins were divided into portions of 10 µmol for coupling of the warheads.

Method 3.1.: Synthesis of diphenyl phosphoramidates. Resin (1 eq.) was swollen in 0.5 mL DMF per 10 µmol of resin, to which DIEA (5 eq.) and Diphenylphosphoryl chloride (5 eq.) were added. Reactions were shaken overnight at room temperature and checked for completion using LC/MS. After completion, the resin was washed three times with DMF and twice with DCM. Probes were then cleaved from the resin by using a 95:2.5:2.5 mixture of TFA:TIS:water.

Method 3.2.: Synthesis of hydroxysuccinimidylcarbamates. Resin (1 eq.) was swollen in 0.5 mL DMF per 10 µmol of resin, to which DIEA (5 eq.) and Disuccinimidylcarbonate (3 eq.) were added. Reactions were shaken overnight at room temperature and checked for completion using LC/MS. After completion, the resin was washed three times with DMF and twice with DCM. Probes were then cleaved from the resin by using a 95:2.5:2.5 mixture of TFA:TIS:water.

Method 3.3.: Synthesis of aminopyridine ureas. Resin (1 eq.) was swollen in 0.5 mL DMF per 10 µmol of resin, to which were added DIPEA (5 eq.) and phenyl 2-pyridinylcarbamate (3 eq.; synthesized from 2-aminopyridine and phenyl chloroformate according to the method described by Swanson et al.[32] and isolated in 29% yield). Reactions were shaken overnight at room temperature and checked for completion using LC/MS. After completion, the resin was washed three times with DMF and twice with DCM. Probes were then cleaved from the resin by using a 95:2.5:2.5 mixture of TFA:TIS:water.

Method 3.4.: Synthesis of phenylcarbamates: Resin (1 eq.) was swollen in 0.5 mL DMF per 10 µmol of resin, to which DIEA (10 eq.) and Phenyl chloroformate (10 eq.) were added. Reactions were shaken overnight at room temperature and checked for completion using LC/MS. After completion, the resin was washed three times with DMF and twice with DCM. Probes were then cleaved from the resin by using a 95:2.5:2.5 mixture of TFA:TIS:water.

Method 3.5.: Synthesis of *p*-nitrophenylcarbamates: Resin (1 eq.) was swollen in 0.5 mL DMF per 10 µmol of resin, to which DIEA (10 eq.) and *p*-nitrophenyl chloroformate (10 eq.) were added. Reactions were shaken overnight at room temperature and checked for completion using LC/MS. After completion, the resin was washed three times with DMF and twice with DCM. Probes were then cleaved from the resin by using a 95:2.5:2.5 mixture of TFA:TIS:water.

Method 3.6.: Synthesis of triazole ureas: Resin (1 eq.) was swollen in 1 mL dry DCM per 10 µmol of resin, to which DIEA (15 eq.) and triphosgene (3 eq.) were added. Reactions were shaken at room temperature for 30 min, after which the cartridge was drained into a solution of 10% NaOH in water. The resin was washed three times with dry DCM, which was drained into a 10%NaOH solution. Next, the resin was resuspended in 1 mL dry DCM, to which 10 equivalents of 1*H*-1,2,3-triazole was added. Reactions were shaken overnight at room temperature and checked for completion using LC/MS. After completion, the resin was washed three times with DCM. Probes were then cleaved from the resin by using a 95:2.5:2.5 mixture of TFA:TIS:water. Note that with this on resin synthesis, the N1-isomer of the triazole ureas was formed (Figure S7).

N-(Diphenylphosphoryl)-isonipecotyl- L-phenylalanyl-6-aminohexanoyl-L-ε-azidolysine amide (4a)

Probe **4a** was synthesized using subsequently methods 1, 2.3 and 3.1 and purified using HPLC. The product was obtained as a white powder. (1.84 mg, yield = 23.7%) HRMS (MALDI-TOF): m/z calcd. for $C_{39}H_{51}N_8O_7P$ [M+H]$^+$ 775.3691, found: 775.3412.

N-(Succinimidyloxycarbonyl)-isonipecotyl-L-phenylalanyl-6-aminohexanoyl-L-ε-azidolysine amide (4b)

Probe **4b** was synthesized using subsequently methods 1, 2.3 and 3.2 and purified using HPLC. The product was obtained as a white powder. (3.31 mg, yield = 48.4%) HRMS (MALDI-TOF): m/z calcd. for $C_{32}H_{45}N_9O_8$ [M+H]$^+$ 684.3464, found: 684.3167.

N-(2-aminopyridin-2-yl-carbonyl)-isonipecotyl-L-phenylalanyl-6-aminohexanoyl-L-ε-azidolysine amide (4c)

Probe **4c** was synthesized using subsequently methods 1, 2.3 and 3.3 and purified using HPLC. The product was obtained as a white powder. (2.99 mg, yield = 45.1%) HRMS (MALDI-TOF): m/z calcd. for $C_{34}H_{46}N_{10}O_5$ [M+H]$^+$ 663.3725, found: 663.3597.

N-(Phenyloxycarbonyl)-isonipecotyl- L-phenylalanyl-6-aminohexanoyl-L-ε-azidolysine amide (4d)

Probe **4d** was synthesized using subsequently methods 1, 2.3 and 3.4 and purified using HPLC. The product was obtained as a white powder. (3.37 mg, yield = 50.8%) HRMS (MALDI-TOF): m/z calcd. for $C_{34}H_{46}N_8O_6$ [M+H]$^+$ 663.3613, found: 663.3211.

N-(4-Nitrophenyloxycarbonyl)-isonipecotyl- L-phenylalanyl-6-aminohexanoyl-L-ε-azidolysine amide (4e)

Probe **4e** was synthesized using subsequently methods 1, 2.3 and 3.5 and purified using HPLC. The product was obtained as a white powder. (1.93 mg, yield = 27.3%) HRMS (MALDI-TOF): m/z calcd. for $C_{34}H_{45}N_9O_8$ [M+H]$^+$ 708.3464, found: 708.3064.

_N_-(1H-1,2,3-triazol-1-yl-carbonyl)-isonipecotyl-L-phenylalanyl-6-aminohexanoyl-L-ε-azidolysine amide (4f)

Probe **4f** was synthesized using subsequently methods 1, 2.3 and 3.6 and purified using HPLC. The product was obtained as a white powder. (0.36 mg, yield = 5.6%) HRMS (MALDI-TOF): m/z calcd. for $C_{30}H_{43}N_{11}O_5$ [M+H]$^+$ 638.3521, found: 638.3790.

_N_-(Diphenylphosphoryl)-isonipecotyl-(_N_-benzyl)glycyl-6-aminohexanoyl-L-ε-azidolysine amide (5a)

Probe **5a** was synthesized using subsequently methods 1, 2.1 and 3.1 and purified using HPLC. The product was obtained as a white powder. (0.33 mg, yield = 4.3%) HRMS (MALDI-TOF): m/z calcd. for $C_{39}H_{51}N_8O_7P$ [M+H]$^+$ 775.3691, found: 775.3742.

_N_-(Succinimidyloxycarbonyl)-isonipecotyl-(_N_-benzyl)glycyl-6-aminohexanoyl-L-ε-azidolysine amide (5b)

Probe **5b** was synthesized using subsequently methods 1, 2.1 and 3.2 and purified using HPLC. The product was obtained as a white powder. (1.29 mg, yield = 18.9%) HRMS (MALDI-TOF): m/z calcd. for $C_{32}H_{45}N_9O_8$ [M+H]$^+$ 684.3391, found: 684.3342.

_N_-(2-aminopyridin-2-yl-carbonyl)-isonipecotyl-(_N_-benzyl)glycyl-6-aminohexanoyl-L-ε-azidolysine amide (5c)

Probe **5c** was synthesized using subsequently methods 1, 2.1 and 3.3 and purified using HPLC. The product was obtained as a white powder. (2.82 mg, yield = 42.5%) HRMS (MALDI-TOF): m/z calcd. for $C_{34}H_{46}N_8O_6$ [M+H]$^+$ 663.37301, found: 663.3648.

_N_-(Phenyloxycarbonyl)-isonipecotyl-(_N_-benzyl)glycyl-6-aminohexanoyl-L-ε-azidolysine amide (5d)

Probe **5d** was synthesized using subsequently methods 1, 2.1 and 3.4 and purified using HPLC. The product was obtained as a white powder. (2.80 mg, yield = 42.2%) HRMS (MALDI-TOF): m/z calcd. for $C_{33}H_{46}N_{10}O_5$ [M+H]$^+$ 663.3619, found: 663.3772.

_N_-(4-Nitrophenyloxycarbonyl)-isonipecotyl-(_N_-benzyl)glycyl-6-aminohexanoyl-L-ε-azidolysine amide (5e)

Probe **5e** was synthesized using subsequently methods 1, 2.1 and 3.5 and purified using HPLC. The product was obtained as a white powder. (2.97 mg, yield = 41.9%) HRMS (MALDI-TOF): m/z calcd. for $C_{34}H_{45}N_9O_8$ [M+H]$^+$ 708.3469, found: 708.3151.

_N_-(1H-1,2,3-triazol-1-yl-carbonyl)-isonipecotyl-(_N_-benzyl)glycyl-6-aminohexanoyl-L-ε-azidolysine amide (5f)

Probe **5f** was synthesized using subsequently methods 1, 2.1 and 3.6 and purified using HPLC. The product was obtained as a white powder. (1.06 mg, yield = 16.6%) HRMS (MALDI-TOF): m/z calcd. for $C_{30}H_{43}N_{11}O_5$ [M+Na]$^+$ 660.3346, found: 660.2908.

_N_-(Diphenylphosphoryl)-4-(piperazinyl-methyl)-benzoyl-6-aminohexanoyl-L-ε-azidolysine amide (6a)

Probe **6a** was synthesized using subsequently methods 1, 2.2 and 3.1 and purified using HPLC. The product was obtained as a white powder. (0.93 mg, yield = 12.9%) HRMS (MALDI-TOF): m/z calcd. for $C_{36}H_{47}N_8O_6P$ [M+H]$^+$ 719.3435, found: 719.3851.

_N_-(Succinimidyloxycarbonyl)-4-(piperazinyl-methyl)-benzoyl-6-aminohexanoyl-L-ε-azidolysine amide (6b)

Probe **6b** was synthesized using subsequently methods 1, 2.2 and 3.2 and purified using HPLC. The product was obtained as a white powder. (0.93 mg, yield = 12.9%) HRMS (MALDI-TOF): m/z calcd. for $C_{29}H_{41}N_9O_7$ [M+H]$^+$ 628.3201, found: 628.3192.

N-(2-aminopyridin-2-yl-carbonyl)-4-(piperazinyl-methyl)-benzoyl-6-aminohexanoyl-L-ε-azidolysine amide (6c)
Probe **6c** was synthesized using subsequently methods 1, 2.2 and 3.3 and purified using HPLC. The product was obtained as a white powder. (0.69 mg, yield = 11.4%) HRMS (MALDI-TOF): m/z calcd. for $C_{31}H_{42}N_8O_5$ $[M+H]^+$ 607.3351, found: 607.3222.

N-(Phenyloxycarbonyl)-4-(piperazinyl-methyl)-benzoyl-6-aminohexanoyl-L-ε-azidolysine amide (6d)
Probe **6d** was synthesized using subsequently methods 1, 2.2 and 3.4 and purified using HPLC. The product was obtained as a white powder. (0.49 mg, yield = 8.1%) HRMS (MALDI-TOF): m/z calcd. for $C_{30}H_{42}N_{10}O_4$ $[M+H]^+$ 607.3463, found: 607.3647.

N-(4-Nitrophenyloxycarbonyl)-4-(piperazinyl-methyl)-benzoyl-6-aminohexanoyl-L-ε-azidolysine amide (6e)
Probe **6e** was synthesized using subsequently methods 1, 2.2 and 3.5 and purified using HPLC. The product was obtained as a white powder. (0.63 mg, yield = 9.7%) HRMS (MALDI-TOF): m/z calcd. for $C_{31}H_{41}N_9O_7$ $[M+H]^+$ 652.3202, found: 652.2670.

N-(1H-1,2,3-triazol-1-yl-carbonyl)-4-(piperazinyl-methyl)-benzoyl-6-aminohexanoyl-L-ε-azidolysine amide (6f)
Probe **6f** was synthesized using subsequently methods 1, 2.2 and 3.6 and purified using HPLC. The product was obtained as a white powder. (0.34 mg, yield = 5.8%) HRMS (MALDI-TOF): m/z calcd. for $C_{27}H_{39}N_{11}O_4$ $[M+H]^+$ 582.3259, found: 582.3079.

Preparation of tissue lysates
Mouse brains were thawed on ice, after which the hemispheres were separated using a razor blade and cut into small pieces. The pieces were collected in a Dounce homogenizer and homogenized on ice using 1.5 mL cold (4 °C) lysis buffer (20 mM HEPES, 2 mM DTT, 1 mM $MgCl_2$, 25 U/mL DNAse I, pH 7.2) until thorough lysis of the organ was visually assessed. After homogenization, the suspension was collected into Eppendorf tubes and the Dounce homogenizer was rinsed twice with small aliquots of lysis buffer, which were added to these tubes. The suspension was centrifuged (2500 g, 3 min, 4°C) to remove cell debris. The supernatant was carefully pipetted and transferred to an ultracentrifuge tube. The debris was resuspended in 0.25 mL lysis buffer and centirfuged again using the same procedure. The supernatant was added to the ultracentrifuge tubes, which were then spun in an ultracentrifuge (100,000 g, 45 min, 4 °C, Beckman Optima™ TLX, TLA 120.2 rotor). The supernatant (= cytosolic protein fraction) was collected and the pellet (= membrane protein fraction) was suspended in 1.5 mL storage buffer (20 mM HEPES, 2 mM DTT, pH 7.2). Protein concentrations were determined using BCA assay on a Spectramax ID3 platereader. Aliquots were snap frozen in liquid nitrogen and stored at -80 °C until use.

Competition of probes with FP-rhodamine
30 µL of cytosolic or membrane fraction of mouse brain lysate (1 mg/mL) was incubated for 1 h at room temperature with 0.3 µL of a stock solution of probe (10 mM, DMSO) or 0.3 µL DMSO. Then 0.3 µL FP-rhodamine (100 µM, DMSO) was added to each sample and the samples were incubated for another hour. Next, 10 µL 4x sample buffer was added to the samples, which were subsequently boiled at 95 °C for 2 minutes. Samples were resolved by SDS-PAGE on 12% acrylamide gels and visualized by measuring in-gel fluorescence on a Typhoon FLA 9500 scanner with excitation at 532 nm and detection at 568 nm with the photomultiplier set at 900 V. Patterns of probe-treated samples were compared with an FP-rhodamine treated control sample. Compounds that led to full disappearance of gel bands were considered hits.

Comparison of 5f with JCP-174 alk

30 μL of cytosolic or membrane fraction of mouse brain lysate (1 mg/mL) was incubated for 1 h at room temperature with either 0.3 μL of a stock solution of probe **5f** (10 μM, DMSO), 0.3 μL of a stock solution of JCP-174 alk (1 mM, DMSO) or 0.3 μL DMSO. Then 0.3 μL FP-rhodamine (100 μM, DMSO) was added to each sample and the samples were incubated for 1 hour at room temperature. Next, 10 μL 4x sample buffer was added to the samples, which were subsequently boiled at 95 °C for 2 minutes. Samples were resolved by SDS-PAGE on 12% acrylamide gels and visualized by measuring in-gel fluorescence on a Typhoon FLA 9500 scanner with settings as described above.

Comparison of 5f with ML-348 and ML-349

30 μL of cytosolic fraction of mouse brain lysate (1 mg/mL) was incubated for 1 h at room temperature with either 0.3 μL of a stock solution of probe **5f** (10 μM, DMSO), 0.3 μL of a stock solution of ML-348 or ML-349 (50 mM, DMSO) or 0.3 μL DMSO. Then 0.3 μL FP-rhodamine (100 μM, DMSO) was added to each sample and the samples were incubated for 5 minutes at room temperature. Next, 10 μL 4x sample buffer was added to the samples, which were subsequently boiled at 95 °C for 2 minutes. Samples were resolved by SDS-PAGE on 12% acrylamide gels and visualized by measuring in-gel fluorescence on a Typhoon FLA 9500 scanner with settings as described above.

Cell permeability assay in A431 cells

A431 cells were seeded at 300,000 cells per well into a 6-well plate and allowed to adhere overnight. The media was refreshed with 1 mL DMEM (with 10% FBS and pen/strep), spiked with either 1 μL **5f** or **6f** (1 mM, DMSO) or 1 μL DMSO for 2h at 37 °C. Next, the medium was aspirated and the cells were washed three times with PBS (5 min). Lysates were prepared by incubating cells in 150 μL lysis buffer (20 mM HEPES, 150 mM NaCl, 2 mM DTT, 25 U/mL Benzonase, 0.5% NP-40, pH 7.2) before scraping cells. Lysates were centrifuged (13000 g, 5 min, room temperature) to pellet debris, after which the supernatant was pipetted off. Protein concentrations of all samples were measured using a BCA assay, and normalized to 2.39 mg/mL with storage buffer (20 mM HEPES, 2 mM DTT, pH 7.2). 90 μL of each sample was incubated with either 0.9 μL FP-rhodamine (DMSO, 100 μM) or 0.9 μL DMSO at room temperature for 1 hour. Next, 30 μL 4x sample buffer was added to the samples, which were subsequently boiled at 95 °C for 2 minutes. Samples were resolved by SDS-PAGE on 12% acrylamide gels and visualized by measuring in-gel fluorescence on a Typhoon FLA 9500 scanner with settings as described above.

IC$_{50}$ determination

Apparent IC$_{50}$ values were measured by using six different compound concentrations in a 1:3 serial dilution, starting at a highest concentration of 30 μM or 370 nM, depending on the potency of the compound.. To this end 30 μL of cytosolic or membrane fraction of mouse brain lysate (1 mg/mL) was incubated for 1 h at room temperature with 0.3 μL of a 100x stock solution of probe in DMSO. Then, 0.3 μL FP-rhodamine (100 μM, DMSO) was added to each sample and the samples were incubated for another hour. Next 10 μL 4x sample buffer was added to the samples, which were subsequently boiled at 95 °C for 2 minutes. Samples were resolved by SDS-PAGE on 12% acrylamide gels and visualized by in-gel fluorescence measuring on a Typhoon scanner as for the initial screening. Remaining enzyme activity was determined by measuring the integrated optical gel band intensity using ImageJ software. Values were normalized to the FP-rhodamine labeled control sample without inhibitor, which was set at 100% activity. IC$_{50}$ values were determined from a dose-response curve generated in GraphPad Prism.

Direct labelling of probe targets

30 μL of cytosolic or membrane fraction of mouse brain lysate (1 mg/mL) was incubated for 1 h with 0.3 μL of a 100x stock solution of the appropriate concentration. Next, 0.5 μL TAMRA-alkyne (1.5 mM in DMSO), 0.3 μL THPTA (5 mM in 4:1 t-BuOH: DMSO), 0.6 μL sodium ascorbate (50 mM in water) and

0.6 μL CuSO$_4$ (50 mM in water) were added to each sample and the samples were incubated 1 h at room temperature. Afterwards, 10 μL of 4x sample buffer was added to the samples, which were subsequently boiled at 95 °C for 2 minutes. Samples were resolved on an SDS-PAGE 12% acrylamide gel and visualized by in-gel fluorescence measuring on a Typhoon scanner.

Western blot against APT-1/2

Mouse brain lysates (90 μL, 1 mg/mL of either cytosolic or membrane fraction) were treated for 1 h with 1 μM probe (from a 100x dmso stock) or a corresponding amount of dmso (control sample). All samples were subsequently treated with 1,5 μL tritag (TAMRA-Lys(biotin)-NH-propyne; 1.5 mM in DMSO), 0.9 μL THPTA (5 mM in water), 1.8 μL CuSO$_4$ (50 mM in water) and 1.8 μL sodium ascorbate (50 mM in water), after which they were incubated for another hour at room temperature. Next, 360 μL of cold acetone (-80 °C) was added to each sample to precipitate proteins and eliminate residual click reagents. The samples were incubated at -20 °C for 30 minutes to ensure efficient protein precipitation, after which they were spun down using a microcentrifuge at max speed. The supernatant was discarded, another 360 μL cold acetone was added to the pellet of the samples and the procedure was repeated once more.

Protein pellets were then redissolved in 90 μL PBS with 2% SDS. Next, SDS was diluted with steps of 90 μL to a final concentration of 0.4% SDS. Then, 30 μL of Ultralink Streptavidin resin slurry was added to each sample to pull down all biotin-labeled proteins. To this end, all samples were incubated on a thermomixer (1h, 1200 rpm, 25 °C). Afterwards, the samples were spun down using a microcentrifuge at full speed.

The supernatant was carefully pippeted from the beads, after which the beads were washed with 120 μL of 0.1% SDS in PBS, subsequently with 120 μL of 1M NaCl, then with 120 μL 1M urea, then with 120 μL PBS and finally with 120 μL MilliQ water. After each washing step, the samples were spun down using a microcentrifuge at full speed and the supernatant was discarded. The beads were resuspended in 120 μL sample buffer and boiled for 10 minutes to release the proteins from the beads. Samples were then resolved on a 12% acrylamide gel using SDS-PAGE.

A fluorescent image of the gels was made (Typhoon scanner), after which the proteins were transferred onto nitrocellulose membranes. Both membranes were incubated for 1h with 3% milk/PBST. The milk was discarded and one of the gels was incubated overnight with 15 mL anti-APT-1 antibody Ab 91606 (0.5 μg/mL in PBST), whereas the other membrane was incubated overnight with 15 mL anti-APT-2 antibody Ab 151578 (0.5 μg/mL in PBST). The antibody-solutions were then decanted and the membranes washed four times with PBST. Next, both membranes were incubated with anti-rabbit HRP antibody (0.2 μg/mL in PBST) for 1h. Afterwards, the membranes were washed four times with PBST and incubated with SuperSignal West Pico Plus chemiluminescent substrate (Life Technologies) just prior to development using a BioRad ChemiDoc imaging system.

Covalent docking

The different probes were drawn in Chemdraw professional 15.1, converted to a pdb file using Chem3D 15.1 and converted into a PDBQT by AutoDockTools 1.5.6. Probes were attached with their carbonyl function (with elimination of the leaving group) to the side chain of residue S119 of APT-1 (PDB code: 6QGS, from which water molecules and the palmitate ligand were removed), using the provided script at the autodock website (see for download: http://autodock.scripps.edu/resources/covalentdocking) with a slight modification. Molecules were then docked according to the flexible side chain method of AutoDock 4.2, as described by Bianco et al.[29] The connected molecules were treated as a fully flexible side chain. The binding site was covered by preparing a 60 × 76 × 70 size grid box with grid spacing of 0.375 Å and the center at 7.837, 127.491, 18.586.

3.5. References

[1]   B. F. Cravatt, A. T. Wright, J. W. Kozarich, *Annu. Rev. Biochem.* **2008**, *77*, 383.

[2]   A. M. Sadaghiani, S. H. L. Verhelst, M. Bogyo, *Curr Opin Chem Biol* **2007**, *11*, 20.

[3]   Y. S. Liu, M. P. Patricelli, B. F. Cravatt, *Proc Natl Acad Sci U S A* **1999**, *96*, 14694.

[4]   M. P. Patricelli, D. K. Giang, L. M. Stamp, J. J. Burbaum, *Proteomics* **2001**, *1*, 1067.

[5]   N. Jessani, Y. S. Liu, M. Humphrey, B. F. Cravatt, *Proc Natl Acad Sci U S A* **2002**, *99*, 10335.

[6]   D. A. Bachovchin, B. F. Cravatt, *Nat Rev Drug Discov* **2012**, *11*, 52.

[7]   J. R. Savinainen, S. M. Saario, J. T. Laitinen, *Acta Physiol (Oxf)* **2012**, *204*, 267.

[8]   D. Davda, B. R. Martin, *Medchemcomm* **2014**, *5*, 268.

[9]   J. M. Sontag, V. Nunbhakdi-Craig, M. Mitterhuber, E. Ogris, E. Sontag, *J Neurochem* **2010**, *115*, 1455.

[10]   D. A. Bachovchin, T. Ji, W. Li, G. M. Simon, J. L. Blankman, A. Adibekian, H. Hoover, S. Niessen, B. F. Cravatt, *Proc. Natl. Acad. Sci. USA* **2010**, *107*, 20941.

[11]   R. Cheng, W. Mori, L. Ma, M. Alhouayek, A. Hatori, Y. Zhang, D. Ogasawara, G. Yuan, Z. Chen, X. Zhang, H. Shi, T. Yamasaki, L. Xie, K. Kumata, M. Fujinaga, Y. Nagai, T. Minamimoto, M. Svensson, L. Wang, Y. Du, M. J. Ondrechen, N. Vasdev, B. F. Cravatt, C. Fowler, M. R. Zhang, S. H. Liang, *J Med Chem* **2018**, *61*, 2278.

[12]   Z. Chen, W. Mori, H. Fu, M. A. Schafroth, A. Hatori, T. Shao, G. Zhang, R. S. Van, Y. Zhang, K. Hu, M. Fujinaga, L. Wang, V. Belov, D. Ogasawara, P. Giffenig, X. Deng, J. Rong, Q. Yu, X. Zhang, M. I. Papisov, Y. Shao, T. L. Collier, J. A. Ma, B. F. Cravatt, L. Josephson, M. R. Zhang, S. H. Liang, *J Med Chem* **2019**, *62*, 8866.

[13]   J. W. Chang, R. E. Moellering, B. F. Cravatt, *Angew Chem Int Ed Engl* **2012**, *51*, 966.

[14]   E. J. van Rooden, M. Kohsiek, R. Kreekel, A. C. M. van Esbroeck, A. van den Nieuwendijk, A. P. A. Janssen, R. van den Berg, H. S. Overkleeft, M. van der Stelt, *Chem Asian J* **2018**, *13*, 3491.

[15]   E. J. van Rooden, R. Kreekel, T. Hansen, A. P. A. Janssen, A. C. M. van Esbroeck, H. den Dulk, R. van den Berg, J. D. C. Codee, M. van der Stelt, *Org Biomol Chem* **2018**, *16*, 5250.

[16]   J. W. Chang, A. B. Cognetta, 3rd, M. J. Niphakis, B. F. Cravatt, *ACS Chem Biol* **2013**, *8*, 1590.

[17]   U. R. Haedke, S. C. Frommel, F. Hansen, H. Hahne, B. Kuster, M. Bogyo, S. H. Verhelst, *Chembiochem* **2014**, *15*, 1106.

[18]   K. Otrubova, V. Srinivasan, D. L. Boger, *Bioorg Med Chem Lett* **2014**, *24*, 3807.

[19]   A. Adibekian, B. R. Martin, C. Wang, K. L. Hsu, D. A. Bachovchin, S. Niessen, H. Hoover, B. F. Cravatt, *Nat Chem Biol* **2011**, *7*, 469.

[20]   J. Z. Long, X. Jin, A. Adibekian, W. Li, B. F. Cravatt, *J Med Chem* **2010**, *53*, 1830.

[21]   N. Aaltonen, J. R. Savinainen, C. R. Ribas, J. Ronkko, A. Kuusisto, J. Korhonen, D. Navia-Paldanius, J. Hayrinen, P. Takabe, H. Kasnanen, T. Pantsar, T. Laitinen, M. Lehtonen, S. Pasonen-Seppanen, A. Poso, T. Nevalainen, J. T. Laitinen, *Chem Biol* **2013**, *20*, 379.

[22]   M. Lamani, M. S. Malamas, S. I. Farah, V. G. Shukla, M. F. Almeida, C. M. Weerts, J. Anderson, J. T. Wood, K. L. G. Farizatto, B. A. Bahr, A. Makriyannis, *Bioorg Med Chem* **2019**, *27*, 115096.

[23]   M. P. Baggelaar, A. C. van Esbroeck, E. J. van Rooden, B. I. Florea, H. S. Overkleeft, G. Marsicano, F. Chaouloff, M. van der Stelt, *ACS Chem Biol* **2017**, *12*, 852.

[24]   J. L. Blankman, G. M. Simon, B. F. Cravatt, *Chem Biol* **2007**, *14*, 1347.

[25]   E. J. van Rooden, A. C. M. van Esbroeck, M. P. Baggelaar, H. Deng, B. I. Florea, A. R. A. Marques, R. Ottenhoff, R. G. Boot, H. S. Overkleeft, J. Aerts, M. van der Stelt, *Front Neurosci* **2018**, *12*, 440.

[26]   A. Adibekian, B. R. Martin, J. W. Chang, K. L. Hsu, K. Tsuboi, D. A. Bachovchin, A. E. Speers, S. J. Brown, T. Spicer, V. Fernandez-Vega, J. Ferguson, P. S. Hodder, H. Rosen, B. F. Cravatt, *J. Am. Chem. Soc.* **2012**, *134*, 10345.

[27]   M. Garland, C. J. Schulze, I. T. Foe, W. A. van der Linden, M. A. Child, M. Bogyo, *PLoS One* **2018**, *13*, e0190255.

[28]   G. M. Morris, R. Huey, W. Lindstrom, M. F. Sanner, R. K. Belew, D. S. Goodsell, A. J. Olson, *J Comput Chem* **2009**, *30*, 2785.

[29]   G. Bianco, S. Forli, D. S. Goodsell, A. J. Olson, *Protein Sci* **2016**, *25*, 295.

[30]   S. J. Won, D. Davda, K. J. Labby, S. Y. Hwang, R. Pricer, J. D. Majmudar, K. A. Armacost, L. A. Rodriguez, C. L. Rodriguez, F. S. Chong, K. A. Torossian, J. Palakurthi, E. S. Hur, J. L. Meagher, C. L. Brooks, 3rd, J. A. Stuckey, B. R. Martin, *ACS Chem Biol* **2016**, *11*, 3374.

[31]   W. L. Delano, **2002**.

[32]   D. M. Swanson, A. E. Dubin, C. Shah, N. Nasser, L. Chang, S. L. Dax, M. Jetter, J. G. Breitenbucher, C. Liu, C. Mazur, B. Lord, L. Gonzales, K. Hoey, M. Rizzolio, M. Bogenstaetter, E. E. Codd, D. H. Lee, S. P. Zhang, S. R. Chaplan, N. I. Carruthers, *J Med Chem* **2005**, *48*, 1857.

3.6. Supplementary information

3.6.1. Additional synthetic procedures

Solution phase chemistry
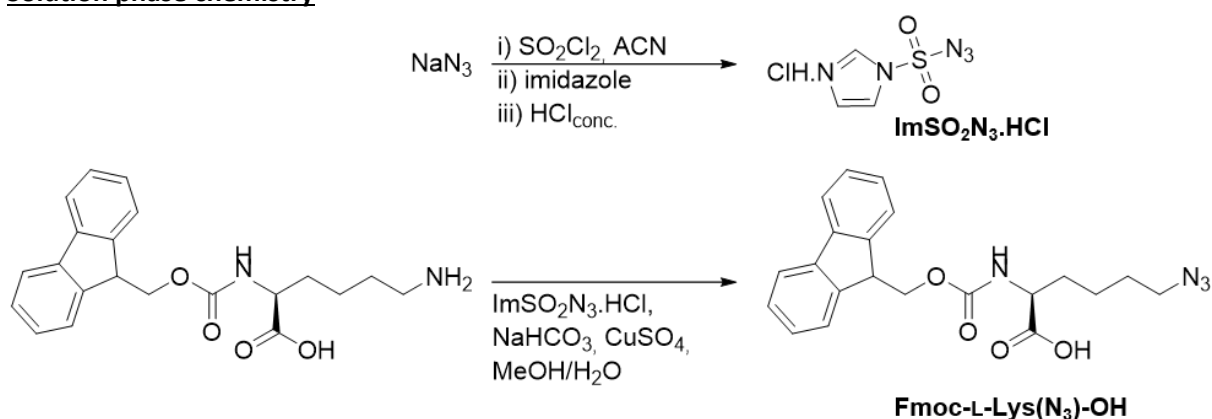
Scheme S3.1. Synthesis of Fmoc-L-Lys(N$_3$)-OH from Fmoc-L-Lys-OH and 1*H*-Imidazole-1-sulfonyl azide.HCl.

1*H*-Imidazole-1-sulfonyl azide.HCl (ImSO$_2$N$_3$.HCl)

1*H*-Imidazole-1-sulfonyl azide.HCl was synthesized according to the method described in Goddard-Borger et al.[1] (Scheme **S1**). The identity was in agreement with the data reported in the literature.

N-(9-Fluorenylmethoxycarbonyl)-2-(S)-amino-6-azidohexanoic acid (Fmoc-L-Lys(N$_3$)-OH)

Fmoc-L-Lys(N$_3$)-OH was synthesized from Fmoc-L-Lys-OH and 1*H*-Imidazole-1-sulfonyl azide.HCl according to the method described in Sminia et al.[2] (Scheme **S1**) and isolated in 73% yield. The identity was in agreement with the data reported in the literature.

N(N$^\alpha$-((9H-fluoren-9-yl)methyl)-N$^\epsilon$-(D-biotinyl)-L-lysyl)-3-amino-1-propyne (**8; Fmoc-Lys(biotin)-NH-propyne**)
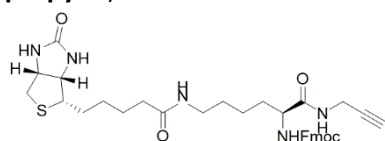
N-α-Fmoc-N-ε-biotinyl-L-lysine (25.0 mg, 42 μmol) was dissolved in 1 ml DMF and heated gently to aid solubilization. DIEA (60 μL, 336 μmol) and HBTU (47.8 mg, 126 μmol) were added to this solution and the reaction mixture was stirred for 15 minutes at room temperature. Then propargylamine.HCl (11.5 mg, 126 μmol) was added to the reaction mixture, which was stirred overnight at room temperature.

Completion of the reaction was checked using LC-MS, after which the solvents were evaporated and the crude mixture purified using HPLC to obtain the title compound as a white powder. (10.70 mg, 40.3%) ^{1}H NMR (600 MHz, DMSO-d6): δ 8.37 (t, 1H, J = 5.4 Hz), 7.89 (d, 2H, J = 7.5 Hz), 7.81-7.70 (m, 3H), 7.51 (d, 1H, J = 8.2 Hz), 7.42 (t, 2H, J = 7.4 Hz), 7.33 (t, 2H, J = 7.1 Hz), 6.53-6.22 (bs, 2H), 4.33-4.17 (m, 4H), 4.14-4.08 (m, 1H), 3.99-3.82 (m, 3H), 3.11 (t, 1H, J = 2.3 Hz), 3.09-3.05 (m, 1H), 3.05-2.94 (m, 2H), 2.8 (dd, 1H, J = 5.1Hz), 2.56 (d, 1H), 2.03 (t, 2H, J = 7.2 Hz), 1.68-1.42 (m, 6H), 1.42-1.20 (m, 6H). HRMS (MALDI-TOF): m/z calcd. for $C_{34}H_{41}N_5O_5S$ [M+H]$^+$ 632.2901, found: 632.2932.

N(N$^\alpha$-((2,4-dicarboxy-tetramethylrhodamin-4-yl)-N$^\epsilon$-(D-biotinyl)-L-lysyl)-3-amino-1-propyne   (7; TAMRA-Lys(biotin)-NH-propyne)
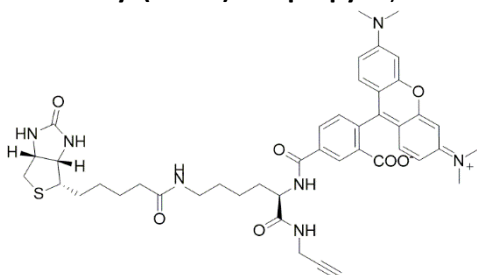
Compound **8** (5.4 mg, 8.47 μmol) was dissolved in 400 μL DMF and heated gently to aid dissolution. Piperidine (50 μL, 506 μmol) was added to this solution, which was subsequently stirred 15 minutes at room temperature to remove the Fmoc group. After 15 minutes the solvents were evaporated and excess piperidine was removed from the crude product by co-evaporation with toluene. The crude product was then redissolved in 1 mL DMF, to which DIEA (7.6 μL, 42.34 μmol) was added. Subsequently TAMRA-OSu (4.5 mg, 8.47 μg) was added to the reaction mixture which stirred overnight at room temperature, covered in aluminium foil. Completion of the reaction was checked using LC-MS, after which the solvents were evaporated and the crude mixture purified using HPLC to obtain the title compound as a pink solid. (0.56 mg, 8.0%) HRMS (MALDI-TOF): m/z calcd. for $C_{44}H_{51}N_7O_7S$ [M+H]$^+$ 822.3643, found: 822.3303.

3.6.2. Supplementary Figures
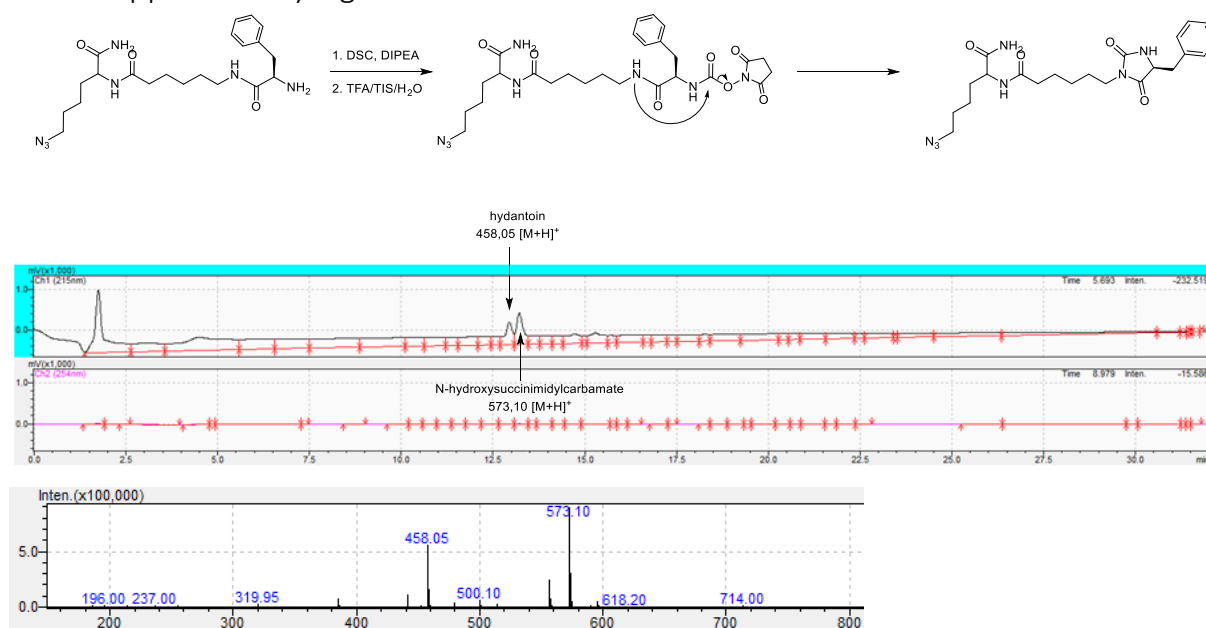
Figure S3.1. Mechanism of the formation of hydantoins from primary NHS-carbamates, after formation of the NHS-carbamate. Illustrated on a Lys(N$_3$)-Ahx-Phe capped as a NHS-carbamate, with LC-MS trace of the crude reaction products.

A

diphenylphosphoramidate
628,15 [M+H]$^+$

B

N-hydroxysuccinimidylcarbamate
537,10 [M+H]$^+$

C

2-aminopyridine urea
516,15 [M+H]$^+$
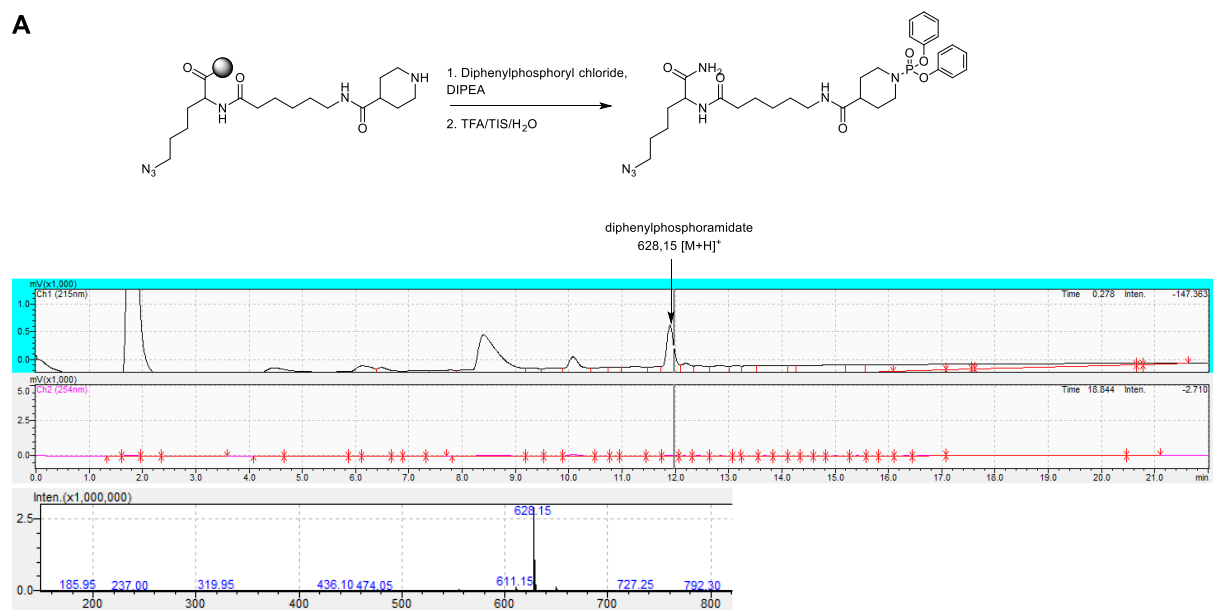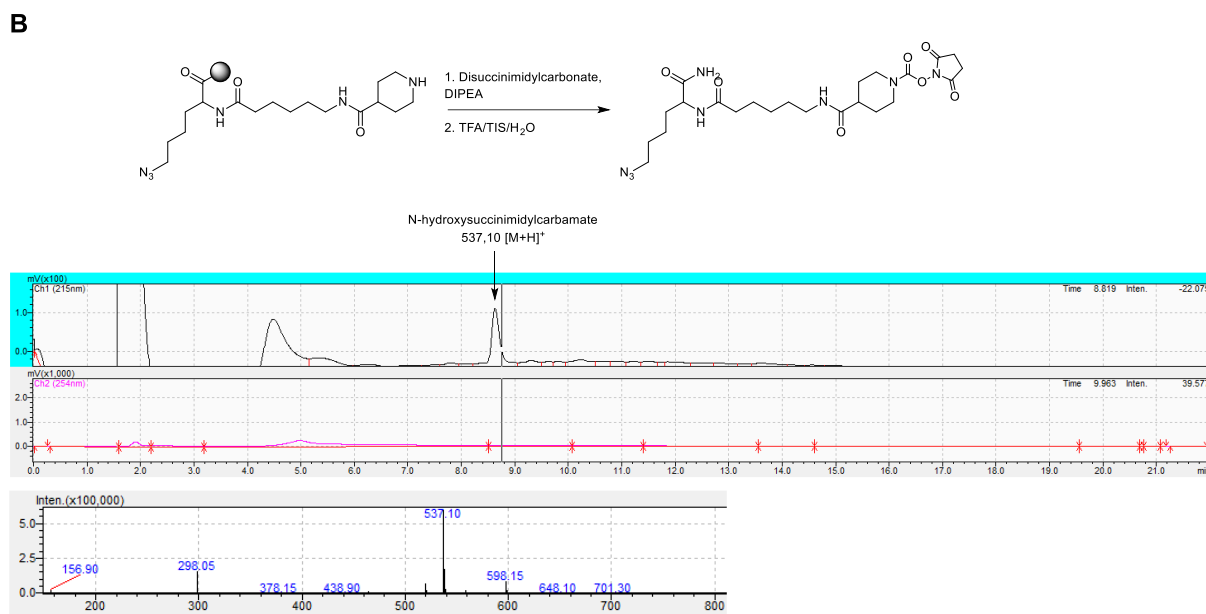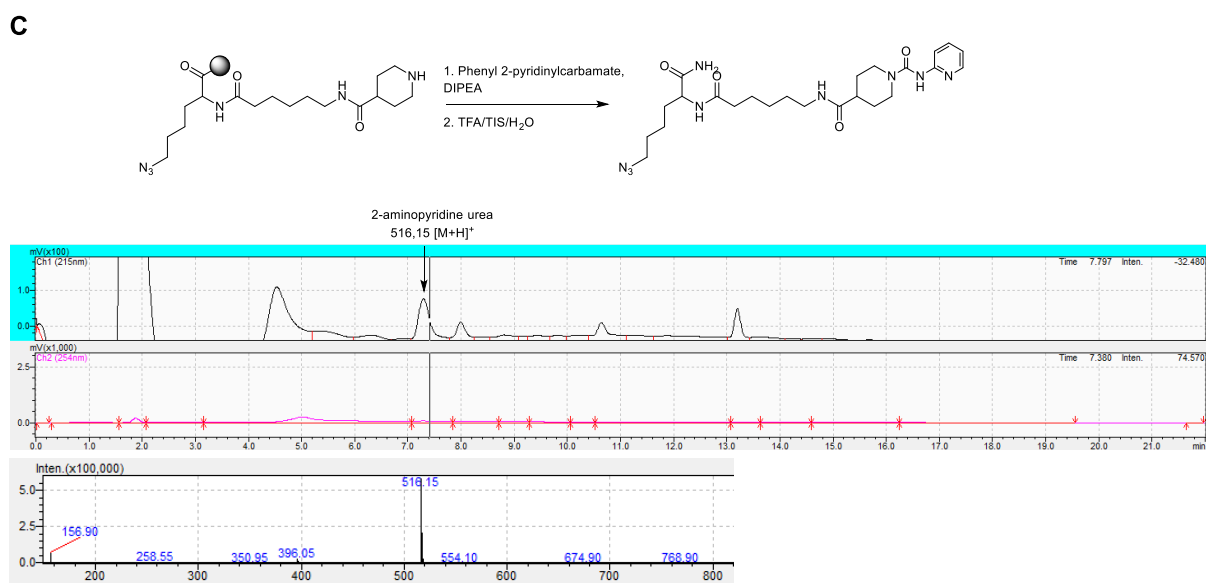
D
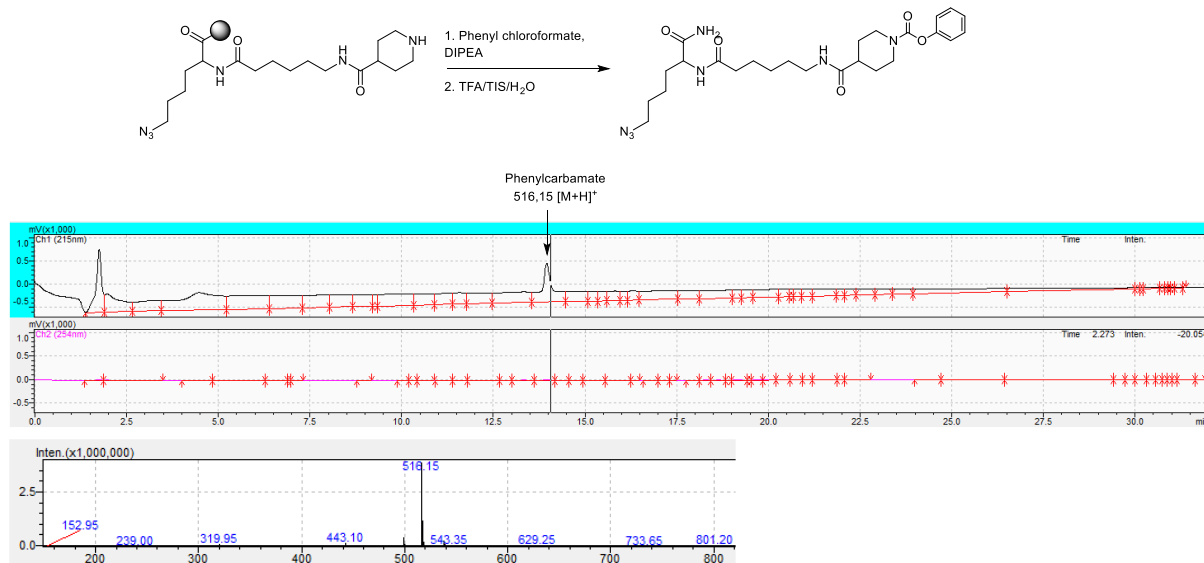
E
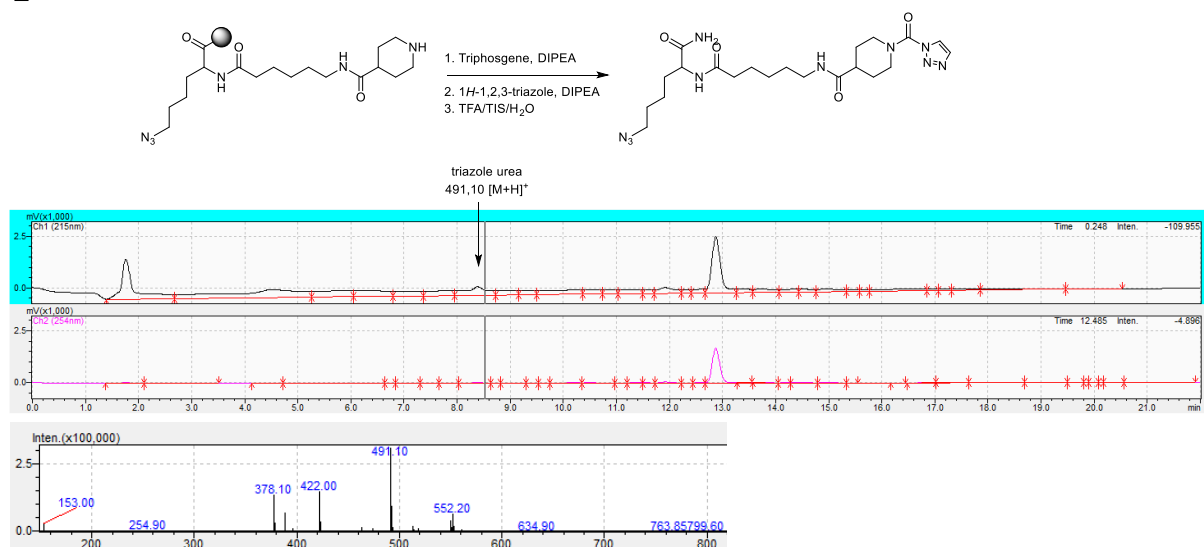
Figure S3.2. Serine reactive warheads can be coupled to a Rink-amide resin-bound Lys(N$_3$)-Ahx-Inp-NH backbone. The figure describes the used coupling conditions and displays crude LC-MS traces for **A.** a diphenylphosphoramidate, **B.** an N-hydroxysuccinimidylcarbamate, **C.** a 2-aminopyridine urea, **D.** a phenylcarbamate and **E.** a 1,2,3-triazole urea.
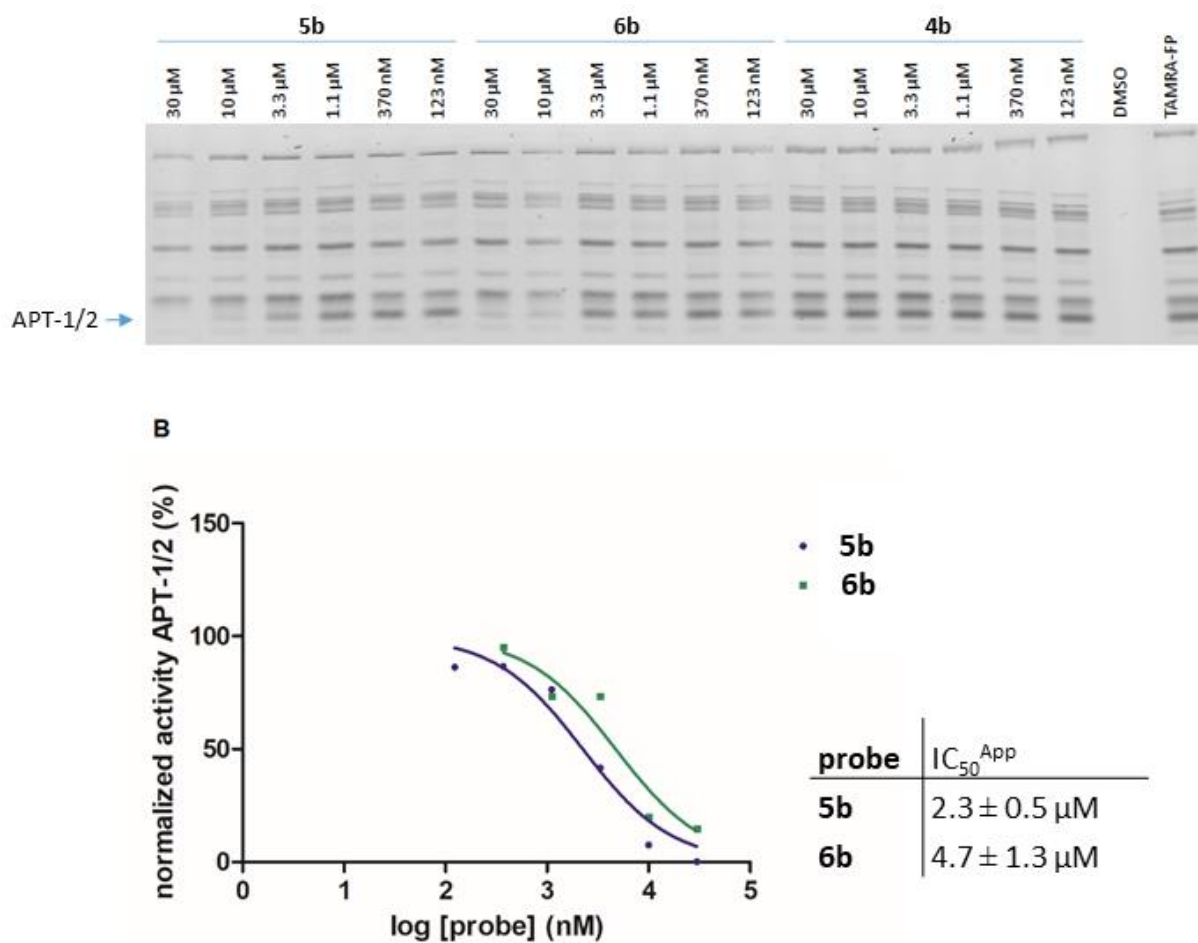
Figure S3.3. A. Gel-based IC_{50}^{App} determination of N-hydroxysuccinimidylcarbamates **4b**, **5b** and **6b** on mouse brain cytosolic fraction. **B.** Inhibition curve of N-hydroxysuccinimidylcarbamates **5b** and **6b** on APT-1/2 with IC_{50}^{App} values.
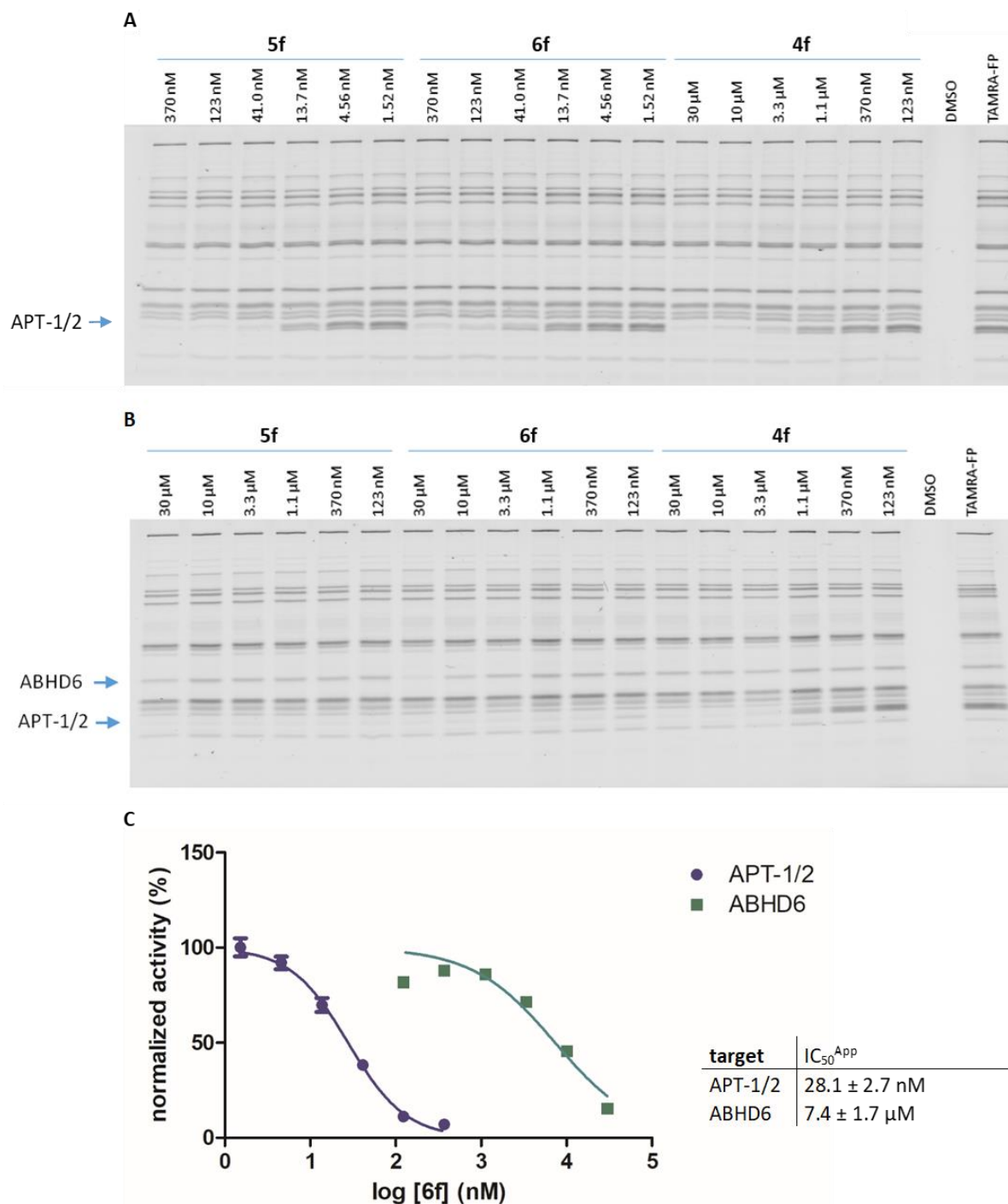
Figure S3.4. A. Representative gel for IC$_{50}$^{App} determination of triazoleureas **4f-6f** on mouse brain cytosolic proteome (relates to Figure 2B). **B.** Similar titration of triazoleureas **4f-6f** on mouse brain cytosolic proteome but at higher concentrations for **5f** and **6f**. No off-targets are identified, except ABHD6 for probe **6f**. **C.** IC$_{50}$^{App} determination for probe **6f** on APT-1/2 and ABHD6 shows a more than 250 fold selectivity for APT-1/2.
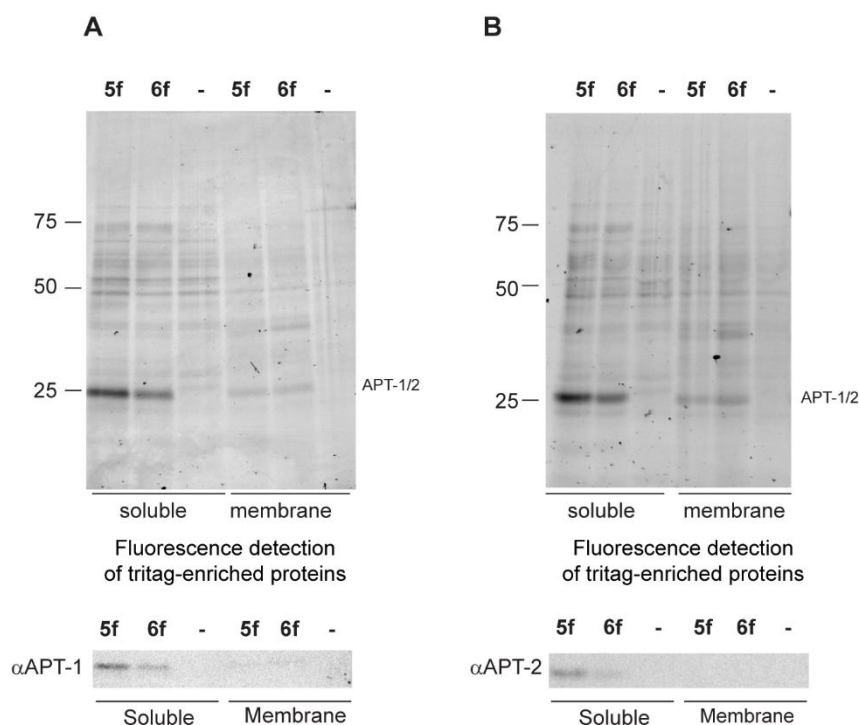
Figure S3.5. Full gels after labeling mouse brain lysate (soluble or membrane fraction) with indicated probe, followed by click chemistry with Biotin-TAMRA-alkyne tag and enrichment of targets on streptavidin resin. Gel in panel A was subjected to Western blot with anti-APT-1 antibody and gel in panel be to anti-APT-2 antibody. Note that APT-1/2 were very low abundant in the membrane fraction.
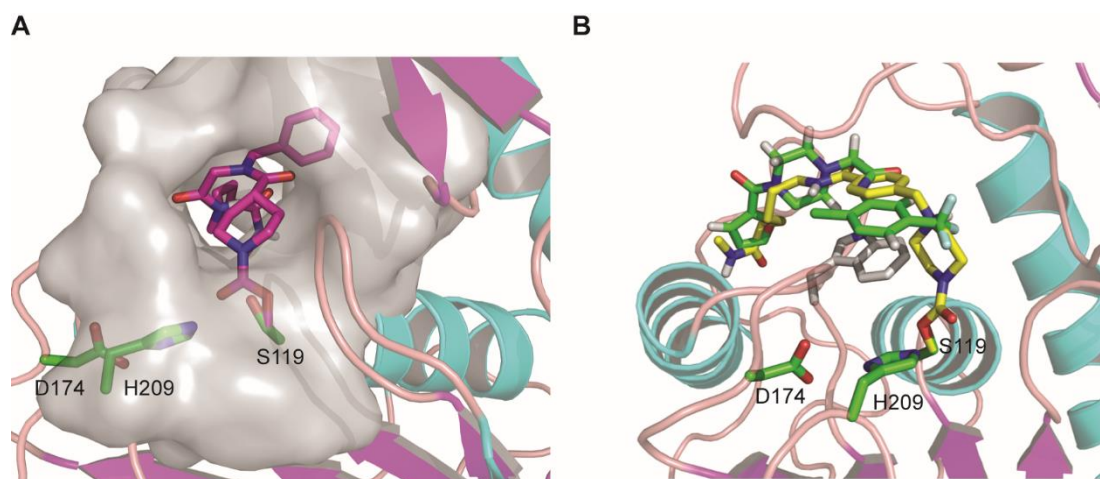
Figure S3.6. Covalent docking of probes in APT-1 (PDB code: 6QGS). **A.** Protein in cartoon format with α-helices in cyan, β-sheets in magenta and random coil in pink. **5f** is shown in magenta in stick format. Active site residues are depicted in green. The hydrophobic palmitate substrate binding channel is depicted as transparent grey surface. **B.** Overlay of **6f** (in yellow) with non-covalent inhibitor ML348 (in green; PDB code: 5SYM). Active site residues also in green and W145 in white. Note the overlapping binding site of the ML348 and the here described covalent inhibitor **6f**.
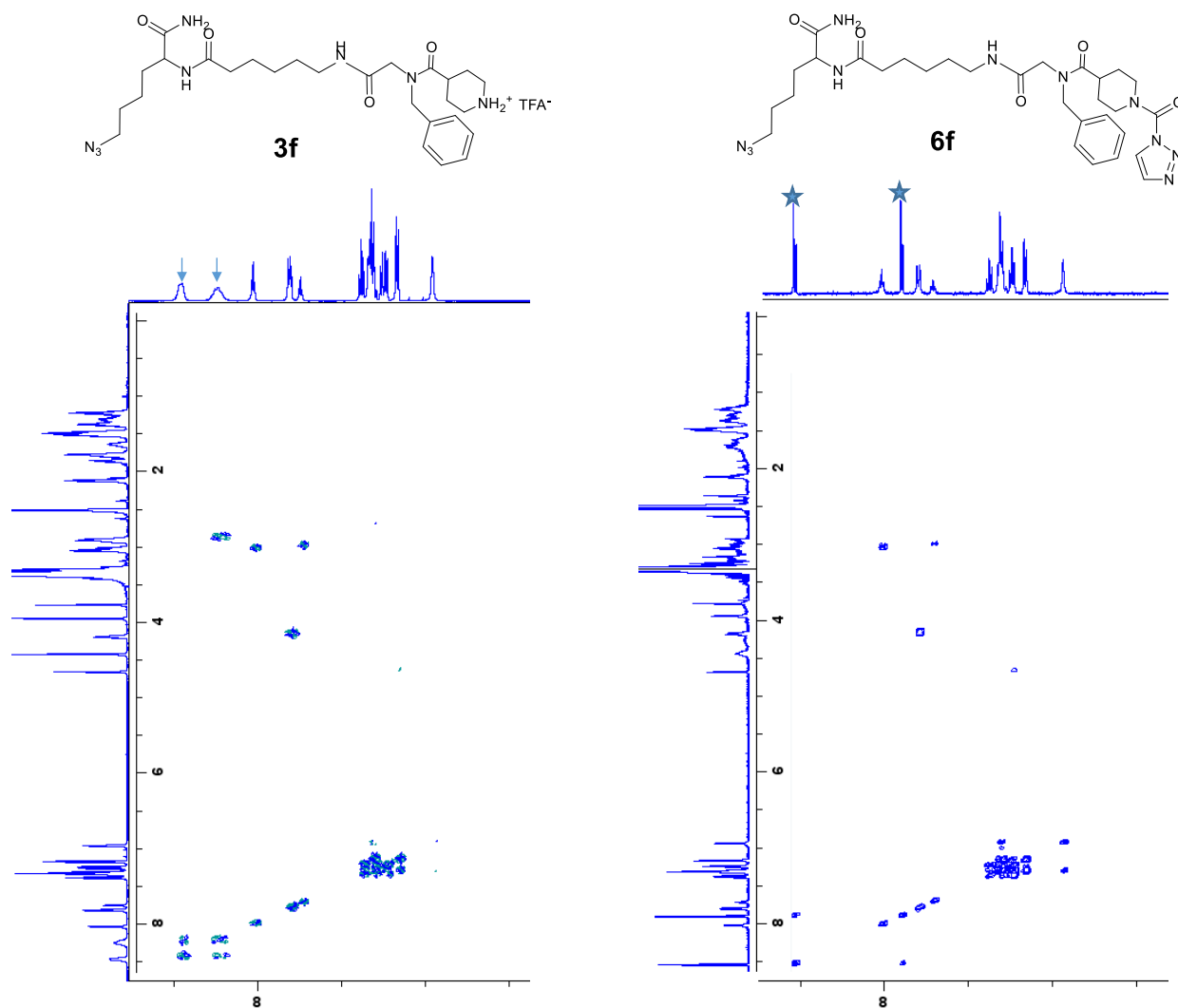
Figure S3.7. Triazole urea structure elucidation. In order to identify whether we formed the N^1- or N^2-isomers for compounds **4f-6f**, we synthesized compounds **3f** and **6f** in larger quantities and measured [1]HH-COSY spectra (DMSO-d6, 600 MHz). In the **3f** spectrum we see two broad signals (↓) at 8.25 and 8.4 ppm. We mark these as the two –NH$_2^+$- protons in the piperidine moiety, because they couple with each other and one couples with aliphatic protons. In the **6f** spectrum, these protons are no longer present and we see two doublets (★) at 8.5 and 7.9 ppm. The fact that they couple to each other leads us to believe that they are the two chemically different triazole protons as we would expect for a N^1-triazole urea.

3.6.3. References supplementary information

[1]   E. D. Goddard-Borger, R. V. Stick, *Org. Lett.* **2007**, *9*, 3797–3800.
[2]   T. J. Sminia, D. S. Pedersen, *Synlett* **2012**, *23*, 2643–2646.

Chapter IV: Recognition element optimization of triazole-urea activity-based probes for acyl protein thioesterases-1/2

This Chapter is based on a manuscript in preparation by Roeland Vanhoutte and Steven H. L. Verhelst

Abstract

Acyl protein thioesterases are enzymes that hydrolyze fatty acid thioesters on cysteine residues of proteins. The two main protein depalmitoylases APT-1 and APT-2 have a very high degree of similarity and show substantial overlap in substrate utility. Activity-based probes that are isoform-selective are needed to study the individual functions and substrate specificities of APT-1 and -2 have not been discovered yet. In this chapter, a solid-phase synthesis procedure is used to synthesize a library of triazole urea probes based on two APT-1/2 dual labelling probes that were reported in Chapter III by altering their recognition elements. Three new ABPs were discovered that are more potent in labeling APT-1/2 than the original hit compounds. The isoform selectivity of these new probes was low however. The binding kinetics of these probes on APT-1 were assessed and their potency to be used in live cell labelling was shown on A431 cells.

4.1. Introduction

Protein palmitoylation is the process of the attachment of the 16-carbon fatty acid palmitate, or other fatty acids that are 14-20 carbons long, onto cysteine residues of proteins.[1,2] It is a dynamic and frequently occurring post-translational modification that alters protein trafficking, membrane localization, stability and conformation of proteins, and protein-protein interactions.[3] The thioester bonds formed in S-palmitoylation can be hydrolyzed by enzymes, in contrast to other similar post-translational modifications involving the attachment of fatty acids, such as *S*-prenylation (thioether) and *N*-myristoylation (amide).[4] Palmitoylation of proteins is catalyzed by zDHHC enzymes. There are 23 zDHHC enzymes known in human, which all share a distinct aspartate-histidine-histidine-cysteine motif in their catalytic domain.[5] Protein depalmitoylases are enzymes that catalyze the removal of fatty acid thioesters on cysteine residues from proteins. Protein depalmitoylases include acyl protein thioesterases 1 and 2 (APT-1, APT-2)[6,7] and the ABHD17-family, which is involved in N-Ras depalmitoylation.[8] The process of protein depalmitoylation remains poorly understood, partly because little is known about APT-1 and APT-2, including the reason why these two seemingly alike enzymes exist simultaneously.[9]

APT-1 and APT-2 are serine hydrolases with an active site Ser-His-Asp catalytic triad. They have an atypical α/β-hydrolase fold and a hydrophobic cleft that facilitates the binding of an acyl chain. Although they are primarily located in the cytoplasm, they can also attach to and detach from the plasma membrane and internal membranes via cycles of acylation and auto-deacetylation. Both enzymes have a large overlap in substrate utilization, with only a handful of preferred substrates identified for APT-1 [10] and APT-2[6,11]. There is a need for selective tools for each of the isoforms of these enzymes to shed light on the differences in their activity and localization as well as their substrate specificity. These tools are hard to develop, because both enzymes have a structural similarity of 81%. The Martin group has managed to create reversible inhibitors ML-348 and ML-349 for respectively APT-1 and APT-2 that allow the selective inhibition of both enzymes.[4] No selective ABPs have been reported for these enzymes however. The aim of the experiments in this chapter was to increase the selectivity of the triazole urea ABPs developed in Chapter III towards isoform-selective ABPs for APTs. To this end, the strength of the solid-phase synthesis approach developed in the previous chapter was used to create many ABPs in a fast manner. Specifically, the strategies employed consisted of adjusting the recognition elements of probes **5f** and **6f** with different aromatic moieties and heterocycles. Two synthetic strategies were applied: adjusting the piperidine/piperazine rings of **5f** and **6f** onto which the triazole urea warhead is formed and substituting the phenyl ring of the Phe peptoid of **5f**. By changing the recognition elements, the binding mode of the probe to the enzymes is altered, which could lead to a structure that binds significantly stronger to one of the isoforms.

4.2. Results and discussion

The first series of probes in this chapter were made by adjusting the the piperazine/piperidine moieties in **6f** and **5f** (Scheme **4.1**). Two analogous structures of **6f** were made: one in which a N^1,N^2-dimethylethane-1,2-diamine was used as ring-opened form of the piperazine ring (**7a**), and one in which the piperazine ring was expanded to a homopiperazine ring (**7b**). In the compounds made analogous to **5f**, **7c** and **7d**, the piperidine ring in **5f** was replaced with two contracted rings, respectively a pyrrolidine and an azetidine. All four probes were synthesized fully analogous to the procedures described in Chapter III for the synthesis of **5f** and **6f**, apart from the different heterocycles that were coupled in reactions g,h,I and j.
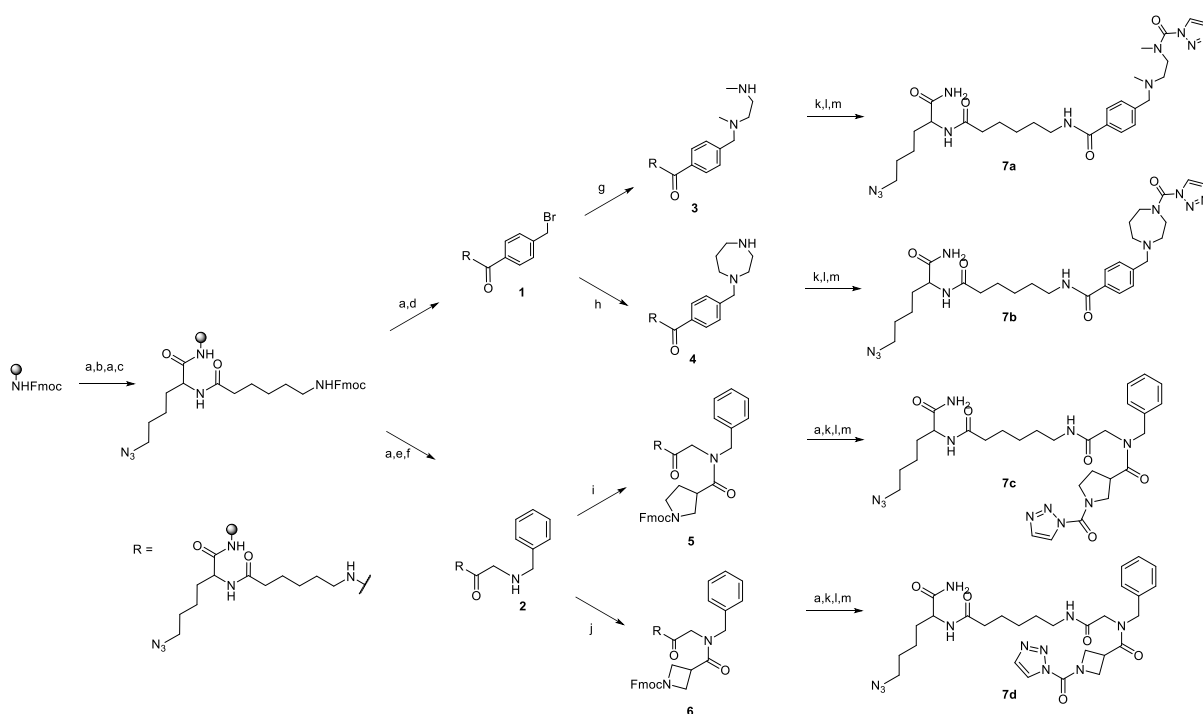
Scheme 4.1. Synthesis towards compounds **7a-d**. a) DMF/piperidine 4/1, 5 min. b) Fmoc-Lys(N$_3$)-OH, HBTU, DIEA, DMF; c) Fmoc-Ahx-OH, HBTU, DIEA, DMF; d) p-Bromomethylbenzoic acid, PyBrOP, DIEA, DMF; e) Bromoacetic acid, DIC, HOBt, DMF; f) Benzylamine, DIEA, DMF; g) N^1,N^2-dimethylethane-1,2-diamine, DIEA, DMF; h) Homopiperazine, DIEA, DMF; i) Fmoc-Pyr-OH, DIC, HOBt, DMF; j) Fmoc-Azt-OH, DIC, HOBt, DMF; (k) Triphosgene, DIEA, DCM, 30 minutes; l) 1H-1,2,3-triazole, DIEA, DCM; m) TFA/TIS/water 95/2.5/2.5.
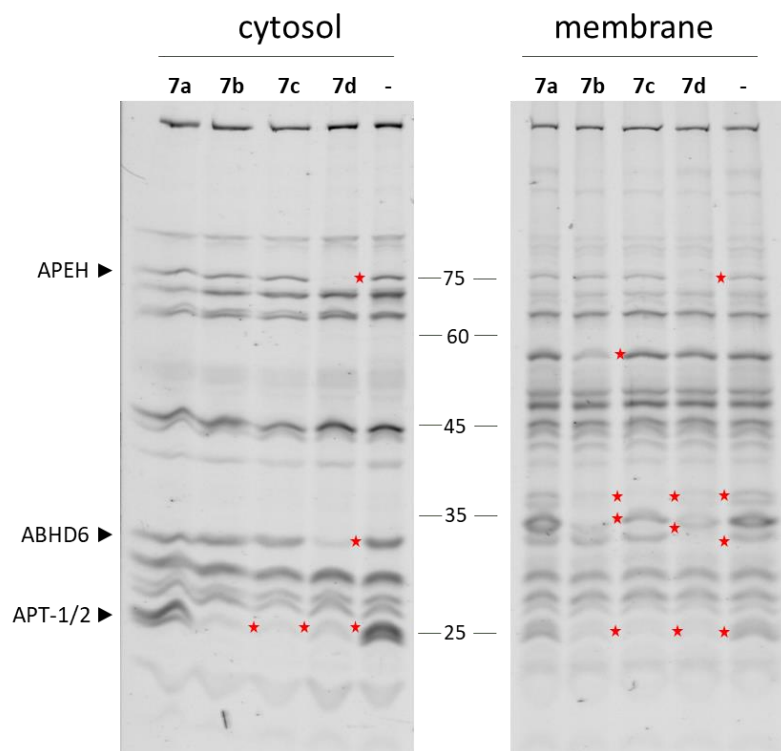
Figure 4.1. Screening of probes **7a-d** for inhibition by competitive ABPP. Fluorescent gels of competitive ABPP in the cytosolic fraction (left panel) or membrane fraction (right panel) of mouse brain lysates. Pretreatment of lysate with the indicated probe (100 µM) was followed by measurement of residual SH activity with FP-Rh.

The resulting probes **7a-d** were first tested for SH reactivity on the cytosolic and membrane fraction of mouse brain lysate (Figure **4.1**). By using this model, it was possible to make a direct comparison with probes **5f** and **6f**, described in Chapter III. At 100 µM probe concentration, probe **7a** was non-reactive for any FP-Rh targets, but probes **7b-d** showed reactivity for APT-1/2 and another 2 or 3 targets labeled by FP-Rh, including bands previously identified as ABHD6 and APEH. Interestingly, ABHD6 was competed by **7d** and not by **7b**, although for their parent compounds, respectively **5f** and **6f**, this reactivity is the other way around.
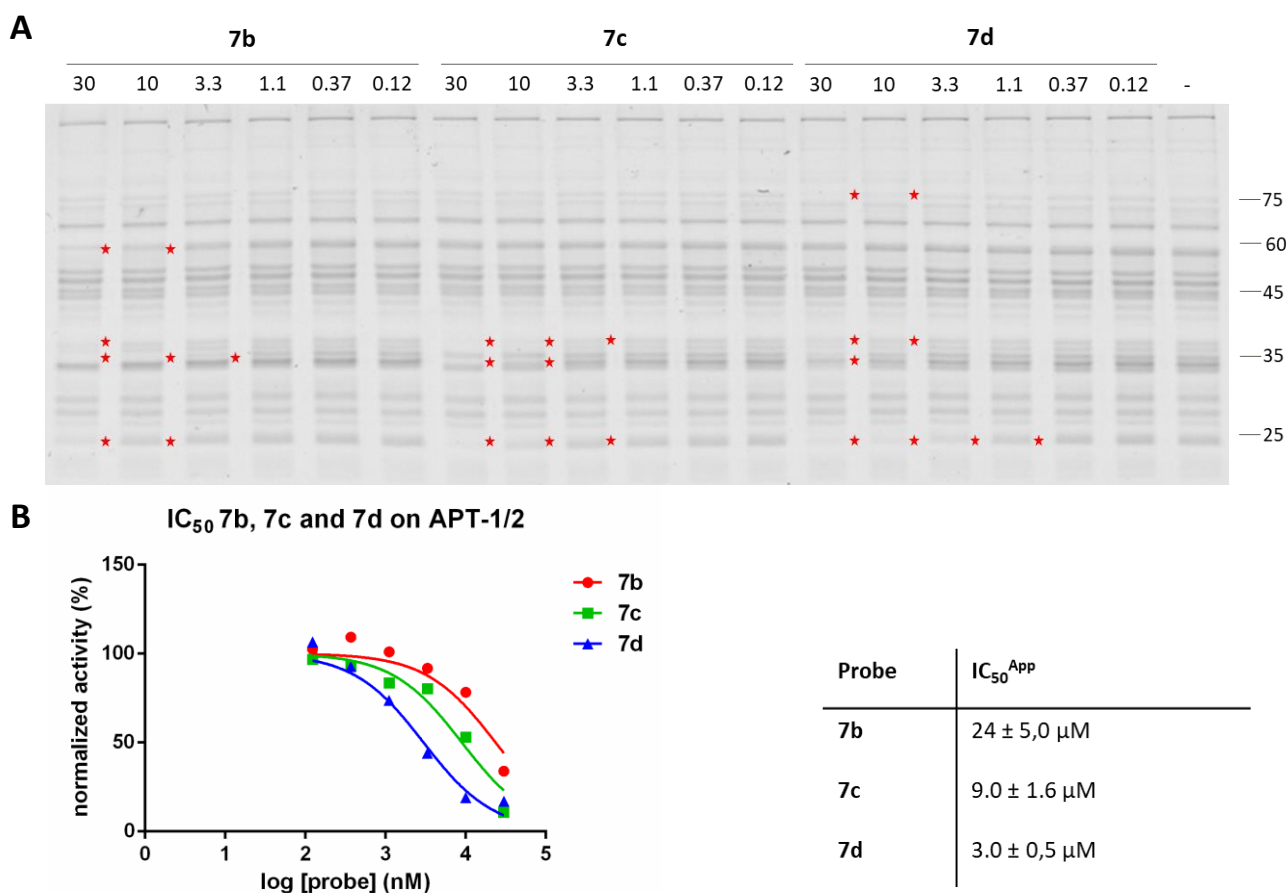
Figure 4.2. A. Gel-based IC_{50}^{App} determination of **7b**, **7c** and **7d** on mouse brain membrane fraction. Inhibited targets are marked with a red star. Probe concentrations are given in µM above gel lanes. **B.** Inhibition curve of **7b**, **7c** and **7d** on APT-1/2 (left) with IC_{50}^{App} values (right). Apparent IC_{50} curves were determined by competitive ABPP of serial dilutions, followed by quantification using gel band densitometry.

Apparent IC_{50} values were assessed on the membrane targets to determine the reactivity of the probes for their targets (Figure **4.2A**). Probe reactivity on all targets was in the low micromolar range, with no probes showing any relevant activity below 1 µM. Probe **7d** showed the most selectivity of all probes for APT-1/2 over its other three targets. For probes **7b** and **7c**, activity and selectivity for all targeted enzymes was low. The IC_{50}^{App} for mouse APT-1/2 decreased for all probes by a factor of more than 100 (Figure **4.2B**), indicating that, while four-, five- and seven-membered rings increase the probe reactivity for other SHs, for APT reactivity a six-membered piperidine or piperazine ring is preferred in the recognition element of this type of ABP.
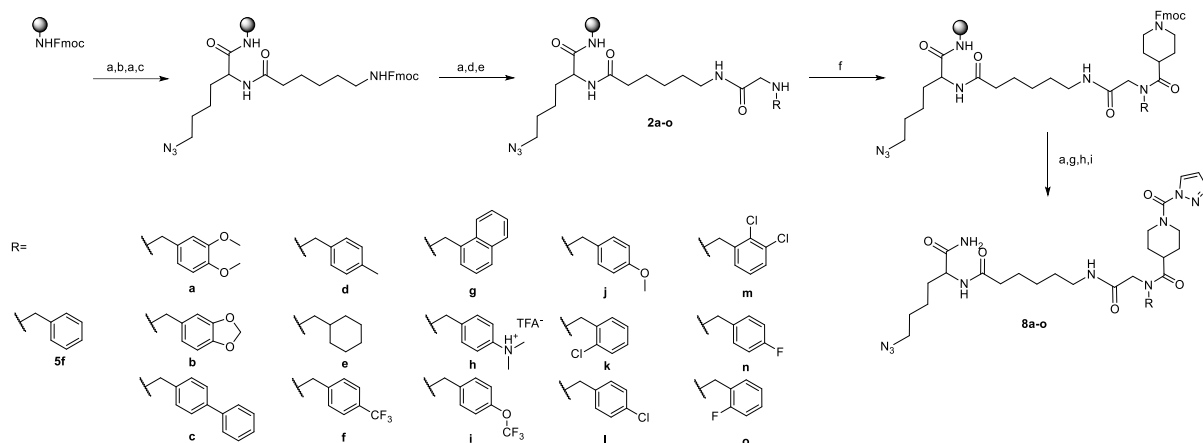
Scheme 4.2. Synthesis towards compounds **8a-o**. a) DMF/piperidine 4/1. b) Fmoc-Lys(N$_3$)-OH, HBTU, DIEA, DMF. c) Fmoc-Ahx-OH, HBTU, DIEA, DMF. d) Bromoacetic acid, DIC, HOBt, DMF. e) R-NH$_2$, DIEA, DMF. f) Fmoc-Inp-OH, DIC, HOBt, DMF. (g) Triphosgene, DIEA, DCM, 30 minutes. h) 1H-1,2,3-triazole, DIEA, DCM. i) TFA/TIS/water 95/2.5/2.5.

Next, it was explored whether modifications of the Phe peptoid in the recognition element of **5f** can lead to a more potent probe for APT-1/2 or a more selective probe for one of the isomers. A new probe library of 15 ABPs was constructed on solid phase with variations in the phenyl group in the recognition element. These variations included the addition of electron donating goups, such as ethers, amines or alkyl groups; the addition of electron withdrawing groups, such as trifluoromethyl groups or halogenides; and changing the phenyl group to a naphthyl, biphenyl or cyclohexyl. For the synthesis of these compounds, the same procedures were followed as described in Chapter III to create **5f**, with the difference being the use of substituted benzylamines or cyclohexyl methylamine instead of benzylamine.
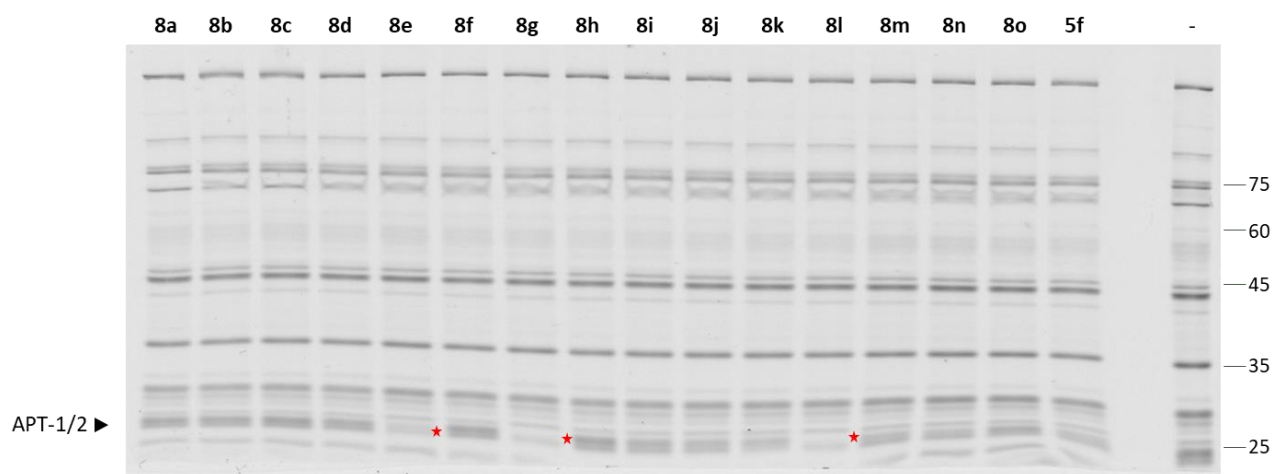
Figure 4.4. Competition of 5 nM probe with 1 µM FP-Rh on mouse brain lysate cytosolic fraction. Probes that show increase in APT-1/2 reactivity compared to **5f** are indicated with a red star.

These compounds were tested on the cytosolic fraction of mouse brain lysate at different concentrations in competition with FP-Rh. A first test was done at 5 nM concentration, which is roughly half the apparent IC_{50} of parent compound **5f** (Figure **4.4**) for mouse APT-1/2. At this concentration, probes **8e** (with no aromatic side chain), **8g** (with a naphthyl sidechain) and **8l** (with a *p*-chlorophenyl sidechain) showed a higher activity for APT-1/2 than **5f**. It is striking that these three probes all have a different type of ring in their recognition element and that similar probes to **8l**, such as **8f** and **8n**, showed no increased activity.
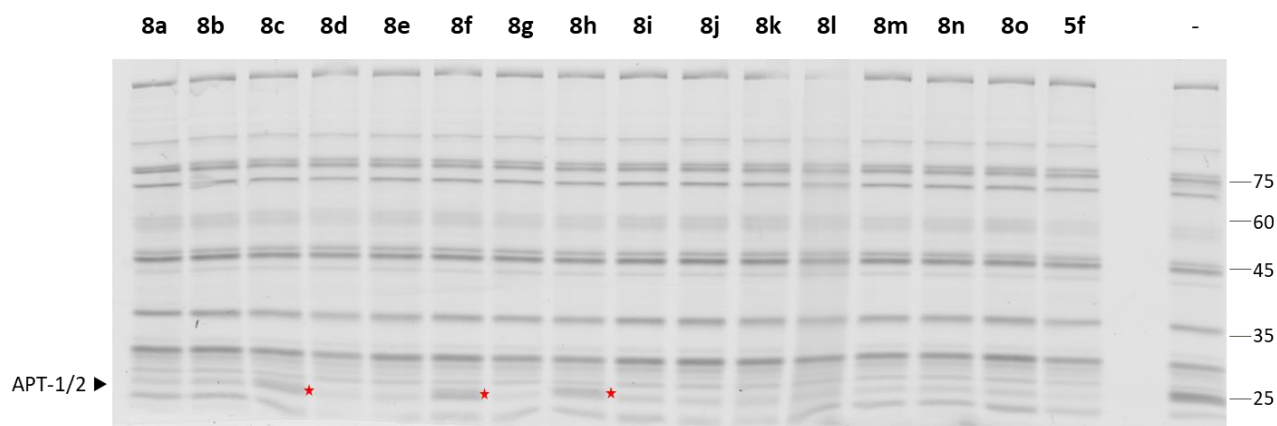
Figure 4.5. Competition of 50 nM probe with 1 µM FP-Rh on mouse brain lysate cytosolic fraction. Probes that show strong decrease in APT-1/2 activity compared to **5f** are indicated with a red star.

A second screening of the probes was done at 50 nM concentration on the same lysate to have an indication of which types of recognition elements have a negative effect on APT-1/2 reactivity (Figure **4.5**). Probes **8c** (with a biphenyl sidechain), **8f** (with a *p*-trifluoromethylphenyl sidechain) and **8h** (with a *p*-dimethylaminophenyl sidechain) showed little reactivity. This result demonstrates a specific tolerance by the enzymes for the substituents on the phenyl rings of the probes, since closely related structures as **8g** to **8c** and **8l** to **8f** cause an increase in the reactivity.
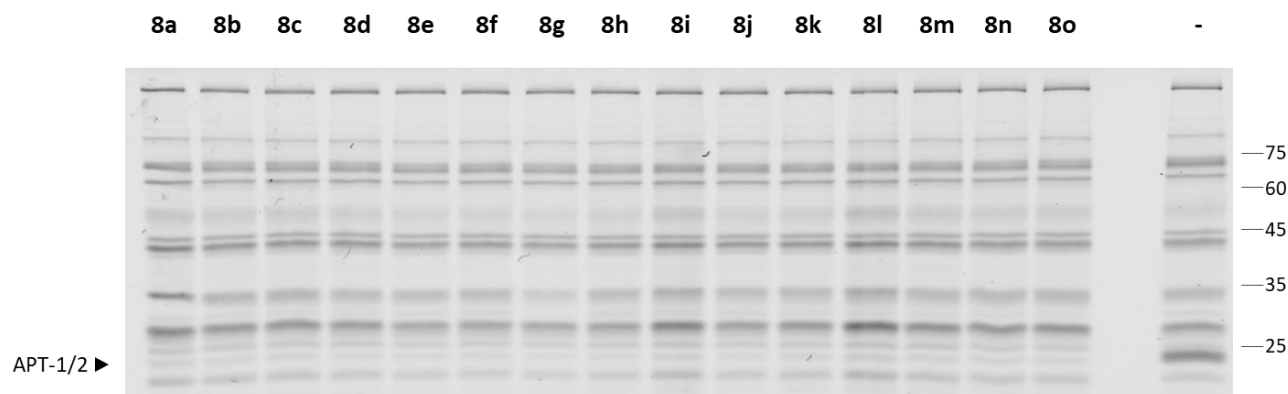
Figure 4.6. Competition of 1 µM probe with 1 µM FP-Rh on mouse brain lysate cytosolic fraction. No probes show labelling of any enzyme that is an FP-Rh target other than APT-1/2.

To assess whether these probes show any significant reactivity for other targets of FP-Rh than APT-1/2, a final variant on this experiment was done at probe concentrations of 1 µM (Figure **4.6**). None of the probes show any measurable activity for off-targets at this concentration, which is much higher than the concentration needed for full labelling of the targets. This shows that the probes can be used to label APT-1/2 selectively to some extent, although assessment on other proteomes and using chemical proteomics is required to get absolute data on their selectivity.

A direct labelling experiment on A431 lysates, in which the proteome was incubated with probes **8e**, **8g**, **8l** and **5f** followed by click chemistry to visualize any targets showed that the probes also do not label any non FP-Rh targets in A431 cells (Figure **4.7**).
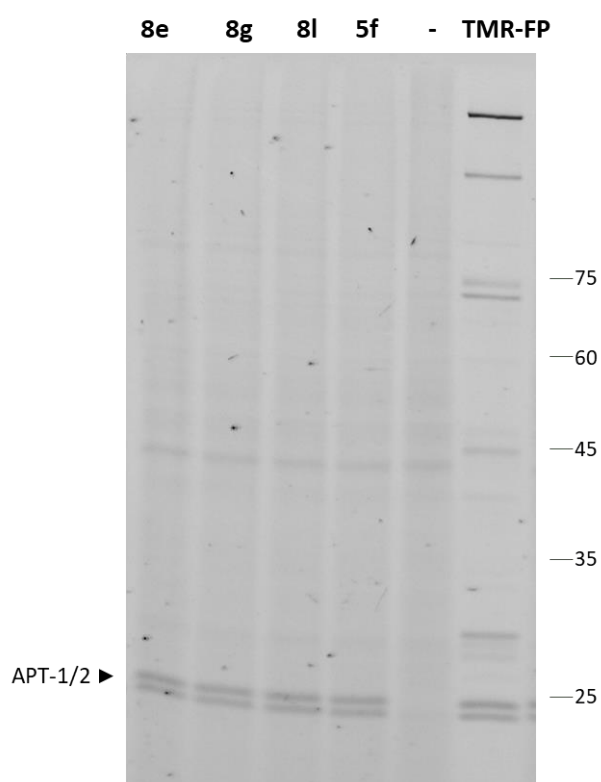
Figure 4.7. Incubation of A431 lysates with probes **8e**, **8g**, **8l** and **5f**, followed by click chemistry with a TAMRA-alkyne fluorophore shows selective no other targets than the ATP-1/2 gel bands. DMSO control (-) shows click background.

IC_{50}

8e: 28 ± 2.6 nM
8g: 17 ± 2.0 nM
8l: 13 ± 1.4 nM
5f: 43 ± 4.8 nM

IC_{50}

8e: 35 ± 5.5 nM
8g: 16 ± 2.3 nM
8l: 22 ± 2.0 nM
5f: 30 ± 7.0 nM
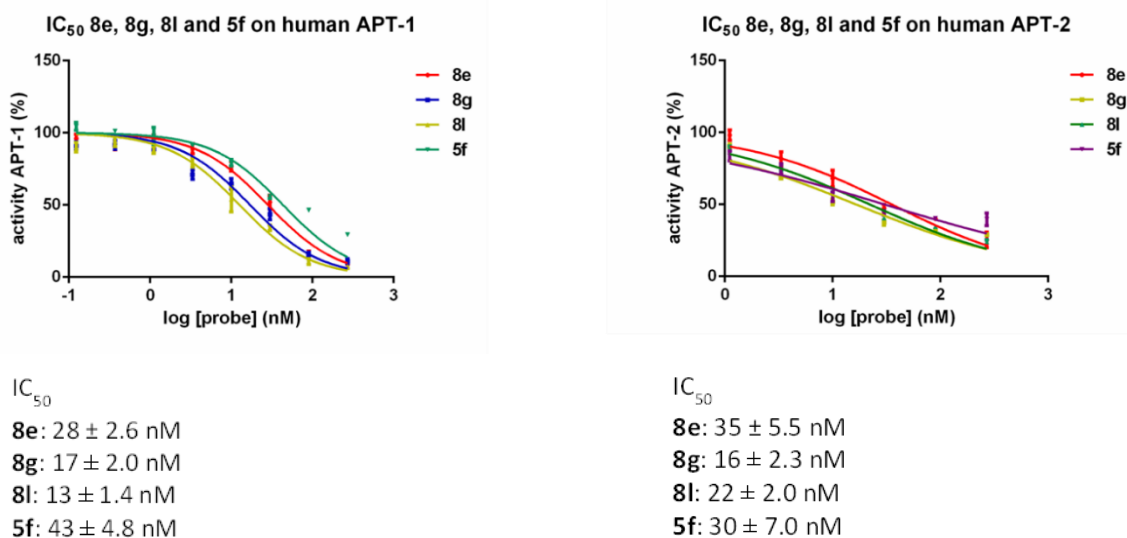
Figure 4.8. Inhibition curve of **8e**, **8g**, **8l** and **5f** on human APT-1 and APT-2 with IC_{50}^{App} values. Apparent IC_{50} curves were determined by competitive ABPP of serial dilutions on purified human APT-1 and APT-2, followed by quantification using gel band densitometry. Inhibition was measured three times for each probe concentration.

To obtain more relevant information about the probes on their applicability in human models, the IC_{50}^{App} was determined on commercially available human APT-1 (Figure **4.8**, left panel) and APT-2 (Figure **4.8**, right panel). This allows us to determine whether the probes show any selectivity for one of the APTs. Gel-based assessment showed however that the IC_{50}^{App} values between APT-1 and APT-2 are very similar for all probes, with a 1.8 factor difference for probe **8l** being the highest difference in reactivity. Although this means that selective labelling of one of the APTs with these probes is not possible, the effect of selective labelling can still be achieved by co-incubation with a dual-labeling APT-1/2 probe and a selective inhibitor of one of the two APTs.
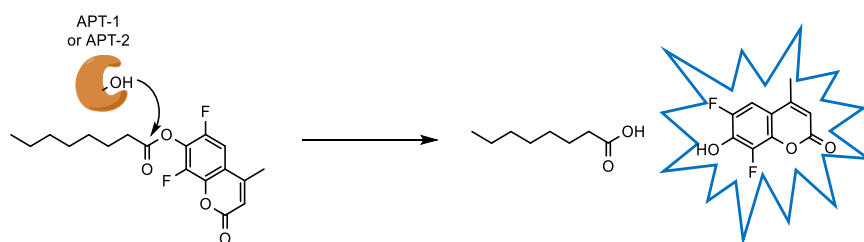
Figure 4.9. Schematic overview of the hydrolysis of DIFMU-octanoate by APT-1 and APT-2 to the fluorescent DIFMU.

As all probes described in this chapter are covalent inhibitors, IC_{50} values are dependent on the time of incubation with the enzyme. To gain an absolute quantification of probe reactivity, the binding kinetics of **8e**, **8g**, **8l** and **5f** to APT-1 were measured. By quantifiying the turnover of the fluorescent DIFMU-octanoate by APT-1 during the simultaneous enzyme inhibition by a titration series of probe concentrations (Figure **4.9**), the k_{obs} was determined for the binding of 5 concentrations per probe.

69
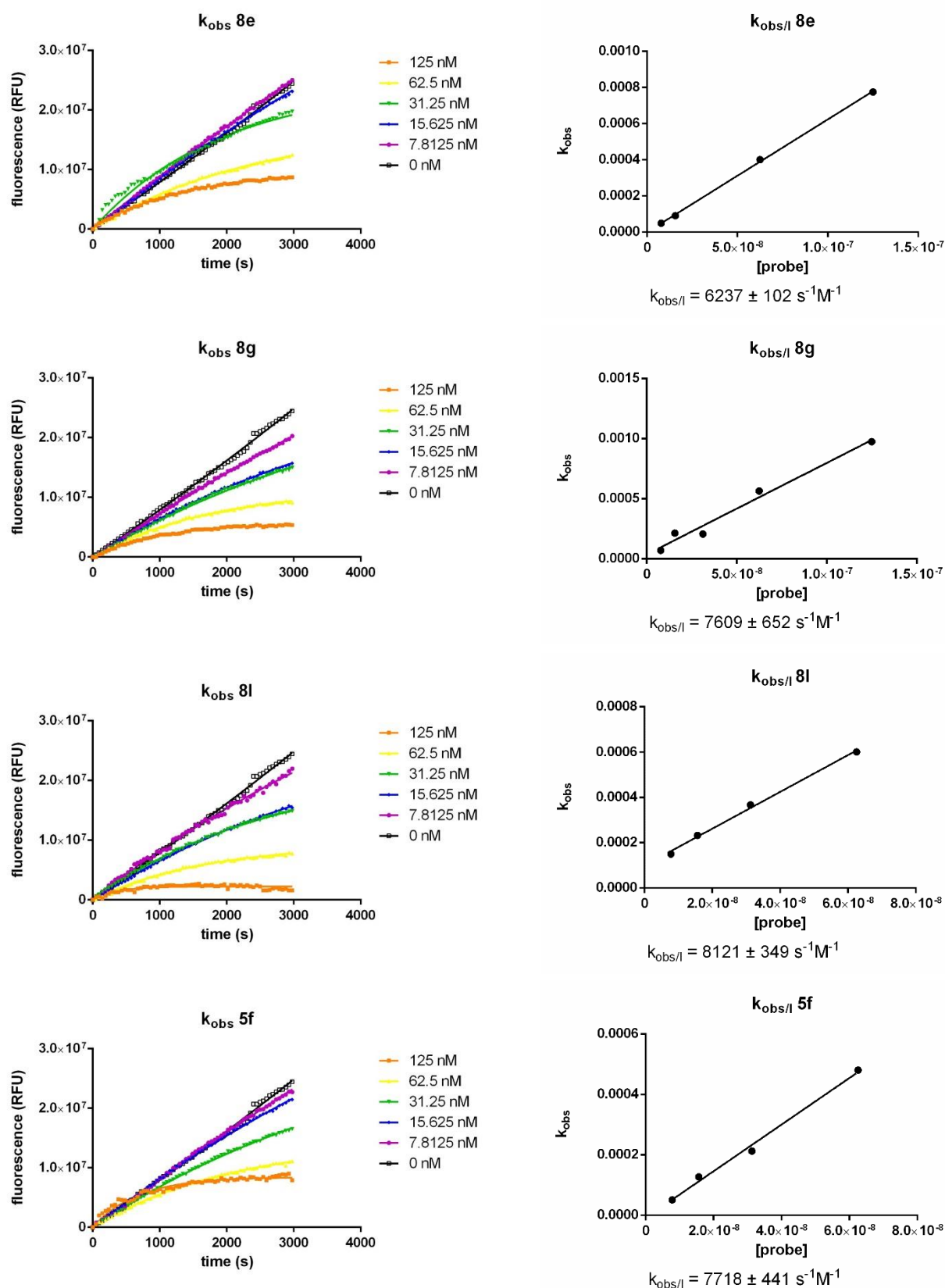
Figure 4.10. Kinetic assessment of APT-1 inhibition with probes **8e**, **8g**, **8l** and **5f**. $k_{obs/I}$ for probes **8e**, **8g**, **8l** and **5f** was calculated by determining the k_{obs} of a range of dilutions on the inhibition of APT-1 via measuring the hydrolysis of DIFMU-octanoate by the enzyme (left panel) and plotting the k_{obs} values to their respective probe concentration (right panel).

Plotting these k_{obs} values to probe concentrations gave a linear slope of k_{obs}/I values (Figure **4.10**), which suggests that the probes form a very short living non-covalent probe-enzyme complex with APT-1 that rapidly forms a covalent bond when formed.[12] The fast binding of these probes correlates with their low IC_{50}^{App} values for APT-1 and could explain the strong difference in potency observed in chapter III between probes with a triazole urea warhead and probes with other serine reactive warheads.[13]

The observed k_{obs}/I values were similar for all four probes, with probe **8l** having a slightly higher k_{obs}/I, ($8.1*10^3 \pm 0.35*10^3$ $s^{-1}M^{-1}$) indicating a slightly faster binding to the enzyme, and probe **8g** ($6.2*10^3 \pm 0.10*10^3$ $s^{-1}M^{-1}$) binding slower. Overall these values indicate that the effect of the different recognition elements of these probes on the inhibition kinetics is rather low.
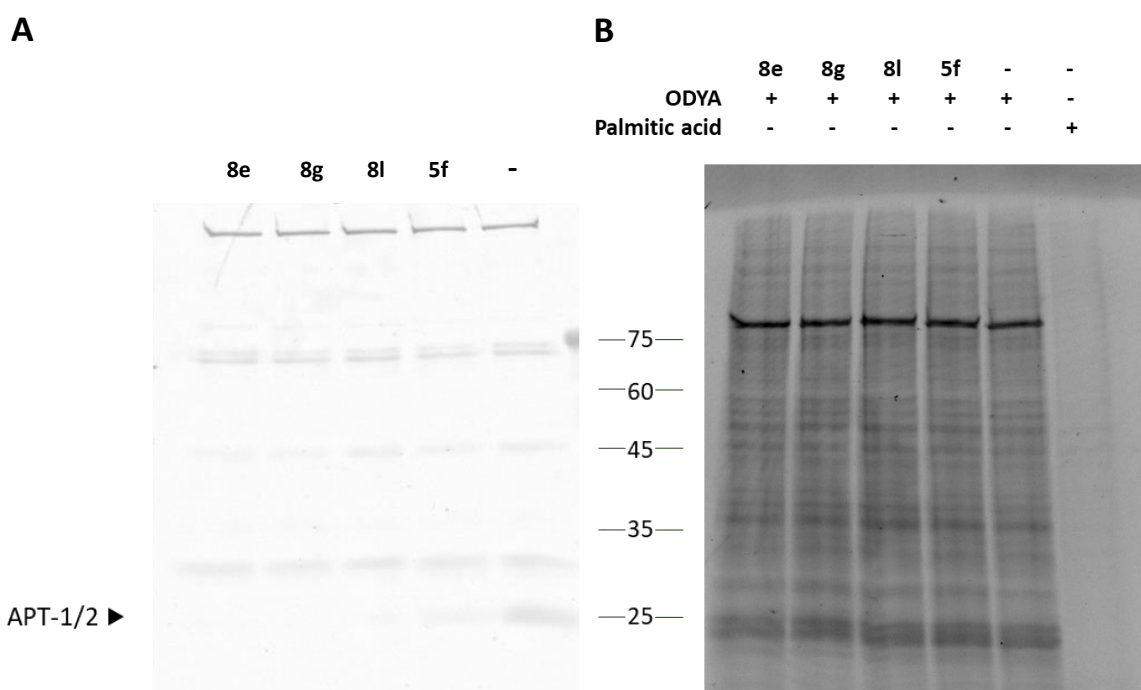
Figure 4.11. A. Inhibition of APT-1/2 by compounds **8e**, **8g**, **8l** and **5f** in live A431 cells. After treatment, compound was washed out, and residual SH activity in cell lysates was detected with FP-Rh. **B.** Metabolic labelling with 17-ODYA on A431 cells. Cells were treated with 17-ODYA and indicated probe, prior to lysis and click labelling with TMR-N_3.

Finally, it was assessed whether the probes can be used for the labeling of APT-1/2 in live cells. To this end, live A431 cells were incubated with probes **8e**, **8g**, **8l** and **5f** and treated with FP-Rh after lysis (Figure **4.11A**). The inhibition of the APT-1/2 bands by all probes show that full inhibition of the targets is achieved after 2h of treatment.

Given the fact that the probes are cell-permeable, it was investigated whether they could affect the inhibition of depalmitoylation of in live cells. To verify this, A431 cells were treated with the clickable palmitic acid analogue 17-octadecynoic acid (17-ODYA), during simultaneous inhibition of APT-1/2 with one of probes **8e**, **8g**, **8l** or **5f** (Figure **4.11B**). After lysis of the cells and click chemistry with TMR-

N_3, no visible increase in palmitoylation was observed in the probe-treated samples compared to the control sample. This indicates that other enzymes such as the ABHD17 enzyme family can depalmitoylate the substrates targeted by APT-1/2. This is in accordance to the results reported by Won et al.[14]

4.3. Conclusion

In conclusion, this chapter describes the optimization of a dual-labelling APT-1/2 probe to more reactive ABPs for APT-1/2 by changing the recognition elements of the probes. The solid-phase synthesis strategies that were used allowed the synthesis of a combinatorial probe library within short time and shows the advantages of full on-resin synthesis of ABPs. It was found that substitution of the piperidine and piperazine moieties in the recognition elements of probes **5f** and **6f** has a negative impact on probe reactivity and selectivity to APT-1/2. On the other hand, several alterations can be made to the Phe peptoid of the recognition element of **5f** increase the probe reactivity. Three probes with higher reactivity were found this way, bearing a *p*-chlorophenyl, naphthyl or cyclohexyl group in their recognition element. The probes showed selectivity for APT-1/2 over other enzymes, cell permeability in live cells and binding kinetics to APT-1 that suggests the rapid formation of a covalent bond between probe and enzyme. Although none of the probes in this study showed any significant selectivity for one of the APT isoforms, selective labelling of one of the APTs could still be achieved in cells by co-incubating the probe with a selective APT-1 or APT-2 inhibitor, such as ML-348 or ML-349. Furthermore, these probes make a good starting point for the development of a selective APT-probe, for example by expanding the peptide sequence of the recognition element.

4.4. Experimental section

General materials and methods
All starting materials for chemical reactions were purchased from commercial suppliers and used without purification. All solvents were of synthesis grade or higher. LC-MS spectra were recorded on a Prominence Ultra-fast Liquid Chromatography system (Shimadzu) using a Waters X-bridge 2.1 mm C18 column with a gradient of 5%-80% acetonitrile in water (with 0.1% formic acid) over 22 min. HPLC purification was performed on a Prominence Ultra-fast Liquid Chromatography system (Shimadzu) using a Waters X-bridge 150 mm C18 prep column with a gradient of acetonitrile in water (with 0.1% trifluoroacetic acid) over 22 min. Purity >95% of all final compounds was assessed by integration of the HPLC spectra.

Solid phase chemistry procedures
Fmoc protected Rink amide resin (1.35 g, 0.74 mmol/g) was treated with 20% piperidine in DMF for 5 min to swell the resin and deprotect the Fmoc group. Next, the resin was washed three times with DMF. All following Fmoc deprotections were performed according to this procedure.

Backbone synthesis

Method 1. Fmoc-L-Lys(N₃)-OH was coupled to 1 mmol of deprotected rink amide resin by adding amino acid (1.5 eq.), HBTU (1.5 eq.) and DIPEA (3 eq.) in 4 mL of DMF to the resin and incubating for 4 hours at room temperature. After this and each following coupling or S_N2 substitution, the resin was washed three times with DMF and three times with DCM. After deprotection, Fmoc-6-aminohexanoic acid was coupled by adding amino acid (2 eq.), HBTU (2 eq.) and DIPEA (4 eq.) in 4 mL DMF to the resin and incubating overnight at room temperature.

Recognition element synthesis

After synthesis of the common peptide backbone, the resin was divided into different batches to form the different recognition elements. Peptide bonds in recognition elements were formed with the corresponding (amino)acid (3 eq.), DIC (3 eq.) and HOBt (3 eq.) in 250 µL DMF overnight at room temperature unless stated otherwise.

Method 2.1. 4-Bromomethyl phenylacetic acid (3 eq.) was coupled to 10 µmol of peptide backbone with PyBrOP (3 eq.) and DIPEA (6 eq.) in 250 µL DMF overnight at room temperature. Subsequently, the bromide was substituted for homopiperazine (20 eq.) using DIPEA (10 eq.) in 250 µL DMF overnight at room temperature to give intermediate **3**.

Method 2.2. 4-Bromomethyl phenylacetic acid (3 eq.) was coupled to 10 µmol of peptide backbone with PyBrOP (3 eq.) and DIPEA (6 eq.) in 250 µL DMF overnight at room temperature. Subsequently, the bromide was substituted for N^1,N^2-dimethylethane-1,2-diamine (20 eq.) using DIPEA (10 eq.) in 250 µL DMF overnight at room temperature to give intermediate **4**.

Method 2.3. Phe-peptoid was formed by coupling Br-acetic acid (3 eq.) to 10 µmol of peptide backbone under standard SPPS conditions and subsequent substitution with benzylamine (20 eq.) and DIPEA (10 eq.) in 250 µL DMF overnight at room temperature. Next, Fmoc-3-Pyrrolidinic acid was coupled using standard SPPS conditions.

Method 2.4. Phe-peptoid was formed by coupling Br-acetic acid (3 eq.) to 10 µmol of peptide backbone under standard SPPS conditions and subsequent substitution with benzylamine (20 eq.) and DIPEA (10 eq.) in 250 µL DMF overnight at room temperature. Next, Fmoc-3-Azetidinic acid was coupled using standard SPPS conditions.

Method 2.5. Phe-peptoid was formed by coupling Br-acetic acid (3 eq.) to 10 µmol of peptide backbone under standard SPPS conditions and subsequent substitution with the indicated amine (20 eq.) and DIPEA (10 eq.) in 250 µL DMF overnight at room temperature. Next, Fmoc-Isonipecotic acid was coupled using standard SPPS conditions.

Warhead coupling

Formation of 1,2,3-triazole urea's was done on the theoretical quantity of 10 µmol after the formation of the recognition elements.

Method 3.: Resin (1 eq.) was swollen in 1 mL dry DCM, to which DIEA (15 eq.) and triphosgene (3 eq.) were added. Reactions were shaken at room temperature for 30 min, after which the cartridge was drained into a solution of 10% NaOH in water. The resin was washed three times with dry DCM, which was drained into a 10%NaOH solution. Next, the resin was resuspended in 1 mL dry DCM, to which 10 equivalents of 1*H*-1,2,3-triazole was added. Reactions were shaken overnight at room temperature and checked for completion using LC-MS. After completion, the resin was washed three times with DCM. Probes were then cleaved from the resin by using a 95:2.5:2.5 mixture of TFA:TIS:water.

N-(1H-1,2,3-triazol-1-yl-carbonyl)-4-(homopiperazinyl-methyl)-benzoyl-6-aminohexanoyl-L-ε-azidolysine amide (7a)
Probe **7a** was synthesized using subsequently methods 1, 2.1 and 3 and purified using HPLC. The product was obtained as a white powder. HRMS (MALDI-TOF): m/z calcd. for $C_{28}H_{41}N_{11}O_4Na$ [M+Na]$^+$ 618.3241, found: 618.3346.

N-(1H-1,2,3-triazol-1-yl-carbonyl)-4-(N^1,N^2-dimethylethynyl-1,2-diaminyl-methyl)-benzoyl-6-aminohexanoyl-L-ε-azidolysine amide (7b)
Probe **7b** was synthesized using subsequently methods 1, 2.2 and 3 and purified using HPLC. The product was obtained as a white powder. HRMS (MALDI-TOF): m/z calcd. for $C_{27}H_{41}N_{11}O_4Na$ [M+Na]$^+$ 606.3241, found: 606.3878.

N-(1H-1,2,3-triazol-1-yl-carbonyl)-pyrrolidinyl-(N-benzyl)glycyl-6-aminohexanoyl-L-ε-azidolysine amide (7c)
Probe **7c** was synthesized using subsequently methods 1, 2.3 and 3 and purified using HPLC. The product was obtained as a white powder. HRMS (MALDI-TOF): m/z calcd. for $C_{29}H_{41}N_{11}O_5Na$ [M+Na]$^+$ 646.3190, found: 646.3519.

N-(1H-1,2,3-triazol-1-yl-carbonyl)-azetidinyl-(N-benzyl)glycyl-6-aminohexanoyl-L-ε-azidolysine amide (7d)
Probe **7d** was synthesized using subsequently methods 1, 2.4 and 3 and purified using HPLC. The product was obtained as a white powder. HRMS (MALDI-TOF): m/z calcd. for $C_{28}H_{39}N_{11}O_5Na$ [M+Na]$^+$ 632.3033, found: 632.3310.

N-(1H-1,2,3-triazol-1-yl-carbonyl)-isonipecotyl-(N-piperonyl)glycyl-6-aminohexanoyl-L-ε-azidolysine amide (8a)
Probe **8a** was synthesized using subsequently methods 1, 2.5 with piperonylamine and 3 and purified using HPLC. The product was obtained as a white powder. (0.40 mg, yield = 5.9%) HRMS (MALDI-TOF): m/z calcd. for $C_{31}H_{43}N_{11}NaO_7$ [M+Na]$^+$ 704.3245, found: 704.3965.

N-(1H-1,2,3-triazol-1-yl-carbonyl)-isonipecotyl-(N-4-methylbenzyl)glycyl-6-aminohexanoyl-L-ε-azidolysine amide (8b)
Probe **8b** was synthesized using subsequently methods 1, 2.5 with 4-methylbenzylamine and 3 and purified using HPLC. The product was obtained as a white powder. (0.21 mg, yield = 3.2) HRMS (MALDI-TOF): m/z calcd. for $C_{31}H_{45}N_{11}NaO_5$ [M+Na]$^+$ 674.3503, found: 674.3741.

N-(1H-1,2,3-triazol-1-yl-carbonyl)-isonipecotyl-(3,4-dimethoxybenzyl)glycyl-6-aminohexanoyl-L-ε-azidolysine amide (8c)
Probe **8c** was synthesized using subsequently methods 1, 2.5 with 4-methylbenzylamine and 3 and purified using HPLC. The product was obtained as a white powder. (0.36 mg, yield = 5.2%) HRMS (MALDI-TOF): m/z calcd. for $C_{32}H_{47}N_{11}NaO_7$ [M+Na]$^+$ 720.3558, found: 720.4536.

N-(1H-1,2,3-triazol-1-yl-carbonyl)-isonipecotyl-(4-phenylbenzyl)glycyl-6-aminohexanoyl-L-ε-azidolysine amide (8d)
Probe **8d** was synthesized using subsequently methods 1, 2.5 with 4-phenylbenzylamine and 3 and purified using HPLC. The product was obtained as a white powder. (0.24 mg, yield = 3.4%) HRMS (MALDI-TOF): m/z calcd. for $C_{36}H_{47}N_{11}NaO_5$ [M+Na]$^+$ 736.3659, found: 736.4139.

N-(1H-1,2,3-triazol-1-yl-carbonyl)-isonipecotyl-(cyclohexanemethyl)glycyl-6-aminohexanoyl-L-ε-azidolysine amide (8e)

Probe **8e** was synthesized using subsequently methods 1, 2.5 with cyclohexanemethylamine and 3 and purified using HPLC. The product was obtained as a white powder. (0.54 mg, yield = 8.4%) HRMS (MALDI-TOF): m/z calcd. for $C_{30}H_{49}N_{11}NaO_5$ [M+Na]$^+$ 666.3816, found: 666.4133.

N-(1H-1,2,3-triazol-1-yl-carbonyl)-isonipecotyl-(4-trifluoromethylbenzyl)glycyl-6-aminohexanoyl-L-ε-azidolysine amide (8f)

Probe **8f** was synthesized using subsequently methods 1, 2.5 with 4-trifluoromethylbenzylamine and 3 and purified using HPLC. The product was obtained as a white powder. (0.29 mg, yield = 4.1%)   HRMS (MALDI-TOF): m/z calcd. for $C_{31}H_{42}F_3N_{11}NaO_5$ [M+Na]$^+$ 728.3220, found: 728.3615

N-(1H-1,2,3-triazol-1-yl-carbonyl)-isonipecotyl-(2-naphtylmethyl)glycyl-6-aminohexanoyl-L-ε-azidolysine amide (8g)

Probe **8g** was synthesized using subsequently methods 1, 2.5 with 2-naphtylamine and 3 and purified using HPLC. The product was obtained as a white powder. (0.19 mg, yield = 2.8%) HRMS (MALDI-TOF): m/z calcd. for $C_{34}H_{45}N_{11}NaO_5$ [M+Na]$^+$ 710.3503, found: 710.3942.

N-(1H-1,2,3-triazol-1-yl-carbonyl)-isonipecotyl-(N-4-(dimethylamino)benzyl)glycyl-6-aminohexanoyl-L-ε-azidolysine amide (8h) trifluoroacetate

Probe **8h** was synthesized using subsequently methods 1, 2.5 with N-4-(dimethylamino)benzylamine and 3 and purified using HPLC. The product was obtained as a white powder. (0.48 mg, yield = 6.0%) HRMS (MALDI-TOF): m/z calcd. for $C_{32}H_{48}N_{12}NaO_5$ [M+Na]$^+$ 703.3768, found: 703.4221.

N-(1H-1,2,3-triazol-1-yl-carbonyl)-isonipecotyl-(4-trifluoromethoxybenzyl)glycyl-6-aminohexanoyl-L-ε-azidolysine amide (8i)

Probe **8i** was synthesized using subsequently methods 1, 2.5 with 4-trifluoromethoxybenzylamine and 3 and purified using HPLC. The product was obtained as a white powder. (0.32 mg, yield = 4.4%) HRMS (MALDI-TOF): m/z calcd. for $C_{31}H_{42}F_3N_{11}NaO_6$ [M+Na]$^+$ 744.3169, found: 744.3694.

N-(1H-1,2,3-triazol-1-yl-carbonyl)-isonipecotyl-(4-methoxybenzyl)glycyl-6-aminohexanoyl-L-ε-azidolysine amide (8j)

Probe **8j** was synthesized using subsequently methods 1, 2.5 with 4-methoxybenzylamine and 3 and purified using HPLC. The product was obtained as a white powder. (0.54 mg, yield = 8.1%) HRMS (MALDI-TOF): m/z calcd. for $C_{31}H_{45}N_{11}NaO_6$ [M+Na]$^+$ 690.3452, found: 690.3846.

N-(1H-1,2,3-triazol-1-yl-carbonyl)-isonipecotyl-(2-chlorobenzyl)glycyl-6-aminohexanoyl-L-ε-azidolysine amide (8k)

Probe **8k** was synthesized using subsequently methods 1, 2.5 with 2-chlorobenzylamine and 3 and purified using HPLC. The product was obtained as a white powder. (0.28 mg, yield = 4.2%) HRMS (MALDI-TOF): m/z calcd. for $C_{30}H_{42}ClN_{11}NaO_5$ [M+Na]$^+$ 694.2957, found: 694.3535.

N-(1H-1,2,3-triazol-1-yl-carbonyl)-isonipecotyl-(4-chlorobenzyl)glycyl-6-aminohexanoyl-L-ε-azidolysine amide (8l)

Probe **8l** was synthesized using subsequently methods 1, 2.5 with 4-chlorobenzylamine and 3 and purified using HPLC. The product was obtained as a white powder. (0.55 mg, yield = 8.2%) HRMS (MALDI-TOF): m/z calcd. for $C_{30}H_{42}ClN_{11}NaO_5$ [M+Na]$^+$ 694.2957, found: 694.3465.

N-(1H-1,2,3-triazol-1-yl-carbonyl)-isonipecotyl-(2,3-dichlorobenzyl)glycyl-6-aminohexanoyl-L-ε-azidolysine amide (8m)

Probe **8m** was synthesized using subsequently methods 1, 2.5 with 2,3-dichlorobenzylamine and 3 and purified using HPLC. The product was obtained as a white powder. (0.22 mg, yield = 3.1%) HRMS (MALDI-TOF): m/z calcd. for $C_{30}H_{41}Cl_2N_{11}NaO_5$ [M+Na]$^+$ 728.2567, found: 728.3266.

N-(1H-1,2,3-triazol-1-yl-carbonyl)-isonipecotyl-(4-fluorobenzyl)glycyl-6-aminohexanoyl-L-ε-azidolysine amide (8n)

Probe **8n** was synthesized using subsequently methods 1, 2.5 with 4-fluorobenzylamine and 3 and purified using HPLC. The product was obtained as a white powder. (1.15 mg, yield = 17.5%) HRMS (MALDI-TOF): m/z calcd. for $C_{30}H_{42}FN_{11}NaO_5$ $[M+Na]^+$ 678.3252, found: 678.3884.

N-(1H-1,2,3-triazol-1-yl-carbonyl)-isonipecotyl-(2-fluorobenzyl)glycyl-6-aminohexanoyl-L-ε-azidolysine amide (8n)

Probe **8n** was synthesized using subsequently methods 1, 2.5 with 2-fluorobenzylamine and 3 and purified using HPLC. The product was obtained as a white powder. (0.32 mg, yield = 4.9%) HRMS (MALDI-TOF): m/z calcd. for $C_{30}H_{42}FN_{11}NaO_5$ $[M+Na]^+$ 678.3252, found: 678.3823.

Preparation of tissue lysates

Mouse brain lysates were prepared and fractionalized as described in Chapter III.

Preparation of cell lysates

A431 cells were grown to confluency in a T175 culture flask using DMEM (with 10% FBS and pen/strep) as medium. The medium was aspirated and cells were washed with PBS, after which they were trypsinized with 5 mL Trypsin-EDTA solution. The cells were collected in a falcon tube and pelleted (500 g, 5 min, room temperature) after which the supernatant was pipetted out. Next, 1 mL of lysis buffer (20 mM HEPES, 150 mM NaCl, 2 mM DTT, 25 U/mL Benzonase, 0.5% NP-40, pH 7.2) was added to the cells, which were lysed by repeated aspiration. The lysate was centrifuged (13000 g, 5 min, room temperature) to pellet debris, after which the supernatant was collected. Protein concentration of the lysate was measured using a BCA assay, and normalized to 1 mg/mL with storage buffer (20 mM HEPES, 2 mM DTT, pH 7.2).

Competition of probes with FP-Rhodamine

30 μL of cytosolic fraction of mouse brain lysate (1 mg/mL) was incubated for 1 h at room temperature with 0.3 μL of a 100x stock solution of probe (DMSO) or 0.3 μL DMSO. Then 0.3 μL FP-Rh (100 μM, DMSO) was added to each sample and the samples were incubated for another hour. Next, 10 μL 4x sample buffer was added to the samples, which were subsequently boiled at 95 °C for 2 minutes. Samples were resolved by SDS-PAGE on 12% acrylamide gels and visualized by measuring in-gel fluorescence on a Typhoon FLA 9500 scanner with excitation at 532 nm and detection at 568 nm with the photomultiplier set at 900 V. Patterns of probe-treated samples were compared with a FP-Rh treated control sample.

IC$_{50}$ determination on human APT-1 and APT-2

Apparent IC$_{50}$ values were measured by using eight (for APT-1) or six (for APT-2) different compound concentrations in a 1:3 serial dilution, starting at a highest concentration of 270 nM. To this end 30 μL of APT-1 (0.5 ng/μL) or APT-2 (3 ng/μL) in 20 mM HEPES, 150 mM NaCl, 0.1% Triton-X100, pH 7.4 was incubated for 1 h at room temperature with 0.3 μL of a 100x stock solution of probe in DMSO. Then, 0.3 μL FP-Rh (100 μM, DMSO) was added to each sample and the samples were incubated for another hour. Next 10 μL 4x sample buffer was added to the samples, which were subsequently boiled at 95 °C for 2 minutes. Samples were resolved by SDS-PAGE on 12% acrylamide gels and visualized by in-gel fluorescence measuring on a Typhoon scanner as for the initial screening. Remaining enzyme activity was determined by measuring the integrated optical gel band intensity using ImageJ software. Values were normalized to the FP-Rh labeled control sample without inhibitor, which was set at 100% activity. IC$_{50}$ values were determined from a dose-response curve generated in GraphPad Prism.

Direct labelling of probe targets

30 µL of A431 lysate (1 mg/mL) was incubated for 1 h with 0.3 µL of a 10 µM stock solution of **8e**, **8g**, **8l** or **5f** (DMSO). Control samples were treated with 0.3 µL of a 100 µM stock of FP-Rh (DMSO) or 0.3 µL DMSO. Next, 0.5 µL TAMRA-alkyne (1.5 mM in DMSO), 0.3 µL THPTA (5 mM in 4:1 t-BuOH: DMSO), 0.6 µL sodium ascorbate (50 mM in water) and 0.6 µL CuSO$_4$ (50 mM in water) were added to all samples except the FP-Rh treated control sample and the samples were incubated 1 h at room temperature. Afterwards, 10 µL of 4x sample buffer was added to the samples, which were subsequently boiled at 95 °C for 2 minutes. Samples were resolved on an SDS-PAGE 12% acrylamide gel and visualized by in-gel fluorescence measuring on a Typhoon scanner.

Cell permeability assay in A431 cells

A431 cells were seeded at 200,000 cells per well into a 12-well plate and allowed to adhere overnight. The media was refreshed with 1 mL DMEM (with 10% FBS and pen/strep), spiked with either 1 µL **8e**, **8g**, **8l** or **5f** (1 mM, DMSO) or 1 µL DMSO for 2h at 37 °C. Next, the medium was aspirated and the cells were washed three times with PBS (5 min). 200 µL PBS was added to each plate and the cells were collected by scraping. The cell suspension was subsequently spun down (500g, 5 minutes, room temperature) and the supernatant removed. Lysates were prepared by aspirating cells in 200 µL lysis buffer (20 mM HEPES, 150 mM NaCl, 2 mM DTT, 25 U/mL Benzonase, 0.5% NP-40, pH 7.2). Lysates were centrifuged (13000 g, 5 min, room temperature) to pellet debris, after which the supernatant was collected. Protein concentrations of all samples were measured using a BCA assay, and normalized to 2.14 mg/mL with storage buffer (20 mM HEPES, 2 mM DTT, pH 7.2). 90 µL of each sample was incubated with either 0.9 µL FP-Rh (DMSO, 100 µM) or 0.9 µL DMSO at room temperature for 1 hour. Next, 30 µL 4x sample buffer was added to the samples, which were subsequently boiled at 95 °C for 2 minutes. Samples were resolved by SDS-PAGE on 12% acrylamide gels and visualized by measuring in-gel fluorescence on a Typhoon FLA 9500 scanner with settings as described above.

Assessment of probe binding kinetics on human APT-1

A stock of 100 µM DIFMUO in PBS + 0.05% Triton-X100 + 0.1% DMSO was made by diluting 2 µL 10 mM DIFMUO (DMSO) into 2 mL PBS + 0.05% Triton-X100. Wells of a black, flat-bottomed 96 well plate were loaded with 40 µL of this solution. Each well was incubated with 0.5 µL of a 200x stock (DMSO) of one of the six indicated concentrations of **8e**, **8g**, **8l** or **5f**. 0.5 µL DMSO was added to two control samples. 40 µL of a 0.25 ng/µL (10 nM) dilution of APT-1 in PBS + 0.05% Triton-X100 was added to all samples but one control sample right before measurement. To the remaining control sample, 40 µL PBS + 0.05% Triton-X100 was added. Fluorescence was measured for 50 minutes at 350 nm excitation and 458 nm emission in a SpectraMax iD3 Multi-Mode Microplate Reader (Molecular Devices). The values measured for the sample that was not treated with APT-1 were subtracted from the measurements. The resulting values were plotted into the equation $[P] = \frac{v_i}{k_{obs}}(1 - e^{-k_{obs}t})$, to determine the k_{obs} values for each probe concentration. The k_{obs} values that were determined from curves with an R^2 value >0.99 were plotted against probe concentrations to determine k_{obs}/I.

Metabolic labelling with 17-ODYA on A431 cells

A431 cells were seeded at 200 000 cells/well in a 12-well plate and grown overnight to confluency in 1 mL DMEM. The medium was aspirated and cells were washed once with PBS. Next, four wells were incubated with 1 mL DMEM without FBS, spiked with 1 µL of a 1 mM stock of **5f**, **8e**, **8g** or **8l** (DMSO). Two control wells were incubated with 1 mL DMEM without FBS, spiked with 1 µL DMSO. All cells were incubated for 2h at 37°C. Next, 1 µL of a 20 mM stock of 17-ODYA (10% BSA in water) was added to all samples but one DMSO-treated control. The final control sample was spiked with 1 µL of a 20 mM stock of palmitic acid (10% BSA in water). Cells were incubated overnight at 37°C. Then, the media was aspirated and the cells were washed three times with PBS + 100 µM phenylmethyl sulfonyl fluoride (PMSF). The cells were scraped and collected in 500 µL PBS + 100 µM PMSF, after which they were pelleted (450 g, 5 min, room temperature) and the supernatant was discarded. Cells were lysed by

agitation in 200 μL lysis buffer (20 mM HEPES, 150 mM NaCl, 2 mM DTT, 0.5% NP-40, 20 U/mL DNAseI, 100 μM PMSF, pH 7.2) After BCA assay, the lysates were brought to the same concentration (1.5 mg/mL) with storage buffer (20 mM HEPES, 150 mM NaCl, 2 mM DTT, pH 7.2). 90 μL of each sample was incubated with 0.5 μL 5 mM TMR-N_3 (DMSO); 0.9 μL 5 mM THPTA (DMSO); 1.8 μL 50 mM $CuSO_4$ (water) and 1.8 μL 50 mM sodium ascorbate (water) for 1h at room temperature. 30 μL of 4x Sample buffer was added to each sample. Samples were resolved by SDS-PAGE on 12% acrylamide gels and visualized by measuring in-gel fluorescence on a Typhoon FLA 9500 scanner with settings as described in Chapter III.

4.5. References

[1]   C. Salaun, J. Greaves, L. H. Chamberlain, *J. Cell Biol.* **2010**, *191*, 1229–1238.
[2]   E. Conibear, N. G. Davis, *J. Cell Sci.* **2010**, *123*, 4007–4010.
[3]   I. Mellman, W. J. Nelson, *Nat. Rev. Mol. Cell Biol.* **2008**, *9*, 833–845.
[4]   S. J. Won, D. Davda, K. J. Labby, S. Y. Hwang, R. Pricer, J. D. Majmudar, K. A. Armacost, L. A. Rodriguez, C. L. Rodriguez, F. S. Chong, et al., *ACS Chem. Biol.* **2016**, *11*, 3374–3382.
[5]   Y. Ohno, A. Kihara, T. Sano, Y. Igarashi, *Biochim. Biophys. Acta - Mol. Cell Biol. Lipids* **2006**, *1761*, 474–483.
[6]   V. M. Tomatis, A. Trenchi, G. A. Gomez, J. L. Daniotti, *PLoS One* **2010**, *5*, e15045.
[7]   J. A. Duncan, A. G. Gilman, *J. Biol. Chem.* **1998**, *273*, 15830–15837.
[8]   D. T. S. Lin, E. Conibear, *Elife* **2015**, *4*, 1–14.
[9]   S. J. Won, M. Cheung See Kit, B. R. Martin, *Crit. Rev. Biochem. Mol. Biol.* **2018**, *53*, 83–98.
[10]   N. Adachi, D. T. Hess, P. McLaughlin, J. S. Stamler, *J. Biol. Chem.* **2016**, *291*, 20232–20246.
[11]   L. Abrami, T. Dallavilla, P. A. Sandoz, M. Demir, B. Kunz, G. Savoglidis, V. Hatzimanikatis, F. G. van Der Goot, *Elife* **2017**, *6*, 1–24.
[12]   J. M. Strelow, *J. Biomol. Screen.* **2017**, *22*, 3–20.
[13]   R. Vanhoutte, M. A. T. Van De Plassche, S. H. L. Verhelst, *J. Med. Chem.* **2020**, *63*, 11845–11853.
[14]   S. J. Won, B. R. Martin, *ACS Chem. Biol.* **2019**, *13*, 1560–1568.

Chapter V: Development of azapeptidic activity-based probes for the Sars-CoV-2 M^{pro} using solid-phase synthesis

Abstract

The SARS-CoV-2 virus has caused the largest worldwide viral pandemic in a century. Although the development of vaccines has lowered the incidence of hospitalizations and mortality due to covid-19, new mutants of the virus are emerging for which the vaccines are less effective. Therefore, the development of antiviral drugs remains necessary in the battle against the virus. The main protease (M^{pro}) of the virus cleaves the viral polyproteins expressed by the SARS-CoV-2 virus into non-structural proteins and is essential for the viral replication. Hence, M^{pro} is a target of interest for the development of antivirals. In this chapter, the development of activity-based probes for the M^{pro} is described, which can be applied as study tools to investigate this protease. The probes have an azapeptidic structure and are synthesized on solid support. It was found that three probes have good reactivity with the M^{pro} on the purified protein and in complex proteomes, with one also showing good antiviral activity in infected live cells. The most reactive probe can detect M^{pro} activity at protein concentrations as low as 50 ng/mL. These probes can furthermore serve as leads for the development of azapeptidic M^{pro} inhibitors as potential antivirals.

5.1. Introduction

Coronaviruses that infect mammalian hosts have been known since 1966.[1] Humanity faced the dangers of highly contagious coronaviruses for a first time during the SARS and MERS outbreaks in 2003 and 2012, caused respectively by the Severe Acute Respiratory Syndrome coronavirus[2] and the Middle East Respiratory Syndrome coronavirus[3]. In December 2019, SARS-CoV-2 was discovered in Wuhan, China. This new highly infective coronavirus had infected 221 million people and claimed 4.4 million lives due to covid-19 as of August 19, 2021.[4] The SARS-CoV-2 pandemic has caused a worldwide health crisis, the like of which the world has not been seen in over a century. The multiple viral transmission routes, which include droplets, direct contact, airborne, fecal-oral, ocular, mother-to-child and animal-to-human, make it extremely challenging to contain its spread. [5] The recent development of vaccines, however, has been a game changer. The developed vaccines restrain the advance of the pandemic, and significantly lower the chances of hospitalization and mortality upon infection with the SARS-CoV-2 virus. Unfortunately, new mutants are rapidly emerging to which vaccines are less effective. One example is the B.1.617.2 "Delta" variant, which was first discovered in India and partly stays out of the grasp of the immune response that is triggered by vaccination with the two most used vaccines worldwide.[6]

The lowered efficacy of the vaccines against the mutant strains, together with the demanding distribution and conservation conditions of the vaccines, calls for the urgent development of antiviral drugs. An ideal candidate to be the target of these much needed antivirals, is the main protease (M^{pro}) of the Sars-CoV-2 virus, which is highly conserved and essential for the virus replication. [7] The M^{pro} makes 11 of the 14 cleavages in polyproteins ppa1 and ppa1b expressed by the virus to form its 16 non-structural proteins (nsp's).[8] This includes the proteolytic cleavage of nsp13, which has RNA helicase and NTPase activity and is essential for viral replication.[9] M^{pro} is a cysteine protease, with a His-Cys dyad in its active site.[10] Its strong preference for P_1 glutamine residues[11,12] makes the development of selective peptide-based inhibitors and activity-based probes (ABPs) with P_1 glutamine residues a possibility[13].

5.2. Results and discussion

The outset of this project is to create selective peptide-like ABPs for M^{pro}, which can be used as tools to study this target protease. The probes are made via solid-phase synthesis with the following design: (1) a hexynoic acid residue bearing an alkyne detection tag, connected to (2) a Tle-Leu-azaGln tripeptide, based on the preferred P_3-P_2-P_1 substrate specificity of M^{pro}, which is capped with (3) a cysteine reactive warhead on the P_1 azaGln, which binds covalently onto the catalytic Cys residue of

M^{pro}. The primary amide of the P$_1$ azaGln also serves as an anchor point for the probes onto the Rink amide resin to make the solid-phase synthesis procedure clean and efficient.

To incorporate the P$_1$ Gln substrate as an azapeptide, a double protected N^1-Fmoc, N^2-Alloc protected 3-hydrazino-propionic acid building block was made (Scheme **5.1A**). This building block can be coupled with its carboxylic acid function to Rink amide resin to form the Gln side chain on the resin and allows the formation of the recognition element and detection tag via Fmoc-based peptide synthesis on the N^1 nitrogen. The Alloc group on the N^2 nitrogen is compatible with Fmoc deprotection conditions and can be deprotected separately for warhead coupling.

A

B   **C**
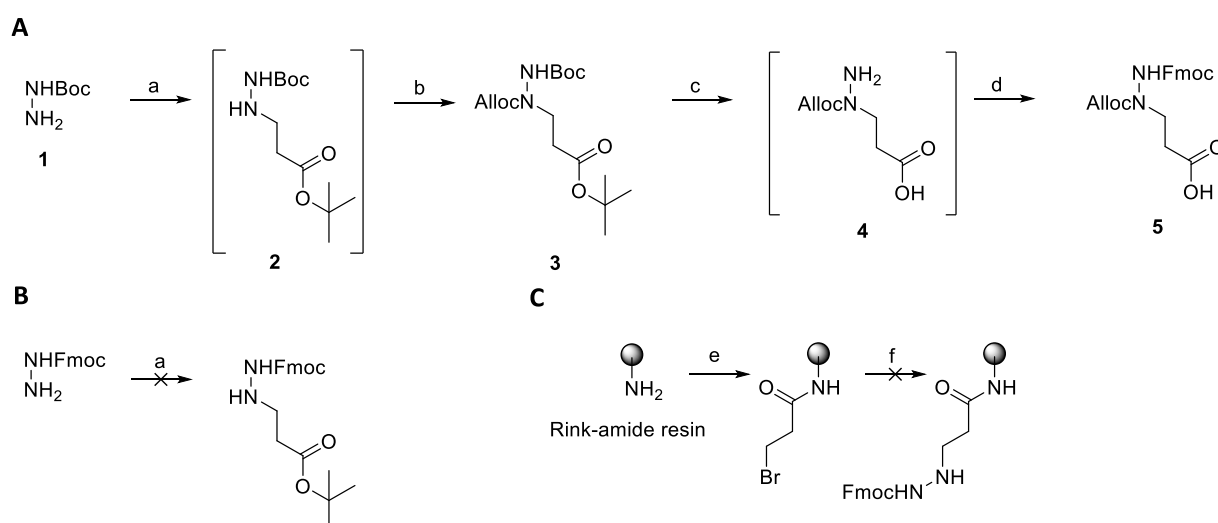
Scheme 5.1. A. Synthesis of compound **5**, an orthogonal N^1-Fmoc, N^2-Alloc protected aza-3-propionic acid building block for Fmoc-based SPPS. a) 3-Bromo tert-butylpropionate, DIEA, DMF, rt. b) Alloc-Cl, DIEA, DMF, rt, yield = 26% over two steps. c) TFA, DCM, rt. d) Fmoc-Cl, DIEA, DCM, rt, yield = 69% over two steps. **B.** Unsuccessful attempt to synthesize building block **5** by reacting Fmoc-hydrazine and 3-Bromo tert-butylpropionate. **C.** Unsuccessful attempt to synthesize the P$_1$ azaGln substrate on Rink-amide resin. e) 3-Bromo propionyl bromide, DIEA, DCM. f) Fmoc-hydrazine, DIEA, DCM.

Synthesis of this building block began by substituting 3-Bromo tert-butylpropanoate with tert-butyl carbazate **1** to give compound **2**. The resulting compound was Alloc-protected on the N^2 nitrogen with Alloc chloride to give **3**, after which the tert-butyl and Boc group were removed simultaneously with TFA. The N^1 nitrogen was reprotected with Fmoc-Cl to give the final compound **5**. A shorter synthetic route via the substitution of Fmoc-hydrazine with 3-Bromo tert-butylpropanoate was not possible due to the poor nucleophilicity of the N^1 nitrogen of Fmoc-hydrazine (Scheme **5.1B**). Another attempt to construct the P$_1$ residue on solid phase with 3-Bromo propionyl bromide followed by substitution with Fmoc-hydrazine failed because of the same reason (Scheme **5.1C**).
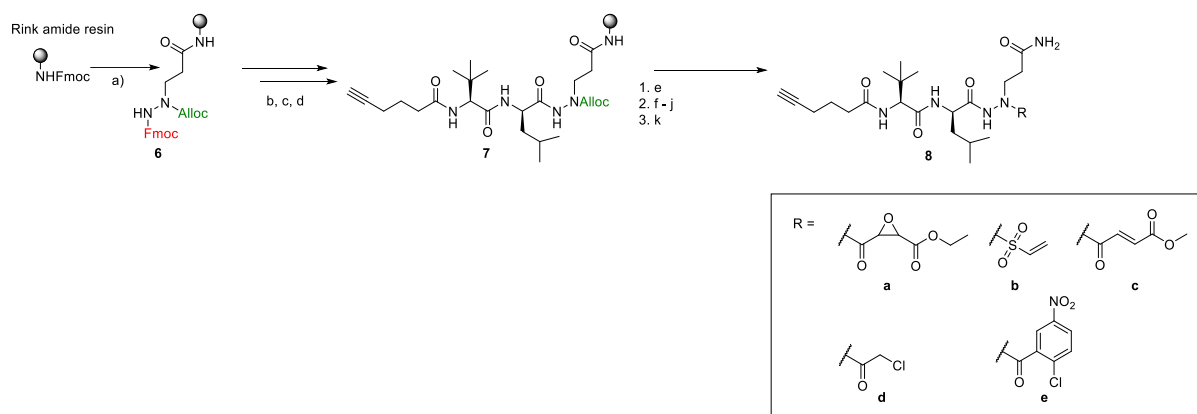
Scheme 5.2. On-resin synthesis of azapeptidic ABPs for the Sars-CoV-2 M^{pro}. a) 1. piperidine/DMF 1/4, 5 minutes; 2. **5**, HBTU, DIEA, DMF, rt, overnight. b) 1. piperidine/DMF 1/4, 5 minutes; 2. Fmoc-Leu-OH HBTU, DIEA, DMF, rt, overnight. c) piperidine/DMF 1/4, 5 minutes; 2. Fmoc-Tle-OH HBTU, DIEA, DMF, rt, 3h. d) piperidine/DMF 1/4, 5 minutes; 2. Hexynoic acid, HBTU, DIEA, DMF, rt, 3h. e) Pd(PPh$_3$)$_4$, PhSiH$_3$, DCM, 30 minutes. f) mono-ethyl epoxysuccinate, HBTU, DIEA, DMF, rt, overnight. g) 2-Chloroethane sulfonylchloride, HBTU, DIEA, DCM, rt, overnight. h) mono-methyl fumarate, HBTU, DIEA, DMF, rt, overnight. i) chloroacetyl chloride, DIEA, DCM, rt, overnight. j) 2-Chloro-5-nitrobenzoic acid, HBTU, DIEA, DMF, rt, overnight. k) TFA/TIS/water 95/2.5/2.5, 30 minutes.

The construction of the probes is described in Scheme **5.2** and started by coupling compound **5** to Rink amide resin using HBTU to form resin backbone **6**. After Fmoc deprotection of this resin backbone, Fmoc-Leu-OH was coupled using HBTU. A high concentration of 2.25M activated Fmoc-Leu-OH was used as driving force to couple this amino acid to the N^1 nitrogen, which is electron-poor due to the allyl carbazate that it forms with the N^2 nitrogen and its Alloc protection group. The subsequent couplings with Fmoc-Tle-OH and hexynoic acid were done at lower concentrations, to form the resin-bound peptide backbone **7** bearing the recognition element and detection tag. Alloc deprotection of the N^2 nitrogen of the P$_1$ residue with Pd(PPh$_3$)$_4$ was done next, followed by the coupling of one of five cysteine reactive electrophiles onto this nitrogen. Selected electrophiles were: ethyl epoxysuccinate (**8a**), vinyl sulfonamide (**8b**), mono-methyl fumarate (**8c**), chloroacetamide (**8d**) and 2-Chloro-5-nitrobenzamide (**8e**). These five warheads employ four different ways of cysteine reactivity: nucleophilic addition (with epoxide ring opening), Michael addition, S$_N$2 substitution and S$_N$Ar substitution. After warhead coupling, the probes were cleaved from the resin with TFA, releasing the resin-bound primary amide on the azaGln sidechain.

As a first assessment of reactivity, the probes were tested in competition with the previously reported M^{pro}-reactive ABP TAMRA-Abu-Tle-Leu-Gln-AOMK on purified M^{pro} at a concentration of 10 µM (Figure **5.1A**). The disappearance of the fluorescently labelled M^{pro} band in samples treated with **8a** and **8c-e** showed reaction of these probes with the target, whereas probe **8b** shows no reaction. The reactivity of probes **8a** and **8c-e** was further assessed in a titration series on the purified M^{pro} to determine apparent IC$_{50}$ values (Figure **5.1B**). This revealed nanomolar IC$_{50}$^{App} values for probes **8a**, **8c** and **8d**, going as low as 20.8 nM for probe **8d**.

A

B

Cmp	IC_{50}^{App} (purified M^{pro})	EC_{50} (infected VeroE6)	CC_{50} (Huh7)
8a	206 nM	>10 µM	36.7 µM
8b	Inactive	N/A	N/A
8c	44.0 nM	>10 µM	62.5 µM
8d	20.8 nM	3.25 µM	50.0 µM
8e	>45 µM	N/A	N/A
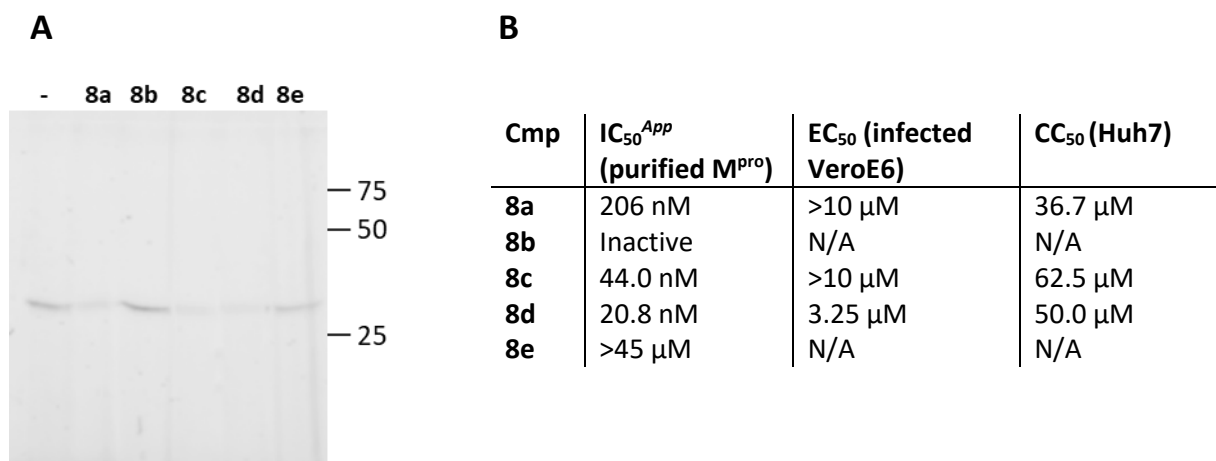
Figure 5.1. A. Competitive labelling between 10 µM **8a-e** and 5 µM of fluorescent probe TAMRA-Abu-Tle-Leu-Gln-AOMK (**probe 9**) on M^{pro} shows labelling activity for probes **8a** and **8c-e**, and no activity for **8b**. **B.** IC_{50}^{App} values calculated for active probes **8a**, **8c** and **8d** on purified M^{pro}, EC_{50} values on antiviral activity in Sars-CoV-2 infected VeroE6 cells and CC_{50} value on Huh7 cells.

The difference in activity between these three probes and probes **8b** (non-reactive) and **8e** (IC_{50} = >45 µM) is striking, especially since the vinyl sulfonamide warhead of probe **8b** is one of the strongest known cysteine-reactive electrophiles.[14] A possible explanation lies in the difference in distance between the recognition element and the electrophilic center of the probes. For probes **8a**, **8c** and **8d**, the attack happens two bonds away from the α-nitrogen of the P_1 azaGln, whereas for probes **8b** and **8e**, the distance between the two moieties is three bonds. Docking studies are needed to further assess the impact on the distance of the recognition element of the probes from the catalytic substrate.
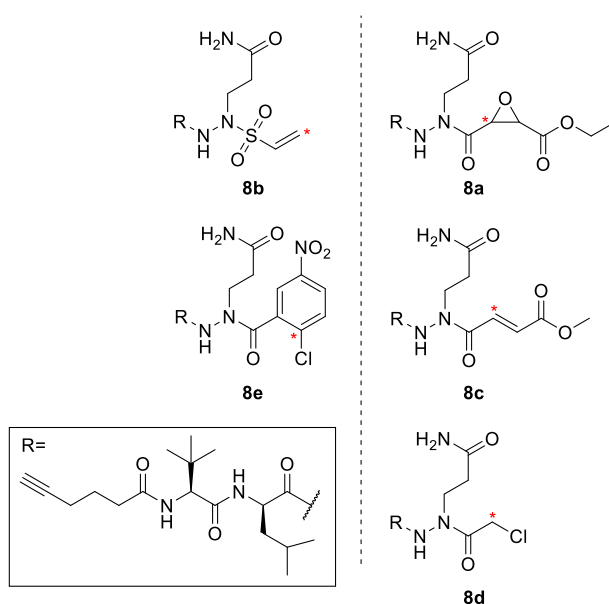
Figure 5.2. Cysteine-reactive warheads used in this series of probes. The cysteine-reactive center is marked with a red asterisk. Warheads onto which the attack happens three bonds away from the α-nitrogen are depicted left, warheads onto which the attack happens two bonds away from the α-nitrogen are depicted right.

Finally, the antiviral activity of probes **8a**, **8c** and **8d** was validated in infected live VeroE6 cells (Figure **5.1B**). To this end, a culture of eGFP-transfected VeroE6 cells was incubated with different concentrations of the probes prior to infection with SARS-CoV-2. After four days, the decrease in GFP-signal was measured and compared between non-infected, infected and infected + probe treated cultures to evaluate the probes' antiviral activity (EC$_{50}$). The effect of the probes on cell viability (CC$_{50}$) was assessed on Huh7 cells via an MTS assay. Probes **8a** and **8c** showed an EC$_{50}$ of >10 µM, whereas probe **8d** had an EC$_{50}$ of 3.25 µM. The difference between these values and the IC$_{50}$ values measured on the purified M^{pro} might be due to cell permeability issues of the probes or their potential to be Pgp substrates because of their peptidic nature. Although the EC$_{50}$ values in live cells are higher, it should nevertheless be possible to use probe **8d** for labelling experiments in infected cells at low micromolar concentrations. In addition, this probe displays enough difference between its EC$_{50}$ and CC$_{50,}$ to create a suitable window for cell treatment.
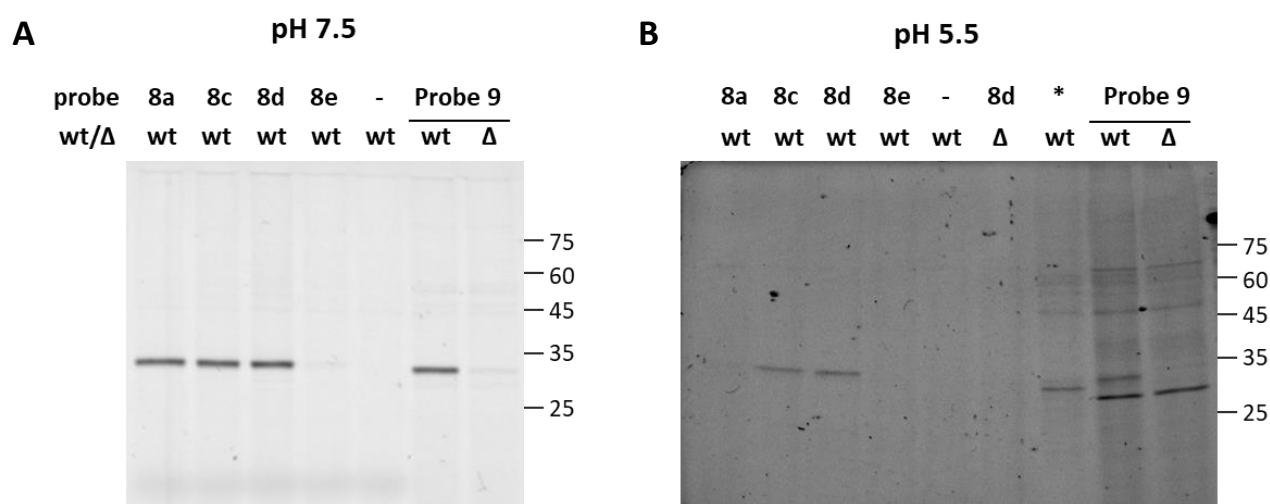
Figure 5.3. A. Probe labelling with probes **8a**, **8c-e** (10 µM concentration) on 30 µg HEK 293T lysate (1 mg/mL), spiked with 600 ng M^{pro}, either wild type (wt) or C145A mutant (Δ) at pH 7.5. Probe-enzyme complexes were visualized through CuAAC "click" chemistry to TAMRA-N$_3$. Lanes labelled "Probe 9" are treated with 10 µM TAMRA-Abu-Tle-Leu-Gln-AOMK. **B.** Probe labelling with probes **8a**, **8c-e** (10 µM concentration) on 30 µg HEK 293T lysate (1 mg/mL), spiked with 600 ng M^{pro}, either wild type (wt) or C145A mutant (Δ), at pH 5.5. Probe-enzyme complexes were visualized through CuAAC "click" chemistry to TAMRA-N$_3$. Lanes labelled "Probe 9" are treated with 10 µM TAMRA-Abu-Tle-Leu-Gln-AOMK. Lane marked (*****) is labelled with cathepsin-reactive ABP DCG-04-alkyne, followed by CuAAC "click" chemistry to TAMRA-N$_3$.

The selectivity of the probes for M^{pro} over other enzymes was assessed by treating HEK293T lysates spiked with M^{pro} with 10 µM of the probes which showed reactivity, followed by CuAAC to TAMRA-N$_3$ (Figure **5.3**). At pH 7.5, which is the optimal working pH for M^{pro}, no probe shows cross-reactivity with other targets than M^{pro} (Figure **5.3A**). M^{pro} is verified as the sole visualized band by treatment of a

sample spiked with the wild type M^{pro} and a sample spiked with a catalytically dead C145A M^{pro} mutant with 10 µM of M^{pro}-reactive probe TAMRA-Abu-Tle-Leu-Gln-AOMK (probe 9). The catalytically dead mutant shows no activity for the probe, which both identifies the band as M^{pro} and shows that the probe labeling is activity-based. As expected, probes **8a**, **8c** and **8d** showed a lot of reactivity with the M^{pro} and no observable labeling was detected for probe **8e** at 10 µM concentration. M^{pro}-spiked HEK293T samples were also probe-labelled at pH 5.5, to assess any cathepsin-reactivity of the probes (Figure **5.3B**). A single band is labeled by probes **8c** and **8d.** This band is identified as M^{pro} by the lacking of labelling in a sample spiked with C145A M^{pro} that is treated with probe **8d**. Furthermore, a band that runs at the same molecular mass is labeled by probe 9 in a sample spiked with the wild type M^{pro}, but not in a sample spiked with C145A M^{pro}.

Assessment of active cathepsins present in the M^{pro} –spiked HEK293T lysates was done by labeling with general cathepsin-reactive probe DCG-04-alkyne (*****). As there is only one cathepsin detected by DCG-04-alkyne, that runs between 25 and 35 kDa, no conclusions can be drawn for the reactivity of the M^{pro}-reactive probes for cathepsins other than that there is no reaction with this one cathepsin. It is possible that more cathepsins are present, but not detected because of lower efficiency of CuAAC click chemistry at pH 5.5. This would also explain the difference in intensity of M^{pro} labelling by probe 9, which does not require CuAAC for the visualization of its targets, compared to probes **8a**, **8c** and **8d**. A repetition of this experiment with a buffer change to pH 7.5 between the incubation with probe and CuAAC to TAMRA-N$_3$ would be better to verify cathepsin reactivity.
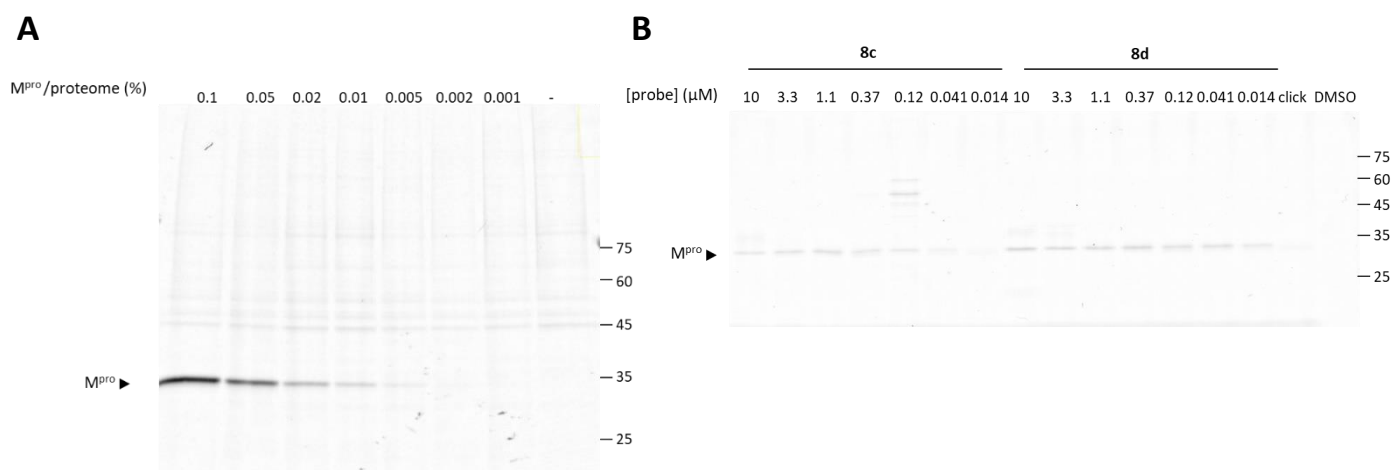
Figure 5.4. A. Labeling of decreasing amounts of recombinant M^{pro} in HEK293T lysates (1 mg/mL total protein concentration, pH 7.4) with probe **8d** reveals the sensitivity of probe **8d** down to 0.005% of total proteome content. **B.** Labelling of 1 µg/mL recombinant M^{pro} (pH 7.4) (activity-adjusted concentration = 20 nM) with decreasing probe concentrations shows probe labelling with **8c** down to 41 nM and with **8d** down to substoichiometric concentration of 14 nM.

The probe sensitivity for probes **8c** and **8d** was assessed on 1 μg/mL of purified M^{pro} (activity-adjusted concentation = 20.6 nM) at different probe concentations, followed by click chemistry to a TAMRA-N$_3$ to determine lowest possible concentrations that are sufficient to detect M^{pro} (Figure **5.4A**). Probe **8c** gave a detectable result up until concentrations as low as 41 nM, for probe **8d**, even a substoichiometric concentration of 14 nM gave a detectable probe-labelling. This shows the strong binding affinity of probe **8d** for the M^{pro} and its ability to react with the target at very low concentrations.

To assess the limit of detection of the probe, HEK293T lysates (1mg/mL protein concentration) were spiked with decreasing amounts of M^{pro}, ranging from 0.1% total proteome concentration to 0.001%, and labeled with 1 μM **8d** followed by CuAAC "click" chemistry to TAMRA-N$_3$ (Figure **5.4B**). At 0.005% of the total proteome (= 50 ng/mL) probe detection was still observed, showing the potential of the probe to detect the M^{pro} in infected cells with low viral loads.

5.3. Conclusion

In conclusion, this chapter describes the development of azapeptidic Sars-CoV-2 M^{pro} reactive ABPs, which consist of a recognition element resembling the preferred substrate sequence of M^{pro} with a P$_1$ aza-amino acid and a cysteine reactive warhead. These probes can be synthesized in a fast manner using solid-phase synthesis, with the P$_1$ aza-glutamine residue being very compatible with synthesis on Rink-amide resin. Out of the five probes that were synthesized, three react strongly with the M^{pro} and are selective for this protease. At the time of writing, Chloroacetamide-based probe **8d** is the molecule with the lowest IC$_{50}$ for M^{pro} of all compounds reported by Covid Moonshot. This is an international consortium of chemists and biologists in academia and industry that collaborates for the synthesis and screening of small molecules as potential antiviral drugs against SARS-CoV-2. Probe **8d** also shows a good inhibition of viral replication in virus-infected cells and low cellular toxicity. This makes the probe potentially suitable for the visualization of M^{pro} in live cells and makes it a good starting point for the development of a new branch of inhibitors for the M^{pro} of the SARS-CoV-2 virus that bear the azapeptide moiety.

5.4. Experimental Section

General materials and methods

All starting materials for chemical reactions were purchased from commercial suppliers and used without purification. All solvents were of synthesis grade or higher. Progress of solution phase reactions was monitored by TLC on pre-coated 0.20 mm thick ALUGRAM® TLC sheets (silicagel-60 with UV indicator) using UV light and/or staining with cerium ammonium molybdate or ninhydrin followed

by heating. Nuclear magnetic resonance spectra were recorded on a Bruker Ultrashield™ 300 or 600 MHz NMR Spectrometer. Chemical shifts are reported in ppm relative to the residual solvent peak. LC-MS spectra were recorded on a Prominence Ultra-fast Liquid Chromatography system (Shimadzu) using a Waters X-bridge 2.1 mm C18 column with a gradient of 5%-80% acetonitrile in water (with 0.1% formic acid) over 22 min. HPLC purification was performed on a Prominence Ultra-fast Liquid Chromatography system (Shimadzu) using a Waters X-bridge 150 mm C18 prep column with a gradient of acetonitrile in water (with 0.1% trifluoroacetic acid) over 32 min. Purity >95% of all final compounds was assessed by integration of the HPLC spectra.

1-allyl 2-(tert-butyl) 1-(3-(tert-butoxy)-3-oxopropyl)hydrazine-1,2-dicarboxylate (3)

tert-butyl carbazate (300 mg, 2.27 mmol) was dissolved in 4 mL dry DMF. DIEA (808 µL, 4.54 mmol) and tert-butyl 3-Bromopropanoate (379 µL, 2.27 mmol) were added to this solution, which was heated to 40°C. The reaction was stirred for 24 hours at room temperature. Upon completion of the reaction (TLC: EtOAc/petroleum ether 3:7), the solvents were evaporated. The crude material was redissolved in 4 mL dry DMF and cooled to 0°C. DIEA (989 µL, 5.67 mmol) and Allyloxycarbonyl chloride (362 µL, 3.4 mmol) were added to the reaction mixture. The reaction mixture was allowed to warm to room temperature and stirred overnight at room temperature. Upon completion of the reaction (TLC: EtOAc/petroleum ether 1:4), the reaction was diluted with 20 mL NaHCO$_3$ (sat. aq.) and extracted five times with 20 mL EtOAc. The organic fraction was dried over MgSO$_4$ and evaporate to dryness. The crude product was purified over column chromatography (EtOAc/petroleum ether 1:4 -> 1:3) to yield the title compound as a colorless oil. (204.53 mg, yield = 26.2%). ^{1}H NMR (300 MHz, CDCl$_3$, 298K): 5.35-5.30 (m, 1H), 4.67-4.58 (m, 2H), 3.82-3.75 (m, 2H), 2.55 (t, 2H, J = 6.5 Hz), 1.63-1.62 (m, 1H), 2.30-2.17 (m, 4H), 1.49-1.46 (m, 9H), 1.44 (s, 9H). ESI-MS: m/z calcd. for C$_{16}$H$_{29}$N$_2$O$_6$ [M+H]$^+$ 345.20, found: 345.00.

2-Fmoc 1-allyl 1-(3-(tert-butoxy)-3-oxopropyl)hydrazine-1,2-dicarboxylate (5)

Compound **3** (120 mg, 348 µmol) was dissolved in 3 mL DCM, to which 3 mL TFA was added. The reaction was stirred for 30 minutes at room temperature. Upon completion of the reaction (EtOAc/petroleum ether 1:4), the solvents were evaporated and the crude material co-evaporated with toluene to remove residual TFA. The crude product was redissolved in 2 mL DCM and cooled to 0°C. DIEA (125 µL, 700 µmol) and Fmoc-Cl (135 mg, 522 µmol) were added to the reaction mixture, which was heated to 40°C and stirred overnight. Upon completion of the reaction (TLC: DCM/MeOH 20:1), the solvents were evaporated and the crude product purified over column chromatography (DCM/MeOH 1:0 -> 20:1) (98.67 mg, yield = 69.0%). ^{1}H NMR (300 MHz, CDCl$_3$, 298K): 7.76 (d, J = 7.7 Hz), 7.62–7.56 (m, 2H), 7.40 (t, 2H, J = 7.5 Hz), 7.31 (t, 2H, J = 7.4 Hz), 6.98-6.92 (m, 1H), 5.96-5.81 (m, 1H), 5.37-5.12 (m, 2H), 4.68-4.42 (m, 4H), 4.28-4.22 (m, 2H), 2.60-2.40 (m, 2H), 1.44 (s, 9H). ESI-MS: m/z calcd. for C$_{22}$H$_{23}$N$_2$O$_6$ [M+H]$^+$ 411.15, found: 410.90.

Solid phase chemistry procedures

Coupling of compound 5 to Rink amide resin (6)

Fmoc protected Rink amide resin (244 mg, 0.74 mmol active sites/g) was treated with 20% piperidine in DMF for 5 min to swell the resin and deprotect the Fmoc group. Next, the resin was washed three times with DMF. All following Fmoc deprotections were performed according to this procedure.

Method 1. Compound **5** was coupled to 180 µmol of deprotected rink amide resin by adding amino acid (1.15 eq.), HBTU (1.15 eq.) and DIPEA (3 eq.) in 1200 µL of DMF to the resin and incubating

overnight at room temperature. After this and each following coupling, the resin was washed three times with DMF and three times with DCM.

Synthesis of the peptide backbone (7)
After deprotection of **6**, Fmoc-L-Leu-OH was coupled to the unprotected nitrogen on the resin by adding amino acid (15 eq.), HBTU (15 eq.) and DIPEA (30 eq.) in 1200 µL DMF and incubating overnight at room temperature. After deprotection of the N-terminus, subsequently Fmoc-L-Tle-OH and hexynoic acid were coupled to the resin by adding (amino)acid (3 eq.), HBTU (3 eq.) and DIEA (10 eq.) in 1200 µL DMF and incubating for 4h.

Warhead coupling
After synthesis peptide backbone **7**, the resins were divided into aliquots of 10 µmol for coupling of the warheads. First, the Alloc group was removed from the resins using general procedure 1.

*General procedure 1: Alloc deprotection of **7***. Alloc groups were removed by first washing the resin three times with dry DCM. Then, the resin was suspended in 1 mL dry DCM, to which Pd(PPh$_3$)$_4$ (0.25 eq.) and PhSiH$_3$ (24 eq.) were added under an Ar atmosphere. Reactions were incubated for 30 min, after which the solutions were drained and the resin was once more incubated with fresh deprotection solution. Afterwards, the resin was washed 3x with DCM.

Ethyl 3-(1-(3-amino-3-oxopropyl)-2-(((S)-2-(hex-5-ynamido)-3,3-dimethylbutanoyl)-D-leucyl) hydrazine-1-carbonyl)oxirane-2-carboxylate (8a)
After deprotection of the resin using the general procedure, the resin (10 µmol active sites) was suspended in 600 µL dry DCM, to which DIEA (27 µL, 150 µmol), monoethyl epoxysuccinate (16 mg, 100 µmol) and HBTU (38 mg, 100 µmol) were added. The reaction was incubated overnight at room temperature and checked for completion using LC/MS. After completion, the resin was washed three times with DCM. The probe was cleaved from the resin by using a 95:2.5:2.5 mixture of TFA:TIS:water and purified using HPLC. The product was obtained as a transparent oil. (0.16 mg, yield = 2.8%) HRMS (MALDI-TOF): m/z calcd. for C$_{27}$H$_{43}$N$_5$O$_8$Na [M+Na]$^+$ 588.3009, found: 588.3500.

methyl (E)-4-(1-(3-amino-3-oxopropyl)-2-(((S)-2-(hex-5-ynamido)-3,3-dimethylbutanoyl)-D-leucyl)hydrazinyl)-4-oxobut-2-enoate (8b)
After deprotection of the resin using the general procedure, the resin (10 µmol active sites) was suspended in 600 µL dry DCM, to which DIEA (27 µL, 150 µmol), monomethyl fumarate (13 mg, 100 µmol) and HBTU (38 mg, 100 µmol) were added. The reaction was incubated overnight at room temperature and checked for completion using LC/MS. After completion, the resin was washed three times with DCM. The probe was cleaved from the resin by using a 95:2.5:2.5 mixture of TFA:TIS:water and purified using HPLC. The product was obtained as a transparent oil. (0.16 mg, yield = 2.8%) HRMS (MALDI-TOF): m/z calcd. for C$_{27}$H$_{43}$N$_5$O$_8$Na [M+Na]$^+$ 558.2904, found: 558.3372.

methyl (E)-4-(1-(3-amino-3-oxopropyl)-2-(((S)-2-(hex-5-ynamido)-3,3-dimethylbutanoyl)-D-leucyl)hydrazinyl)-4-oxobut-2-enoate (8c)
After deprotection of the resin using the general procedure, the resin (10 µmol active sites) was suspended in 600 µL dry DCM, to which DIEA (27 µL, 150 µmol) and 2-chloroethane-1-sulfonyl chloride (11 µL, 100 µmol) were added. The reaction was incubated overnight at room temperature and checked for completion using LC/MS. After completion, the resin was washed three times with DCM. The probe was cleaved from the resin by using a 95:2.5:2.5 mixture of TFA:TIS:water and purified using

HPLC. The product was obtained as a transparent oil. (0.04 mg, yield = 0.8%) HRMS (MALDI-TOF): m/z calcd. for $C_{23}H_{39}N_5O_6SNa$ [M+Na]$^+$ 536.2619, found: 536.2877.

N-((S)-1-(((R)-1-(2-(3-amino-3-oxopropyl)-2-(2-chloroacetyl)hydrazinyl)-4-methyl-1-oxopentan-2-yl)amino)-3,3-dimethyl-1-oxobutan-2-yl)hex-5-ynamide (8d)

After deprotection of the resin using the general procedure, the resin (10 µmol active sites) was suspended in 600 µL dry DCM, to which DIEA (27 µL, 150 µmol) and chloroacetyl chloride (8 µL, 100 µmol) were added. The reaction was incubated overnight at room temperature and checked for completion using LC/MS. After completion, the resin was washed three times with DCM. The probe was cleaved from the resin by using a 95:2.5:2.5 mixture of TFA:TIS:water and purified using HPLC. The product was obtained as a transparent oil. (0.33 mg, yield = 6.2%) HRMS (MALDI-TOF): m/z calcd. for $C_{23}H_{39}N_5O_6SNa$ [M+Na]$^+$ 522.2459, found: 522.2564.

N-((S)-1-(((R)-1-(2-(3-amino-3-oxopropyl)-2-(2-chloro-5-nitrobenzoyl)hydrazinyl)-4-methyl-1-oxopentan-2-yl)amino)-3,3-dimethyl-1-oxobutan-2-yl)hex-5-ynamide (8e)

After deprotection of the resin using the general procedure, the resin (10 µmol active sites) was suspended in 600 µL dry DCM, to which DIEA (27 µL, 150 µmol), 2-chloro-5-nitrobenzoic acid (13 mg, 100 µmol) and HBTU (38 mg, 100 µmol) were added. The reaction was incubated overnight at room temperature and checked for completion using LC/MS. After completion, the resin was washed three times with DCM. The probe was cleaved from the resin by using a 95:2.5:2.5 mixture of TFA:TIS:water and purified using HPLC. The product was obtained as a white solid. (0.23 mg, yield = 4.6%) HRMS (MALDI-TOF): m/z calcd. for $C_{27}H_{43}N_5O_8Na$ [M+Na]$^+$ 558.2904, found: 558.3372

Production of SARS-CoV-2 M^{pro}. The expression and purification of M^{pro} was performed as reported previously.[13]

Production of SARS-CoV-2 M^{pro} mutant C145A.

An overnight culture was prepared from a single colony of freshly transformed bacteria (Escherichia coli strain BL21 (DE3) for Mpro C145A). The overnight culture was diluted 200 times into LB media with 100 µg/mL Ampicillin kept at 37°C and 300 rpm. Once the OD$_{600}$ = 0.7 the expression was induced with 0.5 mM IPTG, and shaken at 18°C for 18h. The cells were pelleted at 5500 rpm at 4°C for 15 min. Pelleted cells were lysed by 5 rounds of sonication (10 sec on, 10 sec off) on ice in lysis buffer (20 mM Tris, pH 7.8; 150 mM NaCl). The mixture was centrifuged at 100,000 × g, 60 min, 4°C to pellet the membrane fraction. The soluble fraction containing the inactive mutant of the SARS-CoV-2 main protease was incubated for 3 h at room temperature with active M^{pro} (0.67 mg/mL in assay buffer) in order to cleave the GST tag and generate the native N-termini of the M^{pro} C145A. After this time the whole was subjected to nickel-nitrilotriacetic acid beads (Qiagen; 1 mL beads per 1 L bacterial expression culture) for 1 h at room temperature. After this time the inactive protease was eluted by increasing imidazole washing steps (25 mM, 50 mM, 200 mM, and 500 mM final elution in 20 mM Tris-NaOH, pH 7.8, 150 mM NaCl). The elution fractions corresponding to 200 mM imidazole were diluted to a final protein concentration of 1 mg/mL in order to avoid protein precipitation (concentration measured using a Bradford colorimetric assay). To those fractions PreScission protease was added to cleave the C-terminal His$_6$ tag, following the instructions of the commercial vendor (Sigma-Aldrich, ref GE27-0843-01). The protease mixture was transferred into a dialysis cassette 10 K cut-off and dialyzed against reaction buffer 1 (20 mM Tris, 150 mM NaCl, 1 mM DTT, 1mM EDTA, pH 7.8) or reaction buffer 2 (20 mM HEPES-NaOH, 150 mM NaCl, 1 mM DTT, 1mM EDTA, pH 7.8) for 22 h at 4°C to ensure cleavage completion. As a final step, the whole was incubated with GST-beads for 1h at room temperature. After that time the sample was spun down at 500g, 4°C, for 10 min and the supernatant

collected, one wash with either reaction buffer 1 or 2 was performed in order to ensure complete elution of M^{pro} C145A. The combined fractions were then concentrated to half of their volume using an Amicon ultra 15 centrifugal filters (10 kDa, Merck Millipore) at 3000 rpm and 4°C.

Detection limit of probes 8c and 8d

Limit of probe detection was measured by using seven different compound concentrations in a 1:3 serial dilution, starting at a highest concentration of 10 μM. To this end, 30 μL of active M^{pro} (1 μg/mL) (50 mM HEPES, 150 mM NaCl, 1 mM DTT, pH 7.5) was incubated for 1 h at room temperature with 0.3 μL of a 100x stock solution of probe in DMSO or 0.3 μL DMSO. Next, 0.5 μL TAMRA-alkyne (1.5 mM in DMSO), 0.3 μL THPTA (5 mM in 4:1 t-BuOH: DMSO), 0.6 μL sodium ascorbate (50 mM in water) and 0.6 μL CuSO$_4$ (50 mM in water) were added to each sample and the samples were incubated 1 h at room temperature. Afterwards, 10 μL of 4x sample buffer was added to the samples, which were subsequently boiled at 95 °C for 2 minutes. Samples were resolved on an SDS-PAGE 12% acrylamide gel and visualized by in-gel fluorescence measuring on a Typhoon scanner.

Detection limit of M^{pro} with probe 8d

Limit of enzyme detection was measured by spiking HEK 293T lysates (1 mg/mL) (50 mM HEPES, 150 mM NaCl, 1 mM DTT, pH 7.5) with a dilution series of seven concentrations of active M^{pro} ranging from 1 μg/mL to 10 ng/mL. A non-spiked sample was used as a negative control. 30 μL of each lysate was labeled with 0.3 μL of a 100 μM stock of probe **8d** (DMSO) for 1h. Next, 0.5 μL TAMRA-alkyne (1.5 mM in DMSO), 0.3 μL THPTA (5 mM in 4:1 t-BuOH: DMSO), 0.6 μL sodium ascorbate (50 mM in water) and 0.6 μL CuSO$_4$ (50 mM in water) were added to each sample and the samples were incubated 1 h at room temperature. Afterwards, 10 μL of 4x sample buffer was added to the samples, which were subsequently boiled at 95 °C for 2 minutes. Samples were resolved on an SDS-PAGE 12% acrylamide gel and visualized by in-gel fluorescence measuring on a Typhoon scanner.

Direct labelling of probe targets

30 μL of HEK 293T lysate (1 mg/mL) (50 mM HEPES, 150 mM NaCl, 1 mM DTT, pH 7.5) was incubated for 1 h with 0.3 μL of a 1 mM stock solution of probe **8a**, **8c**, **8d** or **8e** or with 0.3 μL DMSO. Next, 0.5 μL TAMRA-alkyne (1.5 mM in DMSO), 0.3 μL THPTA (5 mM in 4:1 t-BuOH: DMSO), 0.6 μL sodium ascorbate (50 mM in water) and 0.6 μL CuSO$_4$ (50 mM in water) were added to each sample and the samples were incubated 1 h at room temperature. Afterwards, 10 μL of 4x sample buffer was added to the samples, which were subsequently boiled at 95 °C for 2 minutes. Samples were resolved on an SDS-PAGE 12% acrylamide gel and visualized by in-gel fluorescence measuring on a Typhoon scanner.

IC$_{50}$^{App} determination on purified M^{pro}

Inhibitor compounds at 20 mM in DMSO are dispensed into 384-well plates (Greiner 384PP 781280) using an ECHO 650T dispenser (DMSO concentration < 1%, final volume = 500 nl). A 15 μM enzyme stock solution is prepared in 20 mM HEPES, pH 7.5 and 300 mM NaCl, and subsequently diluted to a working solution of 300 nM Mpro in assay buffer (20 mM HEPES, pH 7.5 and 50 mM NaCl) before the addition of 25 μl to each well using a Multidrop Combi (Thermo Scientific). After a quick centrifugation step (1 000 rpm, 15s) the plate is incubated for 15 min at RT. The reaction is initiated with the addition of 25 μl 4 μM substrate (TSAVLQSGFRK-NH2, initially custom synthesized by the Schofield group, GLBiochem) dissolved in assay buffer. After centrifugation (1 000 rpm, 14s) the reaction is incubated for 10 min at RT before quenching with 10% formic acid. The reactions are analysed with MS using RapidFire (RF) 365 high-throughput sampling robot (Agilent) connected to an iFunnel Agilent 6550 accurate mass quadrupole time-of-flight (Q-TOF) mass spectrometer using electrospray. All

compounds are triaged by testing calculating the % inhibition at 5 and 50 μM final concentration. Dose response curves uses a 11 datapoints range of 100 – 0.0017 μM inhibitor concentrations. RapidFire integrator software (Agilent) was used to extract the m/z (+1) charge states of both the substrate (1191.67 Da) and cleaved N-terminal product TSAVLQ (617.34) from the total ion chromatogram data followed by peak integration. Percentage conversion (product peak integral/ (product peak integral + substrate peak integral))*100) and percentage inhibitions were calculated and normalised against DMSO control with deduction of any background signal in Microsoft Excel. IC50's were calculated using Levenberg–Marquardt algorithm is used to fit a restrained Hill equation to the dose-response data with both GraphPad PRISM and CDD.

EC_{50} determination of probes 8a, 8c and 8d on SARS-CoV-2 infected VeroE6 cells

Cells and viruses

The SARS-CoV-2 isolate used in this study was the BetaCov/Belgium/GHB-03021/2020 (EPI ISL407976|2020-02-03), which was isolated from a Belgian patient returning from Wuhan in February 2020. The isolate was passaged 7 times on VeroE6 cells which introduced two series of aminoacid deletions in the spike protein (PMID: 33203860). The infectious content of the virus stock was determined by titration on Vero E6 cells. The SARS-CoV-2 antiviral assay is derived from the previously established SARS-CoV assay (PMID: 15961169). In this assay, fluorescence of VeroE6-eGFP cells (provided by Dr. K. Andries J&JPRD; Beerse, Belgium) declines after infection with SARS-CoV-2 due to the cytopathogenic effect of the virus. In the presence of an antiviral compound, the cytopathogenicity is inhibited and the fluorescent signal maintained. The compounds were added in serial dilutions to the cells one day before infection with SARS- CoV-2. Four days after infection eGFP fluorescence was assessed with high content imaging. VeroE6 cells were maintained in Dulbecco's modified Eagle's medium (DMEM; Gibco cat no 41965-039) supplemented with heat-inactivated 10% v/v fetal calf serum (FCS; Biowest) and 500 μg/mL Geneticin (Gibco cat no 10131-0275). and kept under 5% CO2 at 37°C.

All SARS-CoV2-related experimental work was performed in the certified, high-containment biosafety level-3 facilities of the Rega Institute at the KU Leuven.

SARS-CoV-2 screening

Stock solutions of the various compounds in DMSO (10 mM) were prepared. The test compounds were serially diluted in assay medium (DMEM supplemented with 2% v/v FCS). Diluted compounds were then mixed with SARS-CoV-2 at 20 TCID50/well and VeroE6-eGFP cells corresponding to a final density of 25,000 cells/well in 96-well blackview plates (Greiner Bio-One, Vilvoorde, Belgium; Catalog 655090). The plates were incubated in a humidified incubator at 37°C and 5% CO2. At 4 days p.i., the wells were examined for eGFP expression using an argon laser-scanning microscope. The microscope settings were excitation at 488 nm and emission at 510 nm and the fluorescence images of the wells were converted into signal values. The results were expressed as EC_{50} values defined as the concentration of compound achieving 50% inhibition of the virus-reduced eGFP signals as compared to the untreated virus-infected control cells.

Toxicity of compounds in the absence of virus was evaluated in a standard MTS-assay as described previously on Huh7 cells.[15]

5.5. References

[1]   D. A. J. Tyrrell, M. L. Bynoe, *Lancet* **1966**, *287*, 76–77.

[2]   T. Kuiken, R. A. M. Fouchier, M. Schutten, G. F. Rimmelzwaan, G. van Amerongen, D. van Riel, J. D. Laman, T. de Jong, G. van Doornum, W. Lim, et al., *Lancet* **2003**, *362*, 263–270.

[3]   A. M. Zaki, S. van Boheemen, T. M. Bestebroer, A. D. M. E. Osterhaus, Fouchier, *N Engl J Med* **2012**, *367*, 1814–1820.

[4]   "www.worldometers.info/coronavirus,"

[5]   K. P. Patel, S. R. Vunnam, P. A. Patel, K. L. Krill, P. M. Korbitz, J. P. Gallagher, J. E. Suh, R. R. Vunnam, **2020**, 2005–2011.

[6]   J. L. Bernal, N. Andrews, C. Gower, E. Gallagher, R. Simmons, S. Thelwall, J. Stowe, E. Tessier, N. Groves, G. Dabrera, et al., *N Engl J Med* **2021**, *385*, 585–594.

[7]   H. M. Mengist, T. Dilnessa, T. Jin, **2021**, *9*, 1–19.

[8]   S. Ullrich, C. Nitsche, *Bioorganic Med. Chem. Lett.* **2020**, *30*, 127377.

[9]   T. Shu, M. Huang, D. Wu, Y. Ren, X. Zhang, Y. Han, J. Mu, **2020**, *12250*, 321–329.

[10]   Z. Jin, X. Du, Y. Xu, Y. Deng, M. Liu, Y. Zhao, *Nature* **2020**, *582*.

[11]   W. Rut, L. Zhang, P. Kasperkiewicz, M. Poreba, R. Hilgenfeld, M. Dra, **2017**, *139*, 88–94.

[12]   L. Zhang, D. Lin, X. Sun, U. Curth, C. Drosten, L. Sauerhering, S. Becker, K. Rox, R. Hilgenfeld, *Science,* **2020**, *368*, 409–412.

[13]   M. A. T. Van De Plassche, M. Barniol-xicota, S. H. L. Verhelst, *ChemBioChem* **2020**, *21*, 3383–3388.

[14]   J. S. Martin, C. J. Mackenzie, D. Fletcher, I. H. Gilbert, *Bioorg. Med. Chem.* **2019**, *27*, 2066–2074.

[15]   D. Jochmans, P. Leyssen, J. Neyts, **2012**, *183*, 176–179.

Chapter VI: Clickable polyamine derivatives as probes for the polyamine transport system

This Chapter is based on

R. Vanhoutte, J. P. Kahler, S. Martin, S. van Veen, S. H. L. Verhelst, Clickable polyamine derivatives as chemical probes for the polyamine transport system, *ChemBioChem* **2018**, *19*, 907–911.

and

N. N. Hamouda, C. van den Haute, **R. Vanhoutte**, R. Sannerud, M. Azfar, R. Mayer, A. C. Calabuig, J. V. Swinnen, P. Agostinis, V. Baekelandt, W. Annaert, F. Impens, S. H. L. Verhelst, J. Eggermont, S. Martin, P. Vangheluwe, ATP13A3 Is a Major Component of the Enigmatic Mammalian Polyamine Transport System. *J. Biol. Chem.* **2021**, *296* (13), 100182.

Abstract

Polyamines are essential for cell growth and differentiation, but their trafficking by the polyamine transport system is not fully understood. In this chapter, the synthesis of several azido-derivatized polyamines for easy conjugation by click chemistry is described. Attachment of a BODIPY-dye gave fluorescent polyamine probes, which were tested in cell culture. The linear probe series showed superior cellular uptake compared with the probes where the dye was attached to a branch on one of the central amines. Interestingly, the linear probes accumulated rapidly in cancer cells (MCF-7), but not in non-tumorigenic cells (MCF-10A). The fluorescent polyamine probes are therefore applicable to the study of polyamine trafficking, whereas the azido-polyamines may be further utilized to transport cargo into cancer cells by exploiting the polyamine transport system.
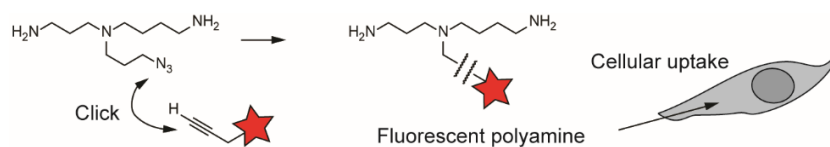
6.1. Introduction

Naturally occurring polyamines, such as spermidine and spermine (Figure **6.1A**), are involved in a variety of critical cellular functions.[1] These include gene expression,[2] cell proliferation and differentiation,[3] as well as cellular stress.[4] Their intracellular concentration, which is in the millimolar range, is tightly regulated by several mechanisms: biosynthesis, catabolism and polyamine transport.[5] Whereas the polyamine biosynthesis and catabolism have been well characterized, the molecular players of polyamine transport remain elusive.[5] As most tumors have elevated activity of the polyamine transport system (PTS),[6] chemical probes that exploit the PTS might be used to target cancer cells for imaging and chemotherapy.[7] In addition, polyamine chemical probes may help in elucidating the transporters constituting the PTS. Interestingly, the structural tolerance of the PTS allows the uptake of substituted polyamines to a large extent. This is illustrated by the report of various fluorescently tagged analogs of spermidine and spermine,[8-15] which include N^4-spermidine-MANT[8], spermidine-C2-BODIPY[9] and spermine-NBD[12] (Figure **6.1B**), all made by different types of linkages to the fluorophore. In order to increase the synthetic flexibility towards polyamine analogs, the synthesis of clickable polyamine derivatives was initiated. In this chapter, the synthesis of five azide-functionalized polyamines suitable for easy click chemistry mediated conjugation to alkyne-functionalized cargo is described, facilitating different research needs. As an example, the polyamines were clicked to an alkyne-functionalized BODIPY to monitor polyamine uptake by cancer cells.
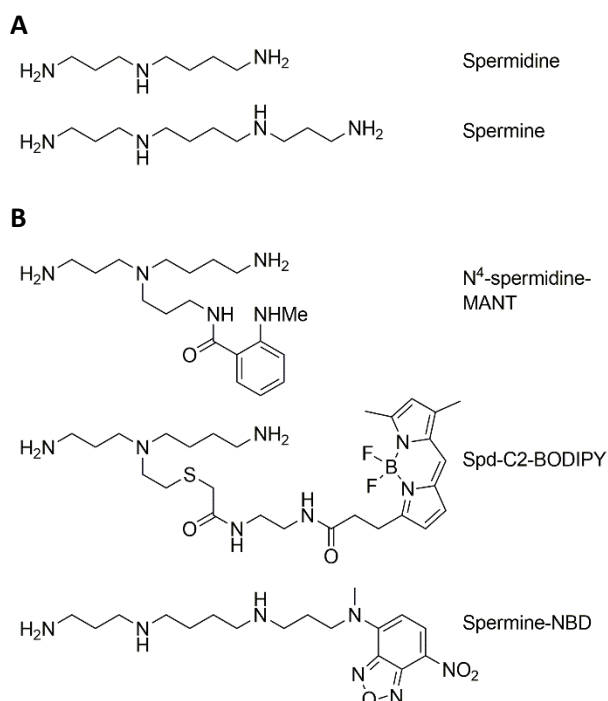

Figure 6.1. Structures of polyamines and fluorescent polyamine probes. **A.** Spermidine and spermine. **B.** Three different fluorophore-polyamine conjugates.
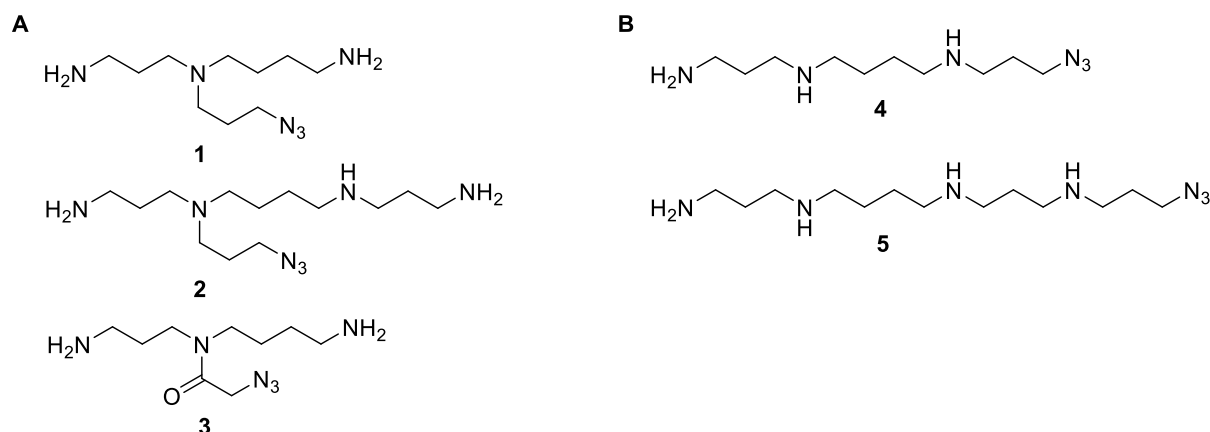
Figure 6.2. A. Branched azido polyamine series comprising compounds **1**, **2**, and **3**. **B.** Linear azido polyamine series comprising compounds **4** and **5**.

6.2. Results and discussion

Synthesis of clickable polyamines. For the design of the azido-polyamine derivatives, the following aspects were taken into consideration: (1) Conjugation can be performed on the terminal primary amine or at a central secondary amine. In the past, spermidine analogues substituted at the secondary amine were shown to exhibit better uptake than analogues with substituents at the primary amine.[16] (2) The polycationic character also seems to be important for uptake into the cell.[17] In view of both of these points, it was decided to synthesize two different series of compounds: a branched series, in which the azido group is located on a substituent at a secondary amine (Figure **6.2A**), and a linear series in which the azide is located on a substituent at a primary amine (Figure **6.2B**). The resulting azido polyamines carry different numbers of positive charges under physiological conditions. In total, the charges are 2 (compound **3**), 3 (compounds **1** and **4**) and 4 (compounds **2** and **5**). This will aid in getting insight into the relationship between charge, linearity and uptake.

For the synthesis of the azido polyamines, commercially available spermidine and spermine were used as starting materials. Different protecting group manipulation strategies were employed in combination with selective N-alkylation, to install a linker containing an azide on a single amine of these polyamines towards Boc-protected derivatives **14**, **15**, **17**, **18** and **22** (Scheme **6.1** and **6.2**). Different approaches were applied for the synthesis of the branched series and for the linear series.

For the branched series, spermidine and spermine were treated with respectively 2 and 3 equivalents Boc-ON in order to protect all amines, except one secondary amine, yielding compounds **8** and **9**, respectively (Scheme **6.1**). The next reactions were the same on both compounds: first, the remaining

free amine was alkylated through Michael addition with acrylonitrile to yield nitriles **10** and **11**. The nitrile on the installed linker was then reduced to an amine via a Raney Nickel catalyzed hydrogenation at elevated pressure, yielding compounds **12** and **13**. In a final step, these resulting amines were converted to azides via diazotransfer with Imidazole-1-sulfonyl azide.HCl to obtain the azide-containg polyamines **14** and **15**.

For azide-functionalized polyamine **17**, in which a tertiary amine is replaced by an amide, double Boc-protected spermidine **8** was treated with chloroacetyl chloride to give compound **16**, followed by a nucleophilic substitution of the chloride with sodium azide to yield compound **17**.
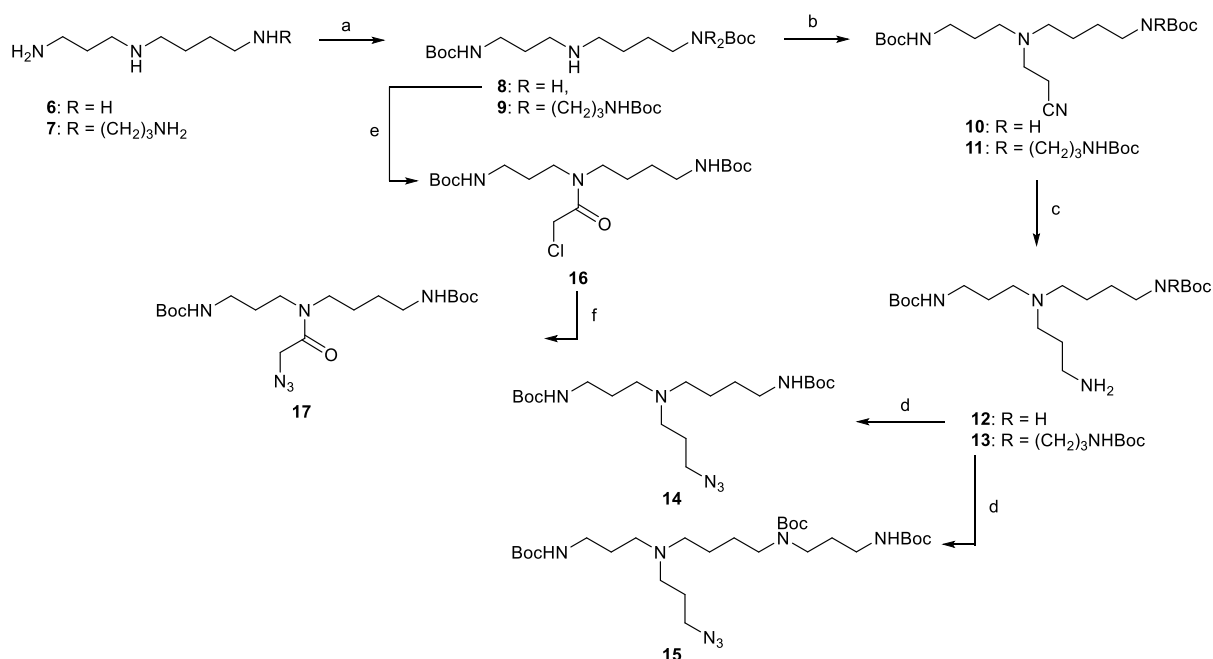
Scheme 6.1. Synthesis of branched probes. a) Boc-ON 2 or 3 eq., THF, rt, 81%. b) acrylonitrile, MeOH, reflux, 84% for **10,** 16% over two steps for **11**. c) Raney Ni, H_2 40 psi, NaOH, EtOH/H_2O, rt, 73-74%. d) Imidazole-1-sulfonyl azide hydrochloride, TEA, CuSO$_4$, MeOH, rt, 22-70%). e) Chloroacetylchloride, DCM, rt. f) NaN$_3$, DIEA, DCM, rt, 33% over two steps.

For the synthesis of the linear series towards compound **18** (Scheme **6.2**), spermine was treated with one equivalent of Imidazole-1-sulfonyl azide.HCl to convert one amine function of a fraction of the spermine starting material to an azide. This was followed by adding an excess of Boc anhydride to the reaction mixture, yielding the fully protected azide-functionalized spermidine **18** in two steps, which could now be purified from the other reaction products.

For the synthesis of linear azide-functionalized spermine **22** (Scheme **6.2**), a desymmetrization sequence of reactions was applied first to create a triple Boc-protected spermine with a single unprotected primary amine (compound **19**). To this end, spermine was treated with one equivalent of ethyl trifluoroacetate, to create a fraction of the starting material in which one primary amine was protected with a trifluoroacetyl group. Next, an excess of Boc anhydride was added to the reaction mixture to protect all non-protected amines in the reaction mixture. The TFA protecting groups were next removed with NaOH, which allowed the separation of compound **19**, which has one unprotected amine function, from the reaction mixture which contains side products with two unprotected amines and no unprotected amines. The free amine of **19** was alkylated with acrylonitrile and subsequently protected using Boc₂O to give compound **20**. The nitrile on **20** was hydrogenated to an amine via a Raney Nickel catalyzed hydrogenation at elevated pressure to yield **21.** The resulting amine function was subsequently converted to an azide via a diazotransfer reaction with Imidazole-1-sulfonyl azide.HCl to yield **22**.
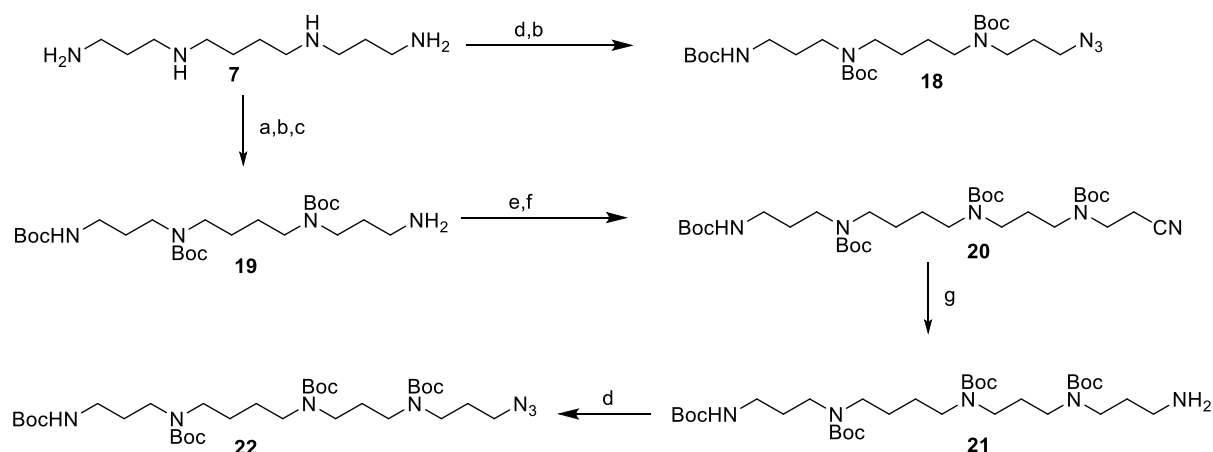
Scheme 6.2. Synthesis of the linear polyamine series. a) Ethyl trifluoroacetate, MeOH, -78 °C to rt. b) Boc₂O 3 eq., DIEA, MeOH, rt, 29% over two steps for **18**. c) NaOH, MeOH, rt, 26% over three steps for **19**. d) Imidazole-1-sulfonyl azide hydrochloride, TEA, CuSO₄ (cat.), MeOH, rt, 93% for **22**. e) acrylonitrile, MeOH, rt. f) Boc₂O 1 eq., MeOH, rt, 66% over two steps. g) Raney Ni, H₂ 40 psi, NaOH, EtOH/H₂O, rt, 96%.

Formation of Polyamine probes from azide-functionalized polyamines through CuAAC. In order to show the applicability of the azido-polyamine derivatives, BODIPY conjugates were synthesized by first deprotection of the Boc-groups on compounds **14, 15, 17, 18** and **22** using 50% TFA. Subsequently, the products underwent copper-catalyzed click chemistry with BODIPY alkyne building block **23**[18] followed by HPLC purification (Scheme **6.3**) to obtain polyamine probes **24-28**.
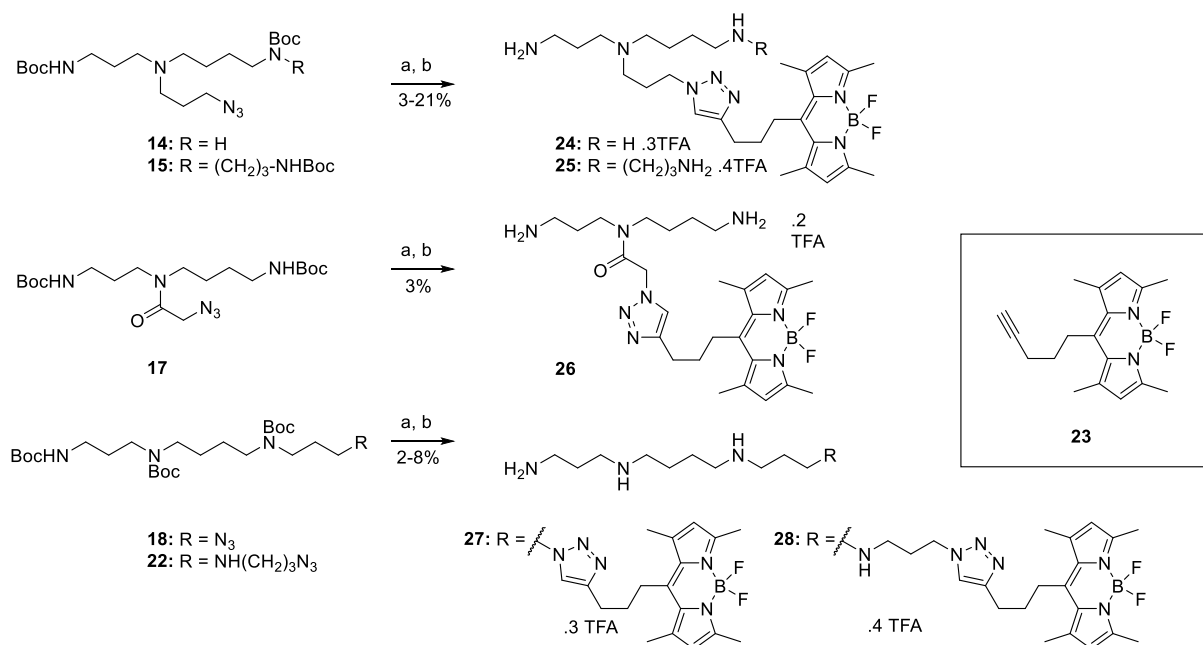
Scheme 6.3. BODIPY click conjugation towards fluorescent polyamine probes. a) TFA/DCM (1/1). b) **23**, DIEA, CuBr, DCM.

Spectral properties of synthesized polyamine probes. The resulting BODIPY-tagged polyamine derivatives display strong absorption and green fluorescence (emission at 504-510 nm; Figure **6.3**). All compounds show Stokes shifts between 10 nm (the alkyne BODIPY **23**) and 16 nm (compound **28**) (Figure **6.3** and Table **6.1**). The spectral properties show only very minor differences between the different BODIPY-tagged polyamines, indicating that the polyamine-probe does not influence the electronic properties of the dye (Table **6.1**).
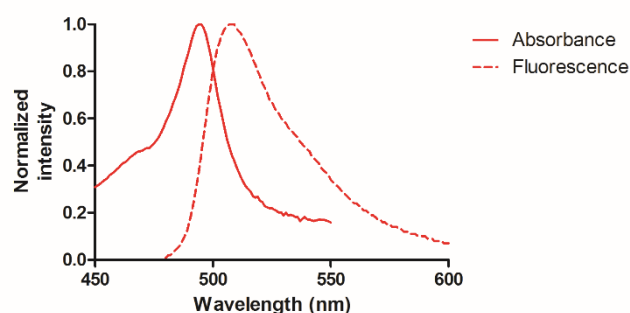
Figure 6.3. Normalized absorption and emission spectra of polyamine-BODIPY conjugate 24.

Table 6.1. Spectral properties of polyamine probes and BODIPY **23**.

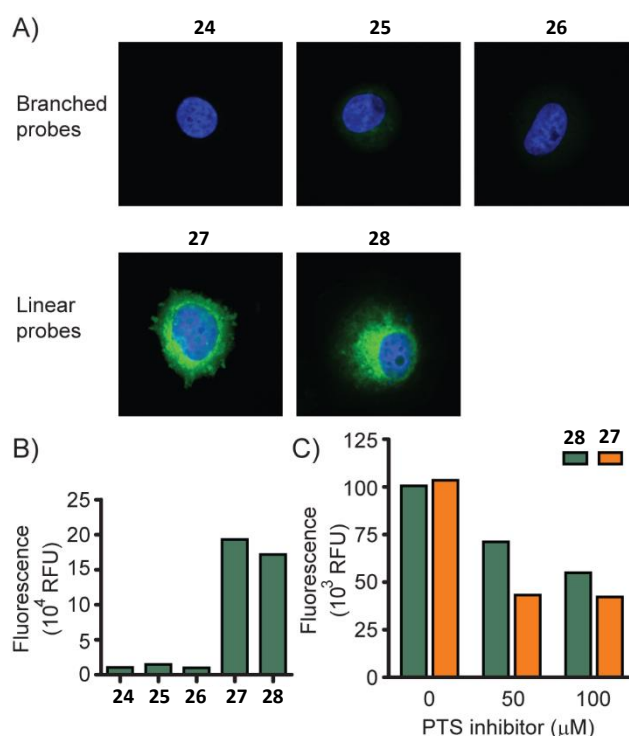| Compound	λ_{Abs} (max) (nm)	λ_{em} (max) (nm)	Stokes shift (nm)
24	495	508	13
25	495	506	11
26	494	508	14
27	494	508	14
28	494	510	16
23	494	504	10

Figure 6.4. Uptake of polyamine probes by MCF-7 cells. A. Representative fluorescent microscopy images of MCF-7 cells after 4 h incubation with 10 μM of indicated probes, followed by washing and fixing. Green color represents BODIPY emission. Nuclei were stained with DAPI (blue color). **B.** Flow cytometry of MCF-7 cells after 4 h incubation with 10 μM of the indicated probes and trypsinization. Depicted is the mean fluorescent intensity of a minimum of 10,000 cells. **C.** Mean fluorescent intensity as measured by flow cytometry of MCF-7 cells after 24h incubation with the PTS inhibitor benzyl viologen followed by addition of probes **27** or **28** for 4h.

Uptake of polyamine probes in MCF-7 and MCF-10A cells. Next, the ability of cells to take up the different fluorescent polyamine conjugates was examined. To this end, the breast cancer cell line MCF-7 was incubated with probes **24**-**28** followed by confocal fluorescent microscopy (Figure **6.4A**). A substantial difference in the uptake of the various probes was obvious from the observed intensities of the intracellular BODIPY fluorescence. Interestingly, branched probes **24**-**26** displayed low uptake efficiency in comparison with linear probes **27** and **28**. Previous studies reported that spermidine analogues with substituents at the central N^4-nitrogen were better in competing for spermidine uptake than those with substituents at the primary amines.[16] However, the substituents only ranged in size from methyl (least bulky) to benzyl (most bulky). Apparently, the biological properties of these substituted polyamines cannot be generalized when attaching larger cargo to the polyamines. In line with our findings, linear fluorophore-conjugated polyamines, such as spermine-NBD (Figure **6.1**) and a cyanine dye connected to the primary amine of various polyamines,[14] have shown efficient cellular uptake, but no direct comparison with branched counterparts was made. Therefore, flow cytometry experiments of MCF-7 cells were performed after 4 h treatment with probes **24**-**28**. Results show that

uptake of linear probes is more than tenfold higher compared with branched probes (Figure **6.4B**). In order to demonstrate that the PTS is responsible for the uptake, MCF-7 cells were treated with benzylviologen, a known inhibitor of the PTS, prior to incubation with probes **27** and **28**. PTS inhibition gave up to 60% reduction of the mean fluorescence of the cells in comparison with untreated cells (Figure **6.4C**), supporting that the probe uptake is mediated by the PTS.
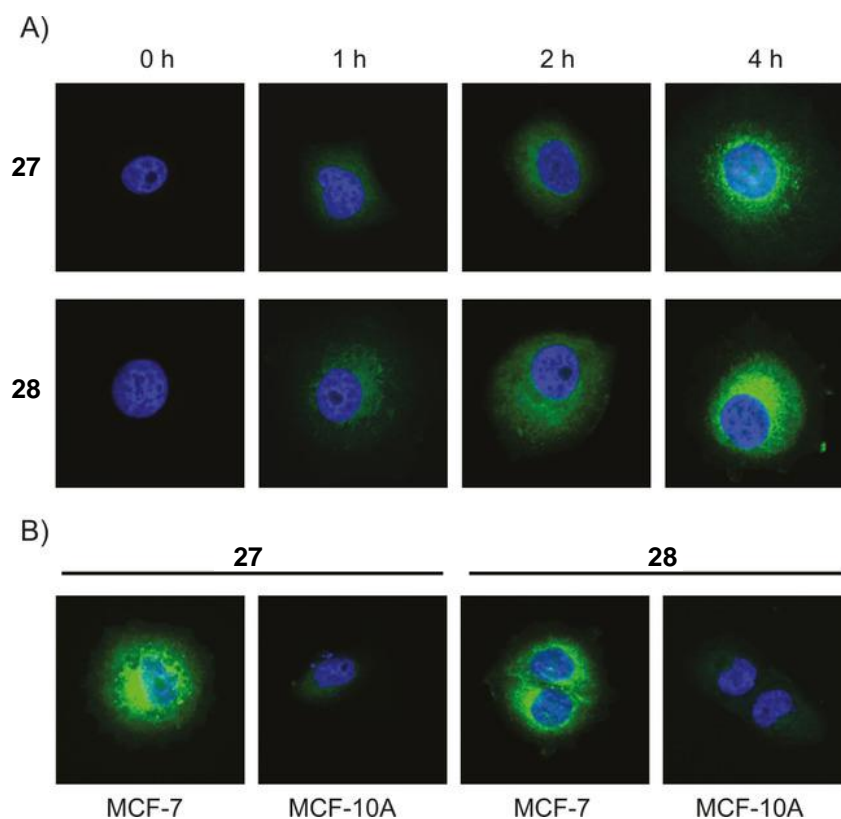

Figure 6.5. Uptake of probes **27** and **28**. A) Representative fluorescent microscopy pictures of representative cells during a time course of uptake in MCF-7 cells. Blue colour represents nuclear staining by DAPI; green colour corresponds to BODIPY emission. B) Comparison of uptake in MCF-7 versus MCF-10A cells after 4h of incubation with 10 μM of the indicated polyamine probes.

Uptake of linear probes **27** and **28** was efficient, and intracellular accumulation was observed as early as 1 h after probe addition (Figure **5A**). Next, the uptake of both linear probes was compared in two different cell lines: the tumorigenic MCF-7 cell line and the non-tumorigenic breast epithelial cell line MCF-10A. Previous studies have shown that polyamine levels in MCF-7 cells are significantly higher than in MCF-10A cells.[19] In this study, a large difference in fluorescent staining was observed, with almost no uptake by the MCF-10A cells (Figure **5B**), in agreement with the higher activity of the PTS in cancer cells.

Synthesis of a Putrescine-BODIPY probe. To complete the set of probes for the most commonly occurring natural polyamines, a Putrescine-BODIPY probe was synthesized to the model of probes **27** and **28**. To this end, an azide-functionalized putrescine **33** was synthesized from of 3-azidopropyl tosylate (**30**), which was made in two reactions, starting from 3-Chloropropanol, and *N*-Boc-putrescine (**32**), which was created by reacting putrescine with Boc-anhydride. (Scheme **6.5**). **37** was coupled to BODIPY **23** through CuAAC and subsequently Boc-deprotected with HCl in dioxane to obtain Putrescine probe **39** as a double HCl salt.
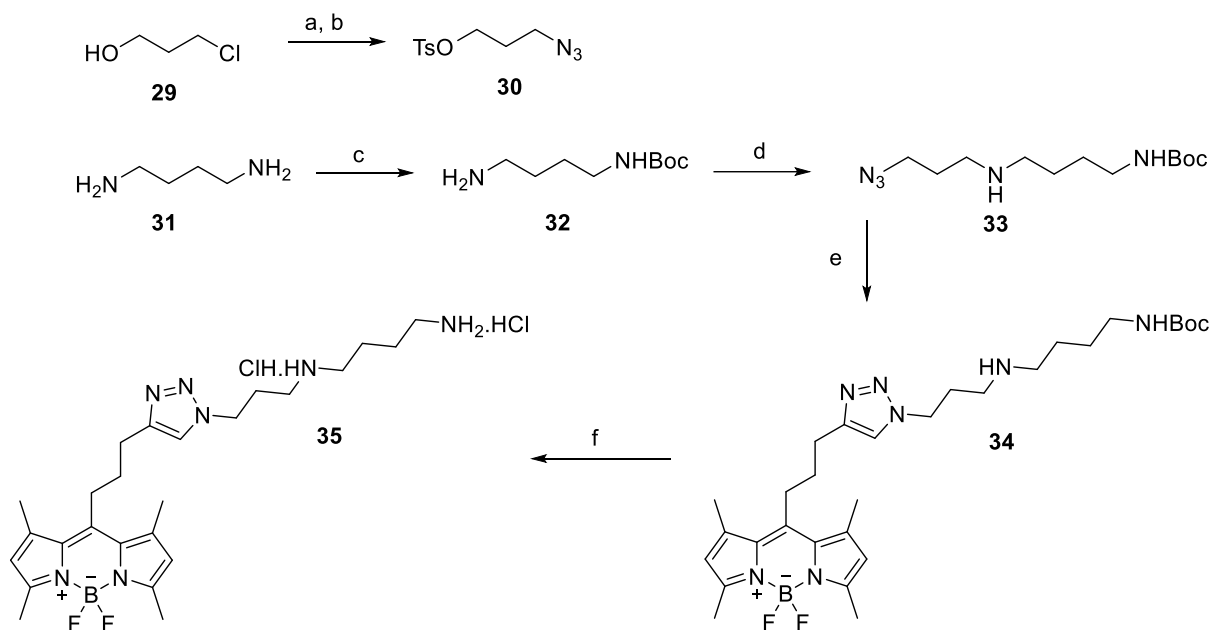
Scheme 6.5. Synthesis of Put-BODIPY **39**. a) NaN$_3$, H$_2$O, reflux. b) TsCl, TEA, DCM, rt., 58% over two steps. c) Boc$_2$O, CHCl$_3$, rt, 98%. d) **34**, DIEA, THF, rt, 30%. e) **23**, DIEA, CuBr, DCM, 63%. f) 4M HCl in dioxane, rt, quant.

6.3. Conclusion

In summary, this chapter describes the synthesis of novel, clickable azido-polyamine derivatives. By clicking these to a BODIPY dye, fluorescent polyamine probes were easily constructed. Cellular uptake of the linear fluorescent polyamines was much more efficient than of the branched ones. Both linear spermine and spermidine probes were taken up similarly, suggesting that spermine and spermidine are both effective in delivering cargo and that the total positive charge in these probes does not seem to matter. It is also show that linear probes **27** and **28** are taken up by tumorigenic MCF-7 cancer cells, but much less by non-tumorigenic MCF-10A cells, which may be explained by a higher activity of the PTS in cancer cells. Hence, these molecules will be useful tools for future interrogation of the PTS, and experiments along these lines will be undertaken and reported in due course. As of 2021, spermine and spermidine probes **27** and **28** have been applied in a study by Van

Veen et al. that identified ATP13A2 as a polyamine transporter with preference for spermine and spermidine over putrescine.[26] Hamouda et al. used putrescine probe **35** to proof that ATP13A3 is a polyamine transporter with preference for putrescine over spermine and spermidine[27].

In addition to the probes, the azido polyamines may also be utilized to shuttle alkyne-containing chemical probes into cancer cells, allowing for selective delivery of potent anticancer modalities that may ultimately reduce off-target effects.

6.4. Experimental section

6.4.1. Biochemistry

Acquisition of absorption and emission spectra: A UV-Visible-NIR Lambda 950 Perkin Elmer spectrometer was used to record the absorption spectra with 1 nm spectral resolution. Attenuators were used to remove the effect of background and noise. The samples placed in a quartz cuvette were sealed and mounted on a Teflon sample holder. Emission spectra were recorded using an Edinburgh Instruments FLS 980 spectrometer on the samples placed in a quartz cuvette (10 mm path length) and sealed by a teflon stopper. The excitation wavelength was set to 470 nm and the emission was collected using a 1-nm step size. The emission was collected in "right-angle mode" through the quartz cuvette and sent to a monochromator and photomultiplier tube (PMT) detector. The wavelength dependence of the detection channel of the fluorimeter was corrected. The optical density of the sample was kept below 0.2.

Cell culture: MCF-7 cells were cultured in Dulbecco's Modified Eagle Medium (DMEM; Sigma-Aldrich) with 10% fetal bovine serum (Invitrogen). MCF-10A cells were cultured in DMEM/F-12 medium (Fisher Scientific) with 5% horse serum (Sigma-Aldrich), 20 ng/mL EGF (Peprotec EC Ltd), 0.5 mg/mL hydrocortisone (TCI Europe), 100 ng/mL cholera toxin (Sigma-Aldrich) and 10 μg/mL insulin (Sigma-Aldrich). Cells were cultured at 37 °C under a 5% CO_2 atmosphere and were split before reaching confluency. Both cell lines were tested for mycoplasma infection and found negative.

Cellular uptake experiments: Cells were seeded in 12 well plates at 25,000 cells/well and cultured overnight in order to adhere. Thereafter, cells were incubated with 10 μM of fluorescent polyamines **14, 15, 17, 18** and **22** for the indicated time, washed with PBS, and fixed with 4% paraformaldehyde. DAPI (1:5000, 10 min) was used as a nuclear stain. Images were acquired using a Zeiss LSM 780 (x63 lens and 2x digital magnification) and processed using Image J.

Flow cytometry: Cells were seeded in a 12 well plate at a density of 100,000 cells/well and allowed to attach overnight. Subsequently, cells were treated with 10 μM of probes **14, 15, 17, 18** and **22** for 4 h and collected by trypsinization. Samples were subjected to flow cytometry on an Attune flow cytometer, where the mean fluorescent intensities were derived from a minimum of 10,000 events per treatment. For the inhibition studies, the experiment was performed as follows: after overnight attachment in 6- or 12-well plates, cells were treated with benzylviologen (50 or 100 μM) or vehicle (PBS) for 24 h. Probes **18** or **22** were added to a final concentration of 10 μM, followed by 4h incubation. Cells were collected by trypsinization and subjected to flow cytometry on an Attune flow cytometer. Each treatment was performed twice in triplicate.

6.4.2. Synthesis

General materials & methods

All starting materials and solvents were bought from commercial vendors and used without further purification. Reactions were analyzed by Thin Layer Chromatoghraphy (TLC) on pre coated 0.20 mm thick ALUGRAM® TLC sheets with fluorescent indicator and by liquid chromatography-mass spectrometry (LC-MS) performed on a Prominence Ultra-fast Liquid Chromatography system equipped with a 2x150 mm C18 analytical column (Waters X-Bridge) coupled to a MS-2020 single quadrupole mass analyzer (Shimadzu). A linear gradient of 5-80% acetonitrile in water (with 0.1% formic acid) was utilized. Silica column chromatography was performed using 230-400 mesh silica (Kieselgel 60). High Pressure Liquid Chromatography (HPLC) purification was performed using a 10x150 mm C18 preparative column (X-Bridge). NMR spectra were recorded in $CDCl_3$ or CD_3OD and measured using a Bruker UltrashieldTM 400 MHz NMR Spectrometer. Chemical shifts are reported in ppm relative to the residual solvent peak and J values are reported in Hz.

General procedure for click chemistry of polyamine-TFA salts to BODIPY 23

CuBr (0.5 equiv) and N,N-diisopropylethylamine (DIEA, 4 equiv.) were added to a solution of the crude material and BODIPY **23** (1 equiv), which was synthesized according to previous reports,[18,22] in CH_2Cl_2. The reaction was stirred for 2–4 days with the addition of extra CuBr, if the progress of the reaction, as monitored by LC-MS, had stalled. The solvent was removed under vacuum and the products purified by reversed-phase HPLC. Fractions containing product were pooled and lyophilized.

N1-(3-aminopropyl)-N1-(3-azidopropyl)butane-1,4-diamine (1)

The title compound was made by Boc-deprotection of **14** (30.0 mg, 70.0 μmol) using 3 mL of a 1:1 mixture of TFA:DCM and was used in crude form in the click chemistry (dark orange-brown solid; 15.4 mg, 96.6%). ^{1}H NMR (400 MHz, CDCl3, 298K): δ = 1.65-1.48 (m, 2H), 1.44-0.97 (m, 14H), 0.92-0.67 (m, 4H). ESI-MS: m/z calcd for $C_{25}H_{48}N_6O_6$ [M+H]$^+$ 229.21, found: 229.15.

N1,N4-bis(3-aminopropyl)-N1-(3-azidopropyl)butane-1,4-diamine (2)

The title compound was made by Boc-deprotection of **15** (60 mg, 102.43 μmol) using 3 mL of a 1:1 mixture of TFA:DCMe[1]H NMR (400 MHz, CDCl$_3$, 298K): δ = 3.15 (t, 2H, J = 6.3 Hz), 3.09 - 2.61 (m, 19H), 1.84 – 1.72 (m, 4H), 1.69-1.60 (m, 2H), 1.58-1.31 (m, 4H). ESI-MS: m/z calcd for $C_{13}H_{31}N_7$ [M+H]$^+$ 286.44, found: 286.10.

N-(4-aminobutyl)-N-(3-aminopropyl)-2-azidoacetamide (3)

The title compound was made by Boc-deprotection of **17** (40.0 mg, 93.3 μmol) using 3 mL of a 1:1 mixture of TFA:DCM and was used in crude form in the click chemistry (brown oil; 39.3 mg, 92.2%). ^{1}H NMR (400 MHz, CDCl3, 298K): δ = 3.94-3.68 (m, 6H), 3.27-2.95 (m, 2H), 2.67-2.29 (m, 4H), 2.19-1.99 (m, 2H), 1.14-0.35 (m, 6H). ESI-MS: m/z calcd for C9H20N6O [M+H]$^+$ 229.17, found: 229.00.

N1-(3-aminopropyl)-N4-(3-azidopropyl)butane-1,4-diamine (4)

The title compound was made by Boc-deprotection of **18** (167 mg, 315.96 μmol) using 3 mL of a 1:1 mixture of TFA:DCM and was used in crude form for click chemistry (white solid, 66.2 mg, 85.4%). ^{1}H NMR (400 MHz, DMSO, 298K): δ = 3.47 (t, 4H, J = 6.4 Hz), 3.01-2.86 (m, 12H), 1.94-1.83 (m, 4H), 1.69-1.59 (bs, 4H). ESI-MS: m/z calcd for $C_{10}H_{24}N_6$ [M+H]$^+$ 229.21, found: 229.05.

N1-(3-aminopropyl)-N4-(3-((3-azidopropyl)amino)propyl)butane-1,4-diamine (5)

The title compound was made by Boc-deprotection of **22** (66.2 mg, 96.5 μmol) using 3 mL of a 1:1 mixture of TFA:DCM and was used in crude form for click chemistry (brown oil, 86.9%). ^{1}H NMR (400 MHz, CD3OD, 298K): δ = 3.02-2.70 (m, 4H), 2.35 (t, 2H, J = 6.1 Hz), 2.07-1.88 (m, 2H), 1.87-1.83 (m, 4H), 1.82-1.74 (m, 2H), 1.71 (t, 2H, J = 6.3 Hz), 1.44-1.29 (m, 2H), 1.28-1.15 (m, 8H), 1.05 (t, 2H, J = 6.2 Hz). ESI-MS: m/z calcd for C13H31N7 [M+H]$^+$ 286.44, found: 286.05.

tert-butyl (3-((4-((tert-butoxycarbonyl)amino)butyl)amino)propyl)carbamate (8)

Spermidine (978 mg, 6.73 mmol) and triethylamine (1.13 mL, 8.08 mmol) were dissolved in 10 mL THF. This mixture was cooled to 0 °C, after which a solution of Boc-ON (3.32 g, 13.47 mmol) in 9 mL THF was added gradually to the reaction mixture over the course of 10 minutes. The mixture was then allowed to slowly warm to room temperature and stirred overnight. After completion of the reaction (TLC: EtOAc:petroleum ether, 3:2), the solvent was evaporated and the product was purified by silica column chromatography (EtOAc:petroleum ether, 3:2 -> EtOAc:triethylamine, 100:1) to give **17** as a colorless oil (1.84 g, 81.1 %). ^{1}H NMR (400 MHz, CDCl$_3$, 298 K): δ = 4.91 (bs, 1H); 4.76 (bs, 1H); 2.91 (bs, 1H); 2.69-2.85 (m, 4H); 1.85-1.76 (m, 2H), 1.69-1.61 (m, 2H); 1.59-1.50 (m, 2H); 1.43 (bs, 22H). ESI-MS: *m/z* calcd for C$_{17}$H$_{35}$N$_3$O$_4$ [M+H]$^+$ 346.26, found 346.05.

tert-butyl (3-((tert-butoxycarbonyl)amino)propyl)(4-((3-((tert-butoxycarbonyl)amino)propyl)amino)butyl)carbamate (9)

Spermine (500 mg, 2.47 mmol) and triethylamine (519 μL, 3.71 mmol) were dissolved in 3 mL THF. This mixture was cooled to 0 °C, after which a solution of Boc-ON (1.82 g, 7.41 mmol) in 5 mL THF was added gradually to the reaction mixture over the course of 10 minutes. The mixture was then allowed to slowly warm to room temperature and stirred overnight. After completion of the reaction, the reaction mixture was evaporated to dryness, and put through to the next step without further purification.

tert-butyl (3-((4-((tert-butoxycarbonyl)amino)butyl)(2-cyanoethyl)amino)propyl)carbamate (10)

Compound **8** (500 mg, 1.45 mmol) was dissolved in 12 mL MeOH. Acrylonitrile (237 μl, 3.62 mmol) was added to this solution, which was subsequently heated to refluxing and stirred overnight. After completion of the reaction (TLC: EtOAc:petroleum ether, 4:1), the mixture was evaporated to dryness and purified by column chromatography (EtOAc:petroleum ether, 4:1) to give the title compound as a colorless oil. (484 mg, 84%). ^{1}H NMR (400 MHz, CDCl$_3$, 298K): δ = 4.98 (bs, 1H), 4.73 (bs, 1H), 3.21-3.05 (m, 4H), 2.74 (t, 2H, J = 6.6 Hz), 2.51-2.38 (m, 6H), 1,62 (quin, 2H, J$_{12}$ = 6.4 Hz, J$_{23}$ = 6.5 Hz), 1.54-1.36 (m, 22H). ESI-MS: *m/z* calcd for C$_{20}$H$_{38}$N$_4$O$_4$ [M+H]$^+$ 399.29, found: 399.10.

tert-butyl (3-((tert-butoxycarbonyl)amino)propyl)(4-((3-((tert-butoxycarbonyl)amino)propyl)(2-cyanoethyl)amino)butyl)carbamate (11)

The crude product of **9** was dissolved in 3.5 mL MeOH. Acrylonitrile (162 μL, 2.47 mmol) was dissolved in 2 mL MeOH and added dropwise to the solution of **9** over the course of 10 minutes. The reaction mixture was subsequently heated until refluxing and stirred

overnight. After completion of the reaction (TLC: DCM:MeOH, 96:4). The reaction mixture was evaporated to dryness and purified by column chromatography (DCM:MeOH, 96:4), to give the title compound as a brown oil (176 mg, 15.6 % over two steps). ^{1}H NMR (400 MHz, CDCl$_3$, 298K): δ = 3.29-3.02 (m, 8H), 2.78-2.70 (m, 2H), 2.50-2.40 (m, 6H), 1.70-1.57 (m, 4H), 1.47-1.34 (m, 33H). ESI-MS: *m/z* calcd for C$_{28}$H$_{53}$N$_5$O$_6$ [M+H]$^+$ 556.40, found: 556.25.

tert-butyl (3-((3-aminopropyl)(4-((tert-butoxycarbonyl)amino)butyl)amino)propyl) carbamate (12)

Compound **10** (1.07 g) was dissolved in 4 mL EtOH (70%) in a Parr bottle. 1 N NaOH in 40 mL EtOH (70%) and 0.5 g of Raney Nickel slurry W-2 were added to this solution. The reaction mixture was shaken under H$_2$ pressure at 2.7 bar overnight. After completion (TLC: EtOAc:petroleum ether, 8:2), the reaction mixture was filtered and most of the solvent evaporated. After confirmation of a pH >13, the crude was extracted twice with 20 mL EtOAc and the organic layer dried and evaporated to give the title compound as a white solid (0.793 g, 73.2% yield). ^{1}H NMR (400 MHz, CD$_3$OD, 298K): δ = 4.77 (bs, 2H); 3.06 (q, 4H, J = 6.3 Hz); 2.76 (t, 2H, J = 6.7 Hz); 2.54-2.42 (m, 6H); 1.90 (s, 2H); 1.72-1.58 (m, 4H); 1.52-1.47 (m, 4H); 1.44 (s, 18 H). ESI-MS: *m/z* calcd for C$_{20}$H$_{42}$N$_4$O$_4$ [M+H]$^+$ 403.32, found: 403.20.

tert-butyl (4-((3-aminopropyl)(3-((tert-butoxycarbonyl)amino)propyl)amino)butyl)(3-((tert-butoxycarbonyl)amino)propyl)carbamate (13)

Compound **11** (148 mg, 267 µmol) was dissolved in 2 mL of EtOH (70%) in a Parr bottle. 1 N NaOH in 10 mL EtOH (70%) and 0.1 g of Raney Nickel slurry W-2 were added to this solution. The reaction mixture was shaken under H_2 pressure at 2.7 bar overnight. After completion (TLC: DCM:MeOH, 96:4), the reaction mixture was filtered and most of the solvent evaporated. After confirmation of a pH >13, the crude was extracted three times with 20 mL DCM and the organic layer dried over $MgSO_4$ and evaporated to give the title compound as a brown oil (111 mg, 74.4% yield). ^{1}H NMR (400 MHz, CDCl$_3$, 298K): δ = 3.29-3.02 (m, 8H), 2.88 (s, 2H), 2.79-2.71 (m, 2H), 2.45-2.34 (m, 6H), 1.69-1.55 (m, 6H), 1.49-1.35 (m, 33H). ESI-MS: *m/z* calcd for $C_{28}H_{57}N_5O_6$ [M+H]$^+$ 560.43, found: 560.30.

tert-butyl (3-((3-azidopropyl)(4-((tert-butoxycarbonyl)amino)butyl)amino)propyl) carbamate (14)

Compound **12** (400 mg, 1.00 mmol) was dissolved in 4 mL methanol. Triethylamine (353 µl, 2.49 mmol) and CuSO$_4$ (3.17 mg, 19.9 µmol) were added to this solution, which was subsequently cooled to 0 °C. 1H-imidazole-1-sulfonyl azide hydrochloride, prepared as described before by Stick and co-workers[23], was added gradually over five minutes. The reaction mixture was allowed to slowly warm to room temperature and was stirred for 10 hours. After disappearance of all starting amine (TLC: EtOAc:petroleum ether, 4:1), the solvent was evaporated. The crude was redissolved in 20 mL EtOAc and extracted twice with 20 mL saturated NaHCO$_3$. The organic fraction was collected, dried over MgSO$_4$ and evaporated to dryness after which the product was purified by silica column chromatography (EtOAc:MeOH, 98:2 -> 90:10), which gave the title compound as a colorless solid (91.4 mg, 21.6%). ^{1}H NMR (400 MHz, CDCl$_3$, 298K): δ = 6.70-6.23 (bs, 1H), 5.66-5.25 (m, 2H), 5.13-4.78 (bs, 1H), 3.32 (t, 2H, J=6.9 Hz), 3.28-3.03 (m, 4H), 2.80-2.39 (m, 6H), 2.09 – 1.96 (m, 2H), 1.71 (t, 2H, J = 6.9 Hz), 1.63 (t, 2H, J = 6.5 Hz), 1.51-1.33 (m, 18H). ESI-MS: *m/z* calcd for $C_{25}H_{48}N_6O_6$ [M+H]$^+$ 429.31, found: 429.15.

tert-butyl (4-((3-azidopropyl)(3-((tert-butoxycarbonyl)amino)propyl)amino)butyl)(3-((tert-butoxycarbonyl)amino)propyl)carbamate (15)

Crude compound **13** (100 mg, 178.64 µmol), was dissolved in 2 mL MeOH. Triethylamine (63 µl, 446.6 µmol) and CuSO$_4$ (3.00 mg, 18.80 µmol) were added to this solution, which was subsequently cooled to 0°C. 1H-imidazole-1-sulfonyl azide hydrochloride (44.9 mg, 214.36 µmol) was added gradually over five minutes. The reaction mixture was allowed to slowly warm to room temperature and was stirred overnight. After disappearance of all 1H-imidazole-1-sulfonyl azide hydrochloride (TLC: DCM:MeOH:TEA, 96:4:1), the solvent was evaporated. The crude was redissolved in 20 mL EtOAc and extracted twice with 20 mL saturated NaHCO$_3$. The organic fraction was collected, dried over MgSO$_4$ and evaporated to dryness after which the product was purified by column chromatography (DCM:MeOH, 95:5), which gave the title compound as a brown oil (73.2 mg, 69.9%). ^{1}H NMR (400 MHz, CDCl$_3$, 298K): δ = 4.74 (bs, 1H), 3.36-2.99 (m, 10H), 2.53-2.30 (m, 6H), 1.75-1.56 (m, 6H), 1.53-1.34 (m, 31H). ESI-MS: *m/z* calcd for $C_{28}H_{55}N_7O_6$ [M+H]$^+$ 586.42, found: 586.30.

tert-butyl (4-(N-(3-((tert-butoxycarbonyl)amino)propyl)-2-chloroacetamido) butyl) carbamate (17)

Compound **8** (150 mg, 434 µmol) and triethylamine (61 µl, 434 µmol) were dissolved in 2 mL dichloromethane. This solution was then cooled to 0 °C, after which chloroacetylchloride (49.0 mg, 434 µmol) was added to the reaction mixture. Then, the reaction mixture was allowed to slowly warm to room temperature and was stirred for 3 hours. After disappearance of **8** (TLC: EtOAc), sodium azide (28.2 mg, 434 µmol) was added to the reaction mixture, which was stirred again overnight. After completion of the reaction (TLC: EtOAc), the solvent was evaporated and the product purified by column column chromatography (DCM:MeOH, 9:1) to give the title compound as a colorless oil (60.7 mg, 32.6%). ^{1}H NMR (400 MHz, MeOD, 298 K): δ = 4.09-4.03 (m, 2H), 3.92-3.83 (m, 2H), 3.45-3.34 (m, 2H), 3.29-3.20 (m, 4H), 1.84-1.68 (m, 4H), 1.62-1.56 (m, 2H), 1.56-1.39 (m, 18H). ESI-MS: *m/z* calcd for $C_{19}H_{36}N_6O_5$ [M+H]$^+$ 429.27, found: 429.10.

tert-butyl (4-((3-azidopropyl)(tert-butoxycarbonyl)amino)butyl)(3-((tert-butoxycarbonyl)amino)propyl)carbamate (18)

Spermine (200 mg, 0.99 mmol), $CuSO_4$ (2.07 mg, 13.0 µmol) and triethylamine (248 µl, 1.78 mmol) were dissolved in 3 mL acetonitrile. Then, the reaction mixture was cooled to 0°C. 1*H*-imidazole-1-sulfonyl azide hydrochloride (186 mg, 0.89 mmol) was added gradually over five minutes, after which the reaction mixture was allowed to slowly warm to room temperature and stirred for 17 h. After disappearance of all diazotransfer reagent (TLC EtOAc:petroleum ether, 4:1), the reaction mixture was cooled to 0°C and Boc_2O (1.29 g, 5.93 mmol) was added gradually over five minutes. The reaction mixture was allowed to slowly warm to room temperature and was stirred overnight. After completion of the reaction (TLC: EtOAc:petroleum ether, 1:2), the solvent was evaporated. The crude product was redissolved in 20 mL EtOAc and washed twice with 20 mL saturated $NaHCO_3$, after which the product was purified by column chromatography (EtOAc:petroleum ether, 1:3) to give the title compound as a colorless oil (152 mg, 29.1%). ^{1}H NMR (400 MHz, CD_3OD, 298K): δ = 3.33-3.26 (m, 2H), 3.26-3.00 (m, 10H), 1.83-1.74 (m, 2H), 1.69-1.61 (m, 2H), 1.52-1.38 (m, 31H). ESI-MS: m/z calcd for $C_{25}H_{48}N_6O_6$ [M+H]$^+$ 529.36, found: 529.20.

tert-butyl (4-((3-aminopropyl)(tert-butoxycarbonyl)amino)butyl)(3-((tert-butoxycarbonyl)amino)propyl)carbamate (19)

Spermine (1.512 g, 7.47 mmol) was dissolved in 40 mL MeOH. This solution was cooled to 0 °C and placed under N_2 atmosphere. Ethyl trifluoroacetate (890 µL, 7.48 mmol) was dissolved in 20 mL MeOH and added dropwise over 30 minutes, under vigourously stirring to the solution of spermine. The reaction mixture was allowed to warm to room temperature and stirred for 16 hours. When all ethyl trifluoroacetate had reacted (TLC: DCM:MeOH:TEA, 85:15:1), the reaction mixture was again cooled to 0°C and Boc_2O (8.17 g, 37.43 mmol) was added to the reaction mixture over 10 minutes. The reaction was then allowed to slowly warm to room temperature and stirred overnight. After completion of the reaction (TLC: petroleum ether:EtOAc, 4:1), the reaction mixture was evaporated to dryness and the crude material purified over a pad of silica (petroleum ether:EtOAc, 4:1 -> petroleum ether:EtOAc:MeOH, 8:2:1) to obtain a mixture of tri-Boc, mono-TFA-protected and di-Boc, di-TFA-protected spermine as a colorless oil. This crude material was dissolved in 25 mL MeOH and cooled to 0°C. To this solution, 25 mL of a 2 N solution of NaOH in water was added dropwise over the course of 15 minutes and the reaction mixture was stirred at room temperature overnight, forming a white precipitate. After completion of the reaction (TLC: DCM:MeOH:NH_3, 80:20:1), most of the solvent was evaporated and water was added until the volume was 50 mL. The aqueous phase was extracted three times with 50 mL DCM. The organic phase was collected, dried over MgSO4 and evaporated to give a yellow oil. This oil was purified over column chromatography (DCM:MeOH, 95:5 -> DCM:MeOH:NH_3, 85:15:1), to yield the title compound as a viscous transparent oil. (986.5 mg, 26.3%). ESI-MS: m/z calcd for $C_{25}H_{50}N_4O_6$ [M+H]$^+$ 503.38, found: 503.25.

tert-butyl(4-((tert-butoxycarbonyl)(3-((tert-butoxycarbonyl)(2-cyanoethyl)amino)propyl)amino)butyl)(3-((tert-butoxycarbonyl)amino)propyl)carbamate (20)

Compound **19** (500.44 mg, 995.5 µmol) was dissolved in 2 mL MeOH. Acrylonitrile (81 µL, 1.24 mmol) was dissolved in 1 mL MeOH and added dropwise to this solution over 1 minute.The reaction mixture was stirred overnight at room temperature. Upon completion of the reaction (TLC: DCM:MeOH, 85:15), Boc_2O (434 mg, 1.99 mmol) was added to the reaction mixture and the reaction was stirred again overnight at room temperature. After completion of the reaction (TLC: EtOAc:petroleum ether, 2/1), the reaction was evaporated to dryness and purified over column chromatography (EtOAc:petroleum ether:AcOH, 1:3:0.01) to obtain the title compound as a colorless oil. (433 mg, yield = 66.4%). ^{1}H NMR (400 MHz, $CDCl_3$, 298K): δ = 5.42-5.14 (bs, 1H), (m, 6H), 3.27-2.95 (m, 2H), 2.67-2.29 (m, 4H), 2.19-1.99 (m, 2H), 1.14-0.35 (m, 6H). ESI-MS m/z calcd for $C_{33}H_{61}N_5O_8$ [M+H]$^+$ 656.88, found: 656.30.

tert-butyl (4-((3-((3-aminopropyl)(tert-butoxycarbonyl)amino)propyl)(tert-butoxycarbonyl)amino)butyl)(3-((tert-butoxycarbonyl)amino)propyl)carbamate (21)

Compound **20** (88 mg, 134 µmol) was dissolved in 3 mL of EtOH (70%) in a Parr bottle. 2 mL of a 1 N solution of NaOH in EtOH (70%) and one spatula of Raney Nickel slurry W-2 were added to this solution. The reaction mixture was shaken under H_2 pressure at 2.7 bar overnight. After completion (TLC: DCM:MeOH, 96:4), the reaction mixture was filtered and most of the solvent evaporated. After confirmation of a pH >13, the crude was extracted three times with 20 mL DCM and the organic layer dried over $MgSO_4$ and evaporated to give the title compound as a white solid (85.2 mg, 96.3% yield). ^{1}H NMR (400 MHz, CDCl3, 298K): δ = 4.90-4.70 (bs, 1H), 3.33-2.97 (m, 14H), 2.66 (t, 2H, J = 6.6 Hz), 2.30-2.17 (m, 4H), 1.75-1.57 (m, 6H), 1.47-1.37 (m, 36H). ESI-MS: m/z calcd for $C_{33}H_{65}N_5O_8$ [M+H]$^+$ 660.91, found: 660.35.

tert-butyl (4-((3-((3-azidopropyl)(tert-butoxycarbonyl)amino)propyl)(tert-butoxycarbonyl)amino)butyl)(3-((tert-butoxycarbonyl)amino)propyl)carbamate (22)

Compound **21** (85.2 mg, 129 µmol) was dissolved in 2 mL methanol. Triethylamine (45 µl, 322.85 µmol) and $CuSO_4$ (2.06 mg, 12.9 µmol) were added to this solution, which was subsequently cooled to 0°C. 1H-imidazole-1-sulfonyl azide hydrochloride (46 mg, 219.51 µmol) was added gradually over five minutes to the mixture. The reaction mixture was allowed to slowly warm to room temperature and was stirred overnight. After disappearance of all 1H-imidazole-1-sulfonyl azide hydrochloride (TLC: EtOAc:petroleum ether, 1:1), the solvent was evaporated. The crude was redissolved in 20 mL EtOAc and extracted twice with 20 mL saturated $NaHCO_3$. The organic fraction was collected, dried over $MgSO_4$ and evaporated to dryness after which the product was purified by column chromatography (EtOAc:petroleum ether., 1:1), which gave 10 as a colorless oil (82.5 mg, 93.1%). ^{1}H NMR (400 MHz, CDCl3, 298K): δ = 3.43-3.28 (m, 4H), 3.28-3.21 (m, 4H), 3.21-2.94 (m, 8H), 1.87-1.77 (m, 4H), 1.77-1.68 (m, 4H), 1.68-1.40 (m, 38H). ESI-MS: m/z calcd for $C_{33}H_{63}N_7O_8$ [M+H]$^+$ 686.91, found: 686.35.

N1-(3-aminopropyl)-N1-(3-(4-(3-(5,5-difluoro-1,3,7,9-tetramethyl-5H-4l4,5l4- dipyrrolo[1,2-c:2',1'-f][1,3,2]diazaborinin-10-yl)propyl)-1H-1,2,3-triazol-1- yl)propyl)butane-1,4-diamine (24)

The title compound was obtained by click chemistry of **1** with alkyne BODIPY **23** following the general protocol as described in the experimental section of the paper. After HPLC purification and lyophilization, the product was obtained as a red solid in 22% yield. HRMS (MALDI-TOF): m/z calcd. for $C_{28}H_{46}BF_2N_8$ [M+H]$^+$ 543.3862, found: 543.3685.

N1,N4-bis(3-aminopropyl)-N1-(3-(5-(3-(5,5-difluoro-1,3,7,9-tetramethyl-5H-4λ^4,5λ^4- dipyrrolo[1,2-c:2',1'-f][1,3,2]diazaborinin-10-yl)propyl)-1H-1,2,3-triazol-1- yl)propyl)butane-1,4-diamine (25)

The title compound was obtained by click chemistry of compound **2** with alkyne BODIPY **23** following the general protocol as described in the experimental section of the paper. After HPLC purification and lyophilization, the product was obtained as a red solid in 3% yield. ESI-MS: m/z: calcd for $C_{31}H_{52}BF_2N_9$ [M+H]$^+$ 600.45, found 600.25. HRMS (MALDI-TOF): m/z calcd. for $C_{31}H_{53}BF_2N_8Na^+$ [M+Na]$^+$ 622.4299, found: 622.3969.

N-(4-aminobutyl)-N-(3-aminopropyl)-2-(5-(3-(5,5-difluoro-1,3,7,9-tetramethyl-5H4λ^4,5λ^4- dipyrrolo[1,2-c:2',1'-f][1,3,2]diazaborinin-10-yl)propyl)-1H-1,2,3-triazol-1- yl)acetamide (26)

The title compound was obtained by click chemistry of compound **3** with alkyne BODIPY **23** following the general protocol as described in the experimental section of the paper. After HPLC purification and lyophilization, the product was obtained as a red solid in 3% yield. ESI-MS: m/z calcd. for $C_{27}H_{41}BF_2N_8O$ [M+H]$^+$ 543.35, found: 543.15. HRMS (MALDI-TOF): m/z $C_{27}H_{40}BF_2N_8ONa^+$ [M+Na]$^+$ 565.3357, found: 565.3093.

N1-(3-aminopropyl)-N4-(3-(5-(3-(5,5-difluoro-1,3,7,9-tetramethyl-5H-4λ^4,5λ^4- dipyrrolo[1,2-c:2',1'-f][1,3,2]diazaborinin-10-yl)propyl)-1H-1,2,3-triazol-1- yl)propyl)butane-1,4-diamine (27)

The title compound was obtained by click chemistry of compound **4** with alkyne BODIPY 16 following the general protocol as described in the experimental section of the paper. After HPLC purification and lyophilization, the product was obtained as a red solid in 2% yield. ESI-MS: m/z: calcd for $C_{28}H_{45}BF_2N_8$ [M+H]$^+$ 543.39, found 543.25. HRMS (MALDI-TOF): m/z calcd. for $C_{28}H_{45}BF_2N_8Na^+$ [M+Na]$^+$ 565.3721, found: 565.3365.

N1-(3-aminopropyl)-N4-(3-((3-(5-(3-(5,5-difluoro-1,3,7,9-tetramethyl-5H-4λ^4,5λ^4-dipyrrolo[1,2-c:2',1'-f][1,3,2]diazaborinin-10-yl)propyl)-1H-1,2,3-triazol-1-yl)propyl)amino)propyl)butane-1,4-diamine (28)

The title compound was obtained by click chemistry of compound **5** with alkyne BODIPY **23** following the general protocol as described in the experimental section of the paper. After HPLC purification and lyophilization, the product was obtained as a red solid in 9% yield. ESI-MS: m/z calcd. for $C_{31}H_{53}BF_2N_9$ [M+H]$^+$ 600.45, found 600.30. HRMS (MALDI-TOF): m/z calcd. for $C_{31}H_{52}BF_2N_9Na^+$ [M+Na]$^+$ 622.4299, found: 622.4135.

3-azidopropyl 4-methylbenzenesulfonate (30)

Tosylate **34** was synthesized based on the procedure of Chan et al.[24] To this end, 3-chloropropanol (1.00 g, 10.58 mmol, 1 eq.) was dissolved in 10 mL H_2O. NaN$_3$ (688 mg, 10.58 mmol, 1 eq.) was added to this solution and the reaction was refluxed overnight. Upon completion of the reaction (petroleum ether/EtOAc 1:1), the reaction mixture was cooled to room temperature and extracted three times with 20 mL DCM. The organic fractions were collected, dried over MgSO$_4$ and evaporated to dryness. The crude product was redissolved in 15 mL dry DCM. Triethylamine (2.95 mL, 2 eq., 21.17 mmol) was added and the mixture was cooled to 0°C. Tosyl chloride (2.44 g, 1.2 eq., 11.64 mmol) was added to the reaction mixture, which was subsequently allowed to warm to room temperature and stirred overnight. Upon completion of the reaction (TLC: petroleum ether:EtOAc 4:1), the solvents were evaporated and the crude product purified over column chromatography (petroleum ether:EtOAc 1:0 -> 9:1) to obtain the title compound as a colorless solid. (1.554 g, yield = 58% over two steps) ESI-MS: m/z calculated for $C_{10}H_{13}N_3O_3S$ [M+H]$^+$ requires 256.07, found 256.90.

Tert-butyl (4-aminobutyl)carbamate (32)

Boc-protected putrescine **36** was synthesized based on the method of Dardonville et al.[25] To this end putrescine (323 mg, 3.67 mmol, 4 eq.) was dissolved in 4 mL CHCl$_3$ and cooled to 0°C. Boc$_2$O (200 mg, 916 μmol, 1 eq.) was dissolved in 10 mL CHCl$_3$ and slowly added to the putrescine solution over the course of 2h. The reaction mixture was then allowed to warm to room temperature and stirred overnight. Upon completion of the reaction (TLC: petroleum ether/EtOAC 1:1), the solvents were evaporated and the crude product redissolved in 20 mL DCM. The crude mixture was extracted three times with H_2O. The organic fraction was collected, dried over MgSO$_4$ and concentrated. The product was further purified using column chromatography (petroleum ether/EtOAc 1:1 -> EA/MeOH/TEA 9:1:0.01) to obtain the title compound as a colorless oil. (169 mg, yield = 98%) ESI-MS: m/z calculated for $C_9H_{20}N_2O_2$ [M+H]$^+$ requires 189.15, found 188.95

Tert-butyl (4-((3-azidopropyl)amino)butyl)carbamate (33)

Boc-putrescine **36** (88 mg, 467 μmol, 1 eq.) was dissolved in 2 mL dry THF under Argon atmosphere. DIEA (333 μL, 1.87 mmol, 4 eq.) was added to this solution, which was subsequently cooled to 0°C. Tosylate **34** (119 mg, 467 μmol, 1 eq.) was added gradually to the reaction mixture, which was subsequently allowed to warm up to room temperature. The reaction stirred overnight at room temperature. Upon completion of the reaction (TLC: DCM/MeOH 9:1), the solvents were evaporated and the crude product purified over column chromatography (DCM/MeOH 9:1) to obtain the title compound as a colorless oil. (38.37 mg yield = 30%) ESI-MS: m/z calculated for $C_{12}H_{25}N_5O_2$ [M+H]$^+$ requires 272.20, found 272.00

Tert-butyl (4-((3-(4-(3-(5,5-difluoro-1,3,7,9-tetramethyl-5H-4l4,5l4-dipyrrolo[1,2-c:2',1'-f][1,3,2]diazaborinin-10-yl)propyl)-1H-1,2,3-triazol-1-yl)propyl)amino)butyl)carbamate (34)
Compound **37** (24 mg, 88.44 µmol, 1 eq.) was dissolved in 2 mL DCM. Alkyne-BODIPY **23** (29.18 mg, 92.86 µmol, 1.05 eq.), DIEA (63 µL, 353.77 µmol, 4 eq.) and subsequently CuBr (6.34 mg, 44.22 µmol, 0.5 eq.) were added to the reaction mixture. The reaction was stirred at room temperature for 3h. Upon completion of the reaction (TLC: DCM/MeOH 9:1), the solvents were evaporated and the crude product purified using column chromatograpy (DCM/MeOH 9:1) to obtain the title compound as a red oil. (32.45 mg, yield = 63%) ESI-MS: m/z calculated for $C_{30}H_{46}BF_2N_7O_2$ [M+H]$^+$ requires 586.37, found 586.20

N1-(3-(4-(3-(5,5-difluoro-1,3,7,9-tetramethyl-5H-4l4,5l4-dipyrrolo[1,2-c:2',1'-f][1,3,2]diazaborinin-10-yl)propyl)-1H-1,2,3-triazol-1-yl)propyl)butane-1,4-diamine dihydrochloride (35)
Compound **38** (32.45 mg, 55.42 µmol) was dissolved in 6 mL 4N HCl in dioxane and stirred for 5 minutes at room temperature. Upon completion of the reaction, the solvents were evaporated to obtain the title compound as a red solid (30.94 mg, yield = 100%). ESI-MS: m/z calculated for $C_{25}H_{40}BCl_2F_2N_7$ [M+H-HCl]$^+$ requires 486.32, found 486.15. ^{1}H NMR (400 MHz, CDCl3, 298K): δ = 7.91 – 7.48 (m, 2H), 7.24 – 6.94 (m, 1H), 6.44 – 5.66 (m, 2H), 3.83 – 3.53 (m, 4H), 3.22 – 3.00 (m, 4H), 2.71 – 1.81 (m, 8H), 1.63 – 1.32 (m, 14H).

6.5. References

[1]   A. E. Pegg, *J Biol Chem* **2016**, *291*, 14904.
[2]   A. C. Childs, D. J. Mehta, E. W. Gerner, *Cell Mol Life Sci* **2003**, *60*, 1394.
[3]   O. Heby, *Differentiation* **1981**, *19*, 1.
[4]   H. J. Rhee, E. J. Kim, J. K. Lee, *J Cell Mol Med* **2007**, *11*, 685.
[5]   L. Miller-Fleming, V. Olin-Sandoval, K. Campbell, M. Ralser, *J Mol Biol* **2015**, *427*, 3389.
[6]   T. Thomas, T. J. Thomas, *J Cell Mol Med* **2003**, *7*, 113.
[7]   A. J. Palmer, H. M. Wallace, *Amino Acids* **2010**, *38*, 415.
[8]   P. M. Cullis, R. E. Green, L. Merson-Davies, N. Travis, *Chem Biol* **1999**, *6*, 717.
[9]   D. Soulet, L. Covassin, M. Kaouass, R. Charest-Gaudreault, M. Audette, R. Poulin, *Biochem J* **2002**, *367*, 347.
[10]   C. Wang, J. G. Delcros, J. Biggerstaff, O. t. Phanstiel, *J Med Chem* **2003**, *46*, 2672.
[11]   M. Wolf, U. Bauder-Wust, R. Pipkorn, H. Eskerski, M. Eisenhut, *Bioorg Med Chem Lett* **2006**, *16*, 3193.
[12]   Y. Guminski, M. Grousseaud, S. Cugnasse, V. Brel, J. P. Annereau, S. Vispe, N. Guilbaud, J. M. Barret, C. Bailly, T. Imbert, *Bioorg Med Chem Lett* **2009**, *19*, 2474.
[13]   S. Rehm, V. Stepanenko, X. Zhang, T. H. Rehm, F. Wurthner, *Chemistry* **2010**, *16*, 3372.
[14]   S. G. Konig, S. Oz, R. Kramer, *Chem Commun* **2015**, *51*, 7360.
[15]   F. Dai, Q. Li, Y. Wang, C. Ge, C. Feng, S. Xie, H. He, X. Xu, C. Wang, *J Med Chem* **2017**, *60*, 2071.
[16]   C. W. Porter, P. F. Cavanaugh, Jr., N. Stolowich, B. Ganis, E. Kelly, R. J. Bergeron, *Cancer Res* **1985**, *45*, 2050.
[17]   R. J. Bergeron, J. S. McManis, W. R. Weimar, K. M. Schreier, F. Gao, Q. Wu, J. Ortiz-Ocasio, G. R. Luchetta, C. Porter, J. R. Vinson, *J Med Chem* **1995**, *38*, 2278.
[18]   C. Thiele, C. Papan, D. Hoelper, K. Kusserow, A. Gaebler, M. Schoene, K. Piotrowitz, D. Lohmann, J. Spandl, A. Stevanovic, A. Shevchenko, L. Kuerschner, *ACS Chem Biol* **2012**, *7*, 2004.
[19]   M. Wolf, W. E. Hull, W. Mier, S. Heiland, U. Bauder-Wust, R. Kinscherf, U. Haberkorn, M. Eisenhut, *J. Med. Chem.* **2007**, *50,* 139.
[20]   R. F. Minchin, A. Raso, R. L. Martin, K. F. Ilett, *Eur. J. Biochem.* **1991**, *200,* 457.
[21]   K. K. H. Vong, K. Tsubokura, Y. Nakao, T. Tanei, S. Noguchi, S. Kitazume, N. Taniguchi, K. Tanaka, *Chem Commun,* **2017**, *53*, 8403.

[22]   J. Spandl, D. J. White, J. Peychl, C. Thiele, *Traffic* **2009**, *10*, 1579.

[23]   E. D. Goddard-Borger, R. V. Stick, Org. Lett. **2007**, 9, 3797–3800.

[24]   E. W. C. Chan, P. Baek, D. Barker, J. Travas-Sejdic, *Polym. Chem.* **2015**, *6*, 7618–7629.

[25]   C. Dardonville, C. Fernandez-Fernandez, S. L. Gibbons, G. J. Ryan, N. Jagerovic, A. M.
        Gabilondo, J. J. Meana, L. F. Callado, *Bioorganic Med. Chem.* **2006**, *14*, 6570–6580.

[26]   S. van Veen, S. Martin, C. Van den Haute, V. Benoy, J. Lyons, R. Vanhoutte, J. P. Kahler, J. P.
        Decuypere, G. Gelders, E. Lambie, J. Zielich, J. V. Swinnen, W. Annaert, P. Agostinis, B.
        Ghesquière, S. H. L. Verhelst, V. Baekelandt, J. Eggermont, P. Vangheluwe, *Nature* **2020**, *578,*
        7795.

[27]   N. N. Hamouda, C. van den Haute, R. Vanhoutte, R. Sannerud, M. Azfar, R. Mayer, Á. C.
        Calabuig, J. V. Swinnen, P. Agostinis, V. Baekelandt, W. Annaert, F. Impens, S. H. L. Verhelst, J.
        Eggermont, S. Martin, P. Vangheluwe, *J. Biol. Chem.* **2021**, *296*, 13.

Chapter VII: General conclusion and future prospects

This thesis describes the synthesis and application of activity-based probes (ABPs) for acyl-protein thioesterases 1 and 2 (APT-1/2) and the SARS-CoV-2 main protease (M^{pro}) as well as the synthesis and application of fluorescent polyamine probes.

Chapter III describes the development of solid-phase synthesis procedures that allow the full on-resin synthesis of serine-reactive ABPs. Creating ABPs on solid-phase allows probes to be formed faster and in higher numbers simultaneously compared to solution-phase synthesis, as the work-ups in between reactions are less tedious. On-resin synthesis of serine-reactive ABPs could speed up the process of finding a selective ABPs for more members of this enzyme family, which is needed as most serine hydrolases are poorly characterized and lack a selective probe.

The probe design used in this chapter consists of (1) an azide tag, incorporated in a Lys(N_3)-Ahx spacer and (2) a recognition element of natural and unnatural amino acids that is connected to (3) a serine reactive warhead, which is installed as an N-terminal cap on the recognition element. The synthesis of the detection tag-spacer-recognition element moiety could be done by using amended solid phase peptide chemistry, which is well described. Less is known about which warheads can be coupled on solid support. In this thesis, this was explored for five different serine reactive warheads. It was attempted to couple them to recognition elements consisting of a single amino acid with an uncapped primary amine, secondary amine or secondary cyclic amine. It was possible to create diphenyl phosphoramidates, phenyl carbamates and 2-aminopyridineureas on all three types of amines on resin. N-hydroxysuccinimidyl carbamates (NHS carbamates) and 1,2,3-triazole ureas could only be formed on secondary amines however. None of the probes in this first library reacted with serine hydrolases in mouse brain lysate. The knowledge that all warheads could be formed on resin on the piperidine moiety of an Inp residue was used to create a second 3x6 library, with three different recognition elements and six warheads (five that were used to create the first library and p-nitrophenyl carbamate). The three different recognition elements consisted of an aromatic residue and a moiety bearing a piperidine or piperazine ring. These types of recognition elements have previously been used to create serine-reactive inhibitors for FAAH and MAGL.[1–3] All recognition elements could be coupled to all six warheads. Probes of this library that bore a NHS carbamate or 1,2,3-triazole urea warhead showed reactivity against acyl-protein thioesterases 1 and 2 (APT-1/2). The other four classes of probes showed no reactivity against the serine hydrolases in mouse brain lysate. Titration of the probe concentration showed that 1,2,3-triazole urea probes **5f** and **6f** were much more potent against APT-1/2 (IC_{50}^{App} **5f** = 11.8 ± 1.8 nM; IC_{50}^{App} **6f** = 27.9 ± 2.8 nM) than their NHS carbamate counterparts. Furthermore, these probes were cell-permeable and showed no detectable off-targets at concentrations as low as 100 nM in mouse brain lysate. As APT-1/2 are not

well understood, these probes could be of good use to further elucidate their activity regulation and trafficking between cytosol and membrane.

In **Chapter IV**, the development of selective probes for APT-1 or APT-2 was attempted. Selective ABPs would allow the study of one of the isoforms without targeting the other and would be valuable tools to elucidate the distinct roles of the individual APTs. Using the on-resin synthetic procedures developed in Chapter III, 1,2,3-triazole urea probes **5f** and **6f** were further optimized to create probes by amending the structure. Two synthetic strategies were attempted to achieve this goal: contraction, expansion and opening of the amine-bearing heterocycle in the recognition element of **5f** and **6f**, and substitution of the phenyl ring in the recognition element of **5f** for a different ring. This resulted in the fast synthesis of another two probe libraries of respectively four and fifteen compounds. The compounds in which the piperidine and piperazine rings were changed showed worse reactivity and/or selectivity for APT-1/2 than their lead compounds. Three of the compounds in which the phenyl ring was substituted (**8e**, **8g** and **8l**), did show higher reactivity on mouse APT-1/2 than the original hit **5f** however, as well as no cross-reactivity with other FP-rhodamine targets on mouse brain lysate. The activity of these three new probes and the original hit **5f** against human APT-1 and APT-2 was measured. Although they were very potent against both enzymes (APT-1: IC_{50}^{App} = 13 - 43 nM, APT-1: IC_{50}^{App} = 16 - 35 nM), none of the compounds showed good selectivity for one of the isoforms. The most selective compound, **8l**, was only 1.8 times more selective for APT-1 over APT-2.

The active probes found in Chapter III and Chapter IV can potentially be further optimized to isoform-selective probes by expanding the recognition element with other amino acids. Such a library can be made relatively fast using the on-resin synthesis procedures used to create the first two libraries. As mentioned before, these procedures can also be applied to create serine-reactive probes for other serine hydrolases. The group of Cravatt has recently synthesized several ABHD17 family inhibitors bearing a pyrazole urea leaving group.[4] Using the solid-phase approach used in this thesis, a library of analogous compounds can be made by amending the 1,2,3-triazole urea synthesis to a pyrazole urea synthesis (Figure **7.1**). This could lead to a speed up in the development of more selective probes for the members of the ABHD17 family and further elucidation of protein depalmitoylation.
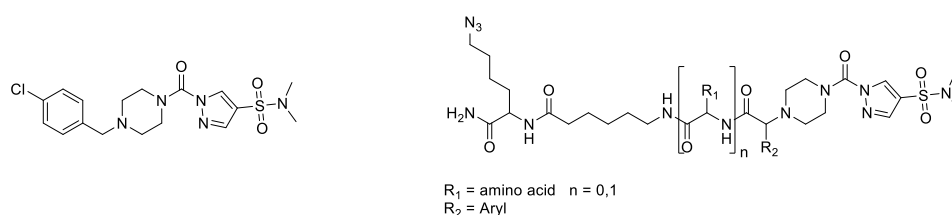

R_1 = amino acid   n = 0,1
R_2 = Aryl

Figure 7.1. Structure of general ABHD17-inhibitor made by Cravatt group (left). Proposed synthesis of derivatives using solid-phase approach established in this thesis (right).

Chapter V describes the development of azapeptide ABPs for the SARS-CoV-2 M^{pro}. M^{pro} is the most promising drug target in the development of antivirals for the treatment of Covid-19, as it is the main switch in the proteolytic activation of the non-structural proteins of the virus.

A library of five probes was created bearing a Tle-Leu-azaGln recognition element, based on the preferred substrate specificity of the enzyme. A cysteine reactive warhead was placed on the azaGln residue and a hexynoic acid detection tag was connected to the Tle residue. These probes were also made using solid-phase synthesis, which allowed for them to be made in a fast manner. The P_1 azaGln served both as an anchor to the resin via its side chain and as a site for the on-resin capping of the probes with a warhead on its α-nitrogen. Three of the synthesized probes were found to have a mid to low nanomolar IC_{50} for the M^{pro}, with chloroacetamide probe **8d** being the most potent probe with an IC_{50} of 20.6 nM. This probe can also be detect low M^{pro} concentrations and shows good antiviral activity. At the time of writing, this is the most potent M^{pro} inhibitor reported in the portfolio of Covid Moonshot.

The antiviral properties of this probe on infected live cells show that the probes inhibit cell death, by inhibiting the M^{pro} of the virus in these cells. Therefore, the probes can be applied to visualize active M^{pro} in live cells. This can be done via click chemistry with an azide-tagged fluorophore after probe binding, or by creating a "pre-clicked" probe by coupling the probe to an azide-tagged fluorophore before incubation on cells. Currently, such experiments are being undertaken in collaboration with the Rega institute on SARS-CoV-2 infected VeroE6 cells.

The probes can be further optimized as well to enhance their activity. The current library is very small and several other cysteine warheads can be coupled to the recognition element. It is striking that warheads that bind with the active site cysteine residue of the M^{pro} two bonds away from the P_1 residue create probes that are much more potent than warheads that bind three bonds away. This suggests that the positioning of the electrophile needs to be very accurate to allow binding of the substrates in their binding pockets. Molecular dynamics simulations with the non-covalently docked molecule in the active site could verify this. Other warheads such as an *N*-propargyl, a 2-chloro propylamide or an acetyl bromide, which also bind two bonds away from the P_1 residue are therefore interesting options for further optimizing the probes reactivity (Figure **7.2**). Besides the warheads, changes in the recognition elements can also be made to potentially increase reactivity. Whereas the S_1 and S_2 substrate specificity of the M^{pro} is very strict for respectively L-Gln and L-Leu, the S_3 pocket allows a wider variety of substrates. Besides L-Tle, other P_3 residues on inhibitors cause good M^{pro} inhibition as well, including D-Tyr and cationic residues such as L-Orn and L-hArg (Figure **7.2**).[5]

Another change that might influence the activity is the addition of a P_4 residue, such as the unnatural L-2-aminobutyric acid, of which the Drag group has shown that it is the preferred P_4 substrate of the SARS-CoV-2 M^{pro} (Figure **7.2**).
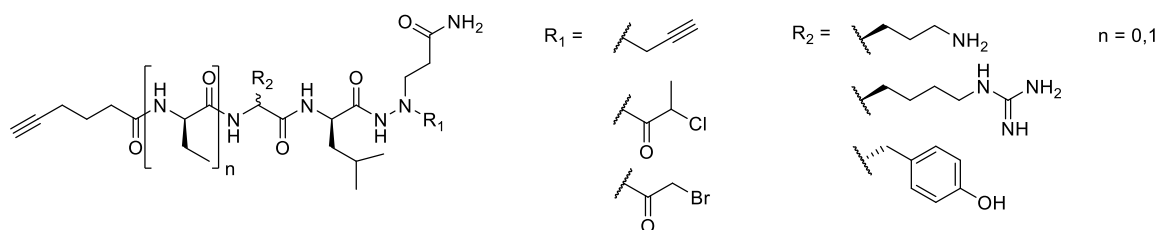

Figure 7.2. Potential optimized probe structures fort he labelling of SARS-CoV-2 M^{pro}.

Chapter VI describes a SAR study on the development of fluorescent polyamine probes. Azide-functionalized polyamines of different lengths, bearing different amounts of amine functions were made, resembling naturally occurring polyamines spermine, spermidine and putrescine. The azide substituent was attached on different positions of the polyamines. These polyamine derivatives were connected to an alkyne-functionalized green fluorescent BODIPY through CuAAC, which resulted in the formation of six different polyamine probes.

It was found that the linear spermidine and spermine probes, on which the fluorophore is connected to an outer primary amine, were taken up far more efficiently by MCF-7 cells than the branched probes, on which the fluorophore is connected to one of the inner secondary amine. These linear spermine and spermidine probes were subsequently used by another research group as tools for the identification of ATP13A2 as the first known mammalian polyamine transporter with preference for spemine and spermidine. The putrescine probe, which was made after the model of the linear spermine and spermidine probes, was used to identify ATP13A3 as a second mammalian polyamine transporter with higher preference for putrescine.
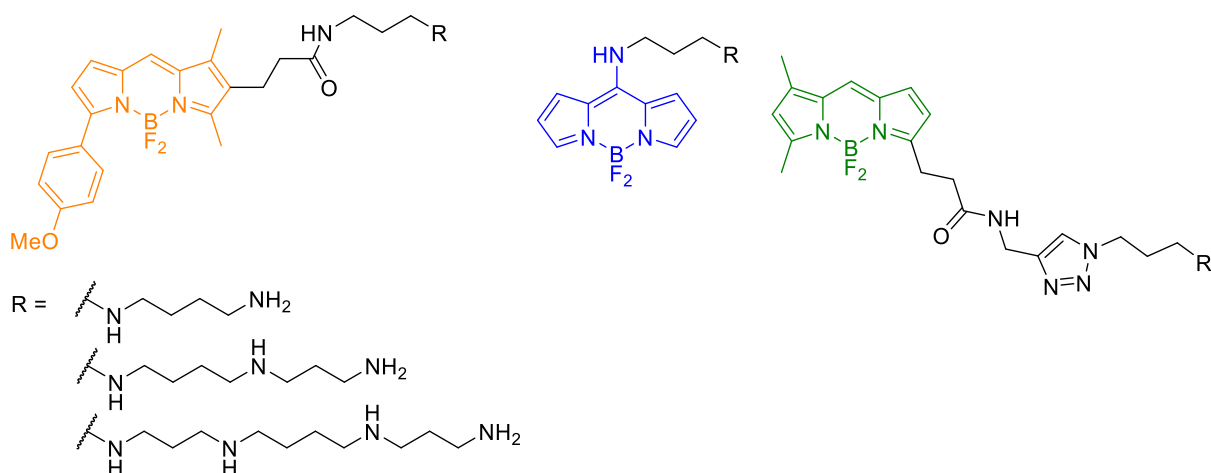

Figure 7.3. Structures of new polyamine probes emitting at different wavelengths: BODIPY-TAMRA (orange), amino-BODIPY (blue), BODIPY-FL (green)

To increase the applicability of these polyamine probes in biochemical research, probes with different colored fluorophores are needed, as the green BODIPY used in the original probes overlaps with the excitation/emission spectrum of green fluorescent protein (GFP), which is frequently expressed in test systems. Therefore, polyamine adducts with different fluorophores are currently being made within our lab. Furthermore, the original probes were found to have relatively low fluorescence in water. To improve this, other green dyes are coupled to the polyamines that can be bought commercially. A first strategy for creating these new probes is by attaching a different alkyne-functionalized BODIPY fluorophores to the azide-functionalized polyamines through CuAAC, such as the green emitting BODIPY-FL (Figure **7.3**). A second strategy uses the polyamine derivatives with one unprotected primary amine, which are intermediates in the synthesis of the azide-functionalized polyamine. These are attached to different colored fluorophores by other linkages. Two examples are TMR-BODIPY (orange emitting), which is connected to the polyamines via an amide coupling and amino-BODIPY (blue emitting) via an S_N2 substitution of 8-SMe-BODIPY with the polyamine.

Furthermore, it was found that the liner spermine and spermidine probes are taken up better in MCF-7 breast cancer cells than in MCF-10A breast epithelial cells. This correlates with the upregulation of polyamine transport in cancer cells[6] and opens the possibility to use these azide-functionalized polyamine derivatives as vectors to shuttle cargo other than fluorophores selectively into cancer cells. Two possible applications were attempted.

The first one is the development of polyamine vectors of Cisplatin-derivatives as a means of creating a chemotherapeuticum with fewer side effects. Due to synthetic problems with the formation of the alkyne-functionalized cisplatin ligand, the desired molecules were not obtained. Nevertheless, these azido-polyamines should be investigated as possible vectors for the selective delivery of chemotherapeutics, e.g. doxorubicin, to cancer cells as there is a need for such drugs.

Secondly, it was attempted to elevate the cellular uptake of biotinylated compounds by creating polyamine-adducts that are taken up through the polyamine transport system. This could overcome the poor cell-permeability of biotinylated probes, which limits their application on live cells. This was attempted with cathepsin-reactive probe DCG-04 as a model. A polyamine-conjugated version of DCG-04 was created by synthesizing the probe with an alkyne handle in the form of a propargylamine residue as a C-terminal cap of the probe (**DCG-04 alk**) and connecting this to Boc-spermidine-N_3 by on-resin click chemistry (**DCG-04 spd**) (Figure **7.4**). This particular probe did no longer react with cathepsins and could not be used for uptake experiments (Figure **7.5A**). It is possible that the polycationic spermidine is detrimental for cathepsin reactivity. Another probe, such as FP-Biotin,

which has a wider reactivity and therefore a higher chance of binding any enzymes when attached to a polyamine, is an alternative to validate this application (Figure **7.5B**).
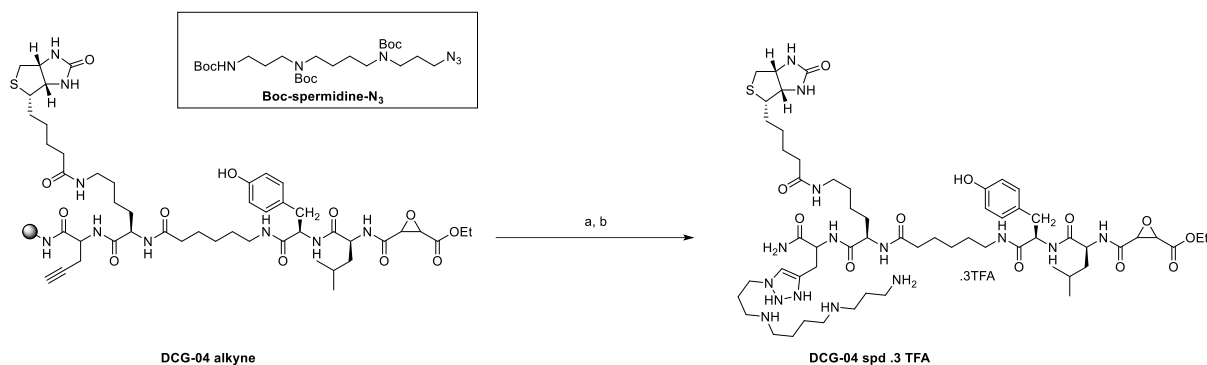

Figure 7.4. Synthesis of **DCG-04 spd** on rink amide resin. a) **Boc-spermidine-N₃**, 2,6-lutidine, TEA, CuBr, sodium ascorbate, DMSO; b) TFA/TIS/water, 95/2.5/2.5.
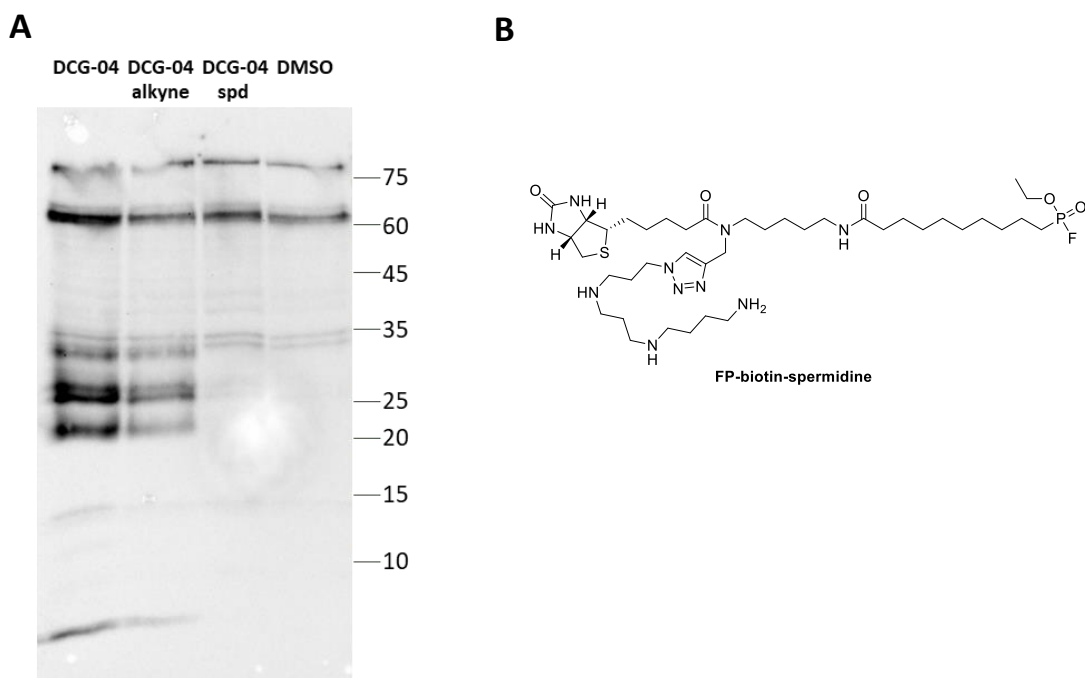

Figure 7.5. A. Incubation of rat liver lysate at pH 5.5 with 50 µM of the indicated compounds or DMSO, followed by biotin detection shows several targets labeled by **DCG-04** and **DCG-04 alkyne**, but not by **DCG-04 spd**. **B.** Proposed structure of FP-biotin-spermidine, a biotinylated probe that can potentially be taken up in cells through the polyamine transport system.

7.1. References

[1]   J. Z. Long, W. Li, L. Booker, J. J. Burston, S. G. Kinsey, J. E. Schlosburg, F. J. Pavon, A. M. Serrano, D. E. Selley, L. H. Parsons, et al., *Nat. Chem. Biol.* **2009**, *5*, 37–44.

[2]   K. Ahn, D. S. Johnson, M. Mileni, D. Beidler, J. Z. Long, K. Mckinney, E. Weerapana, N. Sadagopan, M. Liimatta, S. E. Smith, et al., *Chem Biol.* **2009**, *16*, 411–420.

[3]   D. S. Johnson, C. Stiff, S. E. Lazerwith, S. R. Kesten, L. K. Fay, M. Morris, D. Beidler, M. B. Liimatta, S. E. Smith, D. T. Dudley, et al., *ACS Med. Chem. Lett.* **2011**, *2*, 91–96.

[4]   J. R. Remsberg, R. M. Suciu, N. A. Zambetti, T. W. Hanigan, A. J. Firestone, A. Inguva, A. Long, N. Ngo, K. M. Lum, C. L. Henry, et al., *Nat. Chem. Biol.* **2021**, *17*, 856–864.

[5]   W. Rut, K. Groborz, L. Zhang, X. Sun, M. Zmudzinski, B. Pawlik, X. Wang, D. Jochmans, J. Neyts, W. Młynarski, et al., *Nat. Chem. Biol.* **2021**, *17*, 222–228.

[6]   L. Miller-Fleming, V. Olin-Sandoval, K. Campbell, M. Ralser, *J. Mol. Biol.* **2015**, *427*, 3389–3406.

Scientific Acknowledgements

Conflict of interest statement

Roeland Vanhoutte is an inventor on patent application ZL919090: "Screeningsmethoden ATP13A2".

Curriculum Vitae

Roeland Vanhoutte

Education

KU Leuven

Since 2017 PhD student - Laboratory of Chemical Biology
   Doctoral school track Drug Design and Development

2011-2016 M. Sc. Drug Development
   B. Sc. Pharmaceutical Sciences

Sint-Jozefscollege Aarschot

2005-2011 Sciences-Mathematics

List of Publications

Articles in internationally reviewed academic journals

Hamouda, N.N., Van Den Haute, C., **Vanhoutte, R.**, Azfar, M., Cortés Calabuig, A., Swinnen, J.V., Agostinis, P., Impens, F., Verhelst, S.H.L., Baekelandt, V., Eggermont, J., Martin, S., Vangheluwe, P. "ATP13A3 is a new member of the mammalian polyamine transport system" *Journal of Biological Chemistry,* 2021, 296, 100182.

Vanhoutte, R., Van de Plassche, M.A.T., Verhelst, S.H.L. "Rapid solid phase construction of serine hydrolase probes results in selective activity-based probes for acyl protein thioesterases-1/2" *Journal of Medicinal Chemistry,* 2020, 63, 20, 11845–11853.

Kahler, J.P., **Vanhoutte, R.**, Verhelst, S.H.L. "Activity-Based Protein Profiling of Serine Proteases in Immune Cells", *Archivum Immunologiae et Therapiae Experimentalis,* 2020, 19; 68(4):23.

van Veen, S., Martin, S., Van den Haute, C., Benoy, V., Lyons, J., **Vanhoutte, R.**, Kahler, J.P., Decuypere, J-P., Gelders, G., Lambie, E., Swinnen, J.V., Annaert, W., Agostinis, P., Ghesquière, B., Verhelst, S.H.L., Baekelandt, V., Eggermont, J., Vangheluwe, P. "ATP13A2 deficiency disrupts lysosomal polyamine export" *Nature*, 2020, 578, 419-424.

Modranka, J., Li, J., Parchina, A., Vanmeert, M., Dumbre, S., Salman, M., Myllykallio, H., Becker, H.F., **Vanhoutte, R.**, Margamuljana, L., Nguyen, H., Abu El Asrar, R., Rozenski, J., Herdewijn, P., De Jonghe, S., Lescrinier, E. "Synthesis and structure-activity relationship studies of benzo[b][1,4]oxazin-3(4H)-one analogues as inhibitors of mycobacterial thymidylate synthase X", *ChemMedChem,* 2019, 14(6), 645-662.

Chakrabarty, S., Kahler, J.P., Van de plassche, M., **Vanhoutte, R.**, Verhelst, S.H.L. "Recent applications in activity-based protein profiling", *Current Topics in Molecular Immunology,* 2019, 420, 253-281.

Vanhoutte, R., Kahler, J.P., Martin, S., Van Veen, S., Verhelst, S.H.L. "Clickable polyamine derivatives as probes for the polyamine transport system", *ChemBioChem*, 2018, 19(9), 907–911. *featured as a cover in ChemBioChem

Meeting abstracts, presented at international scientific conferences and symposia

Vanhoutte, R., Verhelst, S.H.L. "Solid phase mix-and-match synthesis of serine hydrolase activity-based probes", *ABPP meeting 2019: Target Discovery and Visualization using Chemical Probes"* (27-29 march 2019, Leuven; poster presentation)

Vanhoutte, R., Kahler, JP., Martin, S., Van Veen, S., Verhelst, S.H.L. "Clickable polyamine derivatives as probes for the polyamine transport system", *Target Discovery using Chemical Probes* (21-23 march 2018, Oxford; oral presentation)
*elected as oral presentation

Vanhoutte, R., Verhelst, S.H.L. "A combinatorial approach towards activity-based probes for serine and cysteine hydrolases", *Merck Organic Chemistry Conference* (7-8 december 2017, Blankenberge; poster presentation)

Meeting abstracts presented at other conferences

Vanhoutte, R., Martin S., Verhelst, S.H.L. "Clickable polyamine derivatives as probes for the polyamine transport system", *Scientific Mixer* (7 june 2018, Leuven; oral presentation)

List of Patents

(Issued 2021) van Veen, S., Martin, S., Van den Haute, C., **Vanhoutte, R.**, Kahler, J.P., Swinnen, J.V., Annaert, W., Agostinis, P., Verhelst, S.H.L., Baekelandt, V., Eggermont, J., Vangheluwe, P., "Screeningsmethoden ATP13A2".

List of awarded Grants

KU Leuven Post-doctoral Mandate type 2, 2021